Development of an Unsteady State Model for the Tank Bioleaching of Sulphide Mineral Concentrates in Flow Reactor Systems

Athanasios Kotsiopoulos

Submitted in total fulfilment of the requirements
of the degree of Doctor of Philosophy

April 2012

Department of Chemical Engineering
University of Cape Town

Publication Declaration

1. Kotsiopoulos A, GS Hansford and R Rawatlal. 2006. Application of population balance modeling in continuous tank bioleaching. Proceedings of the South African Chemical Engineering Congress 2006, 20-22 September 2006, Durban, South Africa. ISBN 1-86840-616-4. [CD-ROM].

2. Rawatlal R, A Kotsiopoulos and G Hansford. 2006. Development of a mathematical model for continuous tank bioleaching. 6th European Symposium on Biochemical Engineering Science, August 27-30, 2006, Salzburg, Austria.

3. Kotsiopoulos A, GS Hansford and R Rawatlal. 2007. Modeling the bioleaching of mineral sulphide particles in a continuous flow reactor systems. South African Institute of Chemical Engineers, R&D Day 2007, Cape Town, South Africa

4. Kotsiopoulos A, GS Hansford and R Rawatlal. An Approach of Segregation in Modelling Continuous Flow Tank Bioleach Systems. AIChE Journal, 54:1592-1599, 2008.

5. Kotsiopoulos A, GS Hansford and R Rawatlal. An investigation into the dynamics of chalcopyrite bioleaching. AIChE Journal, 56:2650-2661, 2010.

6. Kotsiopoulos A, GS Hansford and R Rawatlal. A dynamic analysis of chalcopyrite bioleaching in continuous flow reactor systems, AIChE J, DOI: 10.1002/aic.12753, August 2011.

7. Kotsiopoulos A, GS Hansford and R Rawatlal, The dynamics of chalcopyrite bioleaching in batch and continuous flow reactor systems incorporating time-varying particle surface areas. In: Proceedings of the 19^{th} International Biohydrometallurgy Symposium. Changsha, Peoples Republic of China, 18-22 September 2011.

Development of an Unsteady State Model for the Tank Bioleaching of Sulphide Mineral Concentrates in Flow Reactor Systems

Athanasios Kotsiopoulos
University of Cape Town, Rondebosch, Cape Town, South Africa, 7701

Abstract

In this thesis, it is hypothesized that in bioleaching flow reactor systems, high reaction rate regions exist that can be maintained by application of biological stress trajectories. Reactor models are developed for the purpose of optimising plant operation, understood here as maximising the production rate. Complicating this attempt are a) the non-linear dynamics associated with the kinetics and b) the primary reaction's being multiphase. Mathematical models are developed to establish which particle parameters are necessary to describe reactor performance using the method of segregation. The models are distinguished by the combination of either particle residence time or age and/or particle size distributions. The models evaluated at steady state are validated against pilot plant data obtained from the Fairview Mine in South Africa and were found to be in good agreement with the data. As the model was developed using a segregation approach and thus incorporates age distributions in the model formulation, the model could be extended to unsteady state operation.

Due to the non-linearity of the chemical reaction rates in bioleaching, a dynamics analysis, which is a study of the evolution of steady states in the bioleaching system, was used to optimise and evaluate input conditions for safe operation and maximising the overall production rate. Dynamics analyses of sulphide mineral ores, specifically chalcopyrite, were performed in batch and continuous flow systems with respect to the redox potential, biomass concentration, system temperature, reactor mean residence time and time-varying particle surface area. In either reactor configuration, the existence and stability of system steady states was determined using the dynamics analysis, which revealed that the often reported passivating effect (Third *et al.*, 2000) resulting from physical phenomena may rather be due to dynamical constraints. Procedures to identify optimum operating conditions and to sustain maximum overall bioleaching rates, by either reducing the reactor mean residence time or applying biological stress, were introduced. Gains up to 56% in the leaching rate, for a reactor operating at steady state, were obtained. However, this analysis applies to tanks operating in steady state mode.

To extend the model for the purpose of control, an unsteady state reactor model was developed and validated against experimental data obtained from Mintek, South Africa. Simulation results indicated that the model was in good agreement with the experimental data in which reactor inlet flow conditions were unsteady. As a means of determining the influence of unsteady state operation on the hydrodynamics of the system, perturbations in the reactor flow rate, particle size distribution and solids loading were investigated. A dynamics analysis on the system revealed that leaching rates could be maintained at the maximum by applying a time-varying biological stress rate derived for an unsteady state reactor system thereby increasing the time-averaged overall rate by 58.9%. The dynamics

analysis demonstrated that effective control strategies could be developed to maintain the rate at a maximum when a reactor is operated under unsteady state conditions.

In summary, the novelty of this work lies in the application of the segregation approach, which allows for the development of an unsteady state model that respects variation in particle size and particle age. The unsteady state model could then be analyzed for dynamics features, from which optimal operation points were discovered. It was then demonstrated that the unsteady state model itself could be used to determine an effective control strategy for this desirable steady state not only to be achieved but also to be maintained in the face of potential unsteady sources in the system inputs.

Contents

List of Figures

List of Tables

Nomenclature

Greek Letters

α	Stoichiometric coefficient of Fe^{3+} in solution according the chemical leaching reaction $[-]$
β	Stoichiometric coefficient of Fe^{2+} in solution according the chemical leaching reaction $[-]$
γ_i	Stoichiometric coefficient of species i for reaction 1.2
θ	Age of a particle $[s]$
μ	Mean particle size $[m]$
ξ_i	Stoichiometric coefficient of species i for reaction 2.2
ρ	Density of sulphide mineral $[kg.m^{-3}]$
σ	Standard deviation $[m]$
τ	Mean residence time $[s]$
ϕ_{MS}	Fraction of the pure mineral sulphide in the ore $[-]$

Roman Letters

A^p	Specific surface area of a particle $[m^2.kg^{-1}]$
A^V	Reactor-volume based particle specific surface area $[m^2.m^{-3}]$
A	Temperature dependent rate constant for the chemical leaching of chalcopyrite $[mol.m^{-3}.s^{-1}]$
B	Temperature dependent rate constant for the chemical leaching of chalcopyrite $[mol.m^{-3}.s^{-1}]$
$C_{Fe^{2+}}$	Concentration of ferrous ions $[mol.m^{-3}]$
$C_{Fe^{3+}}$	Concentration of ferric ions $[mol.m^{-3}]$

C_{H+}	Concentration of protons $[mol.m^{-3}]$
C_{MS}	Concentration of the mineral sulphide ore $[mol.m^{-3}]$
C_X	Concentration of biomass $[mol.m^{-3}]$
$C_{X,a}$	Bifurcation biomass concentration at high ferric/ferrous ion ratios $[mol\ carbon.m^{-3}]$
$C_{X,b}$	Bifurcation biomass concentrations at low ferric/ferrous ion ratios $[mol\ carbon.m^{-3}]$
$C_{X,max}$	Biomass concentration required to maintain maximum overall rates $[mol\ carbon.m^{-3}]$
E_a	Activation energy $[kJ.mol^{-1}]$
EPS	Extracellular Polymeric Substance
$f_0(l_0)$	The normal distribution representing the probability of particles in a specific size range $[m^{-1}]$
$f(X_{cpy})$	Topological term $[-]$
g_{py}	Mineral grade $[-]$
H	Reactor holdup $[kg$ or $m^3]$
h_{in}	Inlet flow rate to the reactor $[kg.s^{-1}]$
h_{out}	Exit flow rate from the reactor $[kg.s^{-1}]$
K	Inhibition constant $[-]$
k	Intrinsic surface reaction rate constant $[mol.m^{-2}.s^{-1}]$
k_d	Death rate kinetic constant $[s^{-1}]$
k_{out}	Exit flow rate constant $[kg^{0.5}.s^{-1}]$
k_s	Biological stress rate $[s^{-1}]$
$k_s(t)$	Time-varying biological stress rate $[s^{-1}]$
$I(\theta)$	The internal age distribution of particles $[s^{-1}]$

$I(t,\theta)$	The unsteady state internal age distribution of particles $[s^{-1}]$
l	Current particle size or diameter $[m]$
$l(\theta)$	Current particle size as a function of particle age θ $[m]$
$l(t,\theta)$	Current particle size as function of particle age θ and real time t $[m]$
l_0	Inlet particle size or diameter to the bioleach reactor $[m]$
MM_{MS}	Molar mass of sulphide mineral ore particle $[kg.mol^{-1}]$
MM_{FeS_2}	Molar mass of pyrite ore particle $[kg.mol^{-1}]$
M^p	Mass of a single particle $[kg]$
M^R	Total mass of all particles in the reactor $[kg]$
MS	Sulphide mineral
N^T	The total number of particles in the reactor $[-]$
n	Reaction order $[-]$
PSD	Particle Size Distribution
$q^{max}_{Fe^{2+}}$	Maximum microbial specific ferrous iron utilisation rate $[mol\ Fe^{2+}.mol\ carbon^{-1}.s^{-1}]$
q_0	Maximum microbial specific ferrous iron utilisation rate at the rerference temperature T $[mol\ Fe^{2+}.mol\ carbon^{-1}.s^{-1}]$
Q	Volumetric flow rate $[m^3.s^{-1}]$
RTD	Residence Time Distribution
r''	Intrinsic surface reaction rate $[mol.m^{-2}.s^{-1}]$
$r''(t)$	Time-varying intrinsic surface reaction rate $[mol.m^{-2}.s^{-1}]$
r'	Particle leaching rate $[mol.kg^{-1}.s^{-1}]$
r_{cpy}	Intrinsic chemical leaching rate for chalcopyrite $[mol.m^{-3}.s^{-1}]$

r_{MS}	Intrinsic rate for most mineral sulphides MS $[mol.m^{-2}.s^{-1}]$
$r_{Fe^{2+}}$	Microbial oxidation rate $[mol.m^{-3}.s^{-1}]$
$\overline{r^p}$	Average particle leaching rate $[mol.m^{-3}.s^{-1}]$
$\overline{r^R}$	Average reactor bioleaching rate $[mol.m^{-3}.s^{-1}]$
r^R	Reactor bioleaching rate $[mol.m^{-3}.s^{-1}]$
$r^R(t)$	Time-varying reactor bioleaching rate $[mol.m^{-3}.s^{-1}]$
r^R_{max}	Maximum reactor bioleaching rate $[mol.kg^{-1}.s^{-1}]$
R	ferric/ferrous iron ratio ($R = C_{Fe^{3+}}/C_{Fe^{2+}}$) $[-]$
R_a	Intercept at high ferric/ferrous ion ratios $[-]$
R_b	Intercept at low ferric/ferrous ion ratios $[-]$
$R_{X,a}$	ferric/ferrous ion ratio at bifurcation point $C_{X,a}$ $[-]$
$R_{X,b}$	ferric/ferrous ion ratio at bifurcation point $C_{X,b}$ $[-]$
R_S	Steady state ferric/ferrous ion ratio $[-]$
$R_{X,max}$	ferric/ferrous ion ratio required to maintain maximum overall rates $[-]$
R_g	Universal gas constant $[J.mol^{-1}.K^{-1}]$
SHE	Standard Hydrogen Electrode
t	Time $[s]$
T	Temperature $[K]$
V^R	Reactor volume $[m^3]$
X^p	Particle conversion $[-]$
X^R	Overall reactor conversion $[-]$

Y_{XS} Biomass yield [–]

1

Introduction

1.1 Historical Perspective

BIOLEACHING is the process of utilising iron and sulphur-oxidsing microorganisms to reclaim valuable metals from sulphide mineral ores. The practice of bioleaching covers the fields of microbiology, geochemistry, biotechnology, hydrometallurgy, mineralogy, geology, chemical engineering and mining engineering (Brandl, 2008). The practice of extracting metals from ores and the recovery of these metals by precipitation on metallic iron has been applied since ancient times. Both the Chinese and Europeans used the process of cementation, coming from the Spanish name *cementación* meaning precipitation, to recover copper from copper sulphate (Ehrlich, 2001; Gilbertson, 2000). As far back as second century B.C., the Chinese and Europeans recovered copper sulphate using this principle, using it as an ingredient in bronze (Ehrlich, 2001; Mishra *et al.*, 2005; Acevedo, 2002). The earliest records of the practice of leaching are by Galen from the island of Cypress, where he reported on the extraction of copper in 166 A.D. He described the percolation of water through permeable rock where copper minerals dissolved to release copper sulphate in solution (Figure 1.1). Thereafter, the copper sulphate was recovered by means of crystallisation (Gilbertson, 2000). The Roman writer, Gaius Plinius Secundus (23 - 79 A.D.), reported a similar method of copper sulphate recovery that was widely practiced in Spain (Brandl, 2008; Gilbertson, 2000). Commercial operation of cementation started as early as 1096 A.D. and was described by Paracelsus (1493 - 1541 A.D.), an alchemist, as the transformation of Mars (iron) into Venus (copper) (Gilbertson, 2000).

The biohydrometallurgical process of heap leaching of copper sulphides was carried out at the Rio Tinto (the Red River) mine in Spain as early as 1752 (Brandl, 2008; Gilbertson, 2000; Gericke *et al.*, 2009). The process involved the construction of ore layers alternating with beds of wood, which was then ignited to roast the copper and iron sulphides (Gilbertson, 2000). Water was distributed over the heaps to collect the solubilised copper and iron as sulphates (Gilbertson, 2000). This method of leaching was later banned in 1878 due to the high sulphur emissions and was altered to exclude the roasting step and ran successfully until the early 1970s (Brandl, 2008; Gilbertson, 2000). This method of leaching predated the understanding

Figure 1.1: Leaching of sulphide mineral ores where copper sulphate was collected in wooden basins and concentrated in the sun. Illustration obtained from Brandl (2008) which was recovered from the book written by Georgius Agricola (1494 - 1555).

of the presence and role of microorganisms in the leaching process (Olson *et al.*, 2003; Ehrlich, 2001). The success of the mine in Rio Tinto, at the time, was considered to be due to either the unique quality of the ore in the area or the Spanish climate favouring the leaching of the sulphide ores (Brandl, 2008; Gilbertson, 2000). It was only until the mid twentieth century that mesophiles *Thiobacillus ferrooxidans*, which was later reclassified as *Acidithiobacillus ferrooxidans* (Kelly and Wood, 2000), contributed favourably to the leaching process in the Rio Tinto mine (Olson *et al.*, 2003; Ehrlich, 2001; Brandl, 2008; Gilbertson, 2000; Mishra *et al.*, 2005; Acevedo, 2002). The role of microorganisms in the leaching of sulphide minerals was only realized in 1947 (Colmer and Hinkle, 1947), by the discovery of *Acidithiobacillus ferrooxidans* and other iron- and sulphur-oxidising microorganisms (Brandl, 2008; Ehrlich, 2001; Gilbertson, 2000; Mishra *et al.*, 2005). It was found that these organisms could oxidize elemental sulphur and ferrous ions at higher rates than by convention inorganic chemistry, up to several orders higher (Gilbertson, 2000; Brandl, 2008).

1.2 Basic Elements of the Bioleaching Process

Chemical leaching by means of ferric sulphate to extract metals from sulphide ores was considered a slow process (Zimmerley *et al.*, 1958). With the discovery of iron- and sulphur oxidising microorganisms, the rate of the leaching process could be increased. An early industrial application of bioleaching was reported by Zimmerley *et al.* (1958). The importance of ferric sulphate as an oxidant in the leaching of copper from sulphide minerals from mine wastes at the Kennecott Copper Corporation in Utah, U.S.A. was recognised (Mishra *et al.*, 2005). The authors identified autotrophic bacteria *Acidithiobacillus*

ferrooxidans as a means of converting ferrous sulphate to the active reactant, ferric sulphate, in acidic solutions for the purpose of leaching copper sulphide minerals. At the time, the process was not designed to promote microbial activity (Olson *et al.*, 2003).

The use of microorganisms to facilitate or promote the extraction of metals from sulphide minerals has only recently been applied in industry (Olson *et al.*, 2003; Brierley and Brierley, 2001). Commercially, bioleaching operations have developed into an important and established process for the recovery of copper, cobalt, nickel, zinc and uranium. Presently, iron- and sulphur-oxidising microorganisms are the preferred microorganisms in the development of bioleaching process. These organisms are naturally occurring where sulphide mineral ores are exposed to the surface in the presence of water (Gilbertson, 2000). Commercially, these microorganisms are often adapted for rapid growth on the sulphide mineral that is to be leached. Industrial applications exploiting microbial activity to mobilize metals in ores was first applied in the extraction of copper and gold in heaps and tank biotech reactors, respectively, in the 1980s (Brierley and Brierley, 2001; Olson *et al.*, 2003; Ehrlich, 2001; Mishra *et al.*, 2005). More recently, the technology was successfully applied in the biooxidation of gold, cobalt, uranium and silver (Acevedo, 2000; Rohwerder *et al.*, 2003; Olson *et al.*, 2003). These operations have an economic advantage over conventional pyrometallurgical processes due to low capital investment, relatively mild operating conditions, low energy input and low environmental impact (May *et al.*, 1997; Acevedo, 2000).

At present, industrial bioleaching applications are performed in either irrigation-type process or stirred tank reactors.

Irrigation-Type Process

In irrigation-type processes bioleaching occurs in either dumps or heaps. The leaching of copper at the Kennecott Copper mine in Utah is one of the earliest applications of dump leaching where billions of tons of low-grade copper ore waste is treated (Rawlings, 2002). In this irrigation-type process, dumps consisting of run-of-mine ore, ore taken directly form the mine, are stacked and treated without crushing. The ore is irrigated and conditioned over several years with an iron- and sulphate-rich wastewater recycle in which the chemical leach reactions are promoted by microorganisms growing in the dump (Rawlings, 2002). Similar to heap leaching, the metal sulphate solution is recovered from the base of the dump to extract the valuable metals by solvent extraction and electrowinning. Due to the low cost of operation, dump leaching is suitable for low-grade ores.

In heap bioleaching, constructed mounds or heaps of crushed ore or concentrate are irrigated with an acidic ferric leach solution at the top (Figure 1.2). The process is designed to be more efficient that dump leaching. Contrary to dump leaching, the acidified, crushed ore is agglomerated in rolling drums and stacked on irrigation pads to avoid loss of leach solution (Rawlings *et al.*, 2003; Rawlings, 2002). Often drip irrigation is applied to minimise

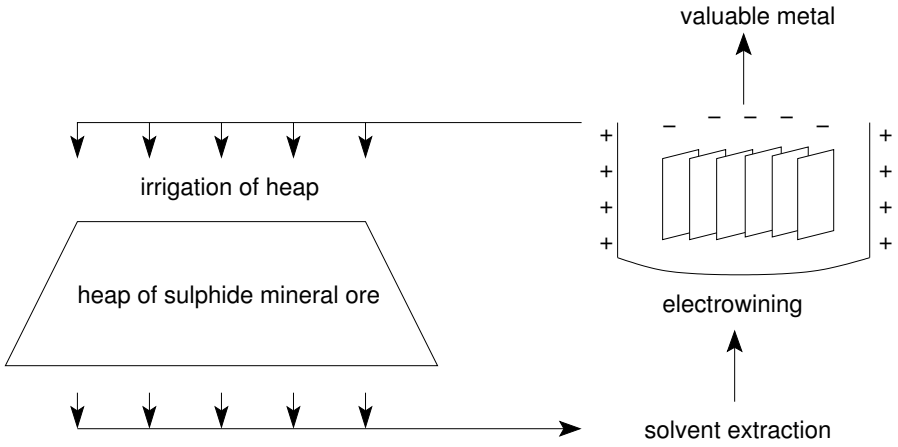

Figure 1.2: Heap bioleaching of sulphide mineral ores (Rawlings, 2002).

evaporation. The leach solution percolates through the heap to come in contact with the crushed ore thus leaching out valuable metals. Aeration of the heaps may either be passive or active. In the case of passive aeration, air is pulled into the heap by the irrigation of the leach solution. Whereas in active aeration, heaps are constructed with aeration pipes installed at the bottom where air is blown into the heap to facilitate the bioleach reactions (Rawlings *et al.*, 2003). The microorganisms that grow in the heap catalyse the extraction of the metals such that insoluble metal sulphides are converted to soluble metal sulphates (Rawlings, 2002). The mineral rich leachate is then recovered for further downstream processing for metal recovery (Rawlings, 2002). Typically, mean residence times for heap bioleaching processes can take up to a few months as opposed to a period of years taken during dump leaching. The low cost to construct and operate heap reactors make the process suitable for the treatment of lower grade ores than those utilized in tank bioleaching (Rawlings *et al.*, 2003).

Stirred Tank Process

Tank bioleaching has been used for the recovery of gold from arsenic-gold bearing concentrates since 1984 (Dew *et al.*, 1997). The Goldfields' BIOX process, previously known as Gencor, at the Fairview mine in South Africa, commissioned in 1986, was the world's first tank bioleaching plant and has one of the longest histories of tank biooxidation applications (Olson *et al.*, 2003; Gilbertson, 2000). The design and commission of the plant was realized after 10 years, which replaced the previously utilized roasting facility to achieved an environmentally favorable process with enhanced gold recoveries (Gilbertson, 2000). Subsequently, several large scale tank bioleaching plants have been established (Table 1.1) with many patent operations arising (BIOX - Fairview, BacTech Mintek, BioCop - BHP Billiton/Coldelco).

The extraction of metals from sulphide minerals involves milling (*ca.* < 75 μm) and floating of the mineral prior to the tank bioleaching process (van Aswegen *et al.*, 2007). Milling of the sulphide mineral ores ensures that the suspension of solids or slurry can be pumped or flow under gravity and that solids remain in suspension when gas is introduced into the

Table 1.1: Plants for the biooxidation of refactory gold minerals (Brierley, 1997; Loayza and Ly, 1999; Acevedo, 2000; Batty and Rorke, 2005)

Plant	Start-up	Technology	Capacity
Fairview, South Africa	1986	Tank leaching	35 tons gold concentrate/day
Sao Bento, Brazil	1990	Tank leaching	150 tons gold concentrate/day
Harbour Lights, Australia	1992	Tank leaching	40 tons gold concentrate/day
Wiluna, Australia	1993	Tank leaching	115 tons gold concentrate/day
Ashanti, Ghana	1994	Tank leaching	1 000 tons gold concentrate/day
Youanmi, Australia	1994	Tank leaching	120 tons gold concentrate/day
Sansu, Ghana	1994	Tank leaching	1 000 tons gold concentrate/day
Kasese, Ghana	1998	Tank leaching	3 tons cobalt concentrate/day
Tamboraque, Peru	1999	Tank leaching	260 000 tons of zinc flotation tailings
Chuquicamata, Chile	1999	Tank leaching	55 tons of copper concentrate/day
Laizhou, China	2001	Tank leaching	5 tons of gold concentrate/day

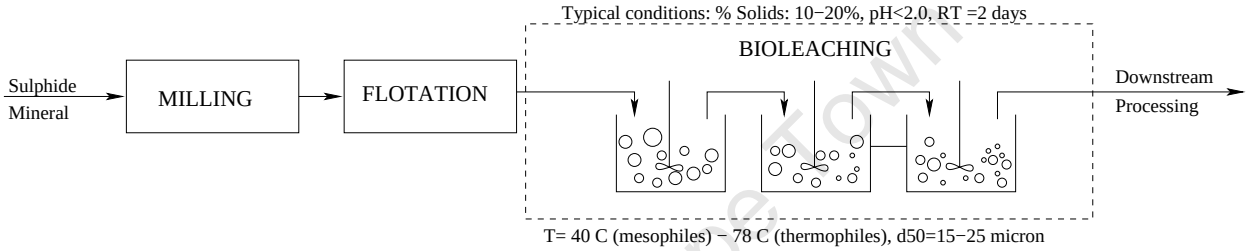

Figure 1.3: The bioleaching process

tanks from the bottom. Tank bioleaching is often carried out in a series of aerated stirred tank reactors with a feed inlet to the first tank in the series and gravity overflow as feed to subsequent tanks in the series (Figure 1.3). Tanks are sufficiently agitated to further ensure uniform suspension of mineral particles and are fitted with baffles which aid in the mixing efficiency. Tank bioleach reactors are large with total design volumes ranging from 440 to 21 600 m^3 with individual tank volumes ranging up to 1 300 - 2 000 m^3 requiring high aeration rates (Rawlings, 2002; Rawlings *et al.*, 2003; van Aswegen *et al.*, 2007). Oxygen supply to these reactors is a major power consumer and therefore significantly contributes to the tank bioleaching operating costs. Approximately 1.8 to 2.6 kg of oxygen is required per kg of sulphide mineral oxidised and is supplied to the reactor by sparging compressed air to tanks (van Aswegen *et al.*, 2007). The axial-flow impeller of the stirred tank reactors is designed such that impeller pumping rate is sufficient to attain high aeration rates and ensure that uniform solid suspension, temperature, pH and concentration profiles are maintained in the reactor (van Aswegen *et al.*, 2007).

The primary reactor(s) usually have higher mean residence times (*ca.* 2 - 2.5 days) than the subsequent tanks in the series and are typically arranged in parallel to facilitate or promote microbial growth and avoid washout (Dew, 1995; Olson *et al.*, 2003). Subsequent tanks in the series are smaller with the total mean residence times over the entire series being about 4 - 6 days (van Aswegen *et al.*, 2007; Olson *et al.*, 2003). As the bioleach reaction is exothermic, the reactors are cooled to remove excess heat (Rawlings, 2002). Due to the high

cost of construction of these bioreactors, tank bioleaching is usually restricted to high-value ores, such as, the bio-oxidation of gold-bearing concentrates (Rawlings, 2002). A major disadvantage of tank bioleaching is that to maintain a uniform suspension of solids and to ensure efficient gas transfer for microbial growth, the quantity of solids within the reactor is limited to *ca.* 20 % [m/v] (van Aswegen *et al.*, 2007; Rawlings *et al.*, 2003).

Microbial Aspects

Tank bioleaching reactors, as opposed to dump or heap reactors, can be controlled within optimal conditions. By controlling these conditions, microbial growth can be maintained at a maximum. However, as the reaction proceeds and metal is leached into the aqueous phase, the density and number of microbial species may significantly be affected (Rawlings and Johnson, 2007).

The advantage of tank bioleaching is that the process is a continuous flow system. This creates an environment in which the most resilient microorganisms are naturally selected and continue to grow (see Table 1.2). The minerals being leached provide a source of energy and nutrients to the microorganisms and are therefore less likely to be subject to washout and continue to thrive, eventually dominating the microbial population. As such, the microorganisms that are most efficient at leaching the minerals remain most active and therefore accelerate the bioleaching process (Rawlings and Johnson, 2007).

The microorganisms present in bioleaching reactions are classified as iron-oxidisers and sulphur oxidisers. These organisms provide ferric ions and sulphuric acid required for the leaching reactions. The proportions and type of microbes present in the reactions depend on the conditions under which the heaps or tank reactors are operated (Ojumu, 2008). These microorganisms may be classified as mesophiles, thermophiles or extreme thermophiles and are largely temperature dependent. Studies have shown that in tank bioleaching reactors operating at moderate temperatures *ca.* 313.15 K, *Leptospirillum* type species are dominant with *Leptospirillum ferriphilum* being the most prevalent as opposed to *Leptospirillum ferroxidans* as previously believed (see Table 1.2; Coram and Rawlings, 2002).

As previously stated, tank bioleaching is an expensive process and is often used in the bioleaching of high-value ores and concentrates, such as, the recovery of gold from asenopyrite concentrates (Rawlings, 2002). Dominant microbial species utilized in the bioleaching of gold-bearing arsenopyrite concentrates at 313.15 K have been identified as consisting of 48 - 57 % *Leptospirillum ferrooxidans*, 26 - 34 % *Acidithiobacillus thiooxidans* and 10 - 17 % *Acidithiobacillus ferrooxidans* mesophilic microorganisms (Dew *et al.*, 1997; Rawlings, 2002). In addition to the aforementioned microorganisms, the presence of *Acidiphilium cryptum* has been detected in the bioleaching of zinc/lead pyrite at 308.15 - 313.15 K (Goebel and Stackebrandt, 1994), while *Sulfobacillus thermosulfidooxidans* was observed in the bioleaching of cobaltiferous pyrite at 308.15 K (Battaglia-Brunet *et al.*, 2002) in stirred tank reactor systems (Table 1.2).

Table 1.2: Acidophiles present in the tank bioleaching of various sulphide mineral concentrates – Table modified from Rawlings and Johnson (2007) and Norris (2007)

Mineral Concentrate	Temperature [K]	Microbial Populations	Reference
Pyrite/Arsenopyrite	313.15	*Leptospirillum ferroxidans* *Acidithiobacillus thiooxidans* *Acidithiobacillus ferroxidans*	Dew *et al.* (1997)
Zinc/Lead Pyrite	308.15 - 313.15	*Leptospirillum ferroxidans* *Acidithiobacillus thiooxidans* *Acidiphilium cryptum* *Acidithiobacillus ferroxidans*	Goebel and Stackebrandt (1994)
Cobaltiferous Pyrite	308.15	*Leptospirillum ferroxidans* *Acidithiobacillus thiooxidans* *Sulfobacillus thermosulfidooxidans*	Battaglia-Brunet *et al.* (2002)
Polymetallic Sulfides	318.15	*Leptospirillum ferriphilium* *Aciditiobacillus caldus* *Sulfobacillus sp.* *Ferroplasma acidophilium*	Okibe *et al.* (2003) Norris (2007)
Pyrite, Arsenical Pyrite and Chalcopyrite	318.15	*Aciditiobacillus caldus* *Sulfobacillus thermosulfidooxidans* *Sulfobacillus montserratensis*	Dopson and Lindström (2004)
Nickel Concentrate	322.15 - 328.15	*Aciditiobacillus caldus* *Acidimicrobium sp.* *Sulfobacillus sp.*	Norris (2007)
Chalcopyrite	348.15 - 351.15	*Sulfolobus sp.* *Metallospheara sp.*	Norris (2007)

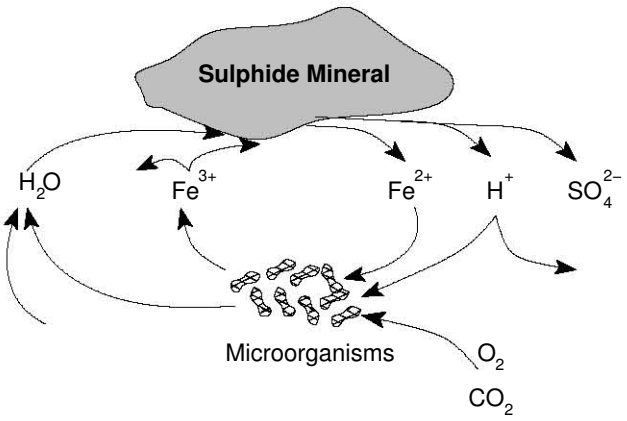

Figure 1.4: The bioleaching mechanism that incorporates the chemical leaching of the sulphide mineral MS *via.* Eq. 1.1 and the microbial ferrous ion oxidation *via.* Eq. 1.2. Figure reproduced from Breed and Hansford (1999b).

While studies by Mikkelsen *et al.* (2006) for the bioleaching of chalcopyrite in stirred tank reactor at 351.15 K were found to be composed of 69 % (total clones) *Sulfolobus shibatae*, 11 % *Stygiolobus azoricus*, 8 % *Metallosphaera sp.*, 2 % *Acidianus infernus*, and 10 % of a novel phylotype related to *Sulfurisphaera ohwakuensis* thermophilic microorganisms.

Bioleaching of sulphide mineral ores are mainly associated with the extraction of gold and copper (Poulin and Lawrence, 1996; Rawlings, 2002). Refractory gold ores are contained in a mixture of pyrite and arsenopyrite that cannot be easily solubilised by cyanidation. The gold is preferentially recovered by sulphur-oxidising microorganisms which oxidise the mineral to release ferric and sulphate ions, where arsenopyrite oxidation occurs more readily over pyrite, releasing the gold for conventional recovery by cyanidation (Poulin and Lawrence, 1996; Rawlings, 2002). The biooxidation process, when compared with conventional roasting processes, has the advantage that no toxic gases are released.

Although heap leaching is an effective technology that can process large volumes of minerals, it suffers from production and yield limitations due to process inefficiencies (Acevedo, 2000). Heap reactors have the disadvantage that they are difficult to aerate efficiently and also are susceptible to pH gradients. Due to the presence of gangue material which are acid-consuming, as opposed to the mineral which acid-producing, makes pH control within optimum bioleaching ranges (*ca.*1.8-2.2) difficult (Rawlings *et al.*, 2003).

Due to these process inefficiencies, there is an increased interest in the application of tank bioleaching (Huberts, 1994). In contrast to heap leaching, the primary operating variables in tank bioleaching, *viz.* temperature, pH, oxygen and carbon dioxide transfer can be effectively controlled to obtain a higher degree of extraction (Acevedo, 2000; Pinches *et al.*, 1987).

1.3 Modeling Considerations

Reduction by ferric ions liberates ferrous ions from mineral sulphide particles into the solution phase transferring particle mass to the aqueous phase (Eq. 1.1, Figure 1.4). Given that

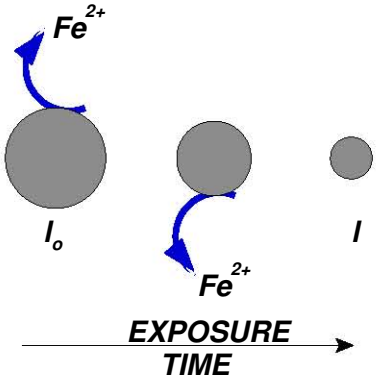

Figure 1.5: The evolution of the a typical particle in a bioleach process. l_0 represents the inlet particle diameter, while l is the final particle diameter.

interphase mass transfer (i.e. from the solid particle to the solution) occurs, it is expected that the particle surface area will change with particle-solution contact time. With microbial oxidation, the ferrous ions are converted back to the ferric ion form, hence the microorganisms maintain a reaction environment at conditions that promote the liberation of ferrous ions from the particles (Eq. 1.2, Boon *et al.*, 1995). The interaction of the solid minerals with the microorganisms in solution facilitates the recovery of metals.

$$MS + 2Fe^{3+} \rightarrow M^{2+} + S^0 + 2Fe^{2+} \quad [1.1]$$

$$4Fe^{2+} + O_2 + 4H^+ \rightarrow 4Fe^{3+} + 2H_2O \quad [1.2]$$

where MS is the sulphide mineral and M^{2+} is the extracted metal ion.

The complexity inherent to bioleaching system arises from the kinetics of the process and the mechanism of dissolution of the solid mineral particles. The liberation of ferrous ion into solution suggests that the particle surface area will change with solution contact time. The change in particle size therefore results in variable particle reaction rates (Figure 1.5). An overall system mass balance, which requires estimation of the overall reaction rate, must then incorporate the rate contribution of all particles in the reactor. One approach to keep track of these surface area changes and their resulting effect on the reaction rate is by Population Balance Models (PBMs).

PBMs are often applied in particulate processes and have been successfully applied in tank bioleaching (Crundwell, 2001). With the exception of Crundwell (2005; 2001; 1994; 1995), the published models fail to incorporate both acid ferric leach and microbial kinetics, variation in particle size and interphase mass transfer (Figure 1.6). None of these models have incorporated the influence of particle age in the reactor and on the acid ferric leach kinetics. In addition, all published models, including the work of Crundwell (2001; 2005), apply only to the steady state mode of operation.

A comprehensive model that incorporates the sub-process mechanism and includes particle surface area changes for a non-uniformly sized population of particles due to variable solution contact times is therefore required for process optimisation. Further, the flow rates to and

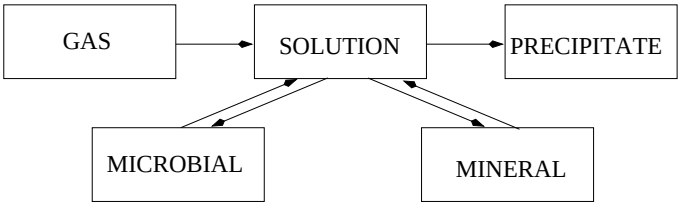

Figure 1.6: The characteristics of bioleaching

from the bioleach reactor are not always constant. These fluctuations in the flow rates influence system performance, thus highlighting the need for the development of a model that considers unsteady state operation.

2

Literature Review

SEVERAL authors have attempted to develop models that predict overall reactor performance. These reactor models may be classified according to the applied assumptions regarding the bioleach mechanism and the nature of the mixing model. Models tend to focus on the aqueous phase components assuming that the fractional conversion of the mineral sulphide ore is directly related to microbial growth, and in most treatments there is less emphasis on the contribution of the solid phase to the overall reaction rate. This is a serious oversight given that the intrinsic leaching rate is surface area dependent. Therefore the mineral particle size and particle-solution contact time are important model inputs when predicting the overall reactor performance. In this chapter, we will attempt to critically review recent continuous flow bioleach reactor models developed from first principles and discuss their suitability to particular applications.

2.1 Bioleaching Mechanism

In bioleaching, two mechanisms are identified namely the direct and indirect mechanisms. The direct mechanism is generally accepted as being the interaction of the microorganisms with the mineral sulphide surface *via.* physical attachment, thereby invoking direct oxidation at the surface inherently gaining energy directly from the sulphide mineral through an enzymatic mechanism (Crundwell, 2003; Rawlings, 2002; Sand *et al.*, 1995). Contrary to this, the indirect mechanism is established as being the chemical reaction of a ferric ion with the metal sulphide surface to release a metal cation, ferrous ion and sulphur compounds. The microorganisms then recycle the ferrous ion by oxidation back to ferric ion to sustain and repeat the oxidation cycle. As opposed to the direct mechanism, attachment of the microorganisms to the mineral sulphide surface is not necessary with the indirect mechanism (Boon *et al.*, 1994). Generally, the indirect mechanism has been adopted, while the direct mechanism of sulphide metal oxidation has been abandoned (Rohwerder *et al.*, 2003).

The observed increased oxidation rate of pyrite in the presence of *Acidithiobacillus ferrooxidans* was described by Silverman and Ehrlich (1964) *via.* the direct mechanism.

They attributed increased oxidation rates to the attachment of the microorganisms to the sulphide mineral surface by reactions 2.1 and 1.2

$$FeS_2 + \frac{7}{2}O_2 + H_2O \rightarrow Fe^{2+} + 2H^+ + 2SO_4^{2-} \quad [2.1]$$

$$4Fe^{2+} + O_2 + 4H^+ \rightarrow 4Fe^{3+} + 2H_2O \quad [1.2]$$

indicating that reaction 1.2 occurs very slowly in the absence of iron-oxidising microorganisms, *Acidithiobacillus ferrooxidans*.

Sand *et al.* (1995) expressed some reservation as to the validity of the direct mechanism after investigating the sulphur metabolic patterns of iron oxidising microorganisms, *Acidithiobacillus ferrooxidans*. No quantifiable depletion in the substrate was observed when the microorganisms were cultivated in an iron-free salt solution, indicating to the authors that cell activity was solely dependent on the availability of iron ions.

Recent work by Tributsch (2001) has shown that the direct bioleaching mechanism should be redefined. Tributsch (2001) indicated that the nature by which different minerals exchange electrons during the release of metal cations is critical to reasoning why sulphides react differently. The direct mechanism (Eqs. 2.1 and 1.2) proposes that all sulphur is converted to sulphate by enzymatic attachment to the mineral without any other sulphur intermediates while the presence of elemental sulphur intermediates supports the indirect mechanism where ferric ions oxidise the mineral sulphide and dissociate to form ferrous ion and elemental sulphur generation during the course of the reaction (Sand *et al.*, 2001). The indirect mechanism is represented by Eqs. 2.2 – 2.3 (Sand *et al.*, 2001):

$$FeS_2 + 14Fe^{3+} + 8H_2O \rightarrow 15Fe^{2+} + 2SO_4^{2-} + 16H^+ \quad [2.2]$$

$$MS + 2Fe^{3+} \rightarrow M^{2+} + S^0 + 2Fe^{2+} \quad [1.1]$$

$$S^0 + \frac{3}{2}O_2 + H_2O \rightarrow 2H^+ + SO_4^{2-} \quad [2.3]$$

The evidence for which mechanism is correct is contradictory. Boon and Heijnen (1998a; b) investigating the oxidation kinetics of pyrite in the presence of *Leptospirillum ferrooxidans* observed that the oxygen utilisation rate decreased with increasing ferric/ferrous ion ratio while the pyrite specific rate increased. Also, in experiments in the absence of pyrite revealed similar results in which the oxygen utilization rate decreased with increasing ferric/ferrous ion ratio. This indicated that ferrous ion is the primary substrate for microbial growth in the aqueous phase. Boon *et al.* (1998) thus concluded that oxygen utilisation occurred exclusively within the bulk liquid rather than at the mineral surface and that the bioleaching of pyrite follows a two-step mechanism in which the pyrite is chemically leached by ferric ion attack and ferric ions are regenerated by microbial ferrous ion oxidation. This finding contradicted the support for a direct mechanism which requires that the attached microorganisms consume all oxygen at the mineral surface, but the contrary was found to be true, thereby confirming an indirect mechanism (Boon and Heijnen, 1998a; b). Visible corrosion pitting of pyrite surfaces

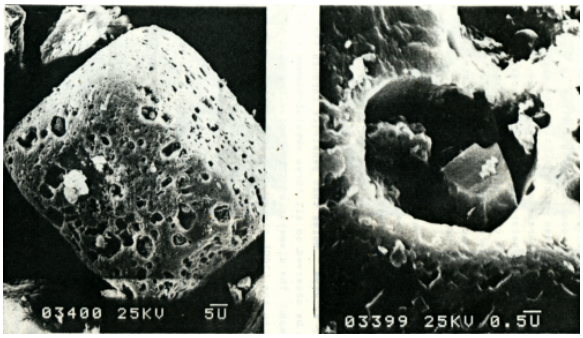

Figure 2.1: Visible generation of pores or pitting of pyrite particles (Hansford and Drossou, 1988).

(Figure 2.1) has been noted by several authors (Hansford and Drossou, 1988; Tributsch, 2001; Sand *et al.*, 1995; Crundwell, 2003) where it is believed that the microorganisms rapidly attach themselves (Rawlings, 1998). This is evident due to the requirement for growing leaching microorganisms to attach themselves to sulphide minerals to sustain growth, multiply and hence leach the mineral (Arrendondo *et al.*, 1994; Sand *et al.*, 1995; Tributsch, 2001).

The amount of microorganisms attached to the sulphide surface depends on the type of microorganism (Sand *et al.*, 1995; Schippers *et al.*, 1996; Tributsch, 2001). For example, sulphur and ferrous ion metabolising *Acidithiobacillus ferrooxidans* microorganisms are less abundant on surfaces as compared to ferrous ion oxidising microorganisms *Leptospirrilum ferrooxidans* which also attach more firmly to the surface (Sand *et al.*, 1995; Schippers *et al.*, 1996). This is because *Acidithiobacillus ferrooxidans* is able to obtain additional energy from the high energy capacitance of sulphur as opposed to *Leptospirillum ferrooxidans* which is solely dependent on ferrous ion as substrate thereby making it more prevelant on mineral surfaces and less abundant in leachates (Sand *et al.*, 1995). It has been shown that very high concentrations of ferric ions are observed in the contact layer between the sulphide mineral and the microorganisms. This contact layer or extracellular polymeric substance (EPS) layer (Figure 2.2) plays an important role in the leaching reactions as it serves as a reaction space whereby the ferric ion reacts with the mineral (Rodriguez-Leiva and Tributsch, 1988; Sand *et al.*, 1995; Rawlings, 1998). It is believed that the majority of the leaching reactions occur within the EPS layer due to the very high concentration of ferric ions (of several orders higher than in the surrounding bulk (Schippers *et al.*, 1996)) within this layer (Schippers *et al.*, 1996; Rodriguez-Leiva and Tributsch, 1988; Tributsch, 2001; Sand *et al.*, 1995). This was supported by experiments by Gehrke *et al.* (1998) and Schippers *et al.* (1996) who found that *Acidithiobacillus ferrooxidans* was unable to leach pyrite when the EPS layer of the microorganisms was stripped, further Norris and Kelly (1982); Norris (1983) and Sand *et al.* (2001) observed that *Acidithiobacillus thiooxidans* cannot dissociate pyrite since it lacks ferrous ion oxidising activity (Schippers *et al.*, 1996). These findings were to further highlight the importance of the ferric ion in the oxidation reactions of sulphide minerals and the support for the indirect mechanism (Sand *et al.*, 2001; Tributsch, 2001; Gehrke *et al.*, 1998; Schippers *et al.*, 1996).

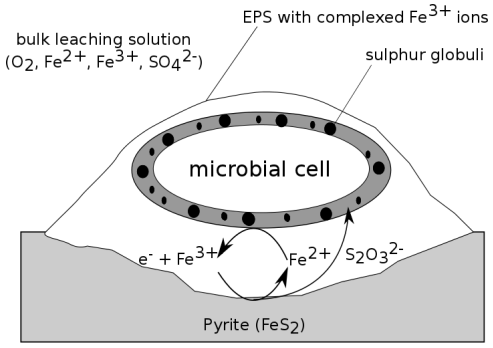

Figure 2.2: Illustration of the contact mechanism. Figure reproduced from Rohwerder *et al.* (2003).

The evidence that microorganisms attach to mineral sulphide surfaces *via.* an EPS layer (Figure 2.2) for certain types of mineral sulphides and not directly to the cell wall (Tributsch, 2001; Rodriguez-Leiva and Tributsch, 1988; Rawlings, 1998; Sand *et al.*, 2001), and that ferric ion is necessary for mineral oxidation reactions has led to the redefining of the bioleaching mechanism terms (Sand *et al.*, 2001; Tributsch, 2001; Crundwell, 2003; Rawlings, 1998; Rohwerder *et al.*, 2003). This has led to the renaming of the indirect mechanism, where close proximity between the cell and the sulphide surface is required, to a contact mechanism which strives to eliminate the ambiguity of the direct mechanism which suggests mineral suphide oxidation occurs *via.* a direct mineral-cell wall membrane contact at the surface (Tributsch, 2001; Rawlings, 1998; Rohwerder *et al.*, 2003).

2.2 Kinetics

2.2.1 Acid-Ferric Leach Kinetics

In mineral leaching the electrochemical potential of the oxidant must be greater than that of the mineral. The potential difference between the oxidant and the mineral is the driving force for the oxidation reaction (Riekkola-Vanhanen and Heimala, 1993; Wadsworth, 1987; May *et al.*, 1997). The greater the difference in the electrochemical potential of the oxidant and the mineral, the faster the rate of reaction (Riekkola-Vanhanen and Heimala, 1993).

Kinetic Models

Chemical ferric leaching can be described by either chemical or electrochemical kinetic models (Breed, 2000). Electrochemical methods assume that the electron transfer from the mineral surface to the surrounding solution is limiting and thus is independent of the total iron concentration (May *et al.*, 1997; Zheng *et al.*, 1986; Garrels and Thompson, 1960; Pletcher, 1984; McKibben and Barnes, 1986; Petrovich, 1981; Holdren, 1981; Wiersma and Rimstidt, 1984; Crundwell, 1987; Kawakami *et al.*, 1988; Boon, 1996; Holmes and Crundwell, 2000; Breed, 2000) while chemical methods assume that the surface reaction

is rate limiting (Williamson and Rimstidt, 1994; Zheng *et al.*, 1986; Moses *et al.*, 1987; Wiersma and Rimstidt, 1984; Tal, 1986; Boogerd *et al.*, 1991; King and Perlmutter, 1977; Reedy *et al.*, 1991). As chemical leaching involves a multi-step mechanism it is important that the rate limiting step is identified. Most authors assume that pyrite oxidation by ferric iron is chemical reaction, rather than diffusion, controlling due to the high activation energies observed (Wiersma and Rimstidt, 1984; Williamson and Rimstidt, 1994; Holmes and Crundwell, 2000). Wiersma and Rimstidt (1984) postulated that in unstirred reactions above 298.15 K, the acid-ferric leaching of sulphide minerals would result in diffusion limiting reactions.

The acid-ferric leaching of pyrite is often considered either first order (Garrels and Thompson, 1960; Wiersma and Rimstidt, 1984; Mathews and Robins, 1972; Kawakami *et al.*, 1988; Boogerd *et al.*, 1991) or approximately half order in ferric ions (McKibben and Barnes, 1986; Tal, 1986; Zheng *et al.*, 1986; Rimstidt and Newcom, 1993; Williamson and Rimstidt, 1994; Holmes and Crundwell, 2000) and *ca.* negative half order in either the proton (Mathews and Robins, 1972; McKibben and Barnes, 1986; Williamson and Rimstidt, 1994; Holmes and Crundwell, 2000) or ferrous ion concentration (Tal, 1986; Zheng *et al.*, 1986; Williamson and Rimstidt, 1994; Holmes and Crundwell, 2000). Assuming that the reacting solid surface area remains constant per unit mass over the short reaction period, Wiersma and Rimstidt (1984) determined that the rate of acid ferric leaching was first order in ferric iron and that the rate constant increased with decreasing ferric iron concentration (see Eq. T 1.4 in Table 2.1). The inverse dependence of the rate constant with ferric iron was consistent to findings obtained by Garrels and Thompson (1960) and Singer and Stumm (1967).

Contrary to results by Wiersma and Rimstidt (1984), the analysis by McKibben and Barnes (1986) on pyrite oxidation in dissolved ferric ion showed that the ferric leaching rate was proportional to the approximate square root of the dissolved ferric iron and negligibly affected by ferrous ions at constant pH with a negative half order rate dependence on proton concentration (McKibben and Barnes, 1986). The authors concluded that pyrite oxidation rates by ferric ion are independent of ferrous ion concentration. The rate law proposed in Eq. T1.5 in Table 2.1 included a rate constant which accounted for the ratio of the exposed mineral surface area, A which was determined using a multipoint BET, to the solution volume V.

Williamson and Rimstidt (1994) used available kinetic rate data from McKibben (1984); Nicholson *et al.* (1988) and Moses and Herman (1991) to generate rate laws for pyrite oxidation by ferric ion and dissolved oxygen over a broad range of solution concentrations (Williamson and Rimstidt, 1994). Based on literature findings, the acid-ferric leaching of pyrite was assumed chemical reaction, rather than diffusion, rate limiting due to the high activation energies observed. From the data accumulated, Williamson and Rimstidt (1994) found that the rate of pyrite oxidation by dissolved oxygen (DO) had a reaction order of 0.5 with respect to dissolved oxygen which was consistent to findings by McKibben (1984). However, unlike the findings by McKibben (1984), Williamson and Rimstidt (1994) showed that the oxidation rate was not independent of pH but inversely proportional to the proton

concentration. Experimental analysis showed that the rate of pyrite oxidation by ferric ion, in the presence of oxygen, was a strong function of ferric and ferrous ions and independent of the concentration of sulphate and chloride ions and ionic strength (Eq. T1.12 in Table 2.1).

Pyrite oxidation by ferric ion, in the absence of dissolved oxygen, revealed similar results obtained by McKibben (1984). In addition to the oxidation rate being a function of the ferric/ferrous ion ratio, the results showed a significant contribution by the proton concentration (Eq. T1.11 in Table 2.1). Similar to findings by McKibben and Barnes (1986), Kawakami *et al.* (1988) determined that the leaching rate was inversely proportional to the acid concentration. An increase in acid concentration resulted in decreased product concentrations. Kawakami *et al.* (1988) proposed that this inverse relationship can be explained by the fact that ferric chloride in solution can form various complexed $FeCl^{2+}$ and $FeCl_2^+$ ions apart from free Fe^{3+} ions, which may be directly related to the oxidising affinity of the ferric complex. The molarity of free ferric ions is greater than ferric complexes in acidic solutions and sulphate is the only observable sulphur-oxygen complex under acidic ferric ion oxidation (Singer and Stumm, 1967; Baes, 1976; Mathews and Robins, 1972; Wiersma and Rimstidt, 1984; McKibben and Barnes, 1986). These observations verify the reaction stoichiometry proposed by Garrels and Thompson (1960), in which the dissolution of 1 mole of pyrite requires the reduction of 14 moles of ferric ion with an additional mole of iron released in solution with sulphate as the only sulphur product in solution (Eq. 2.2).

The relationship of the rate of pyrite oxidation by ferric ion with the ferric/ferrous ion ratio shows that the rate is strongly influenced by the solution redox potential thus indicating an electrochemical mechanism for the reaction (Williamson and Rimstidt, 1994).

Influence of the Ferric-to-Ferrous Ion Ratio

In many instances, the chemical leaching rate of pyrite is found to be a function of the ferric/ferrous ion ratio (Garrels and Thompson, 1960; Mathews and Robins, 1972; Tal, 1986; Zheng *et al.*, 1986; Kawakami *et al.*, 1988; Williamson and Rimstidt, 1994) with an experimentally determined reaction order close to 0.5 (Crundwell, 2001; Petersen and Dixon, 2006; Tal, 1986; Zheng *et al.*, 1986; McKibben and Barnes, 1986). These models are consistent with the hypothesis that the acid-ferric leaching of pyrite occurs *via.* an electrochemical model (May *et al.*, 1997; Breed and Hansford, 1999b; Holmes and Crundwell, 2000).

Table 2.1: Acid-Ferric Leaching Kinetics

Reference	E_a $[kJ.mol^{-1}]$	Rate Constant	Rate Expression	Eq. No.
Garrels and Thompson (1960)	–	3.5×10^{-5} – 8.3×10^{-5} (interpolated)	$r_{FeS_2} = k\frac{C_{Fe3+}}{C_{Fe2+} + C_{Fe3+}}$	T 1.1
Mathews and Robins (1972)	92	1.47×10^{8} mol.dm^{-3}.min^{-1}	$r_{FeS_2} = kexp\left(\frac{-E_a}{RT}\right)\frac{MA}{V}\frac{C_{Fe3+}}{C_{Fe^{tot}}C_{H+}^{0.44}}$	T 1.2
King and Perlmutter (1977)	20 (0.1M) 53 (1.0M)	0.1 M Fe^{3+}, 40^oC: κ=3.1×10^{-6} mol.dm^{-3}.s^{-1}, K=12 dm^3.mol^{-1} 0.1 M Fe^{3+}, 60^oC: κ=6.4×10^{-6} mol.dm^{-3}.s^{-1}, K=3.45 dm^3.mol^{-1} 1.0 M Fe^{3+}, 60^oC: κ=2.0×10^{-4} mol.dm^{-3}.s^{-1}, K=29 dm^3.mol^{-1}	$r_{FeS_2} = \kappa\left(\frac{C_{FeS_2}}{C_{FeS_2,o}}\right)^{\frac{2}{3}}\frac{C_{Fe3+}}{\left(C_{Fe3+} + KC_{Fe2+}\right)^2}$	T 1.3
Wiersma and Rimstidt (1984)	92	1.5×10^{-6} to 7.0×10^{-6} s^{-1}	$r_{FeS_2} = k\frac{A}{M}C_{Fe3+}$ where $\frac{A}{M}$ – 1 m^2.g^{-1}	T 1.4
McKibben and Barnes (1986)	60.3	$10^{-9.74}$ mol.cm^{-2}.min^{-1}	$r_{FeS_2} = k\frac{C_{Fe3+}^{0.5}}{C_{H+}^{0.5}}$	T 1.5
Tal (1986)	–	6.42 mg pyrite.g^{-1}.h^{-1}	$r_{FeS_2} = k\frac{C_{Fe3+}}{C_{Fe2+}}^{0.682}$	T 1.6
Zheng *et al.* (1986)	–	k_1 = 6.10 μmol.kg^{-1}.s^{-1} k_2 = 2.03 μmol.kg^{-1}.s^{-1} k_3 = 3.84 μmol.kg^{-1}.s^{-1} k_4 = 91.1 μmol.kg^{-1}.s^{-1}	$r_{FeS_2} = \frac{k_1 - k_2\left(\frac{C_{Fe2+}}{C_{Fe3+}}\right)^{0.5}}{\frac{1}{C_{Fe3+}^{0.5}} + k_3 + k_4\left(\frac{C_{Fe2+}}{C_{Fe3+}}\right)^{0.5}}$	T 1.7

Continued on next page

Table 2.1 – continued from previous page

Reference	E_a [kJ.mol^{-1}]	Rate Constant	Rate Expression	Eq. No.
Kawakami *et al.* (1988)	95	$k_R = 0.056$ min^{-1} $k_L = 0.33$ mol^2.m^{-5}.min^{-1} $K_R = 19.5$ $K_L = 5.6$	$r_{FeS_2} = (15 - 13\alpha)\frac{6\omega}{\rho d}\left(k_R[R]\frac{C_{Fe^{3+}}}{C_{Fe^{3+}} + K_R C_{Fe^{2+}}} + k_L \frac{C_{Fe^{3+}}}{\left(C_{Fe^{3+}} + K_L C_{Fe^{2+}}\right)^2}\right)$ α – molar fraction of pyrite forming sulphur ω – pyrite concentration, kg.m^{-3}	T 1.8
Boogerd *et al.* (1991)	125 $(30 - 45^oC)$ 50 $(45 - 70^oC)$	k = 64±6 mM.day^{-1} (70^oC) k = 16.6±1.5 mM.day^{-1} (45^oC) k = 1.59±0.18 mM.day^{-1} (30^oC)	$r_{FeS_2} = k \cdot \frac{C_{FeS_2}}{30 + C_{FeS_2}} \cdot \frac{C_{Fe^{3+}}}{95 + C_{Fe^{3+}}}$	T 1.9
Rimstidt and Newcom (1993)	–	3.0 (±2.0)×10^{-5} mol.m^{-2}.s^{-1}	$r_{FeS_2} = kC_{Fe^{3+}}^{0.62\pm0.10}$	T 1.10
Williamson and Rimstidt (1994)	50 – 80	k = 10$^{-8.58}$ mol.m^{-2}.s^{-1}	N_2 purged $r_{FeS_2} = k\frac{C_{Fe^{3+}}^{0.3}}{C_{Fe^{2+}}^{0.47} C_{H^+}^{0.32}}$	T 1.11
		k = 10$^{-6.07}$ mol.m^{-2}.s^{-1}	O_2 present $r_{FeS_2} = k\frac{C_{Fe^{3+}}^{0.93}}{C_{Fe^{2+}}^{0.4}}$	T 1.12
Holmes and Crundwell (2000)	45 – 79.9		$r_{FeS_2} = k[H+]^{-0.5}\left(\frac{k_{Fe^{3+}} C_{Fe^{3+}}}{k_{FeS_2} C_{H^+}^{-0.5} + k_{Fe^{2+}} C_{Fe^{2+}}}\right)^{0.5}$	T 1.13
Salmon and Malmström (2006)	FeS_2 : 56.9 ZnS : 21 $CuFeS_2$: 20	$r_{FeS_2} = (2.54\pm0.39)\times10^{-11}$ mol.m^{-2}.s^1 $r_{ZnS} = (6.52\pm2.57)\times10^{-10}$ mol.m^{-2}.s^1 $r_{CuFeS_2} = (4.05\pm1.65)\times10^{-10}$ mol.m^{-2}.s^1	$r_i - \frac{R_j}{A_i \eta_{I,j}}$	T 1.14

Holmes and Crundwell (2000) confirmed that the dissolution of mineral sulphides, in particular pyrite, are characterised by an oxidation-reduction type mechanism, which involves the oxidation of pyrite and the reduction of ferric ions and oxygen at the pyrite surface. Supporting an electrochemical mechanism, the half order reactions for the oxidation of pyrite (Eq. 2.4) and reduction of ferric ions (Eq. 2.5) and oxygen (Eq. 2.6) were studied (Holmes and Crundwell, 2000).

$$FeS_2 + 8H_2O \rightarrow Fe^{2+} + 2SO_4^{2-} + 16H^+ + 14e^- \quad [2.4]$$

$$Fe^{3+} + e^- \rightleftharpoons Fe^{2+} \quad [2.5]$$

$$O_2 + 4H^+ + 4e^- \rightarrow 2H_2O \quad [2.6]$$

With the condition that the net production of electrons is zero, the half reactions were studied independently and rate expressions for each of the half reactions was derived to obtain an overall rate expression for the chemical leaching of pyrite. Using an electrochemical approach, the anodic oxidation of pyrite (Eq. 2.4) and the oxidation/reduction of ferrous and ferric ions on pyrite (Eq. 2.5) was found to be chemical reaction controlling due to the high activation energies observed (Holmes and Crundwell, 2000). The anodic oxidation of pyrite in Eq. 2.4 was found to be negative half order with respect to the proton ions, approximately first order in ferric and ferrous ions for the oxidation/reduction of ferrous and ferric ions on pyrite (Eq. 2.5) and near first order for the reduction of dissolved of dissolved oxygen on pyrite (Eq. 2.6).

Noting that the net production of electrons is zero and the rate and current density are related by stoichiometry, Holmes and Crundwell (2000) developed a rate expression for the dissolution of pyrite that is half order in ferric ions and either zero order if the production rate of protons $k_{FeS_2}C_{H^+}^{-0.5}$ in Eq. 2.4 is greater that the rate of oxidation of ferrous ions $k_{Fe^{2+}}C_{Fe^{2+}}$ in Eq. 2.5, or negative half order in ferrous ions if $k_{FeS_2}C_{H^+}^{-0.5} \ll k_{Fe^{2+}}C_{Fe^{2+}}$. When $k_{FeS_2}C_{H^+}^{-0.5} \ll k_{Fe^{2+}}C_{Fe^{2+}}$, the reaction orders obtained from the rate expression developed by Holmes and Crundwell (2000) were similar to those obtained by McKibben and Barnes (1986).

Influence of pH

It has been shown that, in acidic solutions, ferric ions are a more effective oxidising agent than gaseous oxygen making ferric ions the preferred oxidant in both anaerobic and aerobic systems (Dutrizac and MacDonald, 1974; McKibben and Barnes, 1986; Moses *et al.*, 1987; May *et al.*, 1997). In acidic environments, the rate of ferrous ion oxidation to ferric ion by molecular oxygen is negligible compared to the ferric ion reduction by pyrite (Wiersma and Rimstidt, 1984). In both instances, where either ferric ions or oxygen is the oxidant, the acid producing reactions form ferrous ions and sulphur as SO_4^{2-} (Eqs. 2.2 and 2.7). In the presence of oxygen, the ferrous ions are converted back to ferric ions by Eq. 1.2, thus

regenerating the oxidant for the reaction in Eq. 2.2.

$$2FeS_2 + 2H_2O + 7O_2 \quad \rightarrow \quad 2Fe^{2+} + 4SO_4^{2-} + 4H^+ \qquad [2.7]$$

At high pH, the oxidation activity of ferric ion decreases due the decreased solubility of the ion at high pH (Moses *et al.*, 1987). The rate of chemical leaching decreases with decreasing ferric/ferrous ion ratio with product inhibition observed with increasing ferrous ion concentration, indicating that the rate is a function of the oxidation potential (Holmes and Crundwell, 2000; Kawakami *et al.*, 1988; Wiersma and Rimstidt, 1984; Singer and Stumm, 1967; Garrels and Thompson, 1960). At low pH levels, ferric ions are the dominant oxidiser of pyrite while dissolved oxygen has little to no effect on the oxidation rate. Williamson and Rimstidt (1994) showed that the pyrite oxidation rate by ferric ion is enhanced by dissolved oxygen at high ferric-ferrous ion ratios, while at low ratios, faster rates are observed in the absence of dissolved oxygen. The differences in the rate laws, with respect to ferric ion, in the presence (see Eq. T1.11 in Table 2.1) and absence of oxygen (Eq. T1.12 in Table 2.1) indicated a change in the reaction mechanism (Williamson and Rimstidt, 1994).

Moses *et al.* (1987) studied the oxidation of mineral sulphides in the presence of ferric iron and molecular dissolved oxygen in the pH range $2 - 9$ and used sulphur as a reaction variable to determine the extent of sulphide mineral oxidation. The objective of the study was to clearly understand which of the two were the dominant oxidative reactants. Of particular interest was the role of ferric iron at circumneutral pH, due to its low activity and solubility at these levels, and to determine whether oxygen is the dominant oxidant of pyrite at these levels. The authors found that ferric iron is the preferred oxidiser of pyrite over dissolved oxygen in the pH range $2 - 9$, and the main oxidant at low pH rather than Fe^{2+} or Fe^{3+}/Fe^{2+} ratio. However, the authors found that the difference in the oxidising potential between ferric iron and dissolved oxygen decreased with increasing pH. This was attributed to the decreased solubility of ferric iron at high pH. Therefore, the oxidation activity at high pH is directly dependent on the conversion of ferrous ion to ferric ion by dissolved oxygen (Moses *et al.*, 1987).

Influence of Sulphur Compounds

The acid-ferric leaching rate decreases with increasing sulphate concentration (Zheng *et al.*, 1986). Among the most abundant ferric ion species are $FeSO_4^+$, $Fe(SO_4)_2^-$ and free Fe^{3+} ions (Zheng *et al.*, 1986). In the BIOX^{TM} process, up to 20 % sulphide content is produced in a plant designed to treat 100 tons per day of a refractory gold concentrate (van Aswegen *et al.*, 2007). With increasing sulphate concentration, the concentration of free ferric ions decreases. The sulphur produced during reaction is frequently observed in the sulphate form (Garrels and Thompson, 1960; Mathews and Robins, 1972; McKibben and Barnes, 1986; Zheng *et al.*, 1986) while some authors have noted sulphur deposits in their experiments

resulting from Eq. 2.8 (Kawakami *et al.*, 1988; King and Perlmutter, 1977).

$$FeS_2 + 2Fe^{3+} \rightarrow 3Fe^{2+} + 2S^0 \quad [2.8]$$

In most cases, sulphur compounds resulting from sulphur-oxygen attachment are attributed to oxygen from water rather than molecular oxygen (Garrels and Thompson, 1960; Mathews and Robins, 1972; McKibben and Barnes, 1986; Zheng *et al.*, 1986; Moses *et al.*, 1987). To verify the reaction stochiometry between Eq. 2.2 and the reaction in which elemental sulphur is produced (Eq. 2.8), Boogerd *et al.* (1991) plotted experimental data against theoretical calculations based on the reaction stoichiometry of Eqs. 2.2 and 2.8. The result showed that a better fit was achieved using Eq. 2.2 at high temperatures and low temperatures. This suggested that pyrite oxidation occurs *via.* Eq. 2.2 which indicated that elemental sulphur is not the major sulphur product in bioleaching.

Influence of Specific Surface Area

Many authors have observed that the ratio of contact mineral surface area to solution volume greatly affects the apparent reaction rate (McKibben and Barnes, 1986; Petrovich, 1981; May *et al.*, 1997; Holdren, 1981; Wiersma and Rimstidt, 1984; Kawakami *et al.*, 1988) and have suggested that the morphology of the mineral surface, which may describe features such as sharp edged surfaces, pits and fractures, can alter the extrinsic rate. McKibben and Barnes (1986) proposed that mineral surface texture could significantly influence the reactive surface area and thus differ from the total mineral surface area. The chemical leaching rate is a function of the available pyrite surface area upon which the ferric ions adsorb (Garrels and Thompson, 1960). Incorporating surface area values into the rate constant calculations are important since the amount of exposed specific surface area to unit mass of solution greatly affects the rate (Wiersma and Rimstidt, 1984). The specific surface area and hence the rate of the reaction are influenced by the type of sulphide mineral under observation (Wiersma and Rimstidt, 1984). Wiersma and Rimstidt (1984) found that samples with larger specific surface area reacted more rapidly than samples with lower surface areas. Holdren (1981); Petrovich (1981); Wiersma and Rimstidt (1984); McKibben and Barnes (1986) and Moses *et al.* (1987) found that mineral surface textures could significantly contribute to the understanding of reactive surface area and total mineral surface area. If an area based rate is considered, the reactor model must predict the available reaction surface area at each time instant.

2.2.2 Microbial Oxidation Kinetics

Microbial oxidation kinetics are often represented by empirical, or Monod/Michaelis-Menton type kinetics (Dempers *et al.*, 2003; Özkaya *et al.*, 2006; Nurmi *et al.*, 2009). In the past, a first order rate expression in the form of Eq. 2.9 was used to describe microbial growth (La

Motta, 1976). However, Eq. 2.9 only represented the exponential growth phase.

$$r_g = \mu C_X \quad [2.9]$$

where r_g [kg.m^{-3}.s^{-1}] is the growth rate of suspension, μ [s^{-1}] the specific growth rate and C_X [kg.m^{-3}] is the microbial concentration.

To overcome the restrictions of Eq. 2.9, La Motta (1976) developed a generic equation that can describe both the growth and stationary phases of a microbial system, commonly known as the logistic equation (Eq. 2.10). The limitation of the logistic equation is that it cannot be used to predict microbial effects over a wide range of conditions, namely, temperature and pH (Breed, 2000).

$$r_g = nC_X \left(1 - \frac{C_X}{C_{X,max}}\right) \quad [2.10]$$

In contrast to the logistic equation, Monod (Monod, 1949) or Michaelis-Menten (Michaelis and Menten, 1913; Johnson and Goody, 2011) type kinetics can be used to incorporate changes in conditions as well as any inhibitory effects resulting from reaction. The Monod equation directly related the specific growth rate to concentration of the limiting nutrient or substrate in the aqueous phase (Eq. 2.11, Monod, 1949; Searby, 2006). The empirical model was based on a succession of phases in which the variation in growth was defined by a lag phase where no growth is observable, an acceleration phase where the growth rate increases, an exponential phase in which the growth rate is constant followed by a decrease in the growth rate called the retardation phase, a stationary phase where no growth was observed followed by a region of negative growth (Monod, 1949).

$$\mu = \frac{\mu_{max} C_S}{K_m + C_S} \quad [2.11]$$

where μ_{max} [s^{-1}] is the theoretical maximum specific growth rate, C_S the limiting substate concentration for growth and K_m is the saturation constant.

The Michaelis-Menten mechanism assumes that the substrate S attaches to the microbial cell or enzyme E to form a complex ES which then reacts to form product P releasing the active enzyme E (Eq. 2.12, Michaelis and Menten, 1913; Johnson and Goody, 2011)

$$E + S \rightleftharpoons ES \rightarrow E + P \quad [2.12]$$

The Michaelis-Menten equation assumes that the adsorption of the enzyme and desorption of the substrate are in equilibrium and the rate of formation of the enzyme-substrate complex is zero (Michaelis and Menten, 1913; Johnson and Goody, 2011). The model further assumes that the concentration of the substrate exceeds that of the enzyme to give the rate of product formation ν as given in Eq. 2.13 (Michaelis and Menten, 1913; Johnson and Goody, 2011).

$$\nu = \frac{V_{max} C_S}{K_m + C_S} \quad [2.13]$$

where V_{max} is the maximum rate, C_S the concentration of the substrate and K_m is the Michaelis constant, which is substrate concentration at which the rate is half the maximum V_{max}.

Unlike the Monod or logistic equation, Michaelis-Menten type kinetics can incorporate product inhibition into the rate expression. In bioleaching, the Michaelis-Menten mechanism follows the reaction path of the iron species in the microbial oxidation reaction. By defining a yield factor, the iron reaction path can be related to the growth kinetics and hence the specific iron utilisation rate $q_{Fe^{2+}}$, which can be represented by a Michaelis-Menten rate expression (Searby, 2006; Boon, 1996). Many authors (see Table 2.2) utilising the Michaelis-Menten model have observed and thus included inhibitory effects resulting from ferric ion inhibition (Kelly and Jones, 1978; Jones and Kelly, 1983; Liu *et al.*, 1988; Nikolov and Karamanev, 1992; Huberts, 1994; Crundwell, 1997; Hansford, 1997; Nemati and Webb, 1998; Breed *et al.*, 1999; Boon *et al.*, 1999a; Kawabe *et al.*, 2003), ferrous iron inhibition (Nemati and Webb, 1997) or a combination of ferric and ferrous ion inhbition (Nikolov and Karamanev, 1992). Few authors have modelled the influence of substrates ferrous ion, oxygen and pH in the microbial kinetics (Crundwell, 1997; Pesic and Olivier, 1989; Ojumu *et al.*, 2006).

The Influence of pH

The kinetics of microbial ferrous ion oxidation has been studied in the pH range from $1.5 - 6.0$ with optimum microbial growth rates observed betweeen 2.0 and 2.5 for *Acidithiobacillus ferrooxidans* and *ca.* pH = 1.7 for *Leptospirillum ferrooxidans* although microbial activity of *Leptospirillum ferrooxidans* at pH levels below one have been observed (Nurmi *et al.*, 2009; Özkaya *et al.*, 2006; Norris and Johnson, 1998; Nemati *et al.*, 1998). Beyond *ca.* pH $= 2.5 - 3.5$, ferrous ion oxidation decreases (Meruane and Vargas, 2003; Pesic and Olivier, 1989; MacDonald and Clark, 1970). Breed and Hansford (1999a) found that there was no clear relationship between the maximum specific Fe^{2+} and O_2 utilisation rates with pH while the affinity kinetic constants $K_{Fe^{2+}}$ and K_{O_2} linearly increased with increasing pH. The pH relationship with the affinity kinetic constant was incorporated into the kinetic rate expressions by means of a linear function (see Table 2.2). The solubility of ferric ions decreases with increasing pH thus forming complex iron precipitates which hinder the transport of protons to the microbial cells (Meruane and Vargas, 2003; Nemati *et al.*, 1998). However, it has been reported that microbial growth is not adversely affected by pH within a small margin of the optimum (Ojumu, 2008; Pesic and Olivier, 1989; Breed and Hansford, 1999a).

Table 2.2: Microbial Oxidation Rate Expressions - Modified from Searby (2006)

Reference	Rate Expression	Microogansim & Constants
Lacey and Lawson (1970)	$\mu = \frac{\mu_{max}[Fe^{2+}]}{Y_{SX}K_m + [Fe^{2+}]}$	*At. ferrooxidans* Batch STR $\mu_{max} = 0.15 - 0.25$ h^{-1} $K_m = 19.7 - 18.1$ mM
MacDonald and Clark (1970)	$\mu = \frac{\mu_{max}[Fe^{2+}]}{K_m + [Fe^{2+}]}$	*At. ferrooxidans* Continuous $\mu_{max} = 0.161$ h^{-1} $K_S = 3.85$ mM $Y_{XS} = 0.0168$ mol carbon.(mol Fe^{2+})$^{-1}$
Guay *et al.* (1977)	$D = \frac{K}{1 - \frac{V_{max}}{V}}$	*At. ferrooxidans* Continuous $V_{max} = 46.51 - 52.08$ mM Fe^{2+}.h^{-1} $K = 0.526 - 0.283$ h^{-1}
Kelly and Jones (1978)	$\mu = \frac{\mu_{max}[Fe^{2+}]}{K_S\left(1 + \frac{[Fe^{3+}]}{K_p}\right) + [Fe^{2+}]\left(1 + \frac{[Fe^{3+}]}{K_c}\right)}$	Monod, batch
Kelly and Jones (1978)	$\mu = \frac{\mu_{max}[S]}{K_S + [S]}$	*At. ferrooxidans* Batch $\mu_{max} = 0.143$ h^{-1} $K_S = 36$ mM Fe^{2+} $Y_{XS} = 0.014$ mol carbon.(mol Fe^{2+})$^{-1}$
Kelly and Jones (1978)	$q_{O_2} = \frac{q_{O_2}^{max}[Fe^{2+}]}{[Fe^{2+}] + K_m\left(1 + \frac{[Fe^{3+}]}{K_I}\right) + [Fe^{2+}]\left(1 + \frac{[Fe^{3+}]}{K_c}\right)}$	*At. ferrooxidans* Batch $K_m = 1.0$ mM Fe^{2+} $K_I = 2.5 - 28$ mM Fe^{3+}

Continued on next page

Table 2.2 – continued from previous page

Reference	Rate Expression	Microogansim & Constants
Jones and Kelly (1983)	$\mu = \frac{\mu_{max}}{1 + \frac{K_S}{[Fe^{2+}]} + \frac{K_S}{K_I}\frac{[Fe^{3+}]}{[Fe^{2+}]}}$	*At. ferrooxidans* Continuous $\mu_{max} = 1.25$ h^{-1} $K_S = 0.8 - 0.9$ mM Fe^{2+} $K_p = 1.0 - 2.0$ mM Fe^{3+} $Y_{XS} = 0.0148$ mol carbon.(mol Fe^{2+})$^{-1}$
Jones and Kelly (1983)	$\mu = \frac{\mu_{max}}{\left(1 + \frac{[Fe^{3+}]}{K_p}\right)\left(\frac{K_S}{[Fe^{2+}]} + 1\right)}$	*At. ferrooxidans* Continuous $\mu_{max} = 1.33$ h^{-1} $K_S = 2.4$ mM Fe^{2+} $K_p = 2.5$ mM Fe^{3+} $Y_{XS} = 0.0141 - 0.054$ mol carbon.(mol Fe^{2+})$^{-1}$
Jones and Kelly (1983)	$\mu = \frac{\mu_{max}}{\frac{K_S}{[Fe^{2+}]}\left(1 + \frac{[Fe^{3+}]}{K_p}\right)\left(\frac{[Fe^{3+}]}{K_c} + 1\right)}$	*At. ferrooxidans* Continuous $\mu_{max} = 1.25$ h^{-1} $K_S = 0.8 - 0.9$ mM Fe^{2+} $K_p = 1.2$ mM Fe^{3+} $Y_{XS} = 0.0148$ mol carbon.(mol Fe^{2+})$^{-1}$
Braddock *et al.* (1984)	$\mu = \frac{\mu_{max}([Fe^{2+}] - [Fe^{2+}]_t)}{K_m + ([Fe^{2+}] - [Fe^{2+}]_t)}$	*At. ferrooxidans* Continuous $\mu_{max} = 0.07$ h^{-1} $K_m = 0.78$ mM $[Fe^{2+}]_t = 0.25$ mM $Y_{XS} = 0.010 - 0.017$ mol carbon.(mol Fe^{2+})$^{-1}$
Smith *et al.* (1988)	$\mu = \frac{Y_{XS}kS}{K_S + S} - b$	*At. ferrooxidans* Continuous $K_S = 3.403$ mM Fe^{2+} $k = 19.7$ mol Fe^{2+}.(mol carbon.h)$^{-1}$ $Y_{XS} = 0.074$ mol carbon.(mol Fe^{2+})$^{-1}$

Continued on next page

Table 2.2 – continued from previous page

Reference	Rate Expression	Microogansim & Constants
Liu *et al.* (1988)	$\mu = \frac{\mu_{max}[Fe^{2+}]}{[Fe^{2+}] + K_S(1 + K_I[Fe^{3+}])}$	*At. ferrooxidans* Continuous $\mu_{max} = 0.12$ h^{-1} $K_S = 1.594$ mM Fe^{2+} $K_I = 0.024$ (mM Fe^{3+})$^{-1}$ $Y_{XS} = 0.0104$ mol carbon.(mol Fe^{2+})$^{-1}$
Norris *et al.* (1988)	$\mu = \frac{\mu_{max}}{1 + \frac{K_m}{[Fe^{2+}]} + \frac{K_m}{K_I}\frac{[Fe^{3+}]}{[Fe^{2+}]}}$	*At. ferrooxidans* Batch $K_S = 1.34$ mM Fe^{2+} $K_I = 3.10$ (mM Fe^{3+})$^{-1}$
Lizama and Suzuki (1989a)	spontaneous $-r_{O_2} = k[FeS_2]$ indirect leaching $-r_{O_2} = \frac{k_3[Fe^{3+}][FeS_2]}{K_m + [FeS_2]}$ *At. f* washed FeS_2 $-r_{O_2} = \frac{k[cell][FeS_2]}{K_m + [FeS_2]}$ *At. f* unwashed FeS_2 $-r_{O_2} = \frac{k[cell][FeS_2]}{K_m(1 + \frac{[cell]}{K_I}) + [FeS_2]}$ *At. f* Fe^{2+} oxidation $-r_{O_2} = \frac{k'_3[cell][Fe^{2+}]}{K_m(1 + \frac{[cell]}{K'_I}) + [Fe^{2+}]}$	Michaelis-Menten, batch (assumed)
Lizama and Suzuki (1989b)	$-r_{O_2} = \frac{k'_3[X][Fe^{2+}]}{[Fe^{2+}] + K_m(1 + \frac{[X]}{K'_I})}$	*At. ferrooxidans* Batch $k'_3 = 0.924 - 1.0567$ mol O_2.(mol carbon.h)$^{-1}$ $K_m = 0.11 - 0.30$ mM Fe^{2+} $K'_I = 1.3 - 5.0$ mM carbon
Pesic and Olivier (1989)	$-\frac{d[Fe^{2+}]}{dt} = 1.62 \times 10^{11}[X][H^+][Fe^{2+}]p_{O_2}e^{-(\frac{58.77}{RT})}$	Nernst, batch electrochemical cell

Continued on next page

Table 2.2 – continued from previous page

Reference	Rate Expression	Microogansim & Constants
Shrihari and Gandhi. (1990)	$\mu = \frac{\mu_{max_0} exp[-K(pH - pH_o)^2] \cdot [Fe^{2+}]}{K_S + [Fe^{2+}]}$	*At. ferrooxidans* Batch $\mu_{max_0} = 0.183$ h^{-1} $K_S = 96.24$ mM Fe^{2+} $K = 3.349$ $Y_{XS} = 0.018$ mol carbon.(mol Fe^{2+})$^{-1}$
Nikolov and Karamanev (1992)	$\mu = \frac{\mu_{max}[Fe^{2+}]}{[Fe^{2+}] + K_S + \frac{K_S}{K_I}[Fe^{3+}] + \frac{([Fe^{2+}])^2}{K_{SI}}}$	*At. ferrooxidans* Continuous $\mu_{max} = 0.227$ h^{-1} $K_S/K_I = 0.939$ $K_{SI} = 210$ mM Fe^{2+} $Y_{XS} = 0.07$ mol carbon.(mol Fe^{2+})$^{-1}$
Miller and Hansford (1992)	$k' = \frac{k'_o e^{(\mu t)}}{1 - \frac{k'_o}{k}[1 - e^{(\mu t)}]}$	Modified Logistic, batch
Nagpal *et al.* (1994)	$r_{Fe_{2+}} = V_1 \cdot \frac{[Fe^{2+}]}{[Fe^{2+}] + K_1\left[1 + \left(\frac{[As(V)]}{K_{I1}}\right)^2\right]} \cdot [cell]$	Monod, stirred batch
Huberts (1994)	$r_{Fe_{2+}} = a_1 \cdot \left(\frac{p_{O_2}}{k_b + p_{O_2}}\right)\left(\frac{[Fe^{2+}]}{[Fe^{2+}] + K_{Fe^{2+}}\left(1 + \frac{[Fe^{3+}]}{K'}\right)}\right)$	*L. ferrooxidans* Continuous $a_1 = 10.29$ mol Fe^{2+}.(mol carbon.h)$^{-1}$ $k_b = 0.22$ atm $K_{Fe^{2+}} = 0.021$ mM Fe^{2+} $K' = 10.2$ mM Fe^{3+}
Nyavor *et al.* (1996)	$V = \frac{\beta k_3 [X][S]}{K_m + \left(1 + \frac{[I]}{K'_I}\right) + [S]}$	*At. ferrooxidans* Batch $K_m = 0.67$ mM $K_I = 6.25$ mM

Continued on next page

Table 2.2 – continued from previous page

Reference	Rate Expression	Microogansim & Constants
Gomez *et al.* (1996)	$\mu_c = \frac{\mu_{max}[Fe^{2+}]}{[Fe^{2+}] + K_S(1 + K_I[Fe^{3+}])}$	*At. ferrooxidans* Batch $\mu_{max} = 0.14$ h^{-1} $K_S = 16.83$ mM Fe^{2+} $K_I = 2.98$
Nemati and Webb (1997)	$\frac{d[Fe^{2+}]}{dt} = \frac{K_0 e^{\frac{68.4}{RT}}[X][Fe^{2+}]}{K'_m(1 + \frac{[X]}{K'_I}) + [Fe^{2+}] + (1 - \frac{[X]}{\beta})\frac{[Fe^{2+}]}{\alpha}}$	*At. ferrooxidans* Batch $K_0 = 8.6 \times 10^{12}$ mol Fe^{2+}.(mol carbon.h)$^{-1}$ $K'_m = 1.2$ mM Fe^{2+} $K'_I = 0.171$ mM carbon $\beta = 5.98$ mM carbon $\alpha = 0.466$ mM Fe^{2+}
Crundwell (1997)	$\mu = k\left(\frac{\frac{[Fe^{2+}]}{[H^+]}}{K_{Fe} + \frac{[Fe^{2+}]}{[H^+]} + K_I[Fe^{3+}]}\right)^{0.5} \times \left(\frac{[O_2]}{K_{O_2} + [O_2]}\right)^{0.5} - m$	Monod, theoretical-chemostat (Electrochemical)
Hansford (1997)	$q_{Fe^{2+}} = \frac{q^{max}_{Fe^{2+}}}{1 + K_{Fe^{2+}}\frac{[Fe^{3+}]}{[Fe^{2+}]}}$	*L. ferrooxidans* Continuous $q^{max}_{Fe^{2+}} = 8.65 - 13.58$ mol Fe^{2+}.(mol carbon.h)$^{-1}$ $K_{Fe^{2+}} = 0.0018 - 0.0033$
Harvey and Crundwell (1997)	$\mu = \frac{\mu_{max}[Fe^{2+}]}{[Fe^{2+}] + K_S(1 + K_I[Fe^{3+}])}$	*At. ferrooxidans* Electrochemical Cell $\mu_{max} = 0.16$ h^{-1} $K_S = 1.31$ mM Fe^{2+} $K_I = 0.072$ mM $(Fe^{3+})^{-1}$ $Y_{XS} = 5.37 \times 10^{-4}$ mol carbon.(mol Fe^{2+})$^{-1}$
Nemati and Webb (1998)	$\frac{d[Fe^{2+}]}{dt} = \frac{K_0 e^{\frac{68.4}{RT}}[X][Fe^{2+}]}{\left(1 + \frac{[Fe^{3+}]}{K_I}\right)(K_m + [Fe^{2+}])}$	*At. ferrooxidans* Batch $K_0 = 8.6 \times 10^{12}$ mol Fe^{2+}.(mol carbon.h)$^{-1}$ $K_m = 4.62$ mM Fe^{2+} $K_I = 36.89$ mM Fe^{3+}

Continued on next page

Table 2.2 – continued from previous page

Reference	Rate Expression	Microogansim & Constants
van Scherpenzeel *et al.* (1998)	$-r_{O_2} = \frac{C_X q_{O_2}^{max}}{1 + K_{O_2} \frac{[Fe^{3+}]}{[Fe^{2+}]}}$	*L. ferrooxidans* Batch $q_{O_2}^{max} = 1.8 - 2.4$ mol O_2.(mol carbon.h)$^{-1}$ $K_{O_2} = 7.0 \times 10^{-4}$
Breed *et al.* (1999)	$q_{Fe^{2+}} = \frac{1.204 \times 10^7 e^{-\frac{35.63}{RT}}}{1 + (0.0002T - 0.0453) \frac{[Fe^{3+}]}{[Fe^{2+}]}}$	*L. ferrooxidans* Continuous $Y_{XS}^{max} = 0.0059$ mol carbon.(mol Fe^{2+})$^{-1}$
Breed and Hansford (1999a)	$q_{Fe^{2+}} = \frac{15.53}{1 + (0.0048pH - 0.0043) \frac{[Fe^{3+}]}{[Fe^{2+}]}}$	*L. ferrooxidans* Continuous $Y_{XS}^{max} = 0.0074$ mol carbon.(mol Fe^{2+})$^{-1}$
Breed *et al.* (1999)	$q_{Fe^{2+}} = \frac{q_{Fe^{2+}}^{max}}{1 + K_{Fe^{2+}} \frac{[Fe^{3+}]}{[Fe^{2+}]}}$	*L. ferrooxidans* Continuous $q_{Fe^{2+}}^{max} = 8.65 - 13.58$ mol Fe^{2+}.(mol carbon.h)$^{-1}$ $K_{Fe^{2+}} = 0.0018 - 0.0033$
Boon *et al.* (1999a)	$q_{O_2} = \frac{q_{O_2}^{max}}{1 + \frac{K_S}{K_I} \cdot \frac{[Fe^{3+}]}{[Fe^{2+}] - [Fe^{2+}]_t}}$	*At. ferrooxidans* Continuous $q_{O_2}^{max} = 1.9$ mol O_2.(mol carbon.h)$^{-1}$ $K_S/K_I = 0.04$ $[Fe^{2+}]^t$=0.5 mM $Y_{XS}^{max} = 0.0012$ mol carbon.(mol Fe^{2+})$^{-1}$
Boon *et al.* (1999b)	$q_{O_2} = \frac{q_{O_2}^{max}}{1 + \frac{K_S}{[Fe^{2+}] - [Fe^{2+}]_t} + \frac{K_S}{K_I} \cdot \frac{[Fe^{3+}]}{[Fe^{2+}] - [Fe^{2+}]_t}}$	Continuous

Continued on next page

Table 2.2 – continued from previous page

Reference	Rate Expression	Microogansim & Constants
Boon *et al.* (1999c)	$\mu = \frac{\mu_{max} + m_0 Y_{OX}^{max}}{1 + \frac{K_S}{[Fe^{2+}]-[Fe^{2+}]_t} + \frac{K_S}{K_I}\frac{[Fe^{3+}]}{[Fe^{2+}]-[Fe^{2+}]_t}} - m_0 Y_{OX}^{max}$	*At. ferrooxidans* Batch $\mu_{max} = 0.060 - 0.105$ h^{-1} $K_S = 0.2$ mM $K_S/K_I = 0.06 - 0.10$ $Y_{OX}^{max} = 0.012$ mol carbon.(mol O_2)$^{-1}$ $m_0 = 0.96$ mol Fe^{2+}.(mol carbon.h)$^{-1}$
Meruane *et al.* (2002)	$q_{Fe^{2+}} = \frac{K_1^* exp[\frac{nF}{2RT}(E^m - E_h^o)]\left(1 - exp[\frac{-nF}{RT}(E^m - E_h)]\right)}{1 + \frac{K_2^*}{[Fe^{2+}]} + K_3^* exp[\frac{nF}{RT}(E_h - E_h^o)]}$	*At. ferrooxidans* Electrochemical Cell $K_1^* = 0.447$ mol Fe^{2+}.(mol carbon.h)$^{-1}$ $K_2^* = 1.31$ mM Fe^{2+} $K_3^* = 0.641$ $E^m = 0.639$ V (SHE)
Meruane *et al.* (2002)	$q_{Fe^{2+}} = \frac{q_{max} - K_2\frac{[Fe^{3+}]}{[Fe^{2+}]}}{1 + \frac{K_S}{[Fe^{2+}]} + K_I\frac{[Fe^{3+}]}{[Fe^{2+}]}}$	*At. ferrooxidans* Electrochemical Cell $q_{max} = 6.128$ mol Fe^{2+}.(mol carbon.h)$^{-1}$ $K_S = 1.31$ mM Fe^{2+} $K_I = 0.641$ $K_2 = 0.0248$ mol Fe^{2+}.(mol carbon.h)$^{-1}$
Gomez and Cantero (2003)	$-r_S = \frac{\mu_{max} S(S_0 - S)}{K_S + S + K_I(S_0 - S)}$	*At. ferrooxidans* Electrochemical Cell $\mu_{max} = 0.22$ h^{-1} $K_S = 16.5$ mM Fe^{2+} $K_I = 3.76$ mM Fe^{3+}
Searby (2006)	$q_{Fe^{2+}} = \frac{q_0 exp\left(\frac{48.0}{RT}\right)}{1 + (aT - b)\cdot\frac{[Fe^{3+}]}{[Fe^{2+}]}}$	*Metallosphaera sp.* Continuous $q_0 = 2.22 \times 10^8$ mol Fe^{2+}.(mol carbon.h)$^{-1}$ $a = 1.39 \times 10^{-3}$ T^{-1} $b = 0.457$ valid T range: $60 - 80^oC$

Continued on next page

Table 2.2 – continued from previous page

Reference	Rate Expression	Microogansim & Constants
Özkaya *et al.* (2006)	$q = \frac{q_{max}[S]}{\left(1 + \frac{I}{K_{ii}}\right) K_S + S + \frac{S^2}{K_i}}$	*L. ferriphilum* Batch $q_{max} = 2.34$ mg Fe^{2+}.(mg VS.h)$^{-1}$ $K_{ii} = 828$ mg.L^{-1} $K_S = 413$ mg.L^{-1} $K_i = 8646$ mg.L^{-1}
Ojumu *et al.* (2009)	$q_{Fe^{2+}} = \frac{K_0 exp\left(\frac{34.46}{RT}\right)}{1 + (aT - b) \cdot \frac{[Fe^{3+}]}{[Fe^{2+}]}}$	*L. ferriphilum* Continuous $a = 6.0 \times 10^{-5}$ T^{-1} $b = 0.0173$ $K_0 = 1.05 \times 10^7$ mmol Fe^{2+}.(mmol carbon.h)$^{-1}$ valid T range: $18 - 45^oC$
Nurmi *et al.* (2009)	$q = \frac{q_{max}[Fe^{2+}]}{\left[K_S\left(1 + \frac{[Fe^{3+}]}{K_{iiFe^{3+}}}\right) + [Fe^{2+}] + \frac{[Fe^{2+}]^2}{K_i}\right] \cdot \left[1 + \frac{[Zn^{2+}]}{K_{iiZi^{2+}}} 1 + \frac{[Ni^{2+}]}{K_{iiNi^{2+}}}\right]}$	*L. ferriphilum* Batch $q_{max} = 2.15 \pm 0.24$ g Fe^{2+}.(g VS.h)$^{-1}$ $K_S = 0.413$ g.L^{-1} $K_{iiFe^{3+}} = 0.828$ g.L^{-1} $K_i = 8.65$ g.L^{-1} $K_{iiMg^{3+}} = 49.1$ g.L^{-1} $K_{iiNi^{2+}} = 62.6$ g.L^{-1}

The Influence of Temperature

Microbial activity increases with increasing temperature. Mesophiles have optimum temperatures between 303.15 K and 313.15 K, while the optimum temperatures for moderate and extreme thermophiles are in the region of 323.15 K and 338.15 K, respecively (Nemati *et al.*, 1998; Ojumu *et al.*, 2006). Although microbial growth of *Acidithiobacillus ferrooxidans* has been recorded at temperatures as low as 275.15 K (Leduc *et al.*, 1993). The temperature at which optimum microbial activity is observed decreases with a decrease in the system pH and often considered microbial strain dependent (Nemati *et al.*, 1998; MacDonald and Clark, 1970). Breed *et al.* (1999); Searby (2006); Ojumu *et al.* (2009) studied the influence of temperature on both mesophilic (Ojumu *et al.*, 2009; Breed *et al.*, 1999) and thermophilic (Searby, 2006) microorganisms (see Table 2.2). Their studies showed that the affinity constant, yield, cell maintenance and maximum specific growth are influenced by temperature (Breed *et al.*, 1999; Searby, 2006; Ojumu *et al.*, 2009). For both mesophilic and thermophilic microorganisms, the affinity constant increases proportionally with an increase in temperature while the maximum microbial yield on ferrous ion Y_{XS}^{max} linearly decreases with an increase in temperature (Searby, 2006; Ojumu *et al.*, 2009).

The greatest influence of temperature on the microbial oxidation rate is on the maximum specific growth rates (Breed *et al.*, 1999; Meruane *et al.*, 2002; Ojumu *et al.*, 2009). These rates increase exponentially with temperature and are often modelled by means of an Arrhenius function (Breed *et al.*, 1999; Searby, 2006; Ojumu *et al.*, 2009) or in the case of extended temperature ranges, the Ratkowsky equation (Ratkowsky *et al.*, 1982; 1983). Microbial activity decreases beyond the optimum temperature and microbial growth ceases at elevated temperatures as weak bonds break resulting in the denaturation of the enzyme cells. As a result, the overall reaction rate, and hence activity, decreases (Dutta, 2008).

The Influence of Ferric and Ferrous Ions

In the literature, several authors have studied the advantage and disadvantage of high and low concentrations of the substrate ferrous ion and ferric ions in the bioleach system (Silverman and Lundgren, 1959; Grishin and Tuovinen, 1988; Barron and Luecking, 1990; Özkaya *et al.*, 2006; Nurmi *et al.*, 2009). Growth rate inhibition by ferrous ions, otherwise referred to as substrate inhibition, beyond a critical concentration (*ca.* 4 g/*l*, Özkaya *et al.*, 2006) have been reported (Silverman and Lundgren, 1959; Braddock *et al.*, 1984; Grishin and Tuovinen, 1988; Barron and Luecking, 1990; Boon *et al.*, 1999b; c; Meruane *et al.*, 2002; Gomez and Cantero, 2003; Özkaya *et al.*, 2006), while a threshold concentration below which no growth is observed has been proposed (Searby, 2006; Braddock *et al.*, 1984; Boon *et al.*, 1999b; Breed and Hansford, 1999a). Substrate inhibition is frequently incorporated into microbial rate expressions using either Monod or Michaelis-Menten type kinetics (see Table 2.2) where it is assumed that an additional molecule of the substrate binds to the enzyme-substrate-complex thereby reducing the activity of the enzyme (Johnson and Goody,

2011; Michaelis and Menten, 1913; Searby, 2006). Similarly, ferric ion inhibition occurs competitively by attaching to the enzyme thus limiting the number of active sites for ferrous ion oxidation and also reducing free ferric ions available for leaching (Kelly and Jones, 1978; Suzuki *et al.*, 1989; Nemati *et al.*, 1998; Harvey and Crundwell, 1997; Kawabe *et al.*, 2003; Özkaya *et al.*, 2006). According to Kelly and Jones (1978) microbial growth and ferrous ion oxidation is subject to competitive (where the ferrous ion substrate competes with ferric ion attachment to the enzyme) or non-competitive (where only the ferric ions attach to the enzyme) ferric ion inhibition where competitive ion inhibition far exceeds non-competitive ferric ion inhibition and thus considered insignificant by comparison (Özkaya *et al.*, 2006). Extended lag phases and in some cases where the initial ferric ion concentration was high, no ferrous ion oxidation was observed due to ferrous ion inhibition (Shrihari and Gandhi., 1990). Ferric ion inhibition is often incorporated in the microbial oxidation rate expressions by means of an inhbition constant K_I and is greatly dependent on the iron-oxidising species in the bioleach system (Norris *et al.*, 1988; Searby, 2006).

Huberts (1994) determined that the inhibiting effect of ferric ions can be countered by the addition of ferrous to the system, thus concluding that the ferric/ferrous ion ratio has greater impact on the microbial growth kinetics that the individual ferric and ferrous ion concentrations (Searby, 2006). Similarly, Özkaya *et al.* (2006) observed instantaneous reaction with no visible lag phase in the presence of ferric ions further indicating that the ferric/ferrous ion ratio is significant in microbial kinetics. Models that account for the change in the microbial oxidation rate as a function of the oxidative reduction potential follow Michaelis-Menten type kinetics which incorporate a substrate affinity constant K_S with a specific ferrous ion utlisation rate that varies according the ferric/ferrous ion ratio (Searby, 2006).

When developing a reactor model for the bioleaching of sulphide mineral ores, it is important that kinetics that fully describe the bioleaching mechanism are applied. In this section, the kinetics of the the acid ferric leaching of pyrite and microbial oxidation of ferrous ion were reviewed.

Most literature pertaining to the acid ferric leaching of pyrite are well developed and agree that the leaching rate is directly proportional to the ferric ions and inversely proportional to either or both the ferrous ions and/or the protons in solution with the order of the reaction *ca.* 0.5. The inverse relationship of the leaching rate expressions with the proton concentration is consistent with the influence of pH which is closely associated with the solubility of ferric ions. Electrochemical experiments clearly show a direct relationship of the pyrite leaching rate with the ferric-to-ferrous ion ratio. Therefore, when developing a reactor model, chemical leaching rates that are either functions of the ferric-to-ferrous ion ratio (Eq. 2.14) or the ratio of the concentration of ferric ions to proton concentration (see Eq. T 1.5 in Table 2.1) should be sufficient to describe the chemical leaching kinetics. However, in biological systems, the ferrous ions are converted to ferric ions by microbial oxidation thus depleting the ferrous ion concentration and replenishing the ferric ion concentration. Consequently,

the chemical leaching rate would be a strong function of the ferric-to-ferrous ion ratio thus supporting kinetics in the form of Eq. 2.14 (Petersen and Dixon, 2006).

$$r''_{MS} = k\left(\frac{C_{Fe^{3+}}}{C_{Fe^{2+}}}\right)^{0.5} \quad [2.14]$$

where the kinetic constant k is a function of the exposed mineral surface area to solution volume.

The microbial oxidation kinetics for mesophilic ferrous ion oxidation are well developed while kinetics for thermophilic microorganisms are limited (Searby, 2006). Most microbial oxidation kinetics are modeled using Michaelis-Menten or Monod type expressions as they are able to describe the change in reaction conditions and incorporate inhibitory effects. The concentration of the ferric and ferrous ions and their ratio are identified as important control parameters in the rate of growth and microbial oxidation and are incorporated in the microbial oxidation rate expressions.

It is clear from the literature that the microbial oxidation kinetics are influenced by the ferric and ferrous ions or the ferric-to-ferrous ion ratio. These ions may have an inhibiting effect on the microbial oxidation rate presenting as either product or substrate inhibition. Observing the proposed kinetic rate expressions in Table 2.2 for the microbial oxidation rate, most rate expressions incorporate these limitations by including the ferric/ferrous ion ratio. The most common, and simplest, representation of the rate expression is the relative ratio of the maximum specific substrate utilisation rate to $1 + K_S(C_{Fe^{3+}}/C_{Fe^{2+}})$ (Eq. 2.15) (see Hansford, 1997; van Scherpenzeel *et al.*, 1998; Breed *et al.*, 1999; Breed and Hansford, 1999a; Searby, 2006; Ojumu *et al.*, 2009 , in Table 2.2).

$$q_S = \frac{q_S^{max}}{1 + K_S\frac{C_{Fe^{3+}}}{C_{Fe^{2+}}}} \quad [2.15]$$

Both Searby (2006) and Ojumu *et al.* (2009) showed that Eq. 2.15 could accurately predict the microbial oxidation rate over a range of experimental conditions for both mesophilic (Ojumu *et al.*, 2009) and thermophilic (Searby, 2006) microorganisms, indicating that the rate expression is sufficient in describing the microbial oxidation reaction at both high ($333.15 - 353.15$ K) and low ($291.15 - 318.15$ K) temperatures when developing a reactor model.

In subsequent chapters, rate expressions in the form of either Eq. 2.14 or Eq. T 1.5 (Table 2.1) will be utilized to describe the acid ferric leaching of pyrite. Eq. 2.15 will be used to represent the microbial oxidation of ferrous ion for both mesophilic and thermophilic microorganisms based on kinetic data obtained from the literature (Table 2.2).

2.3 Hydrodynamic Stress

During bleaching, iron and sulphur oxidising microorganisms are exposed to various hydrodynamic stresses. These stresses are predominantly due to high agitation rates and solid-liquid interactions that may cause minor cell damage or complete cell disruption (Bronnenmeier and Märkl, 1982; Raja, 2005). Cell wall strength is integral in maintaining the cell structure under high hydrodynamic stresses. It has been shown that microorganisms that can survive at high temperatures ($333.15 - 353.15$ K), classified as thermophiles, are more susceptible to cell damage than lower temperature microorganisms such as mesophiles (< 313.15 K) as high temperature microorganisms lack cell rigidity and are more susceptible to mild stresses (Valencia *et al.*, 2003; Sissing and Harrison, 2003; Witne and Phillips, 2001; Nemati and Harrison, 2000; Clark and Norris, 1996; Brock and Madigan, 1991; Bronnenmeier and Märkl, 1982).

Microorganisms are exposed to both hydrodynamic and physicochemical stresses in tank bleaching. Hydrodynamic stress is defined as the stress on the microorganisms generated by the movement of fluid in the reactor caused by mixing and/or aeration, while physicochemical stress is the stress resulting from less than ideal bioleaching conditions such as pH, temperature, nutrient starvation and product inhibition (Raja, 2005). Hydrodynamic stresses may arise from high agitation rates required to suspend solids in the reaction environment and reduced oxygen availability to the microorganisms (Raja, 2005; Valencia *et al.*, 2003; Witne and Phillips, 2001; Bailey and Hansford, 1994; Loia *et al.*, 1994). To maintain a homogeneous suspension of solids in the reacting environment, the solid, gas and liquid phases are well mixed. The solid-solid and solid-cell interactions result in hydrodynamic stress. Bronnenmeier and Märkl (1982) hypothesised that cell damage occurred predominantly at or near the impeller blades during mixing. Due to the reduced cell wall rigidity of thermophiles, compared to mesophiles, it is expected that cell damage would occur at lower solids concentrations in thermophilic operations than in mesophilic systems (Raja, 2005). Cell damage or death may result from high shear stress due to high agitation rates, attrition due to solid-cell interactions; collisions between cells; and cells with either the impeller or reactor walls (Sissing and Harrison, 2003; Michaels *et al.*, 1996; Dunlop and Namdev, 1994; Cherry and Papoutsakis, 1986). The size, shape and density of the solid particles, as well as the frequency of particle-cell collisions in the reactor, can have an influence on the intensity of the damage incurred on the microbial cells present in the reactor (Raja, 2005; Deveci, 2004; Nemati *et al.*, 2000). Deveci (2002; 2004) studied the influence of particle loading, particle size and shape on cell damage. In conflict to observation to Bronnenmeier and Märkl (1982), Deveci (2002; 2004) found that cell damage due to hydrodynamic shear alone was minimal compared to the cell damage achieved when solid particles were introduced to the experiments. Deveci (2002; 2004) thus concluded that, for microbial cells suspended in the liquid phase, cell damage was mostly due to particle-cell interactions promoted by agitation speeds and was influenced to lesser degree by collisions between cells and the cells with the reactor components.

In bioleaching, biological stress may influence the overall reactor performance by decreasing the microbial growth, overall leaching rates as well as rates of particle-cell attachments (Raja, 2005). As low rates of copper extraction are often observed in chalcopyrite bioleaching, Raja (2005) attempted to determine the influence of hydrodynamic stress on the overall performance of slurry-type reactors in the bioleaching of chalcopyrite. The aim of the study was to determine whether low extraction rates are due to such stresses. The study included an investigation into the influence of particle solids loading, defined as the mass of particles relative to the reactor volume [m/v], on the system redox potential and microbial cell concentration. Quartzite solids loading ranging from $0 - 18$ % [m/v] containing 3 % [m/v] chalcopyrite loading at a constant impeller speed of 1.97 $m.s^{-1}$ was investigated. The experimental results showed a decrease in both the solution redox potential and microbial concentrations with increasing solids loading from the baseline experiments conducted at 0 % [m/v] quartzite loading. A critical solids loading of 9 % quartzite was identified in the redox potential experiments at which point the bioleaching system became significantly affected by hydrodynamic stress. The decrease in the redox potential was attributed to the increase in ferrous ion concentration in the reactor due to reduced microbial activity and hence limited ferrous ion oxidation (Eq. 1.2). When monitoring the influence of solids loading on the microbial concentration, Raja (2005) observed a decrease in the microbial concentration with increasing solids loading. Little to no microbial growth was observed at 18 % [m/v] quartzite due to cell death while reactors containing 9 % [m/v] quartzite and above reached stationary phase over a longer time period than experiments conducted at lower quartzite loadings. Similarly, iron and copper solubilisation decreased with increasing solids loading. However, over the initial 48 hours of their experiments, where the redox potential dropped below *ca.* 0.61 V, there was a sharp increase in copper in solution indicating increased copper extraction rates at lower redox potentials.

It is clear from the literature that biological stresses have a negative influence on the microbial growth rate. High agitation rates and increased solids loadings [m/v] are contributing factors to observed decreased microbial concentrations (Deveci, 2002; 2004; Valencia *et al.*, 2003; Sissing and Harrison, 2003; Witne and Phillips, 2001; Nemati and Harrison, 2000; Clark and Norris, 1996; Brock and Madigan, 1991; Bronnenmeier and Märkl, 1982). In addition to reduced growth rates, the findings by Raja (2005) indicate that applied hydrodynamic stresses also influence the solution redox potential. With increased solids loading, a decrease in the solution potential is observed. Consequently, increased copper extraction rates are noted (Raja, 2005). These observations indicate that by applying a biological stress to the bioleaching system, the rate of extraction, especially in the case of chalcopyrite, can be manipulated to maintain the system at maximum overall rates by controlling both the microbial concentration and solution redox potential or ferric/ferrous ion ratio.

2.4 Chalcopyrite Bioleaching

Kametani and Aoki (1985) studied the influence of the ferric/ferrous ion ratio on the chemical

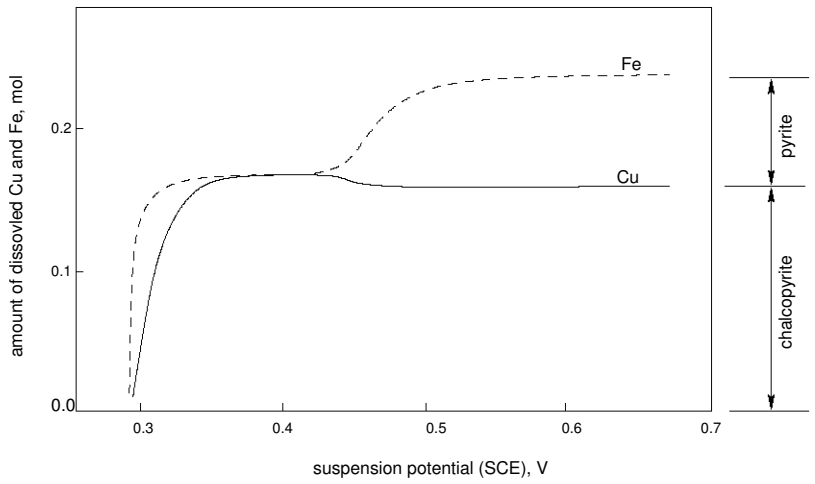

Figure 2.3: Graphical representation of the copper and iron concentrations obtained during the chemical leaching experiments conducted by Kametani and Aoki (1985)

oxidation rate of chalcopyrite. The leaching process was assumed to be an electrochemical process in which the chemical leaching rate was considered dependent on the potential difference between the sulphide mineral particle surface and the leach solution, which they defined as the suspension potential. Different chemical leaching rates were observed when the suspension potential was above or below 0.45 V (Saturated Calomel Electrode, SCE). With increasing suspension potential, Kametani and Aoki (1985) noted a fast increase in the leaching rate up to 0.45 V after which a slow increase in the rate was observed from 0.45 V to 0.60 V (Figure 2.3). Higher total iron extraction rates were achieved than copper when the potential was between 0.3 V and 0.33 V. This was attributed to the precipitation of copper as CuS. From 0.37 V to 0.43 V similar concentrations of copper and iron were observed in the solution phase at which stage the oxidation of chalcopyrite reached completion. Above 0.43 V, the iron concentration in solution increased while the copper concentration remained constant. Kametani and Aoki (1985) postulated that at low suspension potentials below 0.45 V (SCE), predominantly $CuFeS_2$ was leached. As the suspension potential increased, the chemical leaching of pyrite dominated indicating sequential leaching of the sulphide mineral.

In bioleach experiments, Hiroyoshi *et al.* (1999) showed that copper extraction rates were reduced when chalcopyrite was bioleached in the presence of *Acidithiobacillus ferrooxidans* at 303 K. Their experiments showed that ferrous ion oxidation was microbially enhanced when chalcopyrite was bioleached in sulphuric acid solutions containing ferrous sulphate but observed that copper extraction rates were inhibited as the microbial concentration increased. Hiroyoshi *et al.* (1999) initially assumed that low copper extraction rates were due to the formation and precipitation of ferric hydroxide on the chalcopyrite surface thus limiting the transfer of ions to and from the particle surface, but further analysis revealed that the majority of the ferric hydroxide was in solution and therefore would not significantly limit leaching. Further experiments in the absence of microorganisms, revealed that higher extraction rates were achieved when chalcopyrite was leached in the ferrous ion promoted solutions as opposed to a system in which no additional ferrous ions were added to the

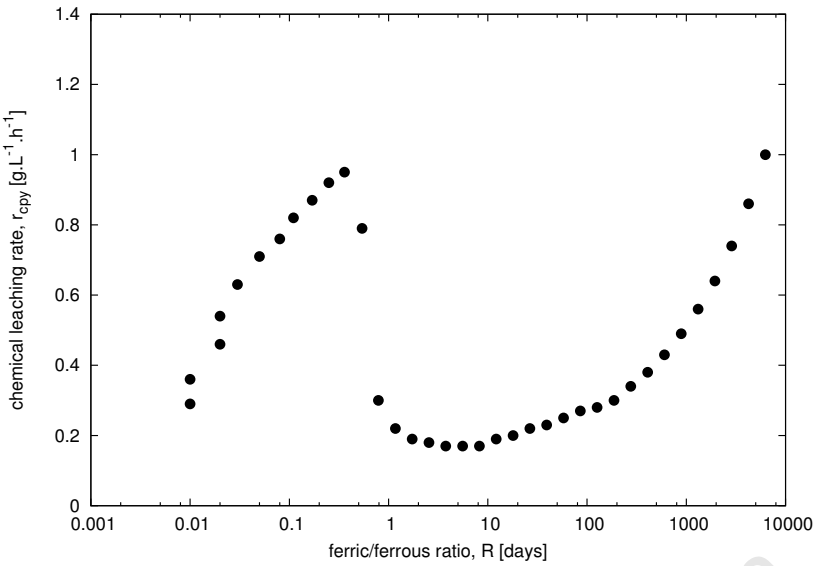

Figure 2.4: The chemical leaching rate of chalcopyrite with increasing ferric/ferrous ion ratio R. Data extracted and reworked from Hiroyoshi *et al.* (2004).

system. Thus concluding that ferrous ions contribute to chalcopyrite leaching.

Ferrous promoted leaching environments ensure that the redox potential, which is related to the ferric to ferrous ion ratio ($C_{Fe^{3+}}/C_{Fe^{2+}}$) *via.* the Nernst equation, are low (Hiroyoshi *et al.*, 2000). Consequently, the results from experiments performed by Hiroyoshi *et al.* (1999) correspond to the observations by Kametani and Aoki (1985) in that high extraction rates were achieved at low redox potentials. These observations indicate that the leaching of chalcopyrite goes through three phases. In the first or active phase high rates are observed at low ferric/ferrous ion ratios, while in the second or passive phase, after a critical ferric/ferrous ion ratio is reached, low leaching rates are observed at high ferric/ferrous ion ratios (*ca.* $R <$ 100 in Figure 2.4). After which in the trans-passive phase, the rate increases again (Hiroyoshi *et al.*, 2004).

Hiroyoshi *et al.* (2001) hypothesised that the enhancement in the leaching rate, in ferrous promoted environments, was due the reduction of chalcopyrite by ferrous ions to Cu_2S (Eq. 2.16). The Cu_2S is then rapidly oxidised by ferric ions to release cupric ions in solution (Eq. 2.17). The summation of the preceding reactions gives the overall reaction in Eq. (2.18). The condition of this mechanism was that there should be sufficient Cu^{2+} and Fe^{2+}, otherwise the chalcopyrite would be directly oxdised by Fe^{3+} ions, in which case the leaching rate would be slower (Eq. 2.18).

$$CuFeS_2 + 3Cu^{2+} + 3Fe^{2+} \rightarrow 2Cu_2S + 4Fe^{3+} \quad [2.16]$$

$$2Cu_2S + 8Fe^{3+} \rightarrow 4Cu^{2+} + 8Fe^{2+} + S \quad [2.17]$$

$$CuFeS_2 + 4Fe^{3+} \rightarrow Cu^{2+} + 5Fe^{2+} + S \quad [2.18]$$

Confirming the above observations, Gericke *et al.* (2010) noted increases between 42 % and 80 % in copper recovery when chalcopyrite was leached in the presence of a moderate

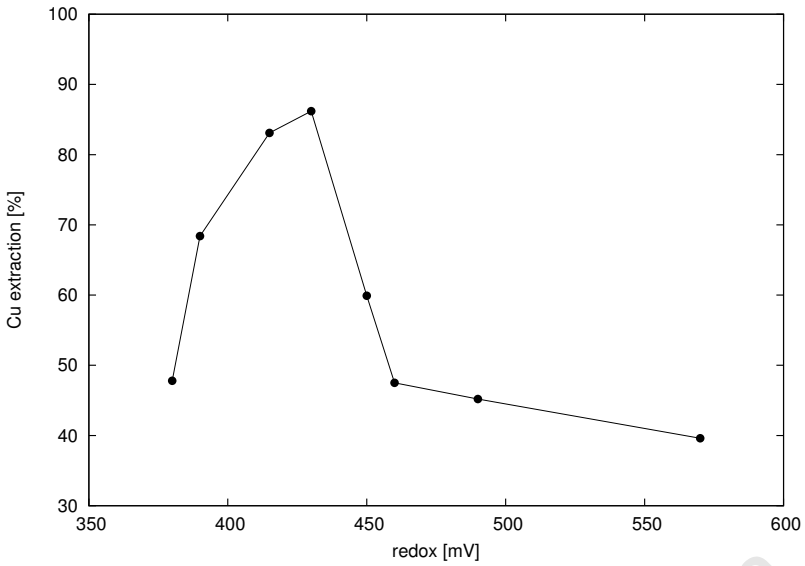

Figure 2.5: The percentage copper extracted from chalcopyrite at 318.15 K as a function of solution redox potential. Figure extracted from Gericke *et al.* (2010).

thermophilic culture at 318.15 K while maintaining the redox potential between 0.41 V and 0.44 V (SCE). At higher solution potentials, copper extraction rates reduced significantly (Figure 2.5). With similar findings from previous authors (Gericke and Govender, 2011; Hiroyoshi *et al.*, 1997; Hirato *et al.*, 1987; Kametani and Aoki, 1985), Petersen and Dixon (2006) noted that chalcopyrite cannot be classified by conventional electrochemical theory. Following the mechanism proposed by Hiroyoshi *et al.* (2004) (Eqs. 2.16 and 2.17), Petersen and Dixon (2006) proposed an empirical leaching rate for chalcopyrite that describes chalcopyrite kinetics as the sum of two parallel reactions with similar kinetics to pyrite which replace each other at some critical ferric to ferrous ion ratio, R_{crit} (Eq. 2.19, Figure 2.6, Petersen and Dixon, 2006).

$$r_{cpy} = g_{py} \cdot f\left(X_{cpy}\right) \cdot R^{0.5} \left[A \cdot exp\left(-\frac{R}{R_{crit}}\right) + B\left(1 - exp\left(-\frac{R}{R_{crit}}\right)\right)\right] \qquad [2.19]$$

where g_{py} is the mineral grade which is the fraction of mineral ore content in the ore body, $f(X_{cpy})$ the topological term which accounts for the change in the mineral reacting surface and A and B the temperature dependent kinetic rate constants.

Observations by several authors concur that unlike most sulphide minerals, increasing the concentration of the conventional oxidant, ferric ions, does not enhance but rather negatively influences the chalcopyrite leaching rate (Dutrizac, 1981; Kametani and Aoki, 1985; Hirato *et al.*, 1987; Almendras *et al.*, 1987; Hiroyoshi *et al.*, 1997; 1999; 2004; Gericke *et al.*, 2010). Similarly, several reports have conflicting opinions about the role of microorganisms in bioleaching experiments (Almendras *et al.*, 1987; Devasia *et al.*, 1996; Hiroyoshi *et al.*, 1997; 1999; Third *et al.*, 2000). The role of microorganisms in most bioleaching processes is clear. The microorganisms create an highly oxidative environment by regenerating ferric ions from ferrous ions which promotes leaching, however this is not always conducive to chalcopyrite bioleaching (Kametani and Aoki, 1985; Hiroyoshi *et al.*, 1997; Third *et al.*,

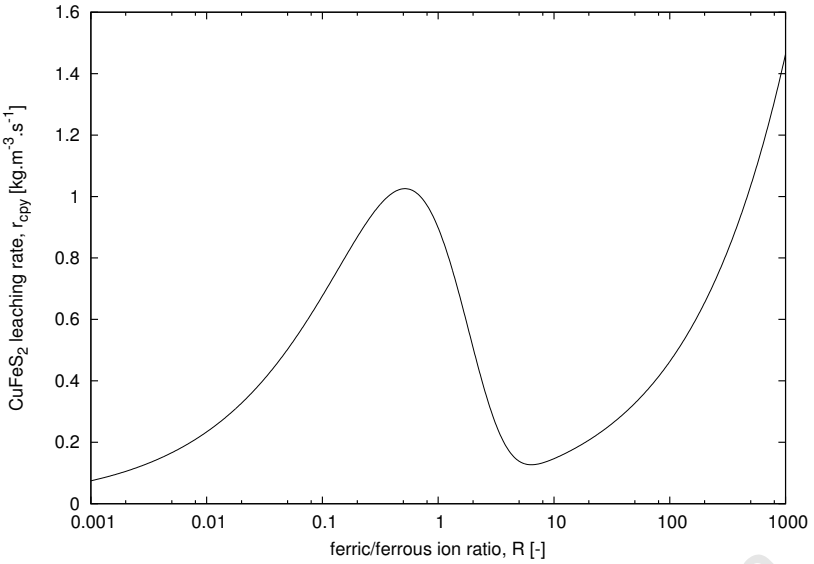

Figure 2.6: The empirical leaching rate proposed by Petersen and Dixon (2006) to describe chalcopyrite kinetics. The general trend of the proposed empirical leaching rate curve corresponds well to the experimental chemical leaching rate data by Hiroyoshi *et al.* (2004) (see Figure 2.4).

2000; Gericke *et al.*, 2010).

Third *et al.* (2000) performed experiments at 310.15 K in the presence of a mixed mesophilic culture. Copper extraction rates were compared with experiments in which the system was inoculated with 1 %, 10 % and 50 % [v/v] of the total solution volume. The highest extraction rates were achieved in experiments that contained 10 % [v/v] inoculum while the lowest rates were observed when 50 % [v/v] inoculum was used. Higher extraction rates were noted in non-inoculated experiments than those achieved when 50 % [v/v] inoculum was used thus verifying the observations by Hiroyoshi *et al.* (1999) that the presence of microorganisms can inhibit rather than enhance the chalcopyrite leaching rate. It is interesting to note however that the experiments conducted by Third *et al.* (2000) resulted in two clearly defined steady states (Figure 2.7). A steady state at *ca.* 0.52 V (SHE), where high rates of extraction were observed using low microbial concentrations (1 % and 10 % [v/v], Figure 2.7) and another steady state at high redox potentials at *ca.* 0.77 V (SHE), in which the microbial concentration was high (50 % [v/v], Figure 2.7). Also, experiments utilising 10 % [v/v] inoculum transitioned from low redox potentials, where high rates were observed, to high redox potentials, while experiments that had little (1 % [v/v]) to no inoculum added to the system remained at low redox potentials with high leaching rates. Clearly this would indicate that, in addition to the system being sensitive to redox potential, the microbial concentration is also a contributing factor to the overall rate.

Most sulphide minerals have intrinsic leaching rates that are proportional to the ferric/ferrous ion ratio to the n^{th} order (Petersen and Dixon, 2006; Crundwell, 2001). These intrinsic leaching rates increase with increasing ferrous/ferrous ion ratio. The chemical leaching rate increases monotonically with an increase in solution redox potential. The rate has a slow initial increase at low potentials, due to ferrous ion inhibition, and gradually increases at

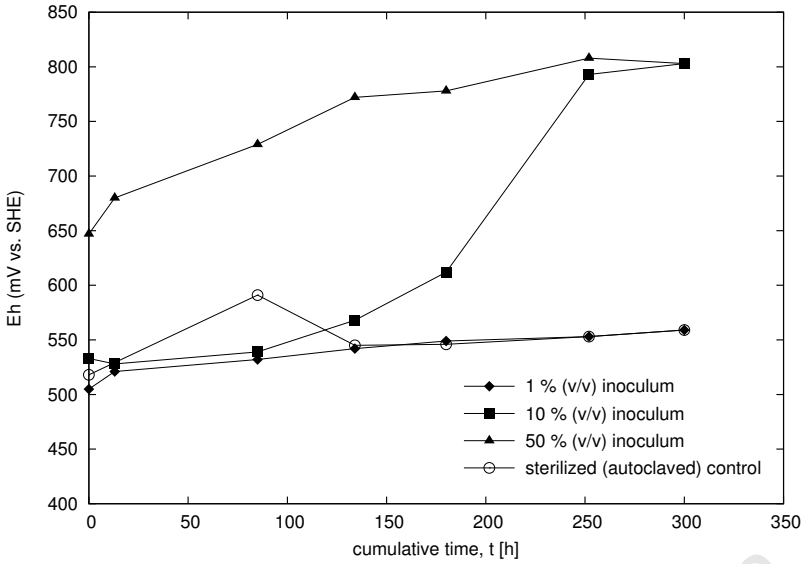

Figure 2.7: Measured redox potentials in chalcopyrite bioleaching experiments conducted by Third *et al.* (2000). Figure extracted from Third *et al.* (2000).

higher potentials when more ferric ions are available for reaction. It has been reported that, in a bioleach system, steady state operation occurs when the rate of ferrous ion production equals the rate of ferrous ion consumption (Eq. 2.20, Breed and Hansford, 1999b).

$$-r_{Fe^{2+}}^{micro} = r_{Fe^{2+}}^{chem} \qquad [2.20]$$

where $r_{Fe^{2+}}^{micro}$ [mol.m^{-3}.s^{-1}] is the rate of microbial ferrous ion consumption and $r_{Fe^{2+}}^{chem}$ [mol.m^{-3}.s^{-1}] the rate of chemical ferrous ion production.

Graphically, these steady states would occur at the intersection of the microbial ferrous ion consumption rate $r_{Fe^{2+}}^{micro}$ and chemical ferrous ion production rate $r_{Fe^{2+}}^{chem}$ (Figure 2.8, Breed and Hansford, 1999b; Hansford and Vargas, 2001). In biological systems, a sustained dynamic equilibrium is reached when there is balance between microbial growth and substrate availability. According to the above definition of stability in a bioleach system (Eq. 2.20), the rate of ferrous ion liberation from the sulphide mineral particle surface must equal the rate at which the ferrous ions are consumed by the microorganisms in solution. The stability of these conditions is largely dependent on the concentration of the biomass, and hence on the microbial activity, as well as the concentration of the sulphide mineral (Boon and Heijnen, 1998a).

If the conditions of steady state in Eq. 2.20 are applied to chalcopyrite bioleaching, and given that the intrinsic leaching rate of chalcopyrite is non-monotonic (Figure 2.4), more than one intersection would occur between the microbial ferrous ion consumption rate $r_{Fe^{2+}}^{micro}$ and chemical ferrous ion production rate $r_{Fe^{2+}}^{chem}$. This indicates that more than one set of conditions would satisfy the equality in Eq. 2.20 for the rate of ferrous ion production and consumption, therefore the bioleach reactor could operate at more than one steady steady state.

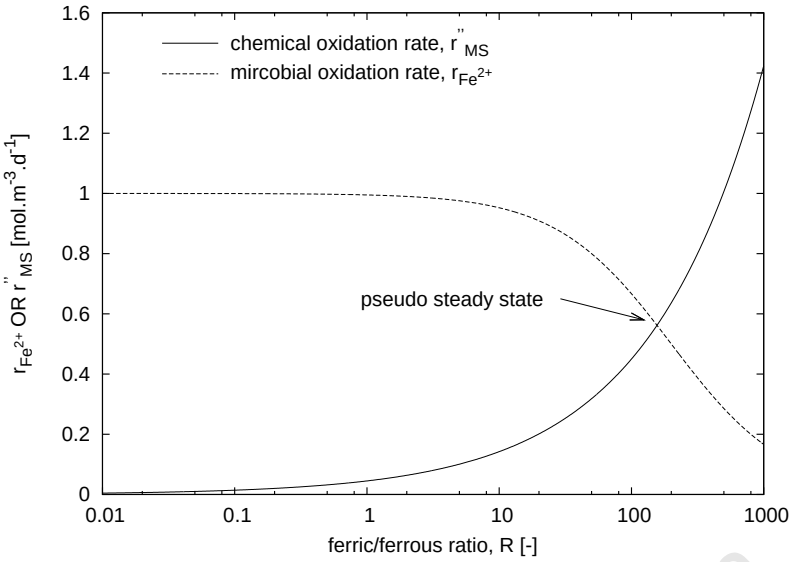

Figure 2.8: Stable pseudo steady state indicated by the point of intersection between the microbial oxidation $r_{Fe^{2+}}^{micro}$ and chemical leaching rate curves $r_{Fe^{2+}}^{chem}$

In the majority of microbial process environments, microorganisms appear as mixed cultures. The interaction and behaviour of these organisms, relative to each other, play an important role in the understanding of their response to changes in their environment (Shuler and Kargi, 2002; Bailey and Ollis, 1986). If we consider that maximum copper extraction rates occur at low solution potentials $0.45 - 0.65$ V (SHE) (Watling, 2006; Third *et al.*, 2000; Hiroyoshi *et al.*, 1997; 1999; 2001; Kametani and Aoki, 1985; Peters, 1976) and assume that the equality in Eq. 2.20 is valid, it would appear that by controlling the microbial oxidation rate by means of the microbial concentration and solution redox potential the chalcopyrite bioleaching rate can be controlled to below 0.65 V (SHE) to obtain high rates. Knowing the sensitivity of the bioleach system to key operating parameters is, therefore, important when developing a process for maximum production.

2.5 Development Of Tank Bioleach Models

Reactor models are developed to facilitate reactor optimisation. Typically optimum plant operation is achieved by maximising the overall production rate. Reactor models are therefore formulated with the objective of identifying appropriate operating conditions to achieve maximum reaction rates.

With the increased interest in tank bioleaching (Rohwerder *et al.*, 2003; Olson *et al.*, 2003) various reactor models have been proposed. These models differ with regard to the assumptions applied and the choice of properties to be analysed, such as, the time the particles reside within the reactor (particle age) and particle size. It is important to note that, at present, none of the reactor models presented in the literature include unsteady state operation in the model development. The main features which differentiate these models, which are summarised in Table 2.3 and illustrated in Figure 2.9, include:

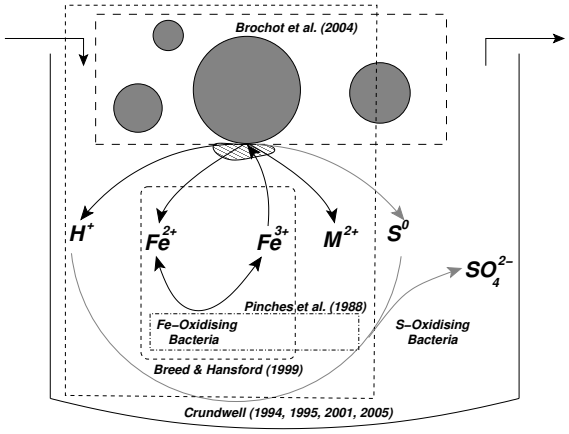

Figure 2.9: Underlying assumptions used when developing tank bioleach models

Table 2.3: Modeling parameters used by various authors when developing tank bioleach reactor models

Author	Logistic equation	First order	Mineral leach	Microbial oxidation	PSD[♭]	RTD[♮]
Pinches *et al.* (1987)	√	–	–	–	–	–
Hansford and Chapman (1992)	√	–	–	–	–	–
Hansford and Miller (1993)	√	–	–	–	–	–
Breed and Hansford (1999b)	–	–	√	√	–	–
Brochot *et al.* (2004)	–	√	–	–	√	√
Crundwell (1994; 1995; 2001; 2005)	–	–	√	√	√	*X*

[♭] Particle Size Distribution (PSD)

[♮] Residence Time Distribution (RTD)

- the choice of kinetics i.e. models that include either or both chemical (see Table 2.1) and microbial oxidation kinetics (Crundwell, 1994; 1995; 2001; 2005; Breed and Hansford, 1999b, see Table 2.2) or models that are purely based on empirical formulae which describe only microbial growth kinetics *via.* the logistic equation (Pinches *et al.*, 1987; Hansford and Chapman, 1992; Hansford and Miller, 1993, see Eq. 2.10) or first order kinetics based on only the shrinking core model (Brochot *et al.*, 2004).

- the inclusion of particle size changes (Crundwell, 1994; 1995; 2001; 2005; Brochot *et al.*, 2004) or lack thereof (Pinches *et al.*, 1987; Hansford and Chapman, 1992; Hansford and Miller, 1993; Breed and Hansford, 1999b).

- the incorporation of either or both residence time distribution and/or particle size distribution (Crundwell, 1994; 1995; 2001; 2005; Brochot *et al.*, 2004)

Models based on the empirical logistic equation often relate the fractional conversion of the mineral sulphide to microbial growth and ignore the effects of chemical leaching (Pinches *et al.*, 1987; Hansford and Chapman, 1992; Hansford and Miller, 1993), and therefore do not account for the change in particle surface area in the overall leaching rate. Similarly the use of first order kinetics which estimate the overall bioleaching rate ignore the effects of the individual bioleach reactions thereby over- or underestimating the change in mineral particle surface area (Brochot *et al.*, 2004). Reactor models that include chemical leach and microbial

kinetics and recognise that a non-uniform distribution of particles reside in the reactor for different time periods, incorporate all aspects of the bioleaching process when predicting reactor performance and are therefore the most comprehensive models (Crundwell, 1994; 1995; 2001; 2005).

In the following sections, the choice of kinetics and particle properties are critically evaluated and their implications in developing overall reactor performance are reviewed from first principles.

2.5.1 Kinetic Rate Expressions

In the bioleaching reactor, sulphide mineral particles come into contact with the reaction environment where they are leached to liberate valuable mineral ions into the aqueous phase. As a result, each of the sulphide mineral particles surface area change over time due to reaction. As performance is often measured by the conversion or rate of dissolution of the sulphide mineral particles, surface area based intrinsic kinetics should be applied when modeling the performance of the bioleach reactor.

Several approaches have been taken to either incorporate or ignore particle-solution dynamics when modeling the bioleach reactor. Early models did not recognise the resulting rate contribution from the change in particle surface area in the reactor, focussing primarily on the microbial kinetics (Pinches *et al.*, 1987; Hansford and Miller, 1993; Hansford and Chapman, 1992).

During the investigation of a gold-bearing concentrate containing a predominance of pyrite, Pinches *et al.* (1987) and Hansford and Miller (1993) developed models under the assumption that the kinetic rate expression could be described by the logistic equation (La Motta, 1976). The fraction of pyrite oxidised was related to microbial growth such that the oxidation rate r was expressed as (Eq. 2.21).

$$\frac{rV^R}{N_{P0}} = \frac{dX}{dt} = k_m X \left(1 - \frac{X}{X_m}\right) \qquad [2.21]$$

where V^R is the volume of the reactor, N_{P0} the initial number of moles of pyrite in the sulphide mineral particles, X the fraction of pyrite oxidised, X_m the maximum fraction of pyrite that could be oxidised and k_m the rate constant (Pinches *et al.*, 1987).

Another approach involves the application of a global rate that takes into account the solid and solution phase kinetics by means of a first order rate equation. Brochot *et al.* (2004) developed a model to predict sulphide and heavy metal recovery. The objective of the model was to optimise equipment configuration to maximise operation from the gravity concentration unit. Since the inlet to each of the tanks in series were fed by gravity-overflow, the solution contact time with the particles in the reaction space varied

from particle-to-particle. The reactor model by Brochot *et al.* (2004) was therefore developed using the segregation approach.

The recovery R of cobalt in solution for a distribution of particle sizes, in a particular size class, was fit to a first order kinetic function (Eq. 2.22)

$$R = R_{max}(1 - e^{-Kt}) \quad [2.22]$$

where R is the cobalt recovered in solution at time t and K the kinetic constant.

The maximum cobalt recovery R_{max} and the kinetic constant K were fit to experimental data for each size class. The results confirmed a linear dependence of the kinetic constant on the inverse of the particle diameter, indicating that the particles reduce in size at a constant rate, similar to the shrinking core model (Brochot *et al.*, 2004)

Although the logistic rate equation can be used to predict the microbial growth and stationary phases for any microbial system (La Motta, 1976), it cannot be used to describe the chemical leach kinetics. While utilising a first order rate expression that describes both the chemical leaching and microbial oxidation reactions as a single reaction and takes into account the interactions between the bioleach phases, it limits the model to steady state operation. This is because the model does incorporate allowances for possible disturbances in either inlet and/or outlet process conditions to the reactor over time or that the conditions within each reactor in the series are not the same. Further, both logistic and first order kinetics exclude product inhibition resulting from the exchange of ions between the phases.

Crundwell (1994) formulated a model for batch and continuous microbial leaching reactors using a population balance approach. The model included chemical and microbial oxidation kinetics to describe the bioleaching mineral sulphides as well as incorporating the variation in particle size distribution resulting from reaction, but was restricted to steady state operation without incorporating possible perturbations in the process conditions. Crundwell (1994) noted, at the time, that the leaching mechanism was unknown and the choice of mechanism (direct or indirect) played an important role in selecting the kinetic model to be applied. The model included the rate of attachment r_a and detachment r_d of microorganisms to the particle surface, assuming that the rate of attachment is proportional to the unoccupied surface area and the rate of detachment proportional to the occupied particle surface area. The rate of microbial growth in solution r_s was incorporated by Monod kinetics, assuming that ferrous ions are the only substrate utilised in solution.

Crundwell (2001; 2005) updated the earlier models (Crundwell, 1994; 1995) by incorporating the generally accepted sub-process mechanism (Boon *et al.*, 1995), applying both microbial growth kinetics and surface area based intrinsic leach kinetics R (Eq. 2.23)

$$R = -k_s \left(\frac{C_{Fe^{3+}}}{1 + kC_{Fe^{2+}}} \right)^{\alpha} \quad [2.23]$$

where k_s is the chemical leaching rate constant [m.min^{-1}] and α is often close to 0.5 (Crundwell, 2001).

The population balance model introduced by Crundwell (1994; 2001) included both bioleach phases thus accounting for the rate contribution due to the change in particle surface area to the overall bioleaching rate. By applying the sub-process mechanism, the kinetics for each of the participating reactions could be independently studied and the influence on the overall reactor performance determined (Breed and Hansford, 1999b).

The model developed by Breed and Hansford (1999b) was similarly based on recent developments by Boon *et al.* (1995) regarding the bioleaching mechanism. Where the acid ferric leaching of the mineral sulphide ore and the regeneration of ferric ions by the microbial oxidation of ferrous ions are considered as two independent reactions. Noting that the redox potential of the solution phase could be represented by the ferric/ferrous ion ratio $C_{Fe^{3+}}/C_{Fe^{2+}}$ *via.* the Nerst equation, Breed and Hansford (1999b) applied Michaelis-Menten/Monod-type kinetics for the microbial oxidation reaction, which account for the ferric ion inhibition (Eq. 2.24), and kinetics in the form of Eq. 2.25 proposed by Boon (1996) for the chemical leaching reaction.

$$r_{Fe^{2+}} = \frac{C_X q^{max}_{Fe^{2+}}}{1 + K\frac{C_{Fe^{3+}}}{C_{Fe^{2+}}}} \quad [2.24]$$

$$\nu_{Fe^{2+}} = \frac{\nu^{max}_{Fe^{2+}}}{1 + B\frac{C_{Fe^{2+}}}{C_{Fe^{3+}}}} \quad [2.25]$$

where $q^{max}_{Fe^{2+}}$ [mol Fe^{2+}.mol carbon^{-1}.s^{-1}] is the maximum microbial specific ferrous iron utilisation rate, K [$-$] the inhibition constant and C_X [$mol.m^{-3}$] the concentration of the biomass and $\nu_{Fe^{2+}}$ [mol Fe^{2+}.mol ${FeS_2}^{-1}$.h^{-1}] is the mineral sulphide specific ferrous ion production rate , $\nu^{max}_{Fe^{2+}}$ [mol Fe^{2+}.mol ${FeS_2}^{-1}$.h^{-1}] the maximum mineral sulphide specific ferrous ion production rate and B [$-$] the chemical ferric leach kinetic constant (Boon and Heijnen, 1998a).

It was assumed by these researchers that, at steady state, the rate of ferrous ion production equals the rate of ferrous ion consumption *via.* the chemical leaching and microbial oxidation reactions, respectively (Eq. 2.20).

$$r^{chem}_{Fe^{2+}} = -r^{micro}_{Fe^{3+}} \quad [2.20]$$

Although the models by Crundwell (1994; 2001) and Breed and Hansford (1999b) both incorporated the multi-step bioleaching mechanism, using independent intrinsic kinetics for each step, the model formulation by Breed and Hansford (1999b) does not show a rate dependence on the solid phase component. The steady state assumption in Eq. 2.20 together with the use of chemical leach kinetics that are independent of the particle surface area, the performance equation evaluated by Breed and Hansford (1999b) reduced to a model in which only the solution phase components were taken into account.

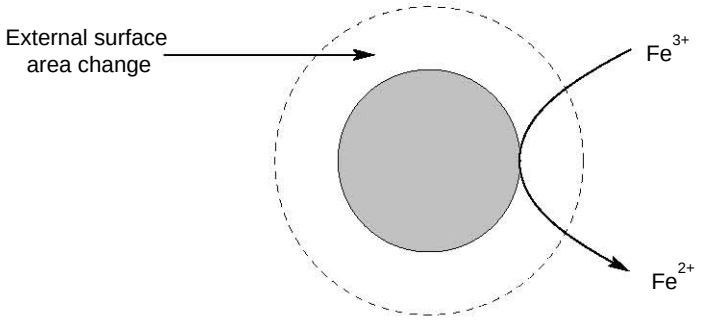

Figure 2.10: The shrinking core model with chemical reaction as the rate limiting step at the particle surface

Bioleaching is a multiphase reaction in which a reduction in the mineral sulphide particle surface area is observed. Therefore, apart from the rate contribution of the solution components to the overall reaction rate, the contribution due to the change in particle mass or size needs to be addressed. This change is frequently modeled for a single particle based on the aforementioned intrinsic kinetics for either a combined or multi-step bioleaching mechanism.

2.5.2 Shrinking particles

In bioleaching, the metal sulphide component of the particles is consumed due to dissolution or reaction, resulting in size changes. This size change is often predicted by application of the shrinking core or shrinking particle model (Yagi and Kunii, 1961).

Reaction controlled shrinking core models generally assume that particles are spherical, reactive, non-porous surfaces in which chemical reaction at the particle surface is the rate limiting step (Crundwell, 1994; Brochot *et al.*, 2004). According to these models, reaction at the particle surface is unaffected by the formation or generation of an unreactive surface (Figure 2.10). The rate of particle shrinkage is therefore proportional to the available unreacted particle surface area (Levenspiel, 1972; Yagi and Kunii, 1961).

Particle-solution dynamics was investigated by Crundwell (1994; 2001) and Brochot *et al.* (2004). In these models, the rate of dissolution of a single particle was initially considered. The difference between their approaches was the choice of bioleaching mechanism and the intrinsic kinetics applied.

Based on the direct and indirect bioleaching mechanism, Crundwell (1994) proposed that the rate of particle dissolution was affected by the nature of the microorganisms attached to the mineral particle surface and the concentration of the ferric ions in solution (Eq. 2.26, Crundwell, 1994). The rate of attachment of microorganisms to the particle surface was assumed to be proportional to the unoccupied surface area.

$$\frac{dl}{dt} = -\frac{k_{dl} N \phi l^2}{3\rho l^2}\left(N_{max}\phi l^2 - N\phi l^2\right) - \frac{k_{il}\phi}{3\rho}\left(\frac{C_{Fe^{3+}}}{C_{Fe^{2+}}}\right)^{\alpha} \qquad [2.26]$$

where l [m] is the particle size, ϕ [$-$] the particle shape factor, N [cells.m^{-2}] the number of microorganisms residing on the mineral particle surface per unit surface area, N_{max} [cells.m^{-2}] the maximum number of microoganims that can occupy the mineral particle surface, ρ [mol.m^{-3}] the mineral sulphide density and k_{dl}, k_{il} the rate constants for direct leaching by the microorganisms and indirect leaching *via.* chemical leaching, respectively.

The shrinking core model proposed by Crundwell (1994) was updated to include transport phenomena of reactants and products to and from the particle surface through a porous product layer surrounding the particle surface (Crundwell, 1995). This was later abandoned as the model was based on both the direct and indirect mechanisms. As the direct mechanism was found not be valid (see § 2.1) the model was simplified to a model in which the direct chemical leaching reaction at the particle surface was rate limiting (Eq. 2.27), thus eliminating diffusion effects (Crundwell, 2001; 2005)

$$\frac{dl}{dt} = -k_s f\left(\underline{C}\right) \qquad [2.27]$$

where the rate of particle consumption is a function of the vector of concentrations in the reactor $f\left(\underline{C}\right)$ and the intrinsic chemical leach kinetics described by Eq. 2.23.

Brochot *et al.* (2004) assumed that the rate of particle dissolution is directly proportional to the combined first order kinetics for both the chemical leaching and microbial oxidation reactions (Eq. 2.28)

$$\frac{dl}{dt} = -k \qquad [2.28]$$

where k [m.s^{-1}] is the first order kinetic constant expressed in terms of the rate of diameter decrease (Brochot *et al.*, 2004).

The shrinking particle models proposed by Crundwell (1994) and Brochot *et al.* (2004) assumed that particles are uniformly distributed with sulphide mineral and free of any inert gangue material. Hence, the rate of particle consumption in these models is constant over the entire surface area.

Several authors have observed the generation of pores or pits on pyrite surfaces (Hansford and Drossou, 1988; Tributsch, 2001; Sand *et al.*, 1995; Crundwell, 2003) where microorganisms have attached themselves (Rawlings, 1998). Attachment of these microorganisms predominates at sharp edged surfaces or other surface imperfections (Bennett and Tributsch, 1978; Shrihari and Gandhi., 1990; Gehrke *et al.*, 1998). It has been shown that high concentrations of ferric ions are observed in the contact layer between the sulphide mineral and the microorganisms. This contact layer or Extracellular Polymeric Substance (EPS) layer plays an important role in the leaching reactions as it serves as a reaction space whereby the ferric ion reacts with the mineral (Rodriguez-Leiva and Tributsch, 1988; Sand *et al.*, 1995; Rawlings, 1998). It is believed that the majority of the leaching reactions occur within the EPS layer due to the high concentration of ferric ions within this region (Schippers *et al.*, 1996; Rodriguez-Leiva and Tributsch, 1988; Tributsch, 2001; Sand

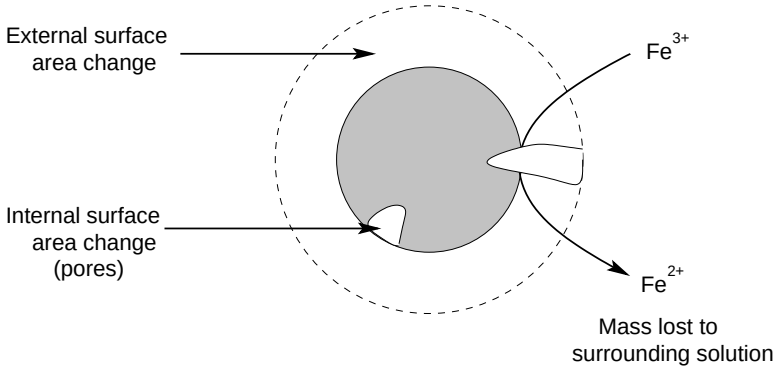

Figure 2.11: The shrinking core model with chemical reaction as the rate limiting step at the particle surface with pore formation

et al., 1995). The evidence that microorganisms attach to mineral sulphide surfaces *via.* an EPS layer for certain types of mineral sulphides and that leaching predominantly occurs at these sites, indicates that a shrinking particle model that incorporates the generation of pores or channels should be investigated.

Hansford and Drossou (1988) developed a propagating pore model in Eq. 2.29 based on the findings by Southwood and Southwood (1986). Hansford and Drossou (1988) assumed that the leaching rate along surface imperfections are constant and that a minimum L_i and maximum L_e pore length, closely related to the particle size, will develop prior to the pores becoming inactive. Further, it was assumed that at the end of the leaching process, all inactive pores had terminating lengths between the minimum and maximum pore lengths with equal diameters (Drossou, 1986).

$$r_v = \frac{6 r_{a_0} M_0}{\rho l_0} \cdot \frac{N^a}{N_0^a} \qquad [2.29]$$

where r_v [kg.m^{-3}.s^{-1}] is the volumetric pyrite oxidation rate, M_0 [kg.m^{-3}] the mass of solids per unit volume of solution, ρ the density of pyrite, l_0 the initial particle diameter, N^a the current number of active pores per unit surface area and N_0^a the initial number of active pores per unit surface area which has a maximum surface area based oxidation rate r_{a_0} [kg.m^{-2}.s^{-1}].

When developing a model to predict the rate of liberation of particle mass into solution, the model proposed by Hansford and Drossou (1988) provides a closer estimation to surface area changes due to the generation of pores or pits observed in bioleaching. The only disadvantage of this model is that pore diameters are considered equal and the external particle surface area or size remains constant.

When modelling the bioleach reactor it is evident that, due to acid-ferric leaching of the sulphide mineral, particle mass is lost to the surrounding aqueous phase. The approach taken determines how closely the change in particle mass can be predicted. Two methods have been proposed in the literature, namely the change in particle mass due to:

1. a uniform change in the external surface area (Crundwell, 1994; 1995; 2001; 2005; Brochot *et al.*, 2004), and

2. the generation of pores along surface imperfections (Hansford and Drossou, 1988)

In the first instance, it is assumed that the entire particle surface area is available for leaching while the second approach, the propagation of pores, assumes that leaching only occurs along active mineral sulphide veins at sharp edged surfaces. The fact that mineral sulphide particles both diminish in size and form pits or pores over the surface (Southwood and Southwood, 1986; Hansford and Drossou, 1988) indicate that both internal and external surface area changes occur and therefore a combination of the proposed models is required. The approach presented by Hansford and Drossou (1988) can be improved by incorporating both external and internal surface area changes with varying pore diameters (Figure 2.11). External surface area changes can be accounted for by the application of the shrinking particle model introduced by Yagi and Kunii (1961), while internal surface area changes can be similarly modeled with mass changes resulting from the formation of pores. By assuming that the pore diameters are normally distributed, the limitation imposed on the Hansford and Drossou (1988) model, in which pore diameters are assumed equal, can be overcome. Thus a shrinking particle model is introduced that can be used to approximate surface area changes frequently observed in bioleaching (Bennett and Tributsch, 1978; Southwood and Southwood, 1986; Hansford and Drossou, 1988; Blight *et al.*, 2000; Sand and Gehrke, 2006). Alternatively, an additional modelling parameter can be introduced that considers that a certain fraction of the particle surface is covered by active sulphide mineral ϕ_{MS}. By application of the shrinking particle model together with the restriction of active particle surface by the introduction of fraction ϕ_{MS}, the accuracy of the average change in the particle surface area can be improved when developing the bioleach reactor model.

In preceding sections 2.5.1−2.5.2, it is evident that both chemical ferric leaching and microbial oxidation kinetics are required when describing the bioleaching process. Further, as the particle surface area changes over time, an appropriate particle model that describes the dissolution of particle mass is necessary. Based on the assumptions made by various authors, the reactor models presented by these authors reflect whether the aforementioned modules have been integrated into their model development. In the following section, the performance equations of various published reactor models are presented.

2.5.3 Bioleach Reactor Modelling

In order to determine the overall reactor performance, material balances of the species in the solid and solution phases and the change in the particle surface area should be incorporated into the model formulation. If the mineral sulphide particles are sufficiently small and agitation is fast enough to uniformly suspend the particles in the aqueous phase, the mass balances can be composed under the simplifying assumption that the mean residence times of the two phases are equal.

When developing their model, Pinches *et al.* (1987); Hansford and Chapman (1992) and Hansford and Miller (1993) applied the steady state assumption to the continuity equation, where the total rate of effluent mass is equal to the rate of consumption of inlet mass. Pinches *et al.* (1987) proposed that the fraction of pyrite oxidised for N reactors in series could be described by Eq. 2.30

$$X_n = \left[X_{n-1}\frac{X_m}{k_m\tau_n} + \left[\frac{X_m}{2}\left(1-\frac{1}{k_m\tau_n}\right)\right]^2\right]^{\frac{1}{2}} + \frac{X_m}{2}\left(1-\frac{1}{k_m\tau_n}\right) \quad [2.30]$$

where τ_n and X_n are the mean residence time and the fraction of pyrite oxidised in tank n, respectively.

From the general CSTR material balance, the overall pyrite oxidation rate r^R over n tanks in series was given by Eq. 2.31, given that X_N is the overall conversion up to and including tank N. The oxidation rate r^R developed by Pinches *et al.* (1987) however is the average rate of pyrite bioleaching over n tanks in series and does not provide any information regarding the differing rates in the individual tanks in the series. As such, the conditions over each tank cannot be predicted and is thus limited to assuming that these are constant over the entire series.

$$r^R = \frac{C_i X_N}{\tau_{ov}} \quad [2.31]$$

where C_i is the concentration of pyrite in the feed to the first reactor and τ_{ov} the overall mean residence time over N reactors in series.

The proposed model was fitted to experimental data for a set of batch and continuous flow reactors. The rate constant k_m and the maximum fraction of pyrite available for oxidation X_M was determined using linear and non-linear curve fitting techniques. Pinches *et al.* (1987) found similar X_M values for both the batch and continuous experiments while the rate constant k_M for the two tests were significantly different with enhanced pyrite oxidation observed in the continuous flow reactors. The difference in the rate constants k_M was associated with the increased survival of the active microorganisms in the continuous flow system and/or the insufficient supply of carbon dioxide in the batch system (Pinches *et al.*, 1987).

Breed and Hansford (1999b) developed their reactor model based on the pseudo-steady state assumption that the rate of ferrous ion production due to chemical leaching equals the rate of microbial ferrous ion consumption 2.20. A steady state mass balance over the bioreactor for the microbial ferrous ion oxidation, which included the rate of microbial production in terms of the Monod microbial growth rate, was formulated. The result, shown in Eq. 2.32, indicated that the ferric/ferrous ion ratio $C_{Fe^{3+}}/C_{Fe^{2+}}$ in the bioreactor was independent of the mineral concentration, total iron concentration or ferrous ion concentration but only dependent on

the reactor residence time and microbial kinetic constants (Breed and Hansford, 1999b).

$$\frac{C_{Fe^{3+}}}{C_{Fe^{2+}}} = \frac{\tau q^{max}_{Fe^{2+}} Y_{Fe^{2+}x} - 1}{K} \quad [2.32]$$

where τ is the reactor mean residence time, $q^{max}_{Fe^{2+}}$ the maximum microbial specific ferrous ion utilisation rate, $Y_{Fe^{2+}x}$ the microbial yield defined as the number of moles of biomass produced per mole of Fe^{2+} oxidised and K the inhibition constant.

Similarly, a steady state balance for the chemical leaching of pyrite over the reactor, assuming kinetics in the form of Eq. 2.25, was formulated. Ignoring the distribution in particle size and that the particle surface area changes with reaction and solution contact time, Breed and Hansford (1999b) showed that the fraction of mineral sulphide leached X in Eq. 2.33 is a function of the solution redox potential, reactor mean residence time and mineral leach kinetics, and independent of the mineral sulphide concentration.

$$X = \frac{\frac{\tau}{15}\nu^{max}_{Fe^{2+}}}{1 + B\frac{C_{Fe^{2+}}}{C_{Fe^{3+}}} + \frac{\tau}{15}\nu^{max}_{Fe^{2+}}} \quad [2.33]$$

where $\nu^{max}_{Fe^{2+}}$ is the maximum specific pyrite oxidation rate and B is a kinetic constant.

The model was compared with data obtained from Breed and Hansford (1999b) for the bioleaching of pyrite in a continuous flow system. Although the microbial species used in the study by Hansford and Chapman (1992) was unknown, similar trends to data were obtained when the kinetic constants for *Leptospirrilum*-like and *Acidithiobacillus ferrooxidans* microorganisms were assumed.

Although the models by Pinches *et al.* (1987); Hansford and Chapman (1992), Hansford and Chapman (1992) and Hansford and Miller (1993) and the model by Breed and Hansford (1999b) are able to predict experimental trends for batch and continuous reactor systems, the reactor models do not take into account the rate contribution due to the change in particle surface area. Crundwell (1995) noted that the change in particle size during reaction can result in significant differences in model predictions and therefore the change in particle surface area should be included in the model formulation.

In the indirect mechanism, ferric ions are converted to ferrous ions liberating an additional Fe centre from the ore particle as ferrous (Eq. 2.2), indicating that particle mass is lost into the aqueous phase (Garrels and Thompson, 1960). In such a mechanism, the overall conversion of the mineral sulphide ore is dependent on the change in particle surface area and hence the particle-reactor exposure time.

Brochot *et al.* (2004) incorporated the solid phase component to their model by assuming that a non-uniformly sized population of particles shrink at a constant rate according to Eq. 2.28. The reduction in the particle size distribution was modelled by defining the partial feed rate for a distribution of particles $f(l)$ with diameter between $[l,\, l + dl]$ as $f(l)dl$. The

product size distribution $q(l)$ was calculated as indicated in Eq. 2.34.

$$q(l) = \int_0^\infty \left(\frac{l}{l+kt}\right)^3 f(l+kt)I(t)dt \qquad [2.34]$$

where $I(t)$ is the residence time distribution in the perfectly mixed reactor.

Assuming that particles in each size class have the same size, the particle size range was divided into equal finite elements $[l_i - \frac{\epsilon}{2},\ l_i + \frac{\epsilon}{2}]$ with element width ϵ. The difference between the resultant partial feed rates f_i and product flowrates q_i in size class i gave the quantity N_i of dissolved material in the solution phase (Eqs. 2.35 - 2.36) and hence the objective of the model.

$$\overline{N}_i = \sum f_i - \sum q_i \qquad [2.35]$$

or

$$N_i = \int_0^\infty f(l)dl - \int_0^\infty q(l)dl \qquad [2.36]$$

The partial flow rates obtained from the model and those obtained experimentally for different size classes were in reasonable agreement with each other, indicating to the the authors that the model developed was suitable for predicting pyrite and chalcopyrite bioleaching trends.

Crundwell (1994) applied a population balance model in which a balance of the solid mineral phase was formulated using a conservation of the particle number in the well mixed CSTR. The rate of leaching was expressed in terms of the rate of particle shrinkage which included terms for the change in particle surface area resulting from the direct and indirect mechanisms (Eq. 2.26, Crundwell, 1994). Reactor performance was evaluated by the solution of Eq. 2.37, the conservation of numbers balance, and 2.38, the reactor conversion, together with the mass balance for the ferrous and ferric ions in solution.

Conservation of numbers (size distribution)

$$V\frac{\partial\left[R(l)n(l,t)\right]}{\partial l} + \frac{\partial n(l,t)}{\partial t} = Qn_f(l,t) - Qn(l,t) \qquad [2.37]$$

Reactor conversion

$$1 - X = \frac{\int_0^\infty l^3 n(l,t)dl}{\int_0^\infty l^3 n_f(l,t)dl} \qquad [2.38]$$

where $R(l)$ is the rate of particle shrinkage represented by Eq. 2.26, $n(l,t)$ the number of particles of size l at time t in the inlet with f being the final number particles and Q the volumetric flow rate of slurry in the reactor.

Crundwell (2001) later simplified Eq. 2.37 to Eq. 2.39 based on the sub-process mechanism.

$$Qn_{in} = Qn_{out} - V\frac{dR(l)n_{out}}{dl} \quad [2.39]$$

where $R(l)$ is the rate of particle shrinkage represented by Eq. 2.27, n_{in} and n_{out} the inlet and outlet size functions, V the reactor volume.

Crundwell (1994) was able to fit the model to experimental data by Konishi *et al.* (1992) by varying the rate constants. The model was found to be in good agreement with the data.

In an attempt to compare models using a Segregation Flow Model (MacMullin and Weber, 1935; Danckwerts, 1953) as opposed to a Population Balance Model (PBM) approach (Hulbert and Katz, 1964), Crundwell (1995) noted that conversions up to 10% higher were erroneously predicted when the segregated approach, that he applied, was used. Using a first order rate of leaching as an example, Crundwell (2005) showed that the tank size required to obtain the same 90% conversion by means of the segregation model would require half the tank size calculated by the population balance model, thus under specifying process equipment.

The difference in these model predictions was attributed to the assumptions regarding the solution phase concentrations between the two model approaches (Crundwell, 2005). In the segregated flow approach, the solution phase concentrations between multiple tanks are evaluated by means of a single residence time distribution function, whereas in the population balance model approach, the concentration profile is predicted for each individual tank thus resulting in very different predictions (Crundwell, 1995).

Based on the literature, when developing a model for the bioleaching of sulphide mineral particles, the kinetics of the sub-process mechanism together with an appropriate model that describes the change in particle surface area is required. Additionally, the change in particle mass due to reaction and particle-solution contact time for all particles in the reactor should be considered. At present, the model proposed by Crundwell (2001; 2005) is the most comprehensive model which integrates all of the preceding factors into a single PBM. The models presented in the literature, however, assume that all particles in the reactor remain in the reaction space for the same period time and assumed steady state operation. This issue can be overcome by introducing the RTD to the model formulation which uncouples the variation in particle surface area with time to explicitly include a distribution in age in the reactor. To address the issue due to the discrepancies between the segregated flow and the PBM approach noted by Crundwell (2005), the diferences can be overcome by considering each reactor in series independently using a perfectly mixed RTD for each tank in series and noting that the particle size distribution entering subsequent tanks in the series change due to leaching. By developing an exit size distribution function, the concentrations and particle size distributions of the intermediate streams, which would be the inlet conditions to the subsequent tanks in the series, could be predicted and thus minimise over predictions associated with the segregation approach (see Chapter 4).

2.6 Conclusions

Reactor models are formulated to determine optimum operating conditions to maintain the system at maximum production rates. In modeling tank bioleaching it is essential that chemical leach and microbial oxidation kinetic rate expressions that are characteristic of the sub-process mechanism be included in the model formulation. Chemical leach rate expressions that are formulated in terms of the exposed mineral surface area per unit mass, and microbial oxidation kinetic rate expressions that incorporate the exchange of ions in solution due to microbial action should therefore be applied. Models focussing primarily on the microbial kinetics do not include the resulting rate contribution from the change in particle surface area in the reactor and therefore do not account for product inhibition resulting from the exchange of ions between the phases. The implication of this assumption is that the overall reaction rate would not include the change in particle mass due to the liberation of ferrous ions into solution. This assumption, however, has no practical application as it is evident in bioleaching experiments that sulphide mineral particles change in size during the leaching process. Also, since iron is liberated from the mineral particles during bioleaching, the implication is the particle mass is changing with time. Since particles of different sizes exist within the reactor with varying reactivities, estimation of the overall reaction rate should consider these changes.

The shrinking core or shrinking particle model is often used to describe the change in particle surface area when modeling the particle dynamics. The morphology and crystalline structure of the sulphide mineral is often ignored when considering the change in particle surface area. These mineralogical aspects are often not considered as the morphology and crystallography consider particle structure at the nano scale. An alternative to incorporating these in the particle model is to consider that the change in particle surface area is at the micro scale. The evidence that pores or pits are formed on the particle surface implies that assuming each spherical particle uniformly shrinks with reaction and is composed of only reactive sulphide mineral is not adequate to describe the change in particle surface area. The presence of inert gangue is ignored and thus particle dissolution due to chemical leaching is over- or underestimated. Improvements to these assumptions can be facilitated by incorporating a propagating pore model, in which pores are generated with particle-solution contact time, or by a combination of the former and latter particle models where both external and internal particle surface area changes are incorporated by defining the fraction of pure sulphide mineral in the ore particle.

By application of a population balance model, the resulting effect of the kinetics of bioleaching and the dissolution of a non-uniformly sized population of particles on the overall reactor performance, can be estimated.

3

Thesis Objectives

The objective of this study is to develop a reactor model for the bioleaching of sulphide mineral concentrates in the unsteady state mode of operation for the purpose of maximising the overall reactor performance. Presently, reactor models are formulated under the steady state assumption. In practice, flow rates to and from the reactor are seldom constant, which influences the reactor mean residence time. Unsteady state flows imply that the reactor inputs, such as, the solids loadings and the particle size distribution to the reactor are not constant. By developing an unsteady state model, the influence of inlet parameters to the reactor can be studied and effective control measures can be implemented to maximise overall production.

To develop such a model, the assumptions associated with previously developed models for bioleaching processes need to be relaxed thus eliminating these simplifying assumptions. As noted in the literature, published models may be classified according to which aspects of the bioleaching process have been considered. It is the aim of this study to incorporate both solid and aqueous phases by incorporating the kinetics of the sub-process mechanism in the model formulation to eliminate any over- or under-estimation of the overall bioleaching rate. The rate contribution of all particles in the reactor, based on the residence time of each of the particles in the reactor will be modeled. In continuous stirred tank reactors, particles ranging in size enter the reactor and remain in contact with the reaction phase for different periods of time. This variation in particle residence time indicates that a distribution in time or age exists within the reactor and that due to the finite rate of dissolution a relationship will exist between particle dissolution rate and particle-solution contact time. A novel approach, based on the segregation model (Danckwerts, 1953), is therefore chosen to model tank bioleach reactors. By application of the segregation approach, the variance in particle properties based on the particle residence time and inlet size can be integrated into the model framework to determine their resultant influence on the overall reactor performance.

Most published reactor models are formulated by applying the assumption that the bioleaching process is under steady state and is perfectly mixed. By developing the model using a generalised population balance famework, the particle age or Residence Time Distribution (RTD) theory into the reactor model, unsteady state operation can be studied.

The reactor model formulated will be used for developing process control strategies under industrial conditions and will be formulated in a generic form to allow for a range of sulphide mineral ores to be investigated.

To optimise the process outputs, a rigorous dynamics analysis of the system will be performed in batch and continuous flow reactor systems. During this analysis, process parameters which influence steady state operation will be identified to establish their impact on the process production rate. A dynamics analysis will initially be performed using a constant particle surface area assumption. Thereafter, the dynamics analysis will be extended to include a time-varying particle surface area determined from the developed PBM. We would expect that this would be a better model with improved prediction accuracy. By applying a constant particle surface assumption prior to including the variances in the particle surface area with solution contact time, a better understanding of the influence of each of the process variables on the dynamic structure of the system can be identified. As such, effective control strategies that maximise the overall bioleaching rate will be attempted.

A steady state reactor model cannot effectively predict unsteady state behaviour nor can the conditions of each individual reactor successfully determined. Generally, when developing reactor models, RTDs are applied to perfectly mixed systems at steady state, assuming flows across the boundaries of the reactor are constant. Any fluctuations in the system flow rates affect the residence time of the particles within the reactor. This type of unsteady behaviour will be incorporated in the formulated steady state reactor model by applying recent developments in RTD theory, where the change in fluid components can be characterised by real time and the exposure period of the particles to the reaction environment. By studying the influence of pertubations to process inputs to the bioleach reactor, the resultant effect on the RTD can be determined. Procedures to maximise the overall rate in the steady state system will be extended to the unsteady state mode of operation. Control strategies based on the influence of unsteady state inlet conditions will be presented with the objective of maximising metal extraction rates.

In this thesis, it is hypothesized that feasible operating points exist at which the rate of bioleaching is higher than those defaulted to by industry. By performing a dynamics analysis on the bioleaching reactor system, it is further hypothesized that operation at these higher rate regions can be identified and achieved. Moreover, the unsteady state model can be used to determine the optimal input trajectory that can be applied to maintain operation in the higher rate region.

Scope and Limitations of this Thesis

This study focusses on maximizing the reactor performance of the bioleach system by investigating the influences of reactor inputs to the overall reaction rate. This is achieved by performing dynamic analyses on both batch and continuous flow reactor systems and

determining the resultant changes in the dynamic structure of the system due to disturbances in the reactor inlet conditions.

The model development in this thesis will assume that the supply of oxygen and carbon dioxide to the bioleach system is sufficient to ignore any mass transfer limitations. Further, the subprocess mechanism of bioleaching will be limited to the acid ferric leaching of the sulphide mineral and the microbial oxidation of ferrous ions to ferric ions. The microbial oxidation of reduced sulphur compounds to elemental sulphur or sulphate is not incorporated in the model formulation. This is due to the complex nature of the sulphur mechanism and the lack of consensus in the literature relating to which reduced sulphur intermediates are present in the bioleaching process.

The primary focus of this study is thus to incorporate both the acid ferric leaching and the microbial oxidation reactions in the reactor model and to explore the rate contribution of changing particle surface areas (due particle-solution contact time) on the overall reactor performance. Also, this study will attempt to introduce various control strategies to maximize the production rate for a tank bioleach system that operates in either steady state or unsteady state mode.

Validation Procedure

In this study, models developed for the bioleaching of sulphide mineral concentrates are coded using SciPy, an open source Python programming language developed by Jones *et al.* (2001). Reactor models are validated against experimental or pilot plant data obtained from literature or industry using optimisation tools *fmin* and/or *leastsq*. The *fmin* package is based on the Nelder-Mead simplex algorithm. The package is used to find the minimum of a function with one or more variables. The Nelder-Mead method is successfully used in optimisation problems, however it can be slow and result in poor performance, converging to non-stationary points in high-dimensional problems (Jones *et al.*, 2001). As such, this method is used as an initial estimate for the *leastsq* package. The *leastsq* package is based on the Levenberg-Marquardt algorithm. The algorithm is commonly used to minimise non-linear functions using the least squares curve fitting method. The algorithm is very robust and can find the minimum of a function even when the initial estimate is far from the solution (Jones *et al.*, 2001; Faires and Burden, 1993).

4

Steady State Continuous Flow Tank Bioleach Modeling

4.1 Introduction

REACTOR models are developed to determine the best operating conditions for maximum production. This is achieved by combining the knowledge of the reaction kinetics and mechanisms of the reactions to obtain a better understanding, design and control of the reactor (Coker, 2001). A number of bioleach reactor models have been published, many of which focus on the biological aspects of the system (Hansford and Miller, 1993; Hansford and Chapman, 1992; Breed and Hansford, 1999b; Pinches *et al.*, 1987). These reactor models fail to consider the impact of acid-ferric leaching on the reactor performance.

The reactor model proposed by Crundwell (1994; 1995; 2001; 2005) incorporated the acid-ferric leach and microbial oxidation kinetics and utilized a distribution of mineral particle sizes to predict reactor performance by means of a population balance model (PBM). However, the model is limited to perfectly mixed systems at steady state. Given the scale of bioleach processes, such assumptions are unrealistic.

One tool for improving the design, operation and control of these processes is an unsteady state reactor model. Before this ambitious goal, the steady state version is attempted here. The model developed in this study incorporates biooxidation kinetics, acid-ferric leach kinetics as well as the effect of particle size and age distributions on reactor performance using a modified PBM approach that requires the numerical solution of only a system of ODEs with well defined initial conditions, rather than boundary value problems.

To develop such a model from first principles, using pyrite as a model compound, the intrinsic kinetics of the reactions involved in the bioleaching process needs to be understood. A multi-step process which includes the acid-ferric leaching and microbial oxidation of pyrite described in reactions Eq. 2.2 and Eq. 1.2 respectively, repeated here for illustration purposes, are used to describe bioleaching.

$$FeS_2 + 14Fe^{3+} + 8H_2O \rightarrow 15Fe^{2+} + 2SO_4^{2-} + 16H^+ \qquad [2.2]$$

$$4Fe^{2+} + O_2 + 4H^+ \rightarrow 4Fe^{3+} + 2H_2O \quad [1.2]$$

The particle-solution dynamics involve the loss of particle mass due to reaction, and consequently the change in particle surface area with the particle residence time resulting from the two bioleaching subprocesses (Eqs. 2.2 and 1.2). Numerous authors have attempted formulating the rate expression for reaction 2.2 in terms of exposed mineral surface area per unit mass of solution (McKibben and Barnes, 1986; Rimstidt and Newcom, 1993; Williamson and Rimstidt, 1994; May *et al.*, 1997). Since the focus in this study is reactor engineering rather than the kinetics, the simplest available kinetics is used for model development. The kinetic rate expression proposed by McKibben and Barnes (1986) (Eq. 4.1, see also Table 2.1) is used.

$$r''_{FeS_2} = k\left(\frac{C_{Fe^{3+}}}{C_{H^+}}\right)^{0.5} \quad [4.1]$$

where k is the intrinsic surface reaction rate constant [mol.s^{-1}.m^{-2}] and $C_{Fe^{3+}}$ and C_{H^+} are the concentrations of the ferric ions and protons in solution [mol.m^{-3}].

The microbial oxidation reaction rate in Eq. 4.2 is based on modified Michaelis-Menton and Monod-type kinetics, and was simplified by Hansford (1997). This rate expression was selected due to its universal application in both mesophilic ($18 - 45^oC$) and thermophilic ($60 - 80^oC$) bioleaching of sulphide minerals over a range of experimental conditions (Ojumu *et al.*, 2009; Searby, 2006). It is important to note that the influence of heavy metals on the overall rate is not the focus of the reactor model development. These inhibitory influences on the overall rate can be easily incorporated into the model by application of a microbial oxidation rate expression similar to those presented by Özkaya *et al.* (2006) and Nurmi *et al.* (2009) (see Table 2.2)

$$r_{Fe^{2+}} = \frac{C_X q^{max}_{Fe^{2+}}}{1 + K\frac{C_{Fe^{3+}}}{C_{Fe^{2+}}}} \quad [4.2]$$

where $q^{max}_{Fe^{2+}} = 0.0019$ mol Fe^{2+}.mol carbon^{-1}.s^{-1} is the maximum microbial specific ferrous iron utilisation rate, $K = 0.0005$ [$-$] the inhibition constant and C_X [mol.m^{-3}] the concentration of the biomass which is obtained by dividing the rate of CO_2 consumed by the dilution rate [s^{-1}]. The microbial oxidation reaction rate constants were taken for the bioleaching of sulphide minerals in the presence of *Leptospirillum ferrooxidans* (Boon and Heijnen, 1998a).

4.2 Model Formulation

When developing the bioleach reactor model, the reactor bioleaching rate r^R and conversion X^R will be assumed to be the variables that determine reactor performance, and hence the objectives of the model formulation. The conversion X^R of pyrite ore to products is given by the relative difference between the inlet pyrite mass $\dot{M}^R_{inlet}$ [kg.s^{-1}] and outlet pyrite mass

$\dot{M}^R_{outlet}$ [kg.s^{-1}] (Eq. 4.3).

$$X^R = 1 - \frac{\dot{M}^R_{outlet}}{\dot{M}^R_{inlet}} \quad [4.3]$$

The average rate of pyrite surface removal per unit mass of particle for a given size is defined as the particle leaching reaction rate r' [mol.s^{-1}.kg^{-1}]. The reaction rate can be described by the shrinking particle model (Yagi and Kunii, 1961) As the reaction proceeds, the unreacted mineral particle is reduced in size while liberating mass into the aqueous phase. The available particle surface area then drops with increasing particle-solution exposure time.

The inlet and outlet mineral sulfide ore mass flowrates are not equal since the bioleaching reaction effectively transfers particle mass to the solution phase. From the continuity equation and applying the steady state assumption, the total rate of effluent pyrite ore mass will be equal to the rate of consumption of the inlet mass (Eq. 4.4).

$$\dot{M}^R_{outlet} = \dot{M}^R_{inlet} - r^R \quad [4.4]$$

where r^R [mol.s^{-1}.m^{-3}] is the reactor bioleaching rate, which is the overall reactor leaching rate (see § 4.3). Since the intrinsic surface reaction rate r'' [mol.s^{-1}.m^{-2}] is area-based, the formulation of the reactor bioleaching rate r^R becomes complicated by the dependence of particle surface area on particle-reactor exposure time (residence time) and inlet particle size. Furthermore, there are distributions of reactor residence time and particle size that complicate developing the reactor bioleaching rate r^R. The following sections develop the relationships among the rates r'', r' , and r^R.

4.3 Particle Dynamics

If the rate at which particle mass is liberated into solution is due to particle-solution contact time, a relationship between the particle size and the particle age should be established.

If we consider a particle entering a reactor at time t_0 [s] and present at time t [s], the particle will have resided there $\theta = t - t_0$ time units.

Generally, the feed stream will have particles of various initial sizes l_0 [m]. In the case of spherical geometry, l_0 may be the initial particle diameter. The corresponding initial specific surface area A^p_0 is then $\frac{\pi l_0^2}{M^p_0}$ [m^2.kg^{-1}] where M^p_0 is the initial mass of the particle.

Assuming steady reaction conditions, the rate of change of particle mass will be the product of the intrinsic surface reaction rate r'' [mol.s^{-1}.m^{-2}], the particle surface area A [m^2] and molar mass MM_{FeS_2} [kg.mol^{-1}] (Eq. 4.5). As particle mass is liberated into the solution phase due to reaction and solution contact time θ, the particle surface area $A(\theta)$ and hence the particle mass $M^p(\theta)$ are functions of the particle age.

$$\frac{dM^p}{d\theta} = -r'' A(\theta) MM_{FeS_2} \quad [4.5]$$

The particle surface area is the product of the specific surface area and the particle mass $A(\theta) = A^p(\theta)M^p(\theta)$.

Assuming spherical particle geometry and constant particle density, the particle surface area and volume can be expressed in terms of size, and substituted into Eq. 4.5 to obtain a differential in particle size (Eq. 4.6 and 4.7).

$$\frac{d}{d\theta}\left(\frac{\pi}{6}l^3\right) = \frac{-r''}{\rho} \cdot \pi l^2 \cdot MM_{FeS_2} \quad [4.6]$$

By chain differentiation of the LHS of Eq. 4.6, the surface area term πl^2 cancels out resulting in Eq. 4.7.

$$\frac{dl}{d\theta} = \frac{-2r''}{\rho} \cdot MM_{FeS_2} \quad [4.7]$$

If the solution concentrations are constant with respect to time, then the intrinsic reaction rate is also constant, and as such Eq. 4.7 can be integrated over particle age θ'=$[0;\theta]$ with initial condition $l(\theta = 0) = l_0$, to yield the relationship between the particle size and age (Eq. 4.8).

$$l(\theta) = \begin{cases} l_0 - \left(\frac{2r''}{\rho}MM_{FeS_2}\right) \cdot \theta & \text{if } 0 \leq \theta < \frac{\rho \cdot l_0}{2r''MM_{FeS_2}} \\ 0 & \text{if } \theta \geq \frac{\rho \cdot l_0}{2r''MM_{FeS_2}} \end{cases} \quad [4.8]$$

Equation 4.8 reinforces that the particle size and hence the particle surface area is a function of age and initial size (Eq. 4.9). Similarly, since the particle leaching rate is the product of the intrinsic surface rate r'' with particle surface area $A(\theta, l_0)$, it follows that the particle leaching rate is also a function of age and size (Eq. 4.10).

$$A(\theta, l_0) = \pi l(\theta, l_0)^2 \quad [4.9]$$

$$r'(\theta, l_0) = r''A^p(\theta, l_0) \quad [4.10]$$

The particle mass M^p can be expressed as a function of the particle age and initial size $M^p(\theta,\, l_0)$ using Eq. 4.8 to obtain the conversion of a single particle X^p (Eq. 4.11).

$$X^p(\theta, l_0) = 1 - \frac{M^p(\theta, l_0)}{M^p(l_0)} \quad [4.11]$$

Figure 4.1 illustrates the dynamics of the particle conversion with the particle age θ [s] and initial size l_0 [m]. Eq. 4.8 indicates the rate at which the particle size or mass decreases with age. Clearly, with an increase in particle age and a decrease in particle size, the particle conversion will increase. The conversion gradually reaches the maximum value (unity) as the particle is consumed with age.

In this section the relationship amongst initial size, age and rate was established for a single particle. Since the particle population in the reactor is distributed with respect to initial size and age, the overall reaction rate can only be predicted by accounting for contributions from all possible initial sizes and ages.

The following section will therefore establish the rate contribution of all particles in the

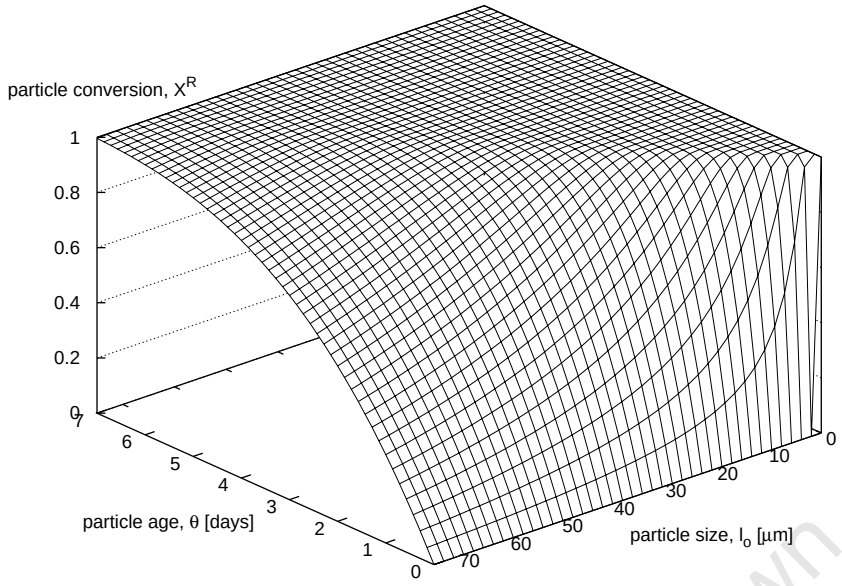

Figure 4.1: Plot of the particle conversion with particle age θ and initial size l_0

reactor by defining the distribution of particles based on their initial size and age.

4.4 Distributions in Particle Age and Size

In developing reactor age and size distribution, we consider a set of particles that enter the reactor at time t_0 with the size distribution $f_0(l_0)$ [m^{-1}], defined such that $f_0(l_0)\Delta l_0$ is the fraction of particles at the inlet in the size range [l_0, l_0+Δl_0]. The size distribution inside the reactor is $f_0(l_0)$ (Figure 4.2).

Furthermore, since a non-trivial distribution in age θ generally exists, we require the internal residence time distribution $I(\theta)$ defined such that $I(\theta)\Delta\theta$ is the fraction of particles in the reactor in the age range $[\theta, \theta + \Delta\theta]$.

When combining the particle size $f_0(l_0)$ and age $I(\theta)$ distributions with the particle dynamics through a complete segregation approach, the overall reactor bioleaching rate r^R [$\mathrm{mol.s}^{-1}.\mathrm{m}^{-3}$] can be predicted.

4.5 Macroscopic Balances

To determine the overall reactor performance, the solution and solid phase contributions to the overall reactor bioleaching rate need to be determined. The first step in modelling the

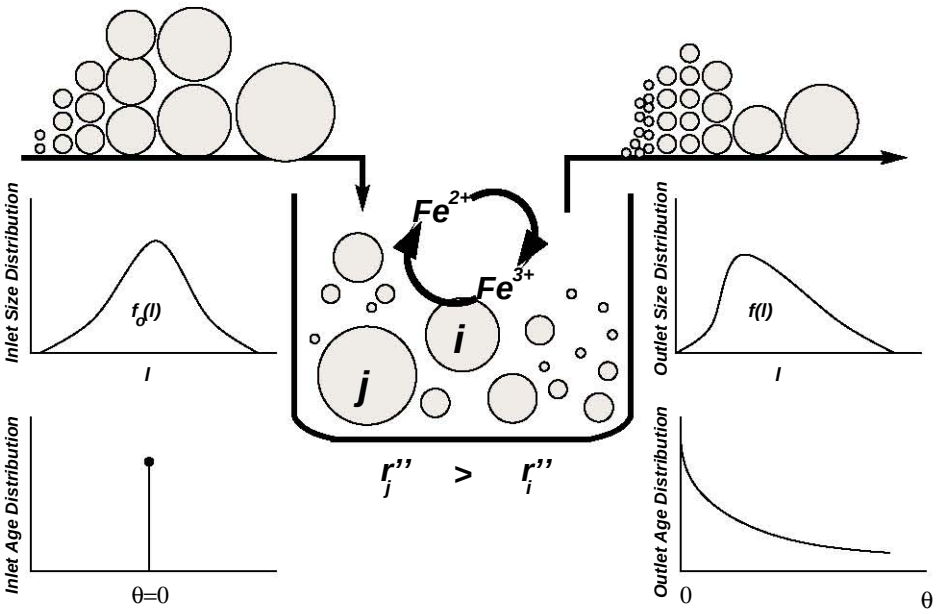

Figure 4.2: Model formulation for the overall reaction rate r^R in a bioleach reactor

reactor is therefore to write material balances for these phases. Assuming perfect mixing in each phase, species balances yield Eqs. 4.12 and 4.13.

Solution phase components

$$\frac{dC_i}{dt} = \frac{C_{i,inlet} - C_{i,outlet}}{\tau_{solution}} \pm \xi_i r^R - \gamma_i r_{Fe^{2+}} \qquad [4.12]$$

Solid particle phase

$$\frac{dC_{FeS_2}}{dt} = \frac{C_{FeS_2,inlet} - C_{FeS_2,outlet}}{\tau_{solid}} - \xi_{FeS_2} r^R \qquad [4.13]$$

where ξ_i and γ_i are the stoichiometric coefficients of species i for reactions 2.2 or 1.2 respectively and and are assigned negative values for reactants and positive values for products. The first terms on the RHSs of the material balances 4.12 and 4.13, assuming perfect mixing, account for the flow of species into and out of the reactor, whereas the other RHS terms are the rates of change due to reaction(s).

Assuming uniform suspension of particles in the reactor, the mean residence times for the solid and solution phases will be equal $\tau_{solid} = \tau_{solution}$.

Since the solution phase is assumed perfectly mixed at the molecular level, the biooxidation rate $r_{Fe^{2+}}$ [mol.s^{-1}.m^{-3}] is the same at all points within the reactor. On the other hand, the concentration of pyrite varies from particle to particle, which complicates estimation of the reactor bioleaching rate r^R. The objective in the following section will be to formulate the reactor bioleaching rate r^R.

The models developed can be distinguished by the initial size distribution used in predicting reactor performance. At the outset a trivial mono-sized particle feed, that remains the same

size during the course of the reaction, is considered. This simplifying assumption is then eliminated in the following models to one that considers an initial size distribution that undergoes a change in size due to reaction and particle solution contact time (Eq. 4.8). The models developed are then validated against pilot data obtained from Hansford and Miller (1993) for a series of cascading tanks to determine the models suitability at predicting reactor performance.

The following model developments are general to metal sulphides, hence the subscript FeS_2 will be replaced by MS.

4.6 Reactor Models

4.6.1 Model 1: Constant, Uniform Specific Surface Area

In Model 1 we consider mono-sized spherical particles that enter the bioleach reactor. It is assumed that all particles entering the reactor are of the same size, and will remain at this size in spite of leaching. The particle specific leaching rate r' will therefore be the same for all particles in the reactor no matter what age they may have resided there. The particle specific leaching rate r' [mol.s^{-1}.kg^{-1}] is the product of the intrinsic surface reaction rate r'' [mol.s^{-1}.m^{-2}] and the particle specific surface area A_0^p [m^2.kg^{-1}](Eq. 4.14).

$$r' = r'' A_0^p \quad [4.14]$$

The overall reactor bioleaching rate r^R may then be obtained as the product of the particle specific leaching rate r' and the constant total reactor solids mass as given by Eq. 4.15.

$$r^R = r' C_{MS,inlet} MM_{MS} \cdot \phi_{MS} \quad [4.15]$$

where $C_{MS,inlet}$ [mol.m^{-3}] is the molar concentration of the mineral sulphide ore in the inlet stream into the reactor, MM_{MS} the molar mass of the pure mineral sulphide ore [kg.mol^{-1}] and ϕ_{MS} the fraction of the pure mineral sulphide in the ore [−].

The overall reactor conversion X^R may then be obtained from the product of the overall reactor bioleaching rate r^R with the mean residence time relative to the inlet mineral sulphide ore concentration $C_{MS,inlet}$ (Eq. 4.16).

$$X^R = \frac{r^R \tau}{C_{MS,inlet}} \quad [4.16]$$

In this model the rate of dissolution and the mass of solids remain constant throughout the course of reaction, the conversion of the mineral sulphide particles X^R is directly proportional to the mean residence time.

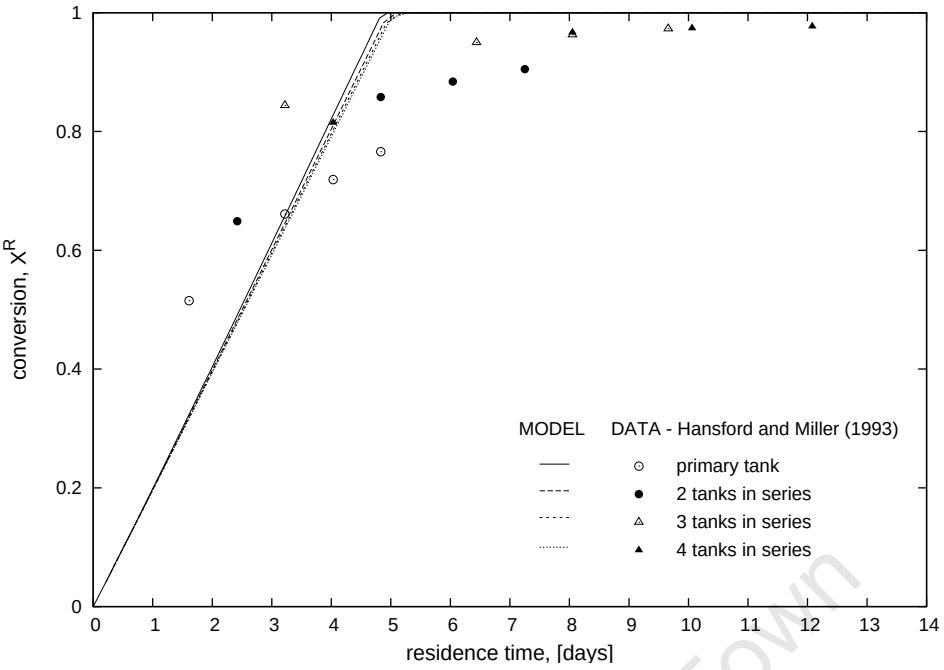

Figure 4.3: Reactor bioleaching conversion for Model 1 (constant specific surface area) versus pilot plant data (Hansford and Miller, 1993)

In reality, sulphide mineral particles of varying particle sizes enter the bioleach reactor and remain in the reactor for different periods of time or age. This model therefore has no practical application but serves to illustrate how restrictive assumptions, such as the bioleaching of sulphide mineral particles with constant, unchanging particle surface areas, in developing a reactor model can result in inaccurate performance predictions.

The model was validated against pilot plant data (Hansford and Miller, 1993) for a cascade of stirred tanks in series with the primary reactor (10 m^3) having a reactor volume twice that of the subsequent reactors (5 m^3). It was assumed during the model validation that the reactor volume for each of the tanks in the series remained constant throughout the bioleaching process. The conversion predicted by the model was fitted to the measured conversions by adjusting only the acid-ferric leaching rate constant k (Eq. 4.1). The solution concentrations of each of the tanks were determined from the material balances (Eq. 4.12) and used as the inlet concentrations for the subsequent tank in the series. As sufficient data points are available at both low and high (close to 100 %) conversions, reasonable data fitting techniques may be applied to determine the suitability of the model to predict reactor performance.

Model validation, with an acid-ferric rate constant $k = 3.9 \times 10^{-3}$ kg.m^{-2}.day^{-1}, with the pilot plant data shows the expected (see Eq. 4.16) linear increase of conversion with residence time for each tank (Figure 4.3). The pilot plant data shows that conversion changes with residence time and with different reactor configurations. This model, however, does not incorporate the effect of different reactor configurations on the overall conversion, making conversion independent of the number of reactors. The conversion for the reactors in the

series is however dependent on the solution concentrations and thus the slope of the modelled conversion changes.

Clearly, the fit is rather poor, and the simplifying assumption of constant particle size must be eliminated. The following model incorporates age and hence surface area distributions.

4.6.2 Model 2: Age-dependent particle size distribution

In Model 2 the inlet stream to the reactor is assumed to contain particles of the same size that will be exposed to the solution phase in the reactor for different periods of time. The particle surface area A^p is therefore age dependent, resulting in a particle leaching rate r' [mol.s^{-1}.kg^{-1}] that varies from particle to particle (Eq. 4.17).

$$r'(\theta) = r'' A^p(\theta) \qquad [4.17]$$

where the intrinsic surface reaction rate r'' [mol.s^{-1}.m^{-2}] depends only on the solution concentrations.

Since $I(\theta)\Delta\theta$ is the fraction of particles in the age range $[\theta,\ \theta + \Delta\theta]$, the average particle leaching rate $\overline{r^p}$ will be the sum of all rate contributions r' [mol.s^{-1}.kg^{-1}] in all particle fractions $I(\theta_i)\Delta\theta_i$ over age intervals $[\theta_i, \theta_i + \Delta\theta_i]$. The overall reactor bioleaching rate r^R is therefore the product of the average particle leaching rate $\overline{r^p}$ [mol.s^{-1}.m^{-3}] with the total number of particles N^T integrated over the age interval $[0, \infty]$ (Eq. 4.18).

$$r^R = \int_0^\infty r'(\theta) \frac{M^p(\theta)}{V^R} \phi_{MS} N^T I(\theta) d\theta \qquad [4.18]$$

Model 2 was validated against the pilot plant data (Hansford and Miller, 1993) using the simplifying assumption that the mean particle size from the preceding tank is the inlet particle size of all particles to the subsequent tank in the series. The conversion data points were fitted using the same method applied in Method 1 for the case of a perfectly mixed reactor (Figure 4.4).

In contrast to Model 1 (§ 4.6.1), the pilot plant data and the model, with an acid-ferric leach rate constant $k = 6.9 \times 10^{-3}$ kg.m^{-2}.day^{-1}, are in close agreement at low conversions, although the model's ability to predict reactor performance at higher conversions is limited. As mentioned previously, particles within the reactor remain in contact with the reaction phase for differing periods of time. In reality, metals leached from the particle would result in a change in particle surface area. The rate contribution per particle should therefore decrease over time. The assumption that the particle size will remain constant from tank-to-tank would subsequently result in an over-estimation of the overall reaction rate. This would account for the poor model predictions at high conversions in Figure 4.4.

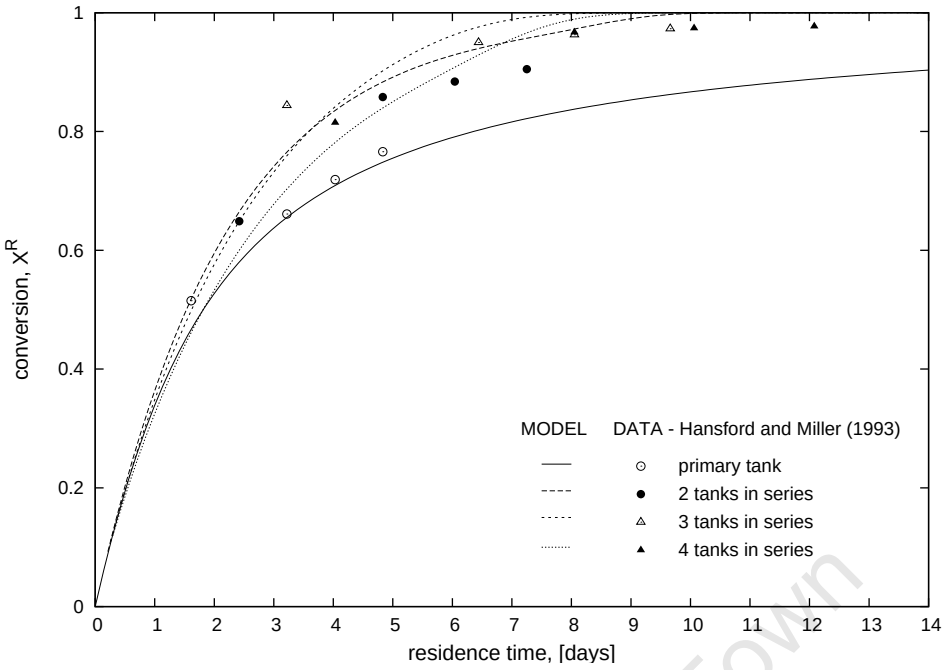

Figure 4.4: Reactor bioleaching conversion for Model 2 (mono-sized feed particles) versus pilot plant data (Hansford and Miller, 1993)

While Model 2 is an improvement on Model 1, it still assumes uniform particle size in the feed stream whereas in reality the typical feed stream is not uniform. In the following model, the size restrictions applied in Models 1 and 2 are relaxed.

4.6.3 Model 3: Non-trivial inlet particle size with age distribution in the reactor

In relaxing the single -size assumptions applied in Models 1 (§ 4.6.1) and 2 (§ 4.6.2), we now acknowledge that the inlet stream contains a non-trivial distribution in particle size. As in Model 2, a reactor age distribution is used.

With regard to the particle dynamics, larger particles will leach at a greater rate than smaller particles due to the larger availability of surface area, therefore the particles will leave the reactor with a different size distribution than upon entering the reactor. If perfect mixing is assumed, the particle age and size distributions within the reactor will be the same as in the outlet stream.

As the particle surface area is a function of the particle residence time and the inlet particle size, the particle leaching rate r' [mol.s^{-1}.kg^{-1}] can be expressed as follows (Eq. 4.19):

$$r'(\theta, l_0) = r'' A^p(\theta, l_0) \qquad [4.19]$$

We assume that the inlet particle size distributions $f_0(l_0)$ is statistically independent of the reactor internal age distribution $I(\theta)$. The assumption of perfect mixing also implies that

the particle size distribution inside the reactor must be the same at the exit, and hence the rate of exit of any particle does not depend on the particle size.

The product of the size and age fractions $f_0(l_0)\Delta l_0 I(\theta)\Delta\theta$ is therefore the fraction of particles in the age range $[\theta, \theta + \Delta\theta]$ and size range $[l_0, l_0 + \Delta l_0]$ in the reactor. Hence, the overall reaction rate can be determined using the segregation approach applied in Eq. 4.20.

$$\bar{r^p} = \sum_{j}^{n}\sum_{i}^{m} r'(\theta_i, l_{0j})\frac{M_i^p(\theta_i, l_{0j})}{V^R}\phi_{MS} I(\theta_i) f_0(l_{0j})\Delta\theta_i \Delta l_{0j} \qquad [4.20]$$

where Eq. 4.21 is the differential form of Eq. 4.20.

$$r^R = \int_0^\infty\int_0^\infty r'(\theta, l_0)\frac{M^p(\theta, l_0)}{V^R}\phi_{MS} N^T I(\theta) f_0(l_0) d\theta dl_0 \qquad [4.21]$$

Alternatively, the segregation model may be used to determine the overall conversion XR in Eq. 4.22

$$X^R = \int_0^\infty\int_0^\infty X^p(\theta, l_0) I(\theta) f_0(l_0) d\theta dl_0 \qquad [4.22]$$

where $X^p(\theta, l_0)$ is the conversion of a single particle in terms of age and size as shown in Eq. 4.11.

The model simulation result was compared with plant data (Hansford and Miller, 1993) and plotted in Figures 4.5 and 4.6 using the same validation method applied for Models 1 and 2, using the outlet size distribution from tank $n-1$ as the inlet size distribution for the subsequent tank n in the series $f_{0,n}(l_{0,n}) = f_{n-1}(l_{n-1})$.

A model that utilises a RTD that only accounts for the distribution in total system age, for example a tanks-in-series RTD, is limited to predicting conditions for only the inlet stream to the first tank and the outlet stream from the last tank in the series assuming that the conditions over each reactor is constant. By considering each reactor independently using a perfectly mixed RTD for each tank in the series and noting that the particle size distribution entering subsequent tanks in the series change due to leaching, the conditions of each of the intermediate streams can be determined.

Since the mass fraction of particles $f_{0,n+1}(l_{0,n+1})\Delta l_{0,n+1}$ entering the subsequent tank is the relative mass difference of all particles M^p in the size range $[l_0, l_0 + \Delta l_0]$, the inlet size distribution of particles in the following tank will be the inverse product of the total initial mass of all particles entering the tank and the differential in particle mass with the inlet particle size (Eq. 4.24)

$$f_n(l_n)\Delta l_n = \frac{M^p(l_{0,n}) - M^p(l_{0,n} - \Delta l_{0,n})}{M^p_{total}} \qquad [4.23]$$

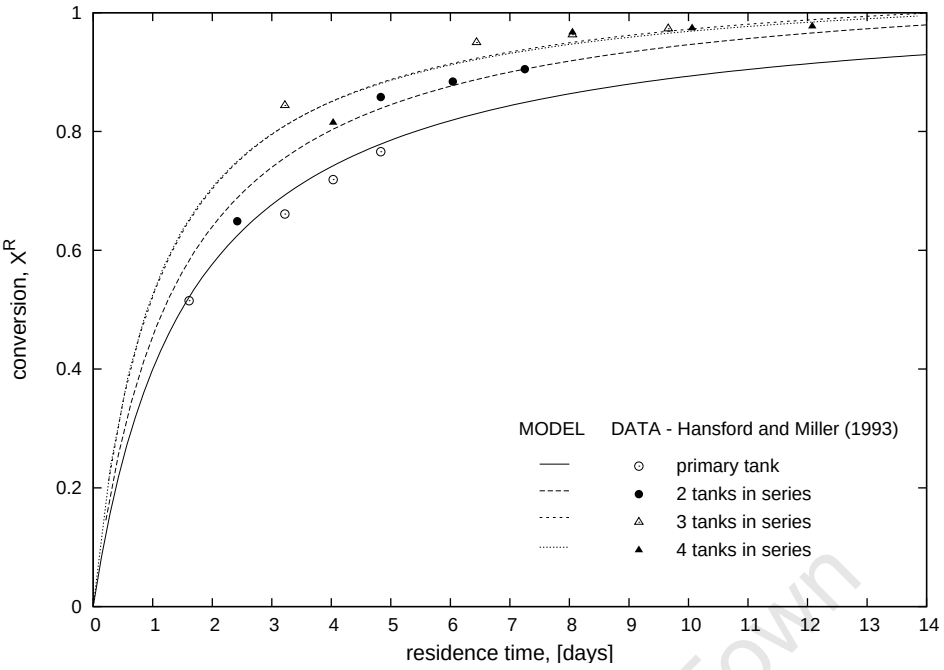

Figure 4.5: Reactor bioleaching conversion for Model 3 (age and size distributional effects) versus pilot plant data (Hansford and Miller, 1993). Note that for the given operating parameters, increasing the number of tanks from 3 to 4 in series does not significantly enhance overall reactor performance.

as such

$$f_{0,n+1}(l_{0,n+1}) = \frac{1}{\int_0^\infty \int_0^\infty M^p(l_{0,n}) I(\theta) f_{0,n}(l_{0,n}) d\theta dl_{0,n}} \cdot \frac{dM^p(l_{0,n})}{dl_{0,n}} \qquad [4.24]$$

The average bioleaching reaction rate $\overline{r^R}$ in each subsequent tank in the series is thus based on the outlet size distribution from the preceding tank $f_{0,n}(l_{0,n}) = f_{n-1}(l_{n-1})$ (Eq. 4.25)

$$\overline{r_n^R} = \int_0^\infty \int_0^\infty r'_n(\theta, l_{0,n}) \frac{M_n^p(\theta, l_{o,n})}{V_n^R} \phi_{MS} f_{0,n}(l_{0,n}) I(\theta) d\theta dl_{o,n} \qquad [4.25]$$

Figure 4.5, with acid-ferric leach rate constant $k = 2.2 \times 10^{-3}$ kg.m^{-2}.day^{-1}, indicates the expected increasing trend in conversion with residence time. With an increase in the number of tanks the conversion increases for the same mean residence time. This is to be expected since more efficient use of reactor volume is made and therefore a higher conversion is achieved as compared to a single tank (Figure 4.5). As such, with an increase in the number of tanks in series, the overall reactor performance approaches plug flow behaviour.

The model was further compared with the average bioleaching reactor rate for each tank in the series. From Figure 4.6 it is clear that the model, which is a function of the age and initial size distribution, is able to predict the rates at each mean residence time.

The model's ability to predict the pilot plant data is greatly improved over Models 1 and 2. In contrast to Model 2, Model 3 is able to achieve good agreement with the data at both

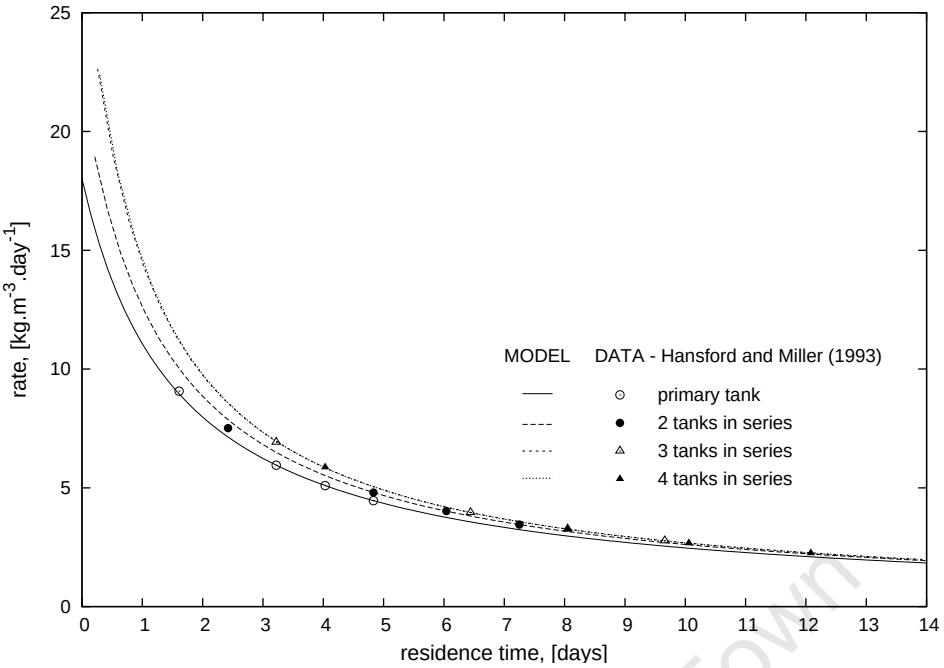

Figure 4.6: Overall reactor bioleaching rate for Model 3 (age and size distributional effects) versus pilot plant data (Hansford and Miller, 1993). As with Figure 4.5, the overall reactor performance is not significantly enhanced when increasing the number of tanks in series from 3 to 4.

high and low conversions.

4.7 Conclusions

Three reactor models were formulated using a segregation approach. The first model did not consider the effects of age or size on the overall reaction rate while the second model incorporated the effects of age on the particle surface area and hence the reactor bioleaching reaction rate. The advantage of including particle age in the latter model was immediately apparent by the improved accuracy of predicting the pilot plant performance data. The third model included the influence of both particle age and size on the overall rate when modelling the bioleach reactor. Of the three models presented, the third model, which incorporated chemical leaching and microbial oxidation kinetics, as well as, particle size and age distributions in the model formulation was the most comprehensive. Comparing the pilot plant data with the three models, it was found that the third model, with the least restrictive assumptions, was able to predict the reactor performance with the greatest accuracy, indicating that both the age and size contributions of all particles in the reactor are necessary to fully describe the reactor performance in tank bioleaching.

In contrast to previous PBMs presented in the literature (Crundwell, 2005; Brochot *et al.*, 2004), the model presented here explicitly describes the overall reaction rate r^R or the overall conversion X^R in the reactor as a function of the age distribution $I(\theta)$. It is therefore a trivial

exercise to now incorporate the recently available advances in residence time distribution theory, in particular the unsteady state solution (Rawatlal and Starzak, 2003).

The application of the present model can therefore be extended to the case in which the particle flowrate is changing with time by incorporating the unsteady state solution to residence time distribution for perfectly mixed vessels (see Chapter 7).

While the model was shown to accurately predict plant operation, it was found in the literature that the leaching rate of chalcopyrite exhibits a non-monotonic relationship with solution redox potential indicating that multiple steady states may exist (see Figures 2.4 and 2.6). Consequently, a dynamics analysis for the bioleaching of chalcopyrite is performed in both batch (Chapter 5) and continuous flow reactor systems (Chapter 6) to determined which process parameters influence the dynamic structure of chalcopyrite bioleaching for the purpose of maximising the overall production rate.

The influence of solution redox potential, biomass concentration, mean residence time, temperature, particle size distribution, solids loading and unsteady state reactor flow rates will be investigated on system steady states in both batch and continuous flow stirred tank reactors in the chapters that follow.

5

A Dynamics Analysis of Chalcopyrite Bioleaching in Batch Reactor Systems

5.1 Introduction

The rate of dissolution of chalcopyrite is very slow in both chemical (Eq. 5.1) and microbial (Eq. 1.2) leaching environments. Low rates of chalcopyrite leaching have been attributed to the formation of a passivating layer thought to evolve from both iron- and sulphur-containing precipitates, hindering the transfer of ions to and from the chalcopyrite surface (Third *et al.*, 2000). Several conflicting reports suggest that an increase in ferrous ion concentration may or may not increase the rate of chalcopyrite leaching (Hiroyoshi *et al.*, 2001; Dutrizac *et al.*, 1969; Hirato *et al.*, 1987). While chalcopyrite bioleaching at elevated temperatures is known to increase the production rate, the reduced cellular rigidity at these temperatures make the cell structure susceptible to mechanical stress, resulting in reduced rates of extraction (Clark and Norris, 1996; Nemati and Harrison, 2000; Sissing and Harrison, 2003; Witne and Phillips, 2001; Valencia *et al.*, 2003). Low rates of dissolution have also been attributed to oxygen transfer limitations (Bailey and Hansford, 1994; Loia *et al.*, 1994; Witne and Phillips, 2001; Valencia *et al.*, 2003).

$$CuFeS_2 + 4Fe^{3+} \rightarrow Cu^{2+} + 5Fe^{2+} + 2S^0 \qquad [5.1]$$

These kinetic considerations were the fundamental building blocks of the model developed in Chapter 4 to predict the overall performance of continuous flow bioleach reactor systems. The model was shown to accurately predict plant operation, but due to the non-linearity of the reaction rate expressions (see § 2.2), a rigorous dynamics analysis of bioleaching kinetics is required to optimise and evaluate input conditions for safe operation and maximising the production rate.

5.2 Model Development

The mechanism of bioleaching is a set of reactions whereby iron is exchanged between the ferric and ferrous ion form *via.* chemical leaching and microbial oxidation reactions (Eqs. 5.1 & 1.2). At steady state, this exchange defines the rate and redox potential at which the bioleach reactor will operate (Breed and Hansford, 1999b). Solution redox potential is related to the ferric to ferrous ion ratio ($C_{Fe^{3+}}/C_{Fe^{2+}}$) *via.* the Nernst equation. The ferrous ions formed from chemical leaching (Eq. 5.1) decreases the solution redox potential while microbial oxidation increases the solution redox potential by the regeneration of ferric ions. The overall solution redox potential therefore only increases if the rate of microbial oxidation is greater than the rate of chemical leaching.

At steady state, the rate at which ferrous ions are liberated from the mineral sulphide particle surface equals the rate at which microbial ferrous ions are consumed in solution. Whether or not this point is stable is largely dependent on the concentration of the biomass, and hence on the microbial activity, as well as the concentration of the sulphide mineral (Boon and Heijnen, 1998a). The chemical leaching and microbial oxidation kinetics must therefore be related to the process conditions as a function of the ferric/ferrous ion ratio in order to determine the steady state(s).

For the sake of clarity, a dynamics analysis is first developed for the simpler case of pyrite bioleaching. As previously stated (see § 2.2), the chemical leach kinetics for most mineral sulphide ores are represented as the ferric to ferrous ion ratio to the n^{th} order (Eq. 5.2)

$$-r''_{MS} = k\left(\frac{C_{Fe^{3+}}}{C_{Fe^{2+}}}\right)^{n} \qquad [5.2]$$

where r''_{MS} is the intrinsic rate [mol.m^{-3}.s^{-1}], k the intrinsic rate constant [mol.m^{-2}.s^{-1}] and n can be approximated to be 0.5 (Petersen and Dixon, 2006).

As such, the chemical leaching rate increases monotonically with an increase in solution redox potential. The rate has a slow initial increase at low potentials, due to ferrous ion inhibition, and gradually increases at higher potentials when more ferric ions are available for reaction (Figure 5.1).

It should be noted that the intrinsic rate r''_{MS} [mol.m^{-3}.s^{-1}] is a surface area based rate (see § 2.2.1) and therefore the overall rate of leaching in the reactor is obtained by multiplying the intrinsic rate by the total particle specific surface area A^p [m^2.m^{-3}]. In reality, the particle surface area may change with time due to reaction. The particle surface area can be considered as constant in flow reactor systems where the mean particle residence time is low with respect to the leaching rate time scale. For simplicity, the total specific surface area available for reaction A^p [m^2.m^{-3}], in the following case studies, is lumped together with the intrinsic leaching rate constant and is assumed constant. More generally, however, the approach of segregation outlined in Chapter 4 should be adopted to account for the varying particle sizes and hence surface area.

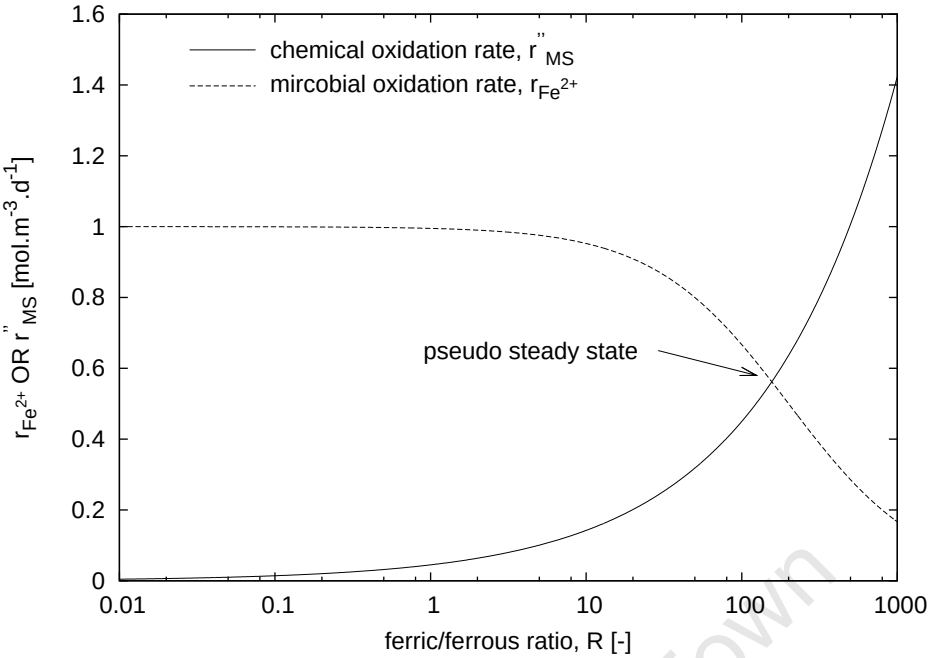

Figure 5.1: Stable pseudo-steady state indicated by the point of intersection between the microbial oxidation and chemical leaching rate curves

Table 5.1: Assumed parameters for the chemical and microbial oxidation rates in Figures 5.1 and 5.2

Chemical Oxidation Rate Constants		Microbial Oxidation Constants	
k	n	$C_X \cdot q^{max}_{Fe^{2+}}$	K
$[mol.m^{-3}.s^{-1}]$	$[-]$	$[mol.m^{-3}.s^{-1}]$	$[-]$
3×10^{-8}	0.5	1.2×10^{-5}	5×10^{-3}

The microbial oxidation rate equation applied in the dynamics analysis is based on Michaelis-Menten/Monod type kinetics developed by Hansford (1997) (Eq. 4.2).

From the microbial kinetics, it is apparent that the microbial oxidation rate is directly proportional to the concentration of the biomass in solution and is a function of the redox potential. Microbial kinetics of this type therefore accounts for the effect of ferric ion inhibition, indicating that the rate of microbial growth decreases with increasing solution potential (Figure 5.1 and Table 5.1).

In the literature review (see § 2.4), it was noted that according to Breed and Hansford (1999b), when a batch system is at equilibrium, the rate of chemical ferrous ion production equals the rate of microbial ferrous ion consumption (Eq. 2.20).

$$-r^{micro}_{Fe^{2+}} = r^{chem}_{Fe^{2+}} \qquad [2.20]$$

However, in the bioleach process, which is inherently multiphase, ions are constantly liberated from the mineral into solution. This forces a never-ending increase of the total concentration

of iron in solution, and therefore a steady state with respect to the absolute concentration of any ionic species is never actually attained. It must be noted that, the rate curves and the point of intersection between the chemical leaching (Eq. 5.2) and microbial oxidation (Eq. 4.2) rate curves determined using kinetic rate constants in Table 5.1, shown in Figure 2.8 and redisplayed in Figure 5.1 for illustration purposes, for a batch reactor, are changing with time. Since the time scale of this move is much less than the reaction time scale, this intersection point, according to Breed and Hansford (1999b), is effectively a pseudo-steady state.

5.3 Model Dynamics

According to Eq. 5.2, the rate of iron turnover in the system increases with the increase in the ferric/ferrous iron ratio ($R = C_{Fe^{3+}}/C_{Fe^{2+}}$). The rate at which the solution redox potential varies is therefore the change in the concentration of ferric ions relative to the change in concentration of the ferrous ions in the multistep mechanism (Eq. 5.3)

$$\frac{dR}{dt} = \frac{C_{Fe^{2+}}\frac{dC_{Fe^{3+}}}{dt} - C_{Fe^{3+}}\frac{dC_{Fe^{2+}}}{dt}}{C^2_{Fe^{2+}}} \qquad [5.3]$$

Since the denominator $C^2_{Fe^{2+}}$ is always positive, $C_{Fe^{2+}}\frac{dC_{Fe^{3+}}}{dt} = C_{Fe^{3+}}\frac{dC_{Fe^{2+}}}{dt}$ at steady state with respect to R.

During batch operation, the change in ferric and ferrous ions with time is the rate at which the ions are produced and consumed. Generally, these material balances can be written as (Eqs. 5.4 and 5.5):

$$\frac{dC_{Fe^{3+}}}{dt} = -\alpha r_{MS} + r_{Fe^{2+}} \qquad [5.4]$$

$$\frac{dC_{Fe^{2+}}}{dt} = \beta r_{MS} - r_{Fe^{2+}} \qquad [5.5]$$

where α and β are the stoichiometric coefficients of the ferric and ferrous ions in solution according the chemical leaching reaction, respectively. In the case of pyrite bioleaching (Eq. 2.2), α and β are the numerical values 14 and 15, respectively, while for chalcopyrite bioleaching $\alpha = 4$ and $\beta = 5$ according to Eqs. 5.1 and 1.2, respectively.

By substituting Eqs. 5.4 and 5.5 into Eq. 5.3, and noting that the redox potential R is the ratio of the ferric to ferrous ions in solution, Eq. 5.3 can be rewritten in the form of Eq. 5.6

$$\frac{dR}{dt} = \frac{(R+1)\cdot r_{Fe^{2+}} - (\beta R + \alpha)\cdot r_{MS}}{C_{Fe^{2+}}} \qquad [5.6]$$

Since the denominator on the right hand side is always positive, the system will reach a pseudo-steady state with respect to R at the condition given by Eq. 5.7.

$$(R+1)\cdot r_{Fe^{2+}} = (\beta R + \alpha)\cdot r_{MS} \qquad [5.7]$$

At any point, when the rate of microbial oxidation exceeds the rate of chemical leaching or *vice versa*, the solution redox potential either increases or decreases, respectively, until the system is at pseudo-steady state.

5.4 Dynamics of Pyrite Bioleaching

Acid ferric sulphate solutions formed from the microbial oxidation of pyrite play an important role in the commercial recovery of, for example, copper from metal sulphide ores. Higher rates of pyrite oxidation would therefore increase rates of leaching (Olson, 1991).

Since bioleaching involves the transfer of ions from the solid particle phase to the surrounding solution phase, the total iron concentration is never constant. As previously stated, in the chemical leaching of pyrite represented by Eq. 2.2, for example, $\alpha = 14$ ferric ions, that are already in solution, are converted to the ferrous form, as well as liberating an additional Fe centre from the ore particle as ferrous, hence $\beta = 15$. Therefore, the analogy proposed by Breed and Hansford (1999b) that the rate of the microbial and chemical oxidation rates are equal at steady state (Eq. 2.20) only applies for the rate of production and consumption of the ferrous ions and does not hold true for the ferric ions. Since the ferric ion concentration is not steady, and due to the existence of a thermodynamic equilibrium between the two ionic forms, the concentration of ferrous ions will also tend to change with time. The only possible pseudo-steady state is therefore with respect to the ferric/ferrous ion ratio R as predicted by Eq. 5.6.

The point of intersection according to the generally reported pseudo-steady state (Eq. 2.20, Figure 5.2 a and b) and the pseudo-steady state rigorously derived here (Eq. 5.6, Figure 5.2 c and d) are shown for a pyrite ore (Eq. 5.7). Clearly, the assumption that pseudo-steady state for the ionic species equates to pseudo-steady state for redox potential is not valid. For this reason, previous attempts at dynamics analyses were not capable of accurately modelling the observed passivation effects. In the following sections, the analysis for the case of chalcopyrite rather that pyrite bioleaching is developed.

5.5 Dynamics of Chalcopyrite Bioleaching

For most mineral sulphide ores, a single stable steady state exists (Figure 5.1). However, according to the studies reported by Kametani and Aoki (1985), the chemical leaching rate of chalcopyrite does not vary monotonically with R, but goes through a maximum followed by a minimum as solution potential increases. On the other hand, the microbial action does vary monotonically with R. As such, there may exist as many as three steady states.

Hiroyoshi *et al.* (2001) proposed that the chemical leaching of chalcopyrite includes a reduction step in which the chalcopyrite is converted to Cu_2S (see § 2.4). The chalcocite

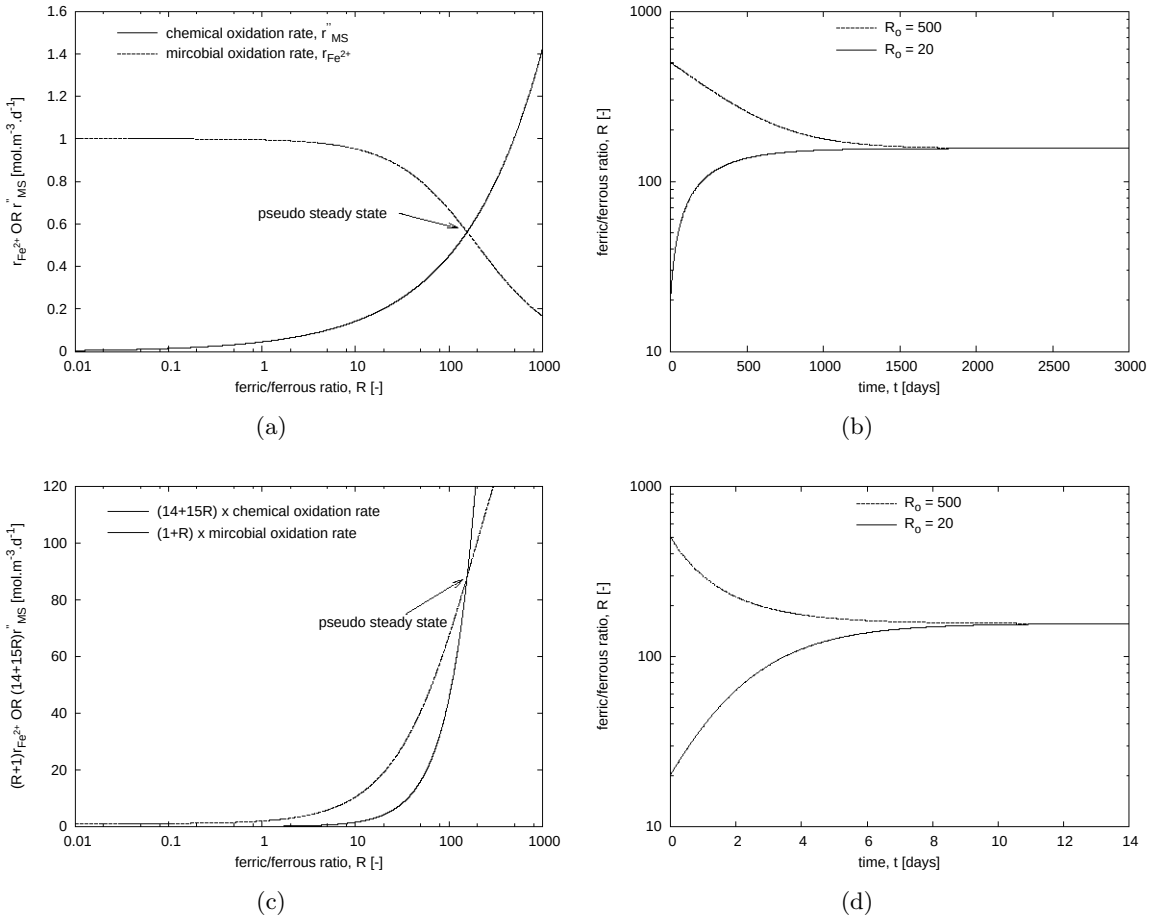

Figure 5.2: Operating point for most mineral sulphide ores. A single stable pseudo-steady state exists at the point of intersection ($R = C_{Fe^{3+}}/C_{Fe^{2+}}$) (a) and (b) correspond to rate and transient plots, respectively, using the generally accepted method in Eq. 2.20; (c) and (d) are rate and transient plots, respectively, determined using Eq. 5.6, derived in the present study.

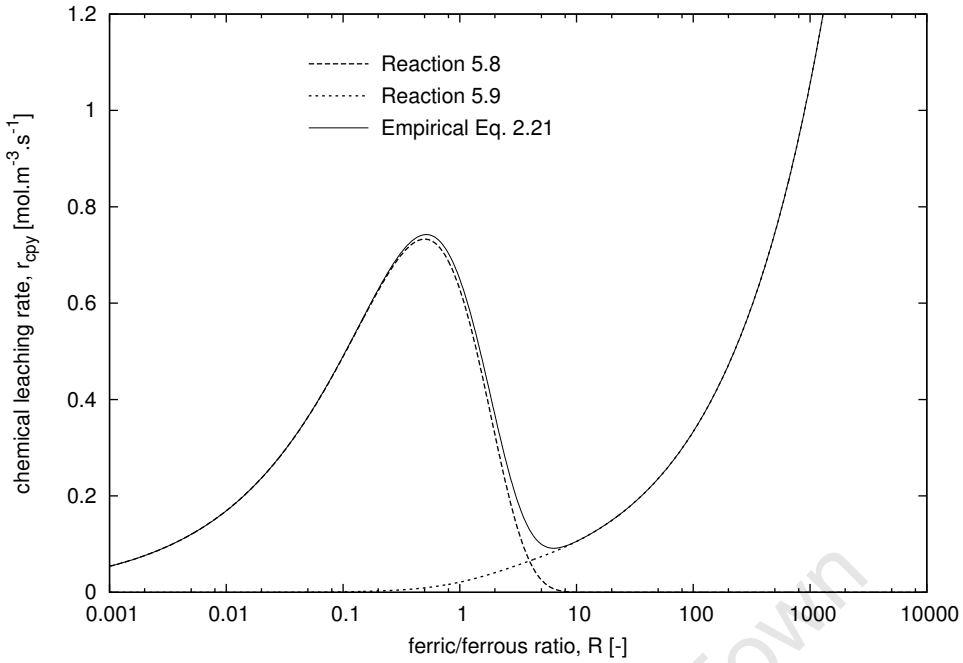

Figure 5.3: Graphical representation of the empirical chalcopyrite leaching rate proposed by Petersen and Dixon (2006)

intermediate is then rapidly oxidised releasing Cu^{2+} ions into solution (Eq. 5.8). Thereafter $Cu_{1.2}S$ undergoes ferric ion oxidation, at a lower rate, further releasing Cu^{2+} ions into solution according to Eq. 5.9 (Petersen and Dixon, 2006).

$$Cu_2S + 1.6Fe^{3+} \rightarrow Cu_{1.2}S + 0.8Cu^{2+} + 1.6Fe^{2+} \quad [5.8]$$

$$Cu_{1.2}S + 2.4Fe^{3+} \rightarrow 1.2Cu^{2+} + 2.4Fe^{2+} + S^0 \quad [5.9]$$

Based on the mechanism proposed by Hiroyoshi *et al.* (2004), Petersen and Dixon (2006) suggested that the rate expression for these two reactions, each producing Cu^{2+}, could be lumped into the single empirical formula given in Eq. 2.19 (see § 2.4). Figure 5.3 illustrates the contributions from each term, representing the contribution from each of the two reactions that give one overall non-monotonic curve.

$$r_{cpy} = g_{py} \cdot f\left(X_{cpy}\right) \cdot R^{0.5} \left[A \cdot exp\left(-\frac{R}{R_{crit}}\right) + B\left(1 - exp\left(-\frac{R}{R_{crit}}\right)\right)\right] \quad [2.19]$$

As with pyrite, the dynamics analysis on chalcopyrite was performed using Eqs. 5.6 and 5.7. Figure 5.4a shows a plot of the microbial oxidation and chemical leaching rate functions $(R+1)r_{Fe^{2+}}$ and $(5R+4)r_{cpy}$, respectively. Points of intersection X, Y and Z in Figure 5.4a indicate pseudo-steady state points at the corresponding redox potential R while the corresponding reaction rates are determined from the chemical leaching rate curve at the corresponding redox potentials R shown in the accompanying Figure 5.4b.

When plotting the leaching rate and the microbial oxidation rate in Figure 5.4a using leaching rate contants $A = 1.40\times10^{-3}$ [mol.m^{-3}.s^{-1}], $B = 1.67\times10^{-5}$ [mol.m^{-3}.s^{-1}] and $R_{crit} = 1$ [$-$]

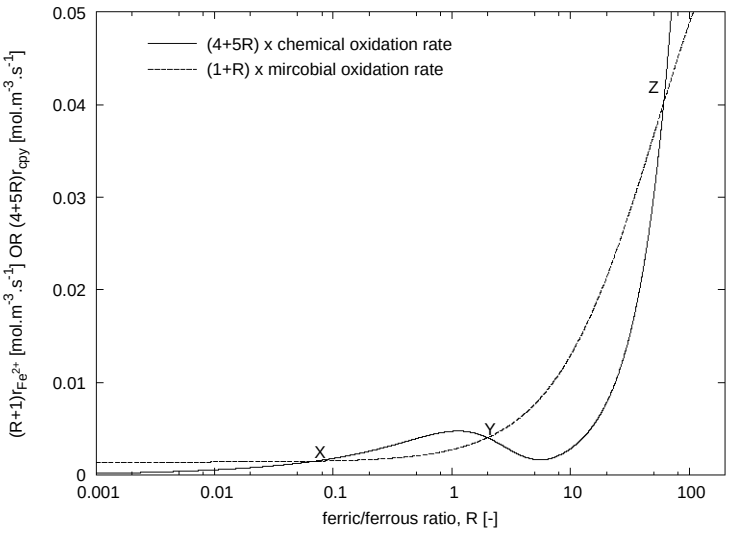

(a) Multiple pseudo-steady states at points of intersection

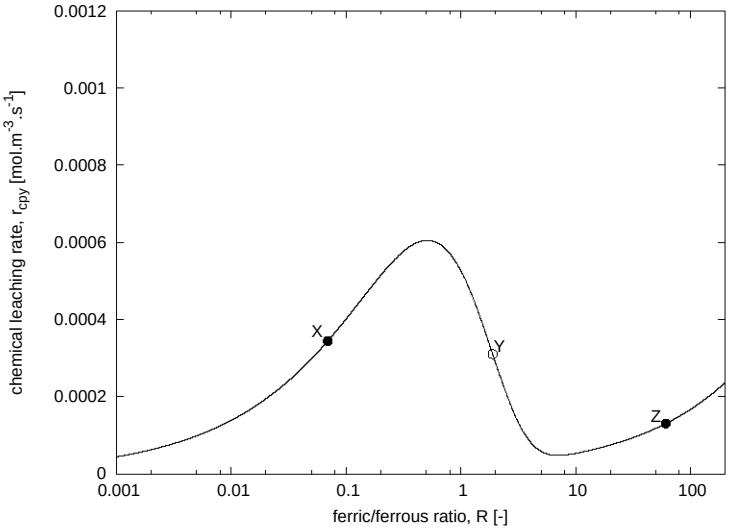

(b) Pseudo-steady states rate points

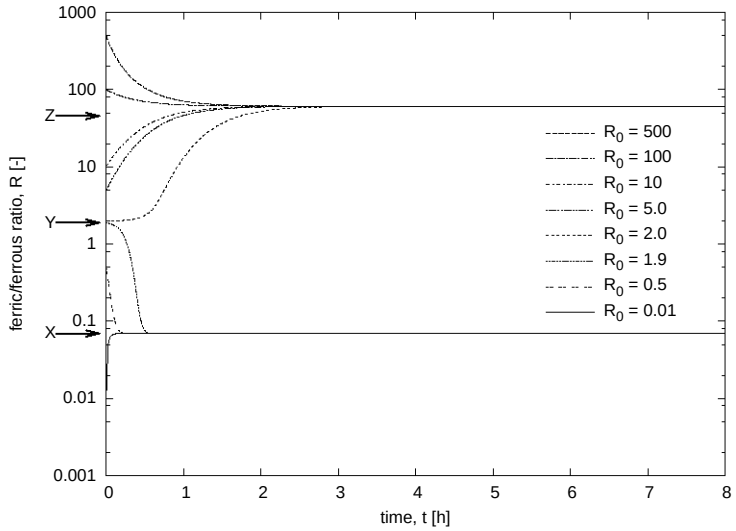

(c) Transient state

Figure 5.4: The dynamics of chalcopyrite indicating multiple pseudo-steady states X, Y, Z ($R = C_{Fe^{3+}}/C_{Fe^{2+}}$)

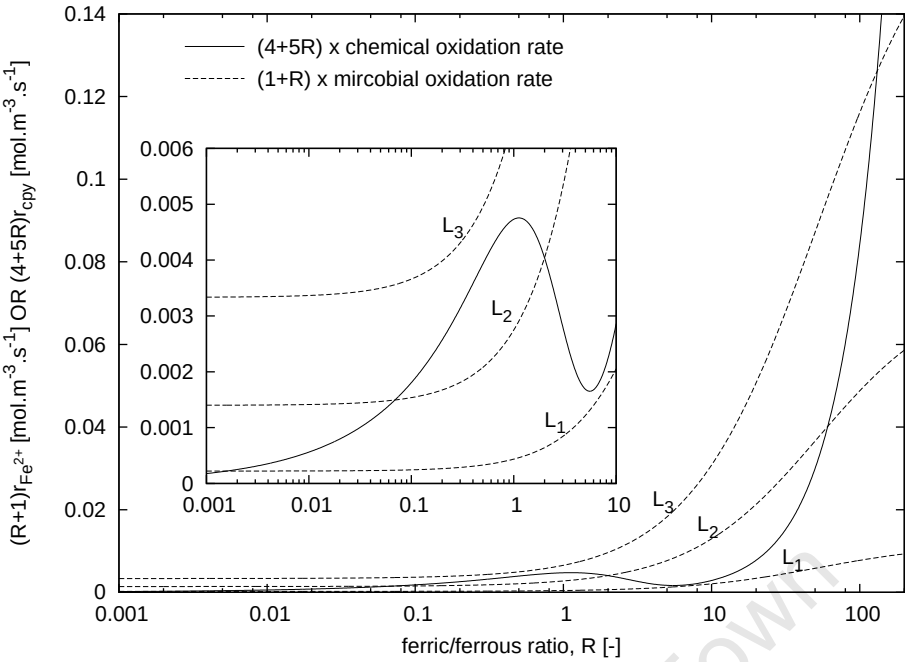

Figure 5.5: Single pseudo-steady state points occur before and after multiple points of stability. Low bioleaching rates occur when one intersection point is observed

and microbial oxidation rate constants $C_X q^{max}_{Fe^{2+}} = 1.40 \times 10^{-3}$ [mol.m^{-3}.s^{-1}] and $K = 0.019$ [$-$], it is clear from Figure 5.4a and b that a maximum number of three pseudo-steady states may occur during chalcopyrite bioleaching. During microbial oxidation (Eq. 1.2), ferrous ions are converted to the ferric form, increasing the ferric/ferrous ion ratio, while ferric ions are converted to ferrous ions during chemical leaching, decreasing the redox potential (Eq. 5.1). Therefore, any region in Figure 5.4 in which the microbial oxidation rate curve lies above the chemical oxidation rate, the overall reaction shifts to higher redox potentials and *vice versa* when chemical leaching exceeds microbial oxidation. A stable pseudo-steady state therefore exists at the intersection of the two rate curves at low solution potentials and another at high solution potentials where microbial oxidation is the dominating reaction (points X and Z in Figure 5.4). An unstable steady state exists at the intermediate potential region (point Y in Figure 5.4) since potentials to the left or right of this intersection, respectively, result in dominant chemical or microbial oxidation rates, which drive the system away from this point to the lower or higher stable pseudo-steady state points X and Z, respectively. A maximum of two stable pseudo-steady states X, Z and one unstable pseudo-steady state Y is therefore observed in chalcopyrite bioleaching.

The time profile for the ferric/ferrous ion ratio R is determined by integrating Eq. 5.6 and plotted in Figure 5.4c, which confirms graphically that only two stable pseudo-steady states are achieved in chalcopyrite bioleaching, with an unstable pseudo-steady state at the intermediate solution potential Y.

In attempting to exploit the dynamics for achieving and maintaining high leaching rates, the biomass concentration C_X, which directly affects the microbial oxidation rate (Eq. 4.2), was varied. The results are shown in Figure 5.5 as curves L_1, L_2 and L_3. Lines L_1 and L_3

intersect with the leaching rate curve only once, indicating that single pseudo-steady states with low leaching rates occur before and after the zone of multiple intersections to which L_2 belongs. Since these intersecting points determine the stability of operation, they must be identified to avoid low bioleaching rates.

A single pseudo-steady state exists at intersecting points R_a and R_b in Figures 5.6a and b . Between these points, there are two stable and one unstable pseudo-steady state (L_2 in Figure 5.5). Points R_a and R_b are therefore bifurcation points. Geometrically, these bifurcation points occur when the microbial oxidation curve is tangent to the chemical leaching rate curve (L_4 and L_5 in Figure 5.6a). Mathematically, redox potentials at bifurcation biomass concentrations $C_{X,a}$ and $C_{X,b}$ in Figures 5.6a and b are obtained when the values of rate functions $(R+1)r_{Fe^{2+}}$ and $(5R+1)r_{cpy}$, as well as their gradients with respect to R, are equal (Eqs. 5.7 and 5.10, respectively).

$$\frac{d\left[(5R+4)\cdot r_{cpy}\right]}{dR} = \frac{d\left[(R+1)\cdot r_{Fe^{2+}}\right]}{dR} \qquad [5.10]$$

When both conditions are satisfied, the rate functions are equal and tangent to each other at the corresponding pseudo-steady state points $C_{X,a}$ and $C_{X,b}$.

It is important to note that $C_X q^{max}_{Fe^{2+}}$ and hence the dynamic structure may change during the operation of even a single batch reactor during a single run, since, as the reaction proceeds, the microbial concentration C_X increases with the generation of ferrous ion substrate during chemical leaching.

If the bioleach reactor operates at any concentration below the bifurcation biomass concentration $C_{X,a}$ (L_4 in Figure 5.6a), chemical leaching becomes the dominating reaction. The ferric ions in solution are converted to the ferrous form thus causing the solution potential to drop until the pseudo-steady state at point R_a is achieved (Figure 5.6b). Alternatively, if the biomass concentration increases beyond bifurcation point $C_{X,b}$ (L_5 in Figure 5.6a), the dominant microbial oxidation reaction converts the ferrous ions back to ferric ions, increasing the solution potential until balance is achieved at point R_b. If, in this dynamics study, the rate of chemical leaching coincides with the rate of microbial oxidation at redox potentials between bifurcation biomass concentrations $C_{X,b} < C_X < C_{X,a}$ as in L_2 in Figure 5.5, the system would be in an unstable steady state region favouring either ferric or ferrous iron production very close to these points. A slight increase or decrease in the solution potential would result in either the rate of microbial oxidation or chemical leaching becoming dominant and thus shifting the balance to higher or lower stable pseudo-steady states, respectively. Stable operation at solution potentials between $C_{X,b} < C_X < C_{X,a}$ can only occur if the solution potential is maintained precisely at the intersection potential. Since the bifurcation biomass concentrations $C_{X,a}$ and $C_{X,b}$ have been identified, it is now possible to control the system into the maximum operating region by investigating the influence of temperature and biomass concentration on the dynamics.

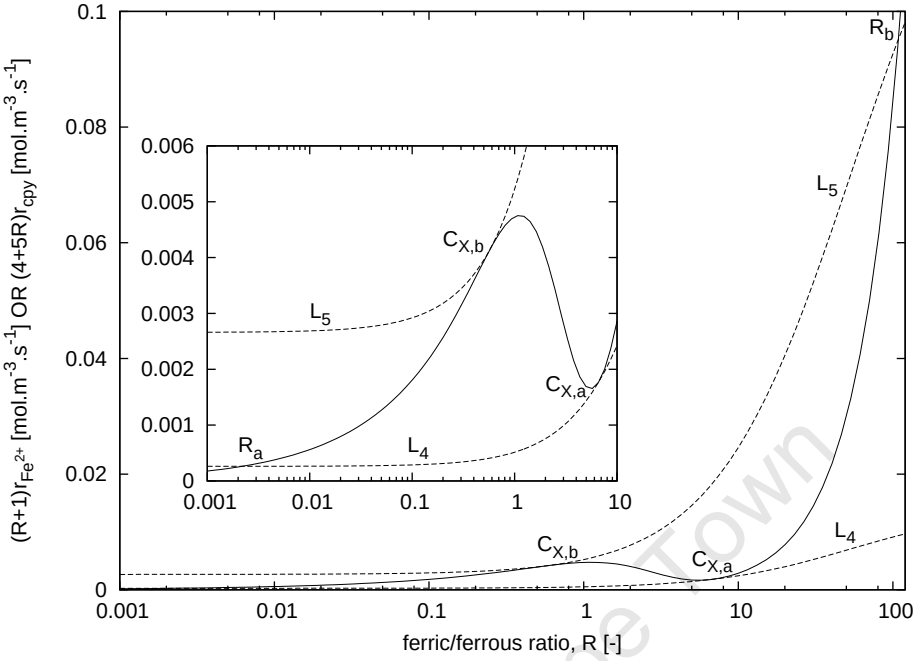

(a) Points of tangency

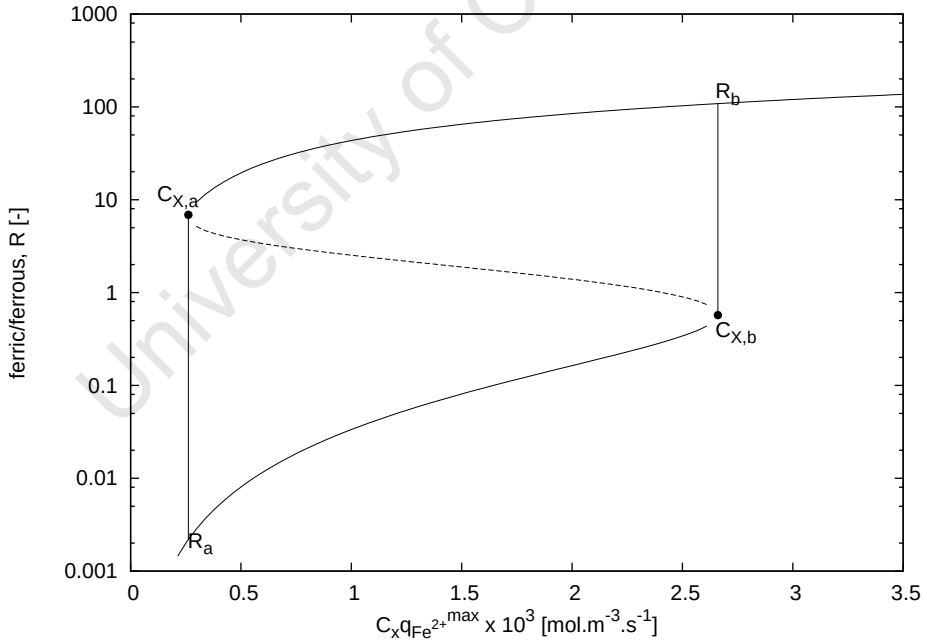

(b) $R - X$ plane

Figure 5.6: Multiple pseudo-steady states achieved by varying the biomass concentration C_X. Points $C_{X,a}$ and $C_{X,b}$ indicate points of tangency of the chemical oxidation rate with the microbial oxidation rate. The solid curves in the phase plane represent stable pseudo-steady states and the dotted curves unstable pseudo-steady states.

5.6 The influence of temperature on system dynamics

Increased bioleaching rates have been observed with increased operating temperatures. Since the chemical leaching and microbial oxidation rates each have different temperature dependencies, the points of pseudo-steady state operation may change with temperature. The temperature dependence of the chemical leaching and microbial oxidation rates is therefore established here.

The temperature dependence for the chemical leaching rate is first considered. The chemical leaching of chalcopyrite and its dependence on temperature was extensively studied by Kametani and Aoki (1985). Reasonable fits to this data are obtained by applying the proposed empirical rate expression in Eq. 2.19 (Figure 5.7). In the absence of a published temperature relationship for the parameters A and B [mol.m^{-3}.s^{-1}] in Eq. 2.19, it is proposed in this study that the Arrhenius dependency be adopted.

The rate fits obtained for the leaching of chalcopyrite over a temperature and redox potential range between $298.15 - 363.15$ K and $0.30 - 0.65$ V (SCE) respectively, were used to obtain the Arrhenius terms in Eqs. 5.11 and 5.12 for the kinetic constants A and B [mol.m^{-3}.s^{-1}] for the chemical leaching rate in Eq. 2.19. The Arrhenius fits to this data are graphically represented in Figure 5.8.

$$A = 1.40 \times 10^{11} e^{-\frac{9.22 \times 10^4}{RT}} \quad [5.11]$$

$$B = 1.72 \times 10^{11} e^{-\frac{1.04 \times 10^5}{RT}} \quad [5.12]$$

Next the temperature dependence for the microbial oxidation rate was also developed. Searby (2006) investigated the influence of temperature on the maximum specific iron utilisation rate $q^{max}_{Fe^{2+}}$, and hence the microbial oxidation rate, for a *Metallosphaera* culture between $333.15 - 353.15$ K. The results indicated that the dependence of $q^{max}_{Fe^{2+}}$ on temperature was Arrhenius (see Eq. 5.13).

$$q^{max}_{Fe^{2+}} = q_0 e^{-\frac{E_a}{R_g T}} \quad [5.13]$$

where $q_0 = 6.17 \times 10^4$ mol Fe^{2+}.mol^{-1} carbon.s^{-1} and $E_a = 48.0 \times 10^3$ J.mol^{-1} (Searby, 2006). This then establishes the temperature dependence for the biooxidation rate.

It is evident from the literature that increasing the operating temperature will increase the rate of chalcopyrite bioleaching. If it is assumed that cell growth inhibition at elevated temperatures resulting from mechanical stresses is negligible, the rate dependencies on temperature established from the Arrhenius terms in Eqs. $5.11 - 5.13$ for the corresponding rate Eqs 4.2 and 2.19 completely describe the system sensitivity to temperature, making it possible to investigate the effect of temperature on system dynamics.

For the sake of illustration, three operating temperatures of 333.15 K, 343.15 K and 353.15 K at constant biomass concentration were simulated. Figure 5.9a indicates the change in

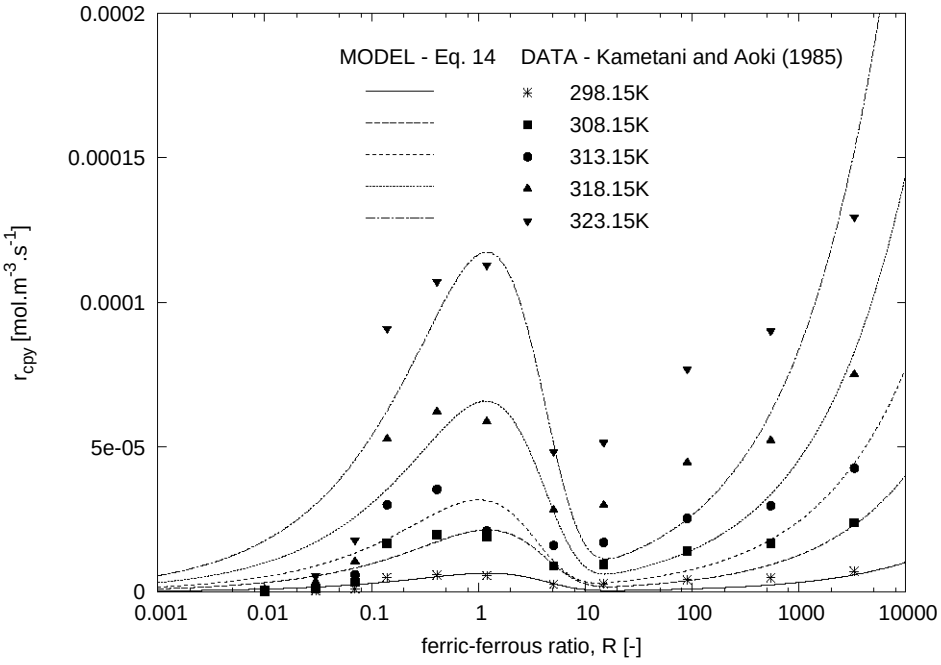

(a)

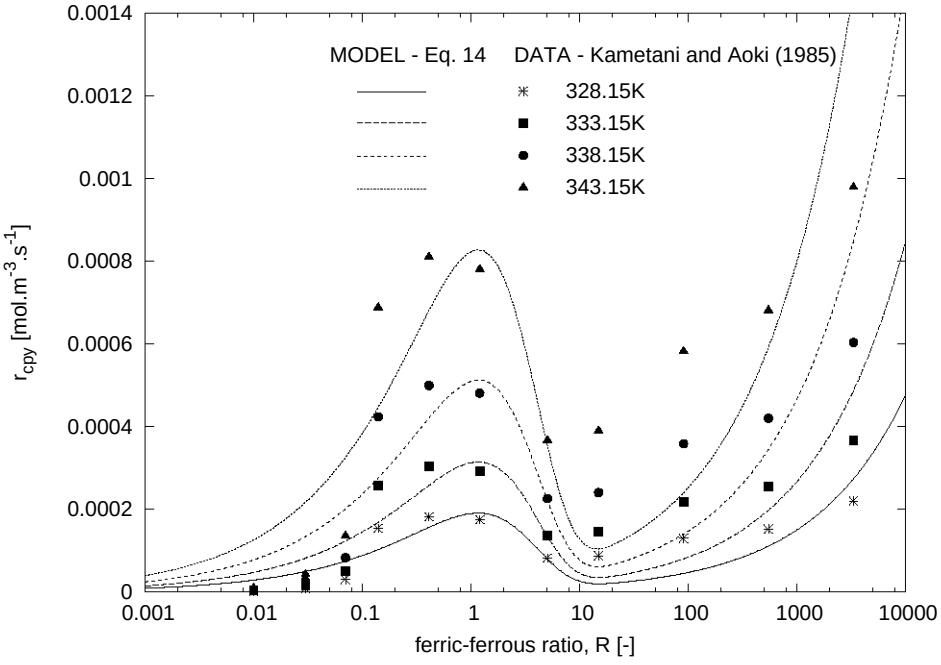

(b)

Figure 5.7: Validation of the empirical leaching rate proposed by Petersen and Dixon (2006) Data extracted from Kametani and Aoki (1985) and Jaffer (2002).

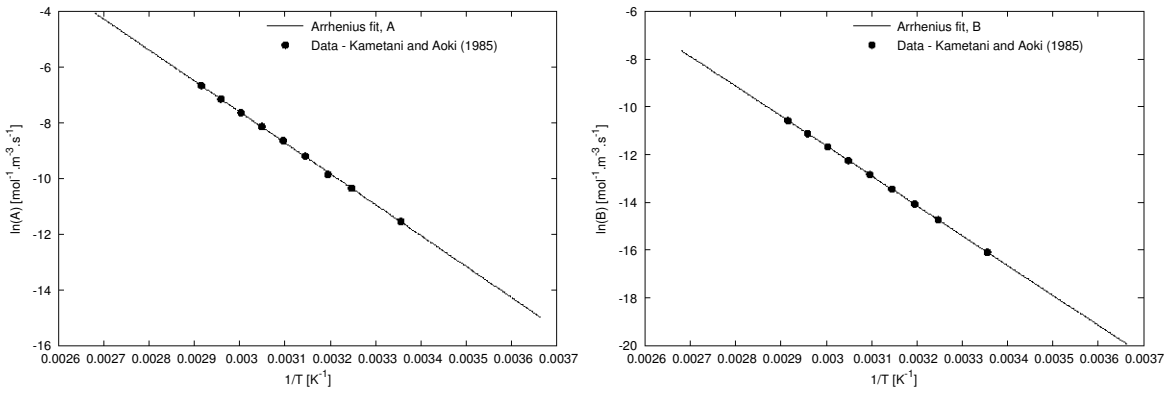

(a) (b)

Figure 5.8: The effect of temperature on the kinetic constants A and B in the chemical oxidation rate of chalcopyrite in Eq. 2.19. Data reworked from Kametani and Aoki (1985) and Jaffer (2002).

pseudo-steady states resulting from the intersection of the chemical leaching rate with the microbial oxidation rate functions $(5R + 4)r_{cpy}$ and $(R + 1)r_{Fe^{2+}}$, respectively. To clearly show the effect of temperature on the chalcopyrite leaching rate, the stable pseudo-steady state points are plotted with the chalcopyrite leaching rate in Figure 5.9b. It is apparent from Figure 5.9 that both the rates of chemical leaching and microbial oxidation increase with temperature in such a way that the pseudo-steady state solution ferric/ferrous ion ratio decreases (Figure 5.10).

The local maximum of the chemical leaching rate curve increases with temperature, thus increasing the operating region at which stable pseudo-steady states occur at low redox potentials. The system thus moves from a single stable pseudo-steady state at low leaching rates, at high solution potentials at 333.15 K (Figure 5.9b), to two stable pseudo-steady states at 343.15 K and 353.15 K (Figures 5.9 and 5.10). For the same given overall biomass concentration, at lower temperatures, the system therefore falls to low rates at lower biomass concentrations than if the system was operated at elevated temperatures (Figure 5.9b).

The influence of temperature on system pseudo-steady state is shown in Figure 5.10. Given that thermal stress influences biomass activity, a feasible limit of 353.15 K does exist, as indicated on the Figure. Temperatures beyond this limit indicate a theoretical representation of the system pseudo-steady states if the thermophiles were active, and the kinetics were valid at the given temperatures. It appears that by increasing the system temperature, low bioleaching rates at solution potentials beyond 0.65 V (SHE) can be overcome with rates comparable to those achieved at low ferric/ferrous ion ratios. However, bioleaching rates at these temperatures depend on the activity of the micro-organisms at such high redox potentials.

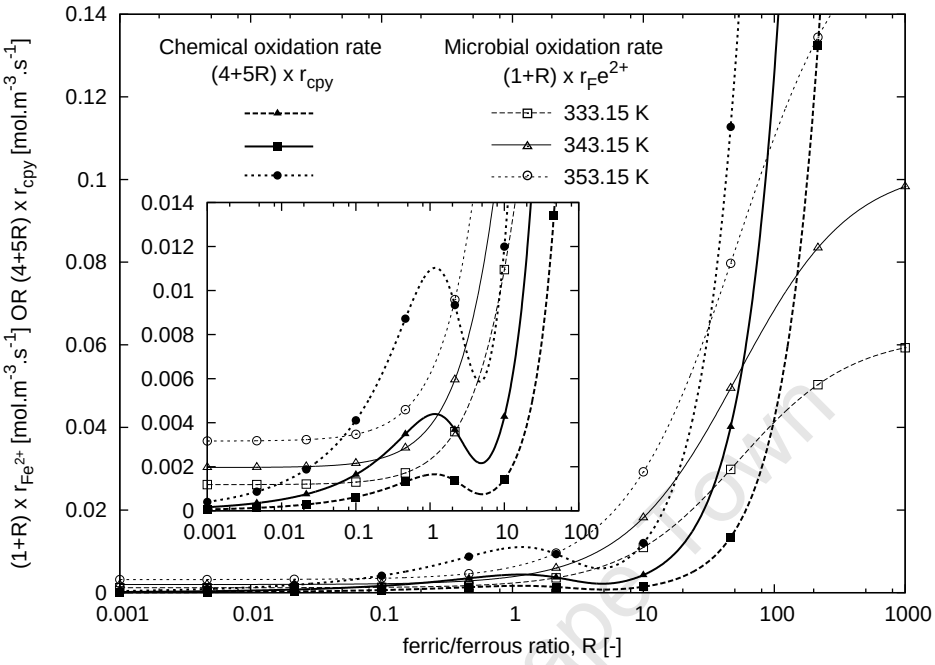

(a) Rate function curves with increasing temperature

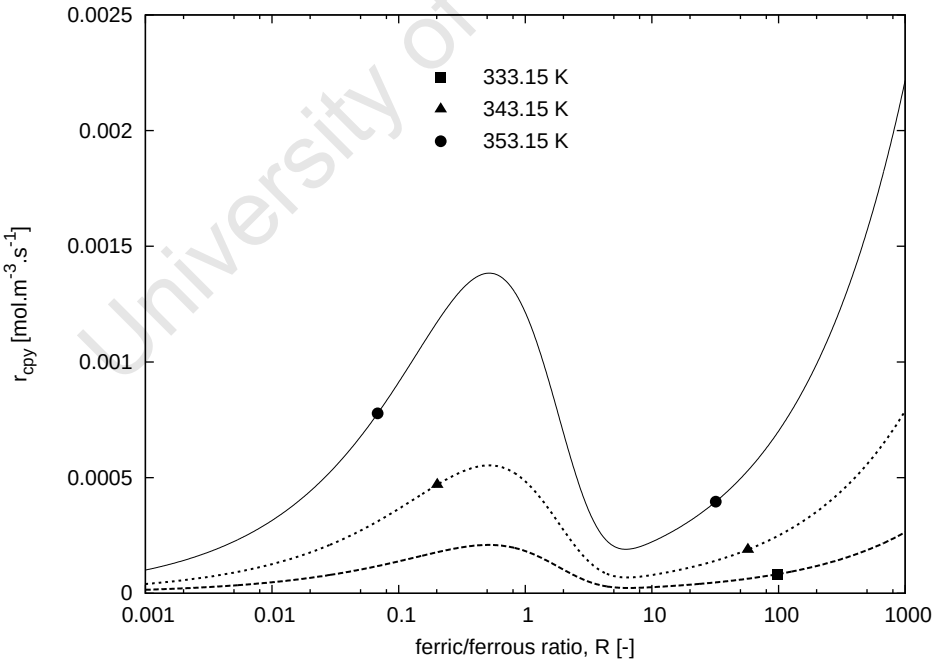

(b) Steady state rates with increasing temperature

Figure 5.9: The effect of temperature on the points of stability and the solution ferric/ferrous ion ratio

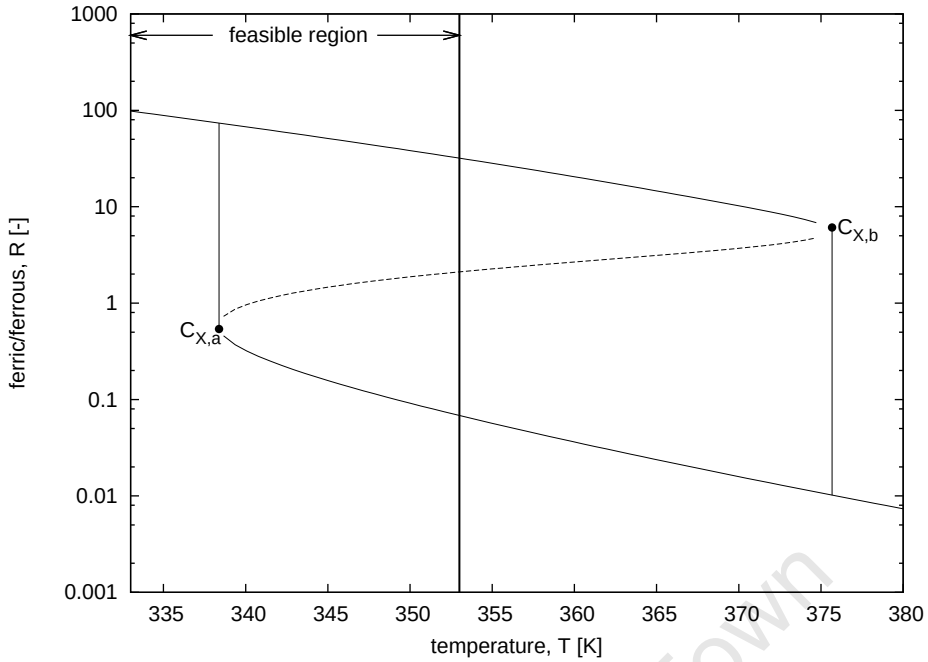

Figure 5.10: The influence of temperature on the points of stability in a bioleach system. Points $C_{X,a}$ and $C_{X,b}$ indicate points of tangency of the chemical leaching rate with the microbial oxidation rate. The solid curves in the phase plane represent stable pseudo-steady states and the dotted curve unstable pseudo-steady states. The solid vertical separator indicates the maximum feasible temperature 353.15K for the thermophiles investigated by Searby (2006)

5.7 The influence of biomass concentration on system dynamics

Since the rate of microbial oxidation is directly proportional to the concentration of biomass (Eq. 4.2), an increase in the biomass concentration, at constant temperature, would therefore increase the rate of microbial oxidation without affecting the leaching rate directly, and hence, increase the overall bioleaching rate in the system. Graphically, this increase is indicated by an upward shift in the microbial oxidation rate curve with biomass.

For the sake of illustration, three biomass concentrations of 0.5, 0.75 and 1.0 mol carbon.m^{-3} were simulated at a constant temperature of 343.15 K. As expected, increased bioleaching rates are observed in Figure 5.11 with increased biomass concentration. The points of operation shift from multiple pseudo-steady states to a single stable pseudo-steady state indicating that a bifurcation concentration exists prior to low overall bioleaching rates (Figure 5.6b).

Increasing the biomass concentration shifted the microbial oxidation rate curve such that the initial availability of multiple pseudo-steady states was reduced to a single stable pseudo-steady state at higher redox potentials with lower overall bioleaching rates (Figure 5.11b). It therefore appears that higher leaching rates cannot be achieved by simply increasing the biomass concentration without bound. The leaching rate does increase at low solution potentials until the microbial oxidation rate is tangent to the chemical leaching rate. Up to this point, two stable pseudo-steady states are observed, one at low solution

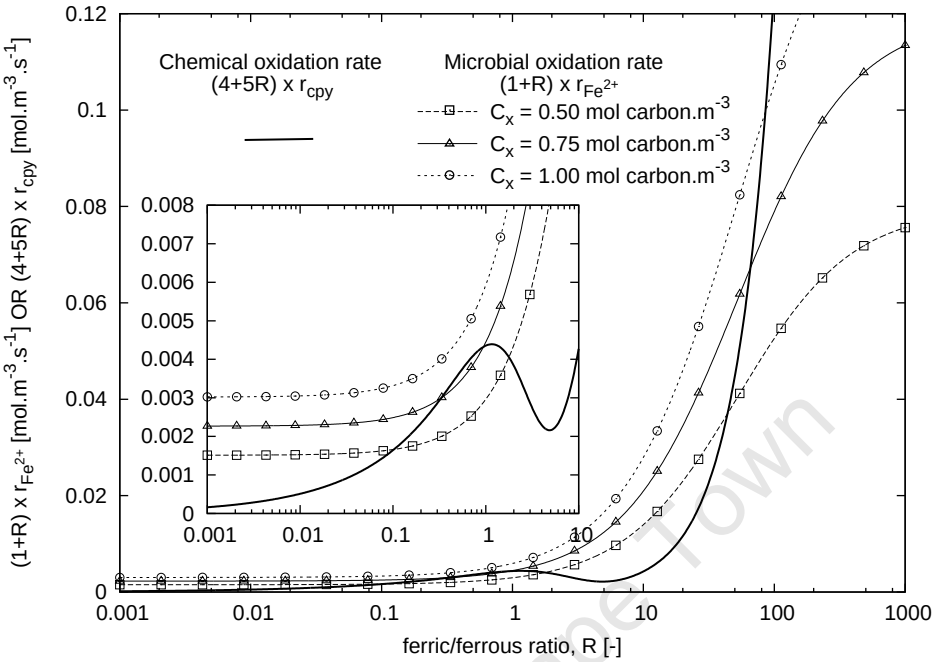

(a) Rate function curves with increasing biomass concentration

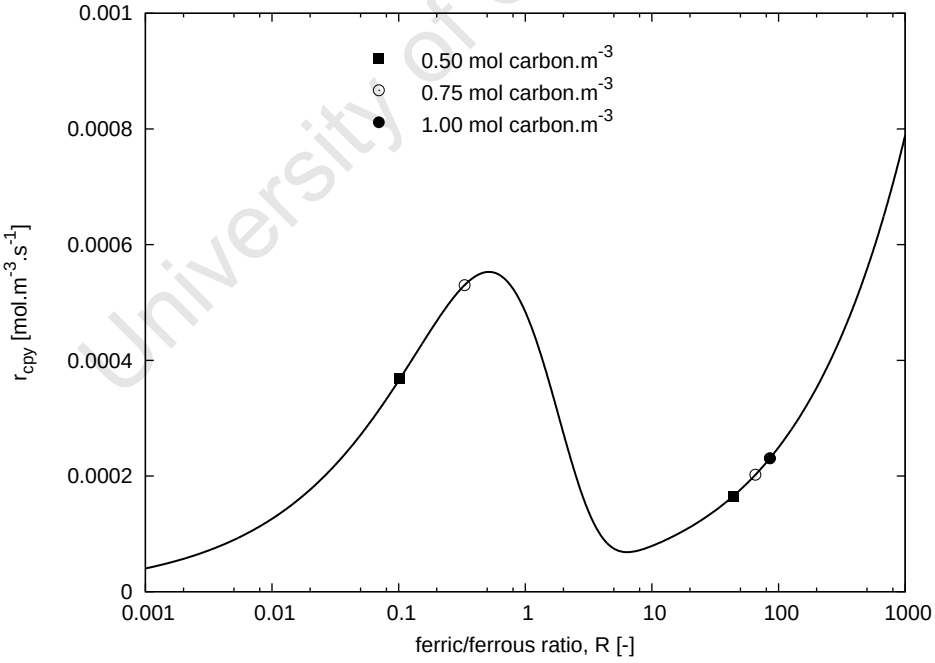

(b) Steady state rates

Figure 5.11: The influence of biomass concentration on the points of stability and the solution ferric/ferrous ion ratio

potentials with high rates and another at high ferric/ferrous ion ratios with low overall bioleaching rates. When the tangent point is exceeded ($C_{X,b}$ in Figure 5.6b), by increasing the biomass concentration, low rates are observed (Figure 5.11b). The point of contention in several studies is whether the presence of micro- organisms or the addition of ferrous ions, increase the rate of leaching (Hiroyoshi *et al.*, 2001; Dutrizac *et al.*, 1969; Hirato *et al.*, 1987) . The analysis reveals that it is the extent to which the biomass concentration shifts the microbial oxidation rate curve with respect to the leaching rate curve. The addition of ferrous ions to the system would only be beneficial if the bioleach reactor operates at high solution potentials where low rates are observed or once the microbial oxidation rate has exceeded the rate of chemical leaching beyond the bifurcation biomass concentration $C_{X,b}$ (Figure 5.6b).

Without a dynamics analysis, it would never be clear which kinetic consideration is causing the behaviour considered, therefore without it, the reports will always appear to be in conflict. The biomass concentration is therefore an important parameter that should be monitored in order to prevent low overall bioleaching rates.

5.8 The combined influence of temperature and biomass on system dynamics

In both temperature and biomass case studies, it emerged that higher leaching rates could be achieved at higher solution potentials by either increasing the system temperature or increasing the biomass concentration.

If Eqs. 5.7 and 5.10 are simultaneously solved at steady state for a range of temperatures with corresponding biomass concentrations, the locus of tangent points, $C_{X,a}$ and $C_{X,b}$, can be obtained (Figure 5.12) from which the optimal operating region can be easily predicted. Multiple pseudo-steady states are achievable between the locus of tangents $C_{X,a}$ and $C_{X,b}$. The stable operating region increases with temperature and biomass concentration increasing the overall bioleaching rate. Any operating point below or above $C_{X,a}$ and $C_{X,b}$ in Figure 5.12, respectively, would result in diminished rates, although at higher temperatures and biomass concentrations competitive rates are possible at high redox potentials (Figures 5.9 and 5.11).

5.9 Experimental validation

Third *et al.* (2000) focussed on the role of microorganisms in the bioleaching of chalcopyrite (see § 2.4). By studying the effects of different inoculum sizes, these researchers reported that bioleaching rates appeared to fall to different extrema when a range of inoculum volumes were introduced to their bioleaching experiments, thus indicating the presence of more than

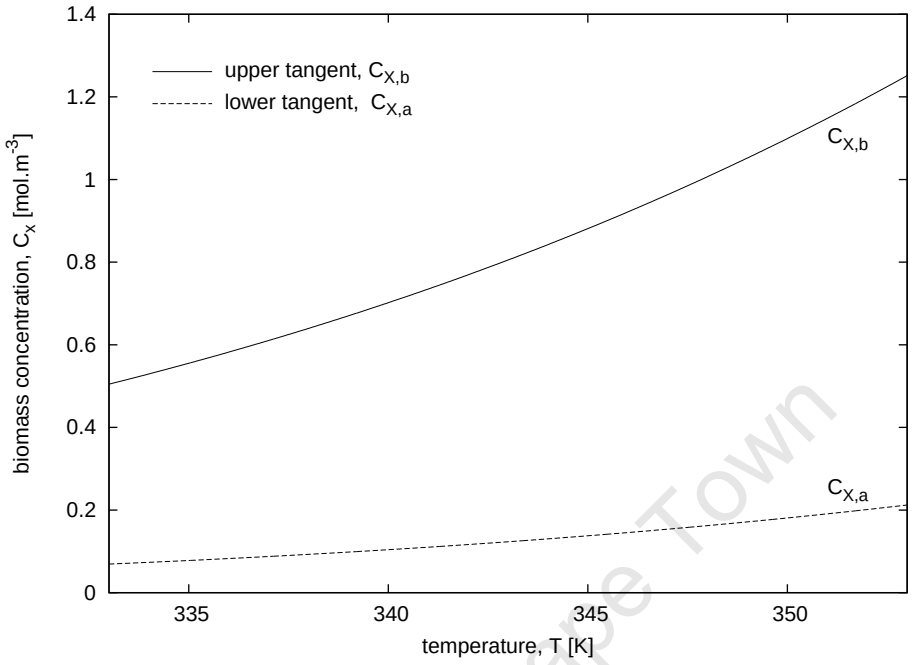

(a) Optimum biomass concentrations as a function of temperature

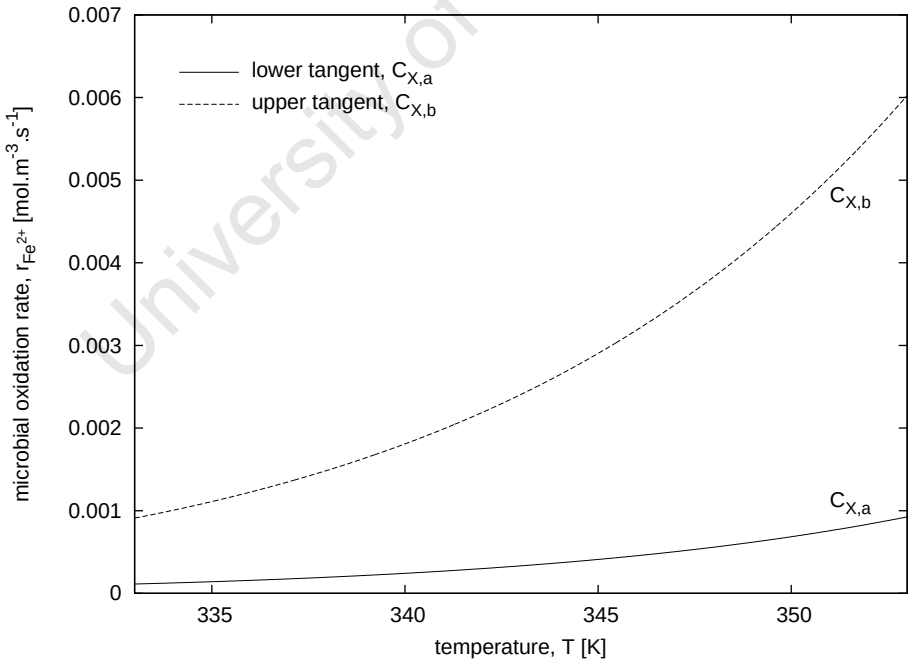

(b) Corresponding microbial oxidation rates

Figure 5.12: Locus of tangent points R_1 and R_2 as a function of temperature and biomass concentration

one pseudo-steady state (see Figures 5.13 and 2.7). The authors hypothesised that the bioleaching rate was not only dependent on the microbial concentration or activity but is also largely dependent on the initial solution redox potential (Third *et al.*, 2000). However, this was the limit of their explanation for this observation, which was largely regarded as an anomaly that did not correspond to the established theoretical frameworks. However, by application of the dynamics analysis introduced in this article, we are able to predict both sets of extrema within one unified model (Figure 5.13).

The leaching rate constants A, B, R_c and the microbial rate constants $q^{max}_{Fe^{2+}}$, K and the final microbial concentration C_X, are unknown for these experiments and are therefore used as the fitting parameters when validating the model with the data.

Two approaches were adopted when applying the dynamics analysis to this experimental data. The first analysis incorporated material balances for the redox potential and the ferrous ion concentration whereas the second analysis incorporated a material balance for the biomass. In the latter case, the biomass was assumed to exhibit growth, inhibition and death. The latter was modelled as a first order reaction rate, in which case the additional parameter k_d, was fit from the data.

In Figure 5.13a, it is shown that in analysis 1 (which does not include a material balance for the biomass concentration), the best parameter fits gave leaching rate constants $A = 6.38 \times 10^{-4}$ kg.m^{-3}.s^{-1}, $B = 3.62 \times 10^{-7}$ kg.m^{-3}.s^{-1}, $R_c = 0.86$ [-] and microbial rate constants $q^{max}_{Fe^{2+}} = 0.0028$ mol Fe^{2+}.mol carbon^{-1}.s^{-1}, $K = 0.027$ [-]. At these values, we are able to predict the observed multiple pseudo-steady states for initial inoculum sizes 1% (v/v) and 50% (v/v) at low and high solution redox potentials, respectively, as well as the transition from fast to slow bioleaching rates observed when a 10% (v/v) inoculum was used. The maximum microbial specific ferrous iron utilisation rate $q^{max}_{Fe^{2+}}$ and inhibition constant K predicted by the model for the mixed mesophilic culture used by Third *et al.* (2000) compares favourably with those reported for pure cultures *Leptospirillum ferrooxidans* $q^{max}_{Fe^{2+}} = 0.0019$ mol Fe^{2+}.mol carbon^{-1}.s^{-1}, $K = 0.0005$ and *Acidithiobacillus ferrooxidans* $q^{max}_{Fe^{2+}} = 0.0024$ mol Fe^{2+}.mol carbon^{-1}.s^{-1}, $K = 0.05$ (Hansford, 1997).

The second analysis (including biomass balance) yields a slightly better fit for the 10% (v/v) inoculum (Figure 5.13b). However, the pseudo-steady state at the lower ferric/ferrous ion ratio was not accurately predicted, and the regressed rate constants $q^{max}_{Fe^{2+}} = 1.0 \times 10^{-4}$ mol Fe^{2+}.mol carbon^{-1}.s^{-1}, $K = 0.033$ for the microbial oxidation rate were not comparable with those reported in literature. Therefore, the rate constants obtained during the first analysis was adopted for the dynamics analysis that follows.

From the chalcopyrite rate curves in Figure 5.14, it is shown that the predicted microbial oxidation rate at low solution potentials and microbial concentration exceeds the chalcopyrite leaching rate. The reaction is thus driven to higher solution potentials with microbial growth. On the other hand, the 1% (v/v) inoculum data shown in Figure 5.14a reveals fast bioleaching rates are achieved when the redox potential remains below the redox potential at bifurcation

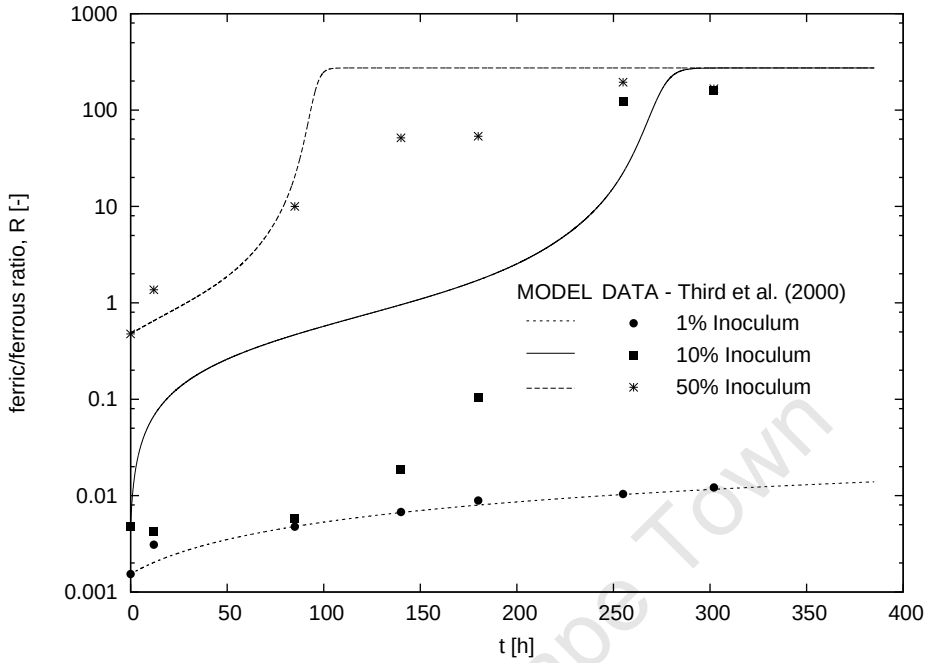

(a) Approach 1

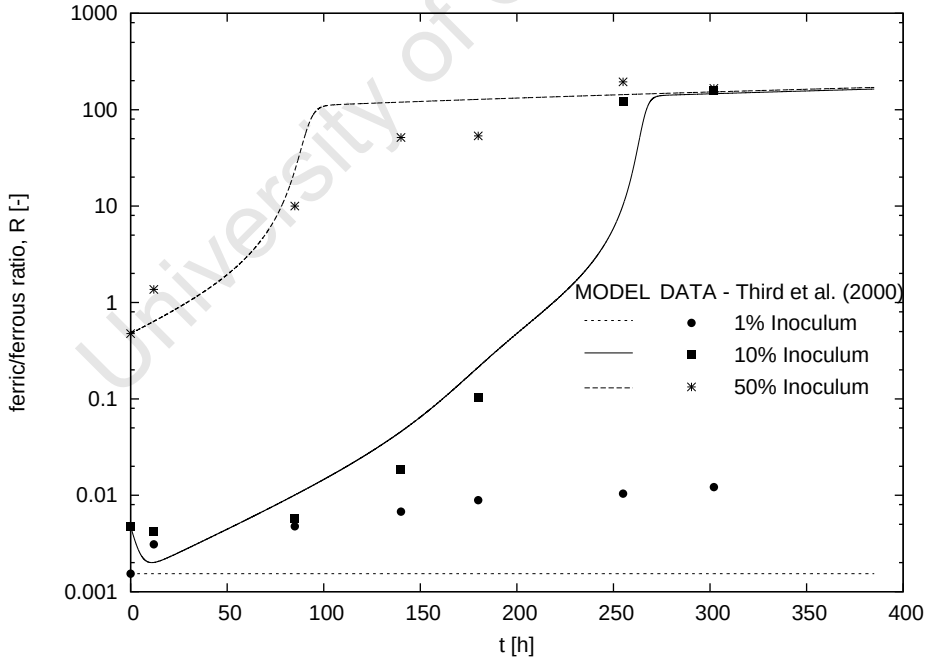

(b) Approach 2

Figure 5.13: Dynamics model validation against chalcopyrite bioleaching data extracted from Third *et al.* (2000)

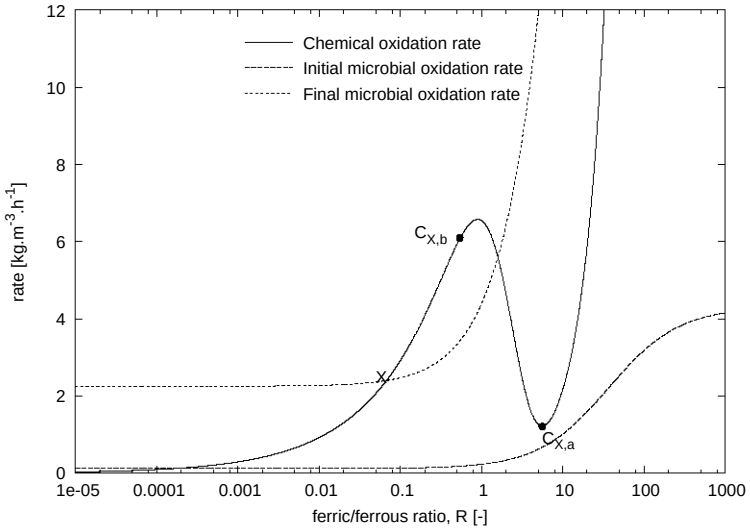

(a) 1% Inoculum

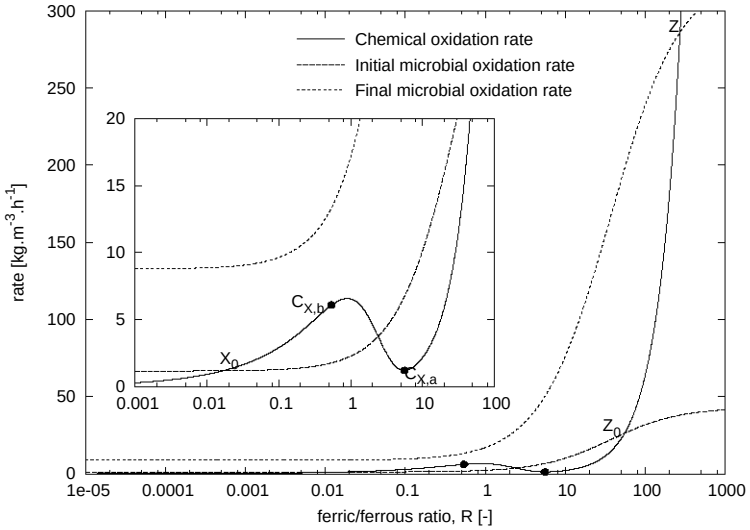

(b) 10% Inoculum

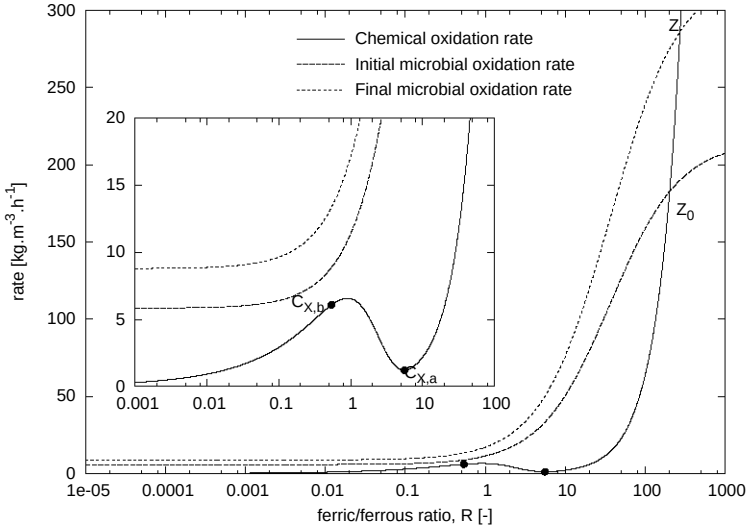

(c) 50% Inoculum

Figure 5.14: Predicted microbial and leaching rates for experimental data extracted from Third *et al.* (2000). Annotations X and Z indicate stable pseudo-steady states at low and high ferric/ferrous ion ratios, respectively.

biomass concentration $C_{X,b}$, $R = 0.54$ [-]. Since ferrous ions are not actively converted to ferric ions and there was no noticeable microbial growth at these conditions, the system remains at the low ferric/ferrous ion ratio range where fast bioleaching rates X are observed.

Similarly, in the 50% (v/v) inoculum experiment low rates are observed at high ferric/ferrous ion ratios, beyond the bifurcation biomass concentration $C_{X,a}$, $R = 5.62$ [-], as predicted by the model (Figure 5.14c). Due to the high initial redox potential combined with a large initial inoculum size, the system immediately falls to slow overall rates Z_0. The system will therefore never attain fast bioleaching rates since the microbial oxidation rate only intersects the chemical leaching rate once at ferric/ferrous ion ratios beyond the bifurcation biomass concentration $C_{X,a}$.

Third *et al.* (2000) noted that with the 10% (v/v) inoculum experiment, the copper leaching rate was fast when microbial activity was low. With microbial growth, and hence an increase in the ferric/ferrous ion ratio, the bioleaching rate moved from fast to slow bioleaching rates when 10% (v/v) inoculum was introduced to the experiment at low solution potentials. At the given conditions, it can be seen in Figure 5.14b that the microbial oxidation rate curve intersects the chemical leaching rate curve thrice, with stable pseudo-steady states observed at low X_0 and high Y_0 ferric/ferrous ion ratios. With increased microbial activity and hence growth, ferrous ions are converted to ferric ions thereby increasing the ferric/ferrous ion ratio. Bioleaching rates therefore move from fast X_0 to slow Z overall rates due to the change in the solution potential and microbial concentration. It is also noted in Figure 5.14b that with microbial growth, there is a transition from two possible stable pseudo-steady states X_0 and Z_0, when three intersections are observed, to a single stable pseudo-steady state Z when the microbial oxidation rate curve intersects the chemical leaching rate curve once, at high ferric/ferrous ion ratios. This transition from multiple X_0, Z_0 to single Z stable pseudo-steady states verifies that a critical microbial concentration exists prior to system inhibition (Figure 5.14b).

5.10 Conclusions

The dynamics analysis shows that the overall rate is inhibited when a certain critical microbial concentration and solution potential is exceeded. Analysis of the experimental data and model indicated that the microbial concentration can be both beneficial and detrimental to the overall bioleaching process and is largely dependent on the initial redox potential. In light of these analyses, the existing experimental observations such as those by Third *et al.* (2000) can now be understood and brought within a single unified theoretical framework.

Now that the dynamics analysis for the bioleaching of sulphide mineral ores in batch reactors has been established, it is important to develop the analysis for continuous flow reactor systems. The above analysis assumes that the particle surface does not change with time and therefore does not influence the dynamic structure of the system. However, the formation

of ferrous ions in the chemical leaching step suggest that the particle surface area changes with particle-solution contact time and reaction. The dynamics analysis should therefore account for this change.

In the following chapter, the dynamics analysis is extended to the case when the particle surface area varies with time by incorporating the modified PBM developed in Chapter 4 for continuous flow reactor systems. Influences of solution redox potential, biomass concentration and mean residence time on system steady states are investigated for the purpose of maximizing overall production.

6

A Dynamic Analysis Of Chalcopyrite Bioleaching In Continuous Flow Reactor Systems

6.1 Introduction

In Chapter 4, a model was developed to determine the reactor performance of continuous flow bioleach reactors. The objective was to develop a reactor model for tank bioleaching using a modified Population Balance Model (PBM) approach that incorporated the bioleaching subprocess mechanism. Since the PBM incorporates non-linear intrinsic rate expressions, a dynamics analysis of the bioleaching of mineral sulphide ores was necessary to ascertain whether more than one steady state may exist in continuous flow bioleach reactor systems. Like in the case with the batch reactor analysis, the dynamics analysis is initially developed assuming a fixed particle surface area during leaching to determine the influence of biomass concentration, the ferric/ferrous ion ratio and mean residence time on steady state operation. Thereafter, by application of the modified PBM, the simplified surface area assumption is eliminated to further establish the influence of time-varying particle surface area on observed steady states.

6.2 Continuous Flow Dynamics

When modeling continuous flow reactors, it is assumed that particles fed to the reactor are instantly perfectly mixed with the other particles already present. The fluid phase concentrations and temperature in the vicinity of each particle in the reactor are therefore considered to be the same. The reactor is normally operated at steady hydrodynamic conditions and since it is assumed to be perfectly mixed, the conditions in the exit stream from the reactor are identical to those inside the reactor.

Due to the system being in a state of continuous flow, the transient change in ferric and ferrous ions is dependent on the mean residence time in the reactor. In performing

a dynamics analysis, the unsteady state balances describing system evolution is initially developed (Eqs. 6.1 and 6.2).

$$\frac{dC_{Fe^{3+}}}{dt} = \frac{C_{Fe^{3+},inlet} - C_{Fe^{3+}}}{\tau} - \alpha r_{MS} + r_{Fe^{2+}} \quad [6.1]$$

$$\frac{dC_{Fe^{2+}}}{dt} = \frac{C_{Fe^{2+},inlet} - C_{Fe^{2+}}}{\tau} - \beta r_{MS} - r_{Fe^{2+}} \quad [6.2]$$

where τ [s] is the mean particle residence time and $C_{Fe^{3+},inlet}$, $C_{Fe^{2+},inlet}$ and $C_{Fe^{3+}}$, $C_{Fe^{2+}}$ [mol.m^{-3}] are the inlet and outlet concentrations of the ferric and ferrous ions, respectively. Since the focus of this section is on the chemistry and not the hydrodynamics of the system, the inlet and outlet flowrates to and from the reactor are assumed constant and hence the mean residence time τ [s] is also constant. Scenarios in which the flow rates are not constant, and hence the mean residence time is a function of time, will be investigated in Chapter 7.

Substituting the material balances in Eqs. 6.1 and 6.2 into Eq. 5.3 and simplifying, yields the transient change in solution redox potential $R = C_{Fe^{3+}}/C_{Fe^{2+}}$ [-] for a continuous flow bioleach reactor (Eq. 6.3).

$$\frac{dR}{dt} = \frac{(R+1)\cdot r_{Fe^{2+}} - (\beta R + \alpha)\cdot r_{MS}}{C_{Fe^{2+}}} + \frac{C_{Fe^{3+}_{inlet}}\left(1 - \frac{R}{R_{inlet}}\right)}{\tau C_{Fe^{2+}}} \quad [6.3]$$

where R_{inlet} [-] is the inlet ferric/ferrous ion ratio to the continuous stirred tank bioleach reactor.

Steady state(s) with respect to R for the continuous flow bioleach reactor are obtained when the LHS in Eq. 6.3 is zero (Eq. 6.4). From Eq. 6.4 we note that the first term on the RHS is the familiar batch term derived in Eq. 5.7 (see § 5.3) while the second term is the change in the ferric/ferrous ion ratio R resulting from flow into and out of the bioleach reactor of the principal ferric and ferrous ions.

Batch Reactor:

$$\underbrace{(R+1)\cdot r_{Fe^{2+}}}_{r_M} = \underbrace{(\beta R + \alpha)\cdot r_{MS}}_{r_L^B} \quad [5.7]$$

Continuous Flow Reactor:

$$\underbrace{(R+1)\cdot r_{Fe^{2+}}}_{r_M} = \underbrace{(\beta R + \alpha)\cdot r_{MS} - \frac{C_{Fe^{3+}_{inlet}}}{\tau}\left(1 - \frac{R}{R_{inlet}}\right)}_{r_L^F} \quad [6.4]$$

where α and β are the stoichiometric coefficients of the ferric and ferrous ions in solution according the chemical leaching reaction (Eq. 5.1), respectively, $r_{Fe^{2+}}$ [mol.m^{-3}.s^{-1}] and r_{MS} [mol.m^{-3}.s^{-1}] the microbial oxidation and chemical leaching intrinsic rates, and for simplicity, the microbial oxidation $(R+1)\cdot r_{Fe^{2+}}$ and chemical leaching $(\beta R + \alpha)\cdot r_{MS}$ rate functions for the batch system are assigned as r_M and r_L^B, respectively (Eq. 5.7). The microbial oxidation rate function on the LHS and the chemical leaching rate function on the

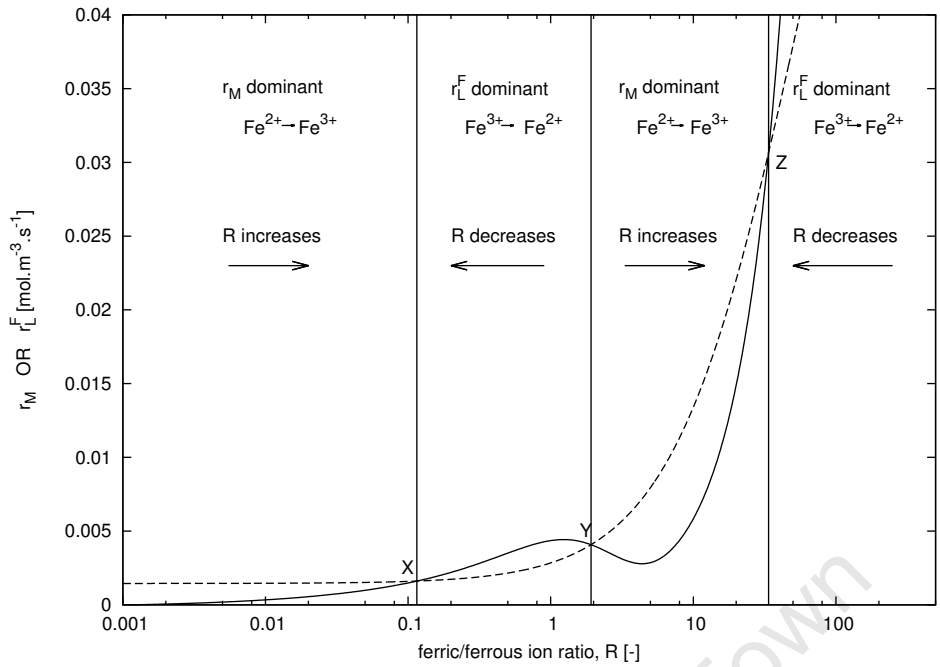

Figure 6.1: Dynamics analysis of chalcopyrite bioleaching in continuous flow systems. Steady states exist at the intersection of the rate function curves. The solid curve indicates the chemical leaching rate function r_L^F and the dotted curve the microbial oxidation rate function r_M in Eq. 6.4

RHS of Eq. 6.4 for the bioleach flow system will, from this point onwards, be referred to by r_M and r_L^F, respectively.

The dynamics analysis of the flow reactor is analogous to the batch case; steady state(s) are the points of intersection between the microbial oxidation rate function curve $(R+1)r_{Fe^{2+}}$ and the chemical leaching rate function curve $(\beta R+\alpha)r_{cpy}$, excepting that the latter term must be offset by the flow contribution $\frac{C_{Fe^{3+}_{inlet}}}{\tau}\left(1-\frac{R}{R_{inlet}}\right)$ (Figure 6.1)

In any region in Figure 6.1 where the microbial oxidation rate function r_M lies above the chemical leaching rate function r_L^F, ferrous ions are converted to ferric ions (Eq.1.2). In this region, the overall rate shifts to higher redox potentials (R increases, see Figure 6.1) where a steady state is observed at the intersection of the rate curves at points X and Z in Figure 6.1. However, when chemical leaching (Eq. 5.1) is the dominant reaction, the overall rate shifts to lower ferric/ferrous ion ratios (R decreases, see Figure 6.1). In the case of chalcopyrite bioleaching, stable steady states are observed at low X and high Z redox potentials. The intersection Y observed between these rate curves is an unstable steady state, since dominating microbial oxidation and chemical leaching reactions are observed at redox potentials to the left and right of this intersection point, respectively, which shift the overall rate to lower X or higher Z ferric/ferrous ion ratios, respectively. In other words, in the vicinity of Y, unless the initial state is exactly on Y, the system tends to fall away from R_Y. As with the batch system, the dynamics analysis of chalcopyrite bioleaching in the continuous flow system reveals two stable steady states at low X and high Z ferric/ferrous ion ratios with an unstable steady state Y at intermediate redox potentials.

Up to this point, the dynamics analysis was developed under a fixed particle surface area assumption, regardless of the disappearance of mineral from the particle due to reaction. For more accurate analysis, however, this simplified assumption has to be eliminated and a Population Balance has to be integrated into the formulation.

6.3 Continuous Flow Dynamics: Application of the modified PBM

In the previous sections, the reactor volume-based leaching rate r_{MS} in Eqs. 6.3 and 6.4 was assumed to be equivalent to the intrinsic leaching rate of chalcopyrite in Eq. 2.19 multiplied by the fixed reactor-volume based particle specific surface area A^V [$m^2.m^{-3}$] which is the product of the particle specific surface area A^p [$m^2.kg^{-1}$] with particle mass M^p [kg] relative to the reactor volume V^R [m^3] (Eq. 6.5).

$$A^V = \int_0^\infty \int_0^\infty A^p(\theta, l_0) \frac{M^P(\theta, l_0)}{V^R} N^T I(\theta) f_0(l_0) d\theta dl_0 \qquad [6.5]$$

These studies were used to establish a basis for the dynamics analysis without the complicating influence of time-varying particle surface area changes. Now that the procedure is established, the more rigorous analysis must be performed.

As determined in Chapter 4, the overall leaching rate r^R [$mol.m^{-3}.s^{-1}$] in Eq. 4.21 is a function of the particle specific surface area A^p [$m^2.kg^{-1}$], particle residence time or age θ [s], inlet particle size l_0 [m] and the intrinsic leaching rate $r'' = r_{MS}$ [$mol.m^{-2}.s^{-1}$]. Accepting that there exists a distribution in age $I(\theta)$ [s^{-1}] within the reactor and that a non-trivial distribution of particle size $f_0(l_0)$ [m^{-1}] applies at to the reactor feed, the overall leaching rate (Eq. 6.7 which is analogous to Eq. 4.25 in Chapter 4) and hence the dynamics analysis for the flow system with changing particle size can be determined (Eq. 6.6).

$$r^R = \phi_{MS} \cdot r_{MS} A^V \qquad [6.6]$$

or

$$r^R = \int_0^\infty \int_0^\infty r_{MS} A^p(\theta, l_0) \frac{M^p(\theta, l_0)}{V^R} \phi_{MS} N^T I(\theta) f_0(l_0) d\theta dl_0 \qquad [6.7]$$

Since the intrinsic leaching rate is reported on a surface area basis, the particle leaching rate will be the product of the intrinsic leaching rate with the particle specific surface area, which itself is a function of the particle residence time and inlet size. The dynamics analysis for bioleaching mineral sulphide ores therefore indicates a shift in steady state due to the time-varying particle surface area and is expected to yield different results from the analysis for a continuous flow system with the fixed surface area assumption.

The time-varying change in particle surface area due to leaching is incorporated in the overall leaching rate r^R (Eq. 6.7). The intrinsic leaching rate r_{MS} in Eq. 6.4, multiplied by

the particle specific surface area (Eq. 6.5), in the dynamics analysis for a continuous bioleach system is consequently equivalent to the overall leaching rate r^R in Eq 6.7 (Eq. 6.8).

$$\underbrace{(R+1)\cdot r_{Fe^{2+}}}_{r_M} = \underbrace{(\beta R+\alpha)\cdot r^R - \frac{C_{Fe^{3+}_{inlet}}}{\tau}\left(1-\frac{R}{R_{inlet}}\right)}_{r_L^S} \qquad [6.8]$$

where r_L^S is the overall chemical leaching rate function that incorporates a time-varying particle surface area due to reaction and flow.

Now that a model has been developed, a rigorous dynamics analysis for the bioleaching of chalcopyrite bioleaching can be performed in continuous flow systems. Process variables which influence the dynamics of the system will be identified using a sensitivity analysis applying the constant surface area assumption. This assumption will then be relaxed to incorporate a reaction rate that includes the change in particle surface area.

6.4 Sensitivity Analysis

In order to exploit the dynamics to achieve high bioleaching rates, the sensitivity of the rates involved to all factors should be examined. It is evident from Eqs. 6.4 and 6.8 that these operating parameters may include the biomass concentration C_X, which directly affects the microbial oxidation rate (Eq. 4.2), the mean residence time τ and the inlet ferric/ferrous ion ratio R_{inlet}. An increase or decrease in any of these parameters will shift either or both of the rate curves resulting in a change to the dynamic structure of the system.

In the following sections, a dynamics analysis for the bioleaching of chalcopyrite will be undertaken to determine the influence of the aforementioned process variables on the dynamic structure of the system. Initially, the dynamics analysis will use the constant particle surface area assumption to compare the influence of mean residence time on steady operation in a CSTR. Thereafter, this assumption will be relaxed by incorporating the modified PBM approach, developed in Chapter 4, in the dynamics analysis that considers particle surface area changes with reaction. Kinetic constants applied in the sensitivity analysis using the constant surface area assumption are reported in Table 6.1. The chemical leaching rate constants A and B are obtained from the Arrhenius terms developed in Chapter 5 at 343.15 K from the chemical leaching experiments performed by Kametani and Aoki (1985) while microbial oxidation rate constants $q^{max}_{Fe^{2+}}$ and K were assumed to follow a Arrhenius relationship established by Searby (2006).

6.4.1 Influence of Biomass

The microbial oxidation rate is directly proportional to the biomass concentration C_X (Eq. 4.2). As such, increases in C_X can be represented graphically by an upward shift

Table 6.1: Chemical leaching and microbial oxidation rate constants utilised in the dynamics analysis for a continuous flow system applying the (a) constant particle surface assumption and (b) a time-varying particle surface area by incorporating the modified PBM.

Chemical Leaching Rate Constants			Microbial Oxidation Constants	
A	B	R_{crit}	$q^{max}_{Fe^{2+}}$	K
(a) Constant Particle Surface Area				
1.27×10^{-3}	2.5×10^{-5}	1	3.02×10^{-3}	0.019
$[mol.m^{-3}.s^{-1}]$	$[mol.m^{-3}.s^{-1}]$	[–]	$[molFe^{2+}.m^{-1}carbon.s^{-1}]$	[–]
(b) Time-Varying Particle Surface Area				
1.63×10^{-7}	3.2×10^{-9}	1	3.02×10^{-3}	0.019
$[mol.m^{-2}.s^{-1}]$	$[mol.m^{-2}.s^{-1}]$	[–]	$[molFe^{2+}.m^{-1}carbon.s^{-1}]$	[–]

in the rate curve from L_1 to L_3 in Figure 6.2 with corresponding biomass concentrations $C_{X,1}$ and $C_{X,3}$, respectively. The microbial oxidation rate function curve passes from a single intersection between L_1 and the chemical leaching rate function curve at low solution redox potentials to multiple intersections between L_2 (at biomass concentration $C_{X,2}$) and the leaching rate curve. Finally, a single intersection L_3 is observed at high ferric/ferrous ion ratios with increasing biomass concentration thus changing the dynamics structure of the system. This change in dynamic structure due to any change in a process variable is known as a bifurcation.

Biomass concentrations below $C_{X,a}$ and above $C_{X,b}$ (corresponding to curves L_a and L_b in Figure 6.2, respectively) are critical values at which the dynamics picture for the system changes from a 3-steady state case to a single stable steady state. Points $C_{X,a}$ and $C_{X,b}$ are therefore bifurcation points. Graphically, bifurcation points $C_{X,a}$ and $C_{X,b}$ with corresponding ferric/ferrous ion ratios $R_{a,B}$ and $R_{b,B}$, respectively, occur when the microbial oxidation and chemical leaching rate function curves are tangent and equal to each other. Mathematically bifurcation points can be obtained when the rate functions r_M and r^F_L, as well as, the gradients with respect to R, are equal (Eqs. 6.4 and 6.9).

$$\frac{d\left[(\beta R+\alpha)\cdot r_{MS}-\frac{C_{Fe^{3+}_{inlet}}}{\tau}\left(1-\frac{R}{R_{inlet}}\right)\right]}{dR}=\frac{d\left[(R+1)\cdot r_{Fe^{2+}}\right]}{dR} \qquad [6.9]$$

The phase plane presented in Figure 6.2b is generated by varying the biomass concentration C_X and re-evaluating the steady states at the corresponding ferric/ferrous ion ratios R. A characteristic S-shaped curve with bifurcation points $C_{X,a}$ and $C_{X,b}$ is obtained. The dynamics analysis on the continuous bioleach reactor reveals similar trends to those observed in the batch system. If a phase plane of steady states for the bioleaching of chalcopyrite are plotted for the continuous flow bioleach reactor together with pseudo-steady states observed for a batch system for given steady state microbial concentrations, the influence of flow can readily be understood (Figure 6.3).

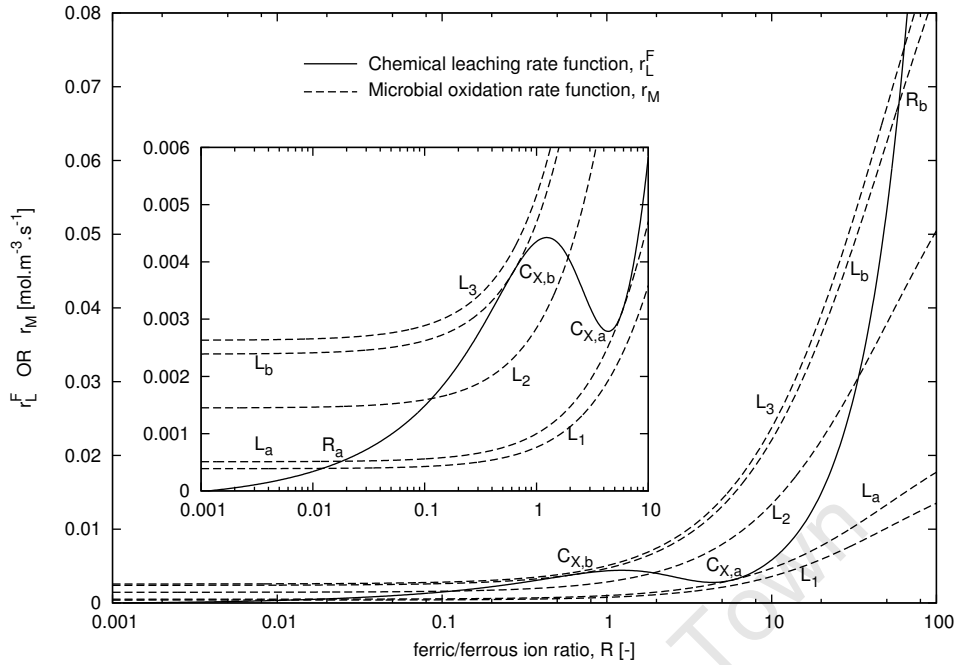

(a) Rate function curves with increasing biomass concentration

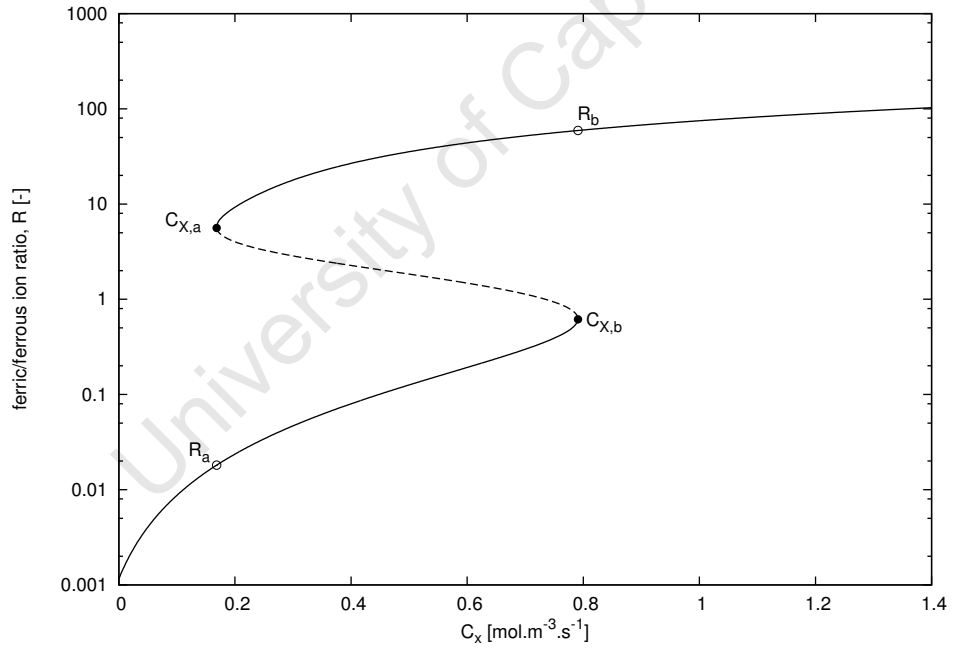

(b) $R - X$ plane

Figure 6.2: Chemical leaching rate function r_L^F with a family of microbial oxidation rate function curves r_M with biomass concentrations $C_{X,1}$, $C_{X,2}$ and $C_{X,3}$ corresponding to curves L_1, L_2 and L_3 respectively and concentrations $C_{X,a}$ and $C_{X,b}$ correspond to curves L_a and L_b, respectively (Figure (a)). $C_{X,a}$ and $C_{X,b}$ are the bifurcation points. In Figure (a) the microbial oxidation rate function curve r_M shifts upwards with increasing biomass concentration $C_{X,1} < C_{X,2} < C_{X,3}$. Single steady states occur when the biomass concentration is less than $C_{X,1}$, L_1 or greater than $C_{X,3}$, L_3. Multiple points of stability are observed when the concentration is $C_{X,2}$, L_2. Low bioleaching rates occur when one intersection point is observed L_1, L_3. Solid curves in the $R - X$ plane in Figure (b) indicate stable steady states and the dotted curve unstable steady states.

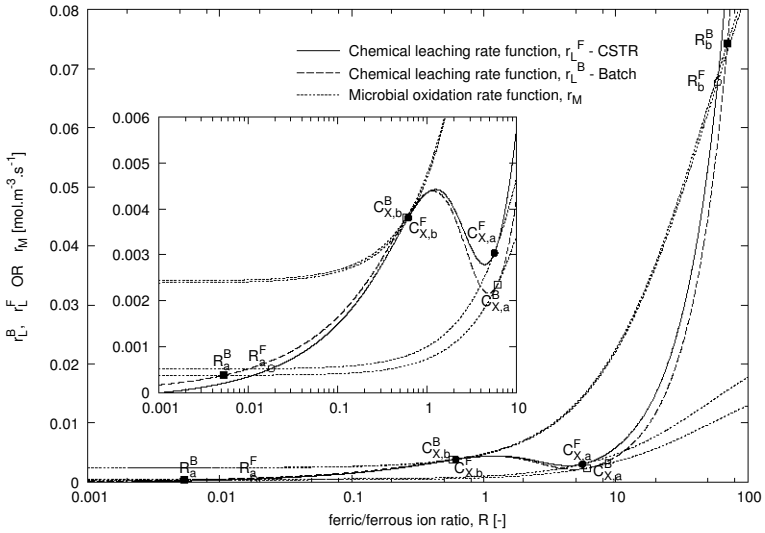

(a) Bifurcation points in batch r_L^B and continuous flow r_L^F systems

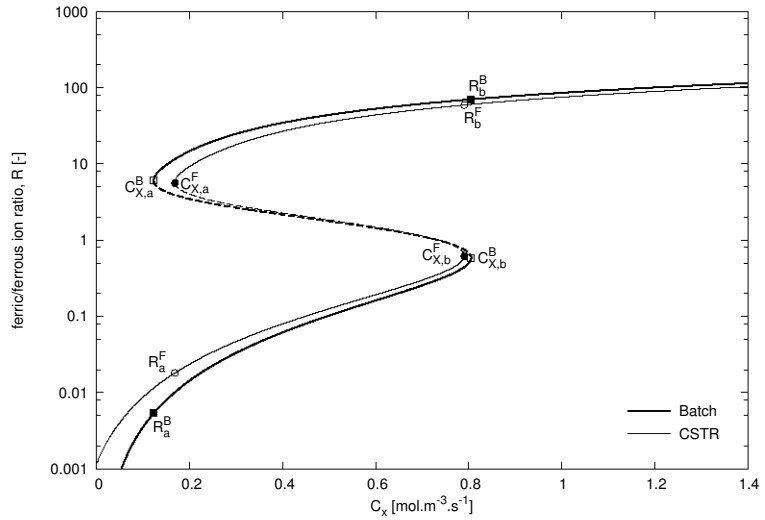

(b) $R - X$ plane of steady-states in batch and continuous flow systems

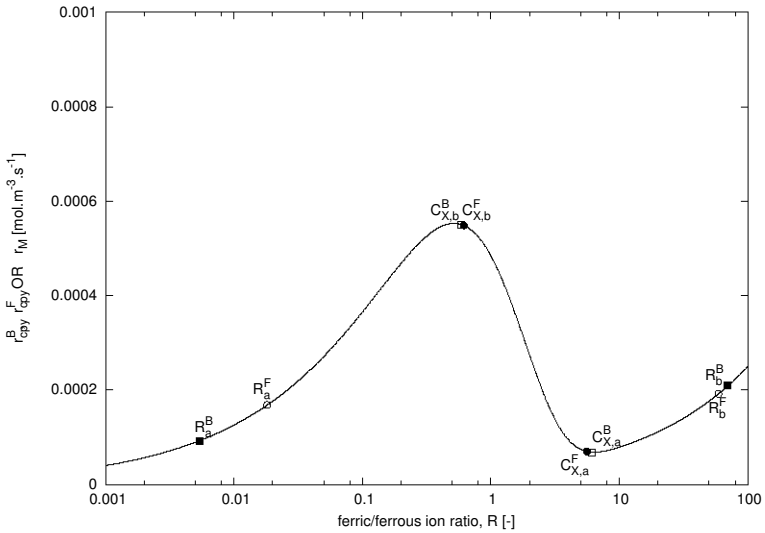

(c) Reaction rate

Figure 6.3: Comparison of the dynamics analysis of chalcopyrite bioleaching in a batch reactor and a CSTR. Parameters superscripted with F and B refer to flow (CSTR) and batch reactor systems, respectively. Reaction rates are determined from the chemical leaching rate curve at the corresponding redox potentials R shown in Figure (c).

The phase plane for the continuous flow bioleach reactor was generated for a reactor operating with a mean residence time of $\tau = 2$ days. In Figure 6.3, it can be seen that when bioleaching chalcopyrite in either a batch or continuous flow reactor, steady states are achieved at slightly different overall solution redox potentials for the same biomass concentrations (*viz.* R_a^B, R_b^B and $C_{X,a}^B$, $C_{X,b}^B$ for the batch reactor and R_a^F, R_b^F and $C_{X,a}^F$, $C_{X,b}^F$ for the continuous flow reactor in Figure 6.3). The similarities in the two dynamics trends in Figure 6.3b is due to the first term on the RHS of Eq. 6.3, the batch term, being much greater than the second term on RHS of Eq. 6.3, the flow term for a mean residence time of 2 days. The magnitude of the flow term is directly proportional to the ferric ion concentration in the feed stream to the CSTR and inversely proportional to the mean residence time. The greater the inlet ferric ion concentration to the continuous flow system, and the smaller the mean residence time, the more pronounced the differences between pseudo-steady states in the batch and steady states in a continuous flow bioleach reactors are. Using low flow rates (hence large residence times) would result in a system which operates close to batch operation and hence it would be expected that when the flow rate is reduced, the CSTR curve approximates the batch curve.

6.4.2 Influence of Mean Residence Time

In order to determine the influence of the mean residence time on the dynamics analysis of the continuous flow bioleach reactor, mean residence times 0.5, 0.75, 1, 2, 5 and 10 days were simulated and the steady state curves plotted together with that for a batch reactor (Figure 6.4). Figure 6.4 reveals that as the mean residence time in the continuous flow reactor is increased the system approaches batch operation. This is expected since large mean residence times would eliminate the flow term in Eq. 6.4 thus driving the system to batch operation (Eq. 5.7).

Steady states in the CSTR at redox potentials below the bifurcation biomass concentration $C_{X,b}^F$ equilibrate at higher ferric/ferrous ion ratios than those achieved in the batch reactor (*viz.* R_a^B and R_a^F for the batch reactor and CSTR, respectively, in Figure 6.3), while steady operation occurs at lower redox potentials for ferric/ferrous ion ratios above bifurcation biomass concentration $C_{X,a}^F$ than in the batch reactor (*viz.* R_b^B and R_b^F for the batch and continuous flow reactors, respectively, in Figure 6.3). This implies that high overall bioleaching rates can be achieved at higher solution redox potentials in the CSTR than in the batch reactor while the critical ferric/ferrous ion ratio prior to the system transitioning to low bioleaching rates (Figure 6.3c) remains relatively constant at bifurcation biomass concentrations $C_{X,b}^F$, $C_{X,b}^B$. However, low rates are observed at lower ferric/ferrous ion ratios that are above bifurcation biomass concentration $C_{X,a}^F$ than at equivalent points in the batch system, hence requiring a higher microbial activity (*viz.* R_a^B and R_a^F for the batch reactor and CSTR, respectively, in Figure 6.3c).

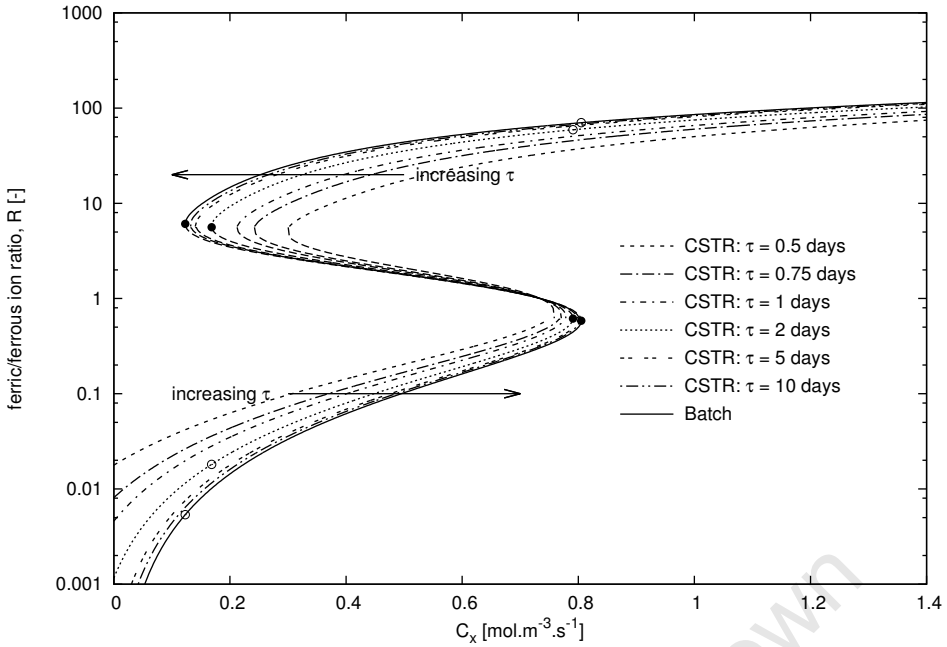

Figure 6.4: The influence of the mean residence time τ on the points of stability and the ferric/ferrous ion ratio R in a continuous flow system.

6.4.3 Influence of ferric-to-ferrous ion ratio

Up to this point the system dynamics has focussed on the influence of the steady state ferric/ferrous ion ratio R on the dynamic structure of the system (Eqs. 5.7, 6.4 and 6.8). This analysis is not sufficient to determine the system steady state since the redox potential continuously increases with microbial oxidation thus driving the bioleaching reaction to high ferric/ferrous ion ratios where low overall steady state bioleaching rates are observed. The biomass concentration C_X explicitly appears in the ferric/ferrous ion ratio R balance in Eq. 6.8 *via.* the microbial oxidation rate expression $r_{Fe^{2+}}$ (Eq. 4.2), which implies that steady state is only possible when both C_X and R are at steady state. As such, the dynamics associated with biomass growth also needs to be developed. To determine the dependence of the system on the biomass concentration, the unsteady state mass balance over the continuous flow bioleach reactor is initially developed (Eq. 6.10).

$$\frac{dC_X}{dt} = \frac{C_{X,inlet} - C_X}{\tau} + Y_{XS} r_{Fe^{2+}} \qquad [6.10]$$

where $C_{X,inlet}$ and C_X [mol carbon.m^{-3}] are the inlet and outlet biomass concentrations, respectively, and Y_{XS} [-] is the biomass yield defined as the moles of biomass produced per mole of substrate.

The biomass concentration in a flow system increases proportionally with the rate of ferrous ion consumption. Since no biomass is present in the inlet stream to the reactor ($C_{X,inlet} = 0$) and incorporating the microbial oxidation reaction rate expression (Eq. 4.2), the steady state

conditions applied to Eq. 6.10 yields Eq. 6.11.

$$R_S = \frac{Y_{XS} q^{max}_{Fe^{2+}} \tau - 1}{K} \quad [6.11]$$

where the subscript S is introduced to emphasize that these are the steady state values. This equation gives an additional constraint which when coupled with the locus of possible steady states on the R-X plane (Figure 6.5a), yields the single possible steady state R-value R_S.

Figure 6.5 was generated to demonstrate the influence of the inlet ferric/ferrous ion ratio to the reactor (Figure 6.5a and b) and the initial ferric/ferrous ion ratio inside the bioleach reactor (Figure 6.5c) on stable steady states in a flow reactor system with changing particle surface area. Ratios ranging from 0.25 to 200 [-] were investigated. The time profile for the ferric/ferrous ion ratio R was determined by integrating Eq. 6.3 assuming a 2 day mean residence time. Irrespective of the inlet conditions to the reactor or the initial ferric/ferrous ion ratio inside the reactor, the system always shifted to a single steady state R-value in the high ferric/ferrous ion ratio region, confirming that the system operating point is determined by the ferric/ferrous ion ratio R_S (Eq. 6.11).

6.4.4 Influence of Time-Varying Particle Surface Area

The preceding sensitivity analyses determined the influence of varying the biomass concentration, mean residence time and inlet ferric/ferrous ion ratio on the dynamic structure of the system without the application of a time-varying particle surface area. In reality, the degree to which particle mass is liberated into the aqueous phase is influenced by the rate of reaction and particle-solution contact time. This change in mass relates to a change in particle surface area and should be incorporated into the dynamics analysis to determine its influence on system steady states. This influence is presented in Figure 6.6 by means of comparing the steady states achieved in a batch reactor (Eq. 5.7) and a continuous flow reactor with (Eq. 6.8) and without (Eq. 6.4) the application of time-varying particle surface area by incorporation of the developed PBM.

The dynamics analyses in the following, and subsequent sections, were performed assuming a mean particle size of 12.5×10^{-6} m and 2 days mean residence time under conditions of perfect mixing in the reactor. Kinetic constants A and B for the intrinsic leaching rate in Eq. 2.19 and the maximum microbial specific ferrous iron utilisation rate $q^{max}_{Fe^{2+}}$ and inhibition constant K for the microbial oxidation rate in Eq. 4.2 applied in the dynamics analysis are reported in Table 6.1.

In Figure 6.6 it can be seen that steady states for the continuous flow system, as predicted using the overall leaching rate r^R formulated in Eq. 6.7, are obtained at lower biomass concentrations than in analyses that do not consider particle surface area changes. As explained before, the overall leaching rate will decrease as the reaction proceeds. This decrease in the leaching rate is graphically presented in Figure 6.7 (*viz.* $C^F_{X,b}$ and $C^S_{X,b}$ for

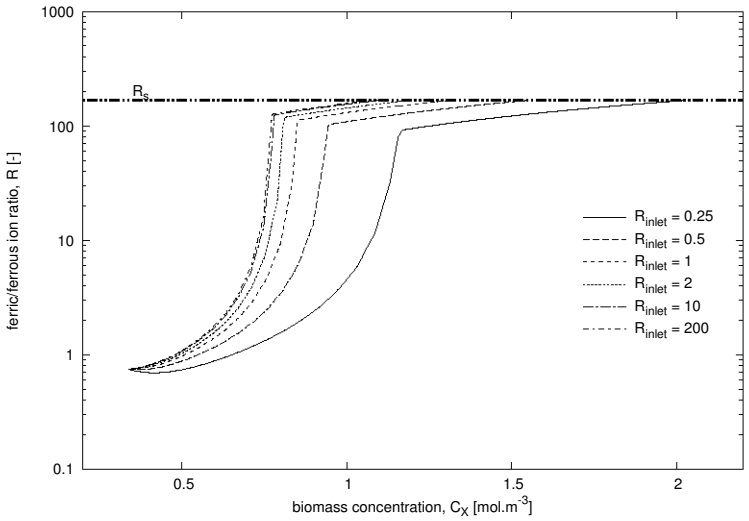

(a)

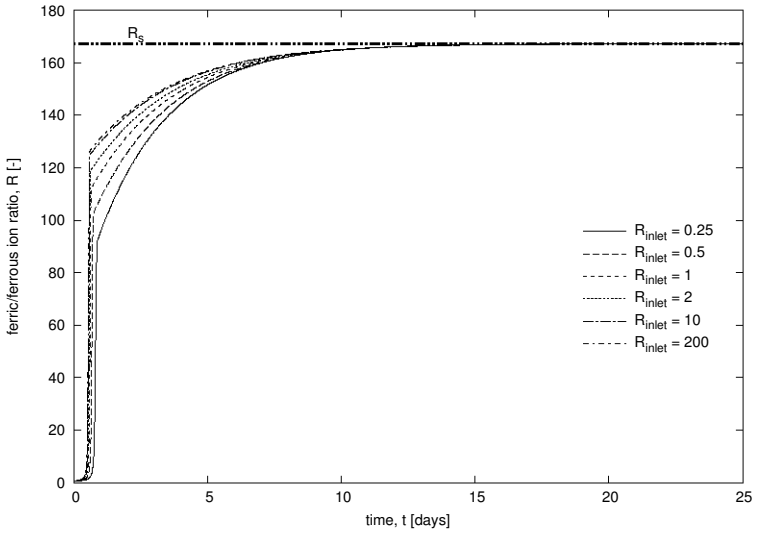

(b)

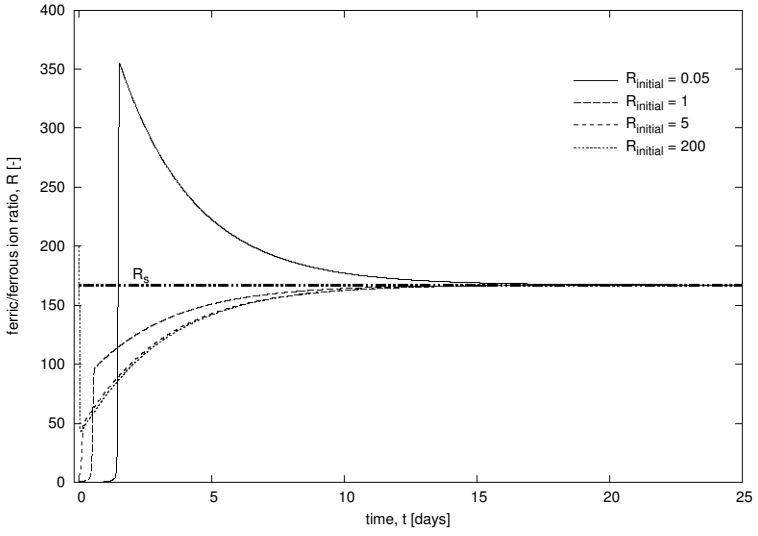

(c)

Figure 6.5: Steady state ferric/ferrous ion ratios R. Only a single stable steady state is achieved at $R_S = 167.2$ [-] for a mean residence time $\tau = 2$ days when either the inlet R_{inlet} (Figures (a) & (b)) or initial $R_{initial}$ (Figure (c)) ferric/ferrous ion ratio is varied.

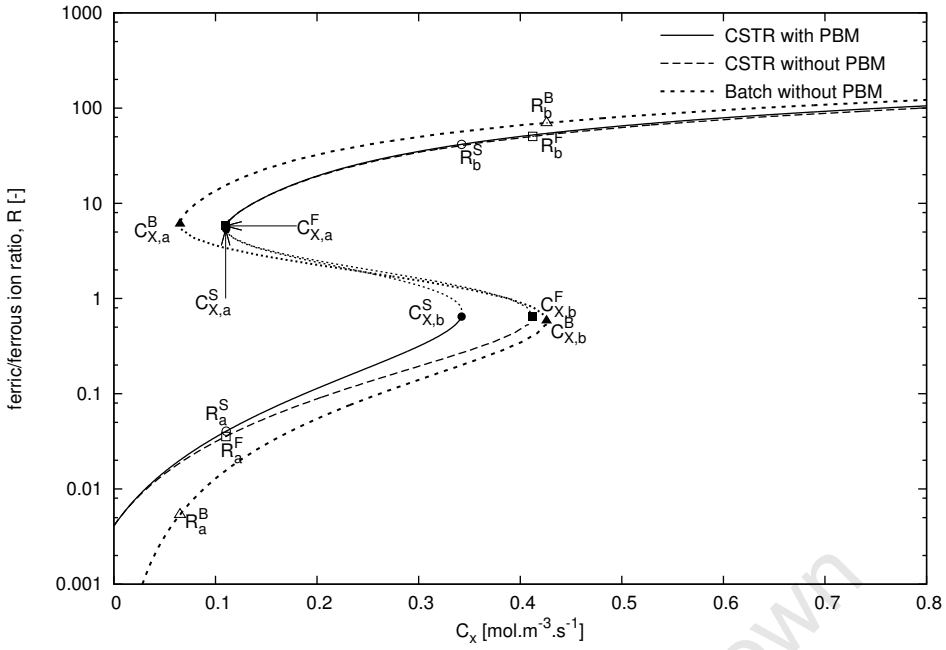

Figure 6.6: Comparison of steady states achieved during the bioleaching of chalcopyrite in a batch and CSTR. The values $C^i_{X,a}$ and $C^i_{X,b}$ indicate bifurcation points. Parameters superscripted with F and B refer to flow (CSTR) and batch reactor systems respectively, with the constant particle surface area, while parameters with superscript S refer to a flow reactor (CSTR) with time-varying particle surface area by application of the modified PBM.

the continuous flow reactor without and with the application of time-varying particle surface area, respectively) by a downward shift in the rate function to lower overall rates at the corresponding redox potential.

As the rate r^S_L is at an optimum at intermediate ferric/ferrous ion ratios *ca.* $R = 1$ the rate of change in the particle surface area is highest at bifurcation point $C^S_{X,b}$ in Figure 6.7. The greatest difference in the two rates r^F_L and r^S_L are therefore observed within this region. However, at low $R < 1$ and high $R > 1$ ferric/ferrous ion ratios the bioleaching rate is slow, therefore the change in particle surface area is small. Consequently, the difference in the rate curve r^S_L that incorporates time-varying particle surface areas with r^F_L that does not include these variances is minimal (*viz.* $C^F_{X,a}$, $C^S_{X,a}$ and R^F_a, R^S_a in Figure 6.7).

Now that the influence of biomass concentration, solution redox potential, mean residence time and time-varying particle surface areas on the dynamics analysis is known and the critical regions have been identified in the light of a dynamics analysis, practical outcomes such as obtaining high bioleaching rates can be investigated.

6.5 Optimisation

To optimise plant operation the process variables required to maximise production yield need to be identified. Optimum plant operation is typically achieved by maximising the

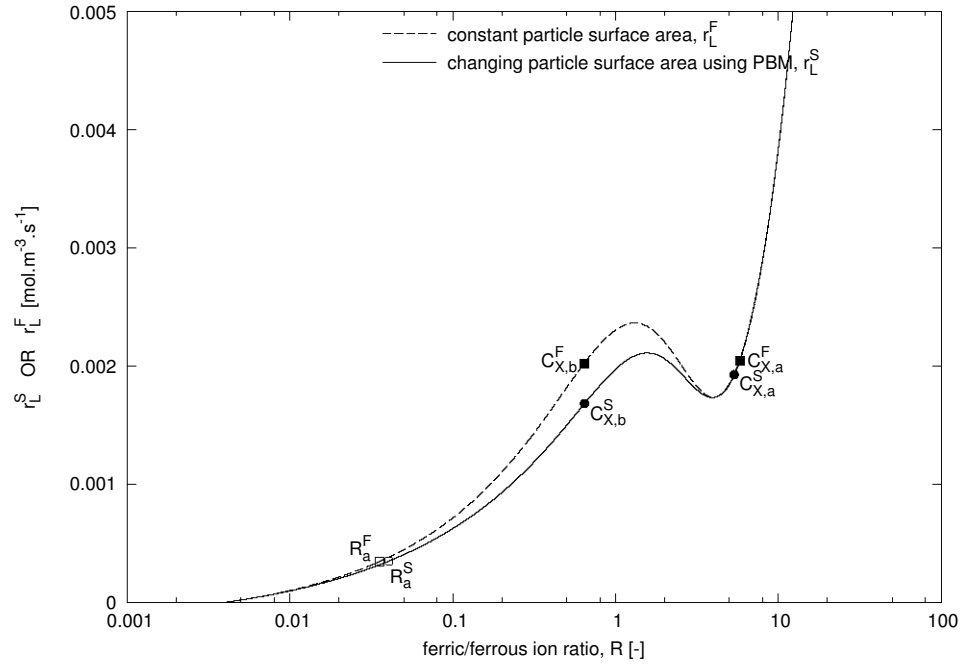

(a)

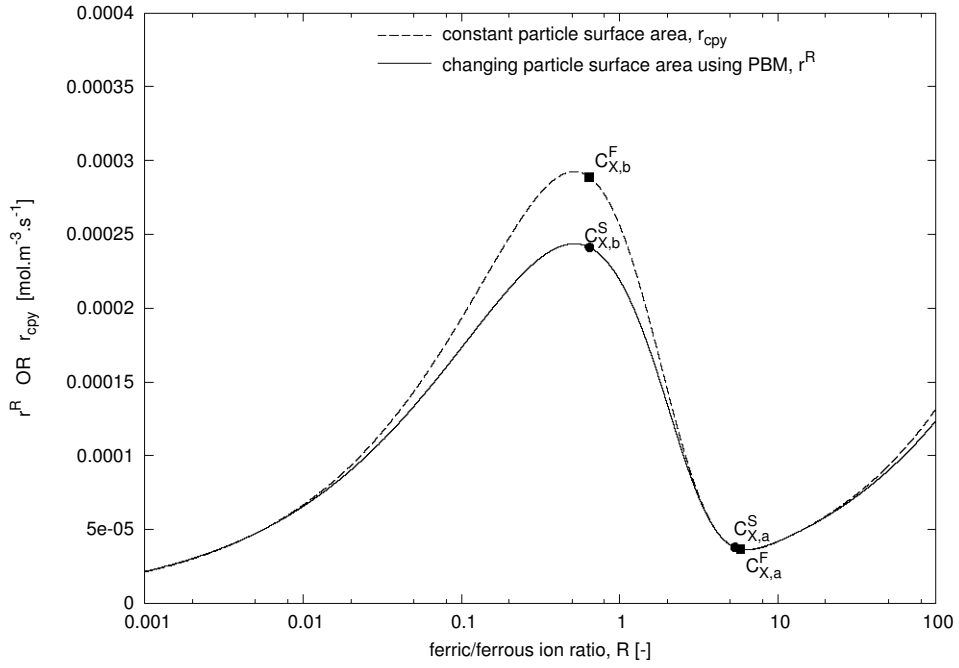

(b)

Figure 6.7: Comparison of the leaching rate for a CSTR with r_L^S and without r_L^F the application of particle surface area changes. Actual leaching rates are shown in Figure (b).

overall reaction rate. In bioleaching, valuable metals are obtained by means of the acid-ferric leaching of the mineral sulphide ore (Eq. 5.1). To achieve maximum product output the overall chemical leaching rate (Eq. 6.7) must be at a maximum thus making the overall chemical leaching rate an important optimisation parameter.

From the dynamics analysis we are able to identify operating conditions which maximise the overall reaction rate. In Figures 6.2 and 6.7, maximum rates are obtained at intermediate ferric-to-ferrous ion ratios ca. $R = 1$ while low rates are achieved at ferric/ferrous ion ratios $R > 1$. From these figures, it is clear that to maintain the rate at the maximum value, the microbial oxidation and chemical leaching rate curves must be tangent and equal to each other, which in this case, coincides with the bifurcation point $C_{X,b}$.

As previously noted, bifurcation points indicate a single branch of stable steady states prior to ($C_{X,a}$ in Figure 6.2) and after which ($C_{X,b}$ in Figure 6.2) the bioleaching system transitions from a three steady state regime to, again, a single branch of stable steady state operation. As such, with regard to system stability, the maximal rate point is actually is an undesirable location since operating near a bifurcation may cause the system to fall away from the design operating point when even small fluctuations occur in the inputs or operating conditions.

Referring to rate curve L_b in Figure 6.2, we noted high rates at point C_X, b with low rates at ferric/ferrous ion ratio R_b. Since the microbial oxidation rate curve L_b in Figure 6.2 is directly proportional to the biomass concentration (Eq. 4.2), any biomass concentration greater than $C_{X,b}$ would result in a single intersection of the microbial oxidation and chemical leaching rate curves at high ferric/ferrous ion ratios R shifting the system to low stable steady state rates (see rate curve L_3 in Figure 6.2). It is clear that when bioleaching chalcopyrite, maximum stable steady state rates can be obtained at point $C_{X,b} = C_{X,max}$ (Figures 6.3 and 6.7) which is sensitive to any small changes in the biomass concentration. Any increase in the biomass concentration $C_X > C_{X,b}$ would shift the system to low rates, therefore when developing a control strategy to maintain high bioleaching rates, the biomass concentration should never exceed $C_{X,b}$.

Optimum operating conditions C_X and R, where maximum bioleaching rates are achieved, which explicitly appear in the microbial oxidation rate expression $r_{Fe^{2+}}$ (Eq. 4.2), can be determined using Eqs. 6.8 and 6.9 and are illustrated in Figure 6.8 as a function of mean residence time. Figure 6.8 reveals that the optimum biomass concentrations $C_{X,max}$ (Figure 6.8a) and ferric/ferrous ion ratios $R_{X,max}$ (Figure 6.8b), where maximum rates are realised (Figure 6.8c), decrease with increasing mean residence time.

As previously stated, optimum operating conditions to sustain maximum rates for the bioleaching of chalcopyrite unfortunately coincide with the system bifurcation point. Thus, maintaining maximum rates at these conditions would require precise control systems that keep the biomass concentration at $C_{X,max}$. If $C_{X,max}$ is exceeded, the system would transition from high to low rates. It is therefore necessary that the biomass concentration is controlled to within some margin below $C_{X,max}$ to ensure that high rates are maintained.

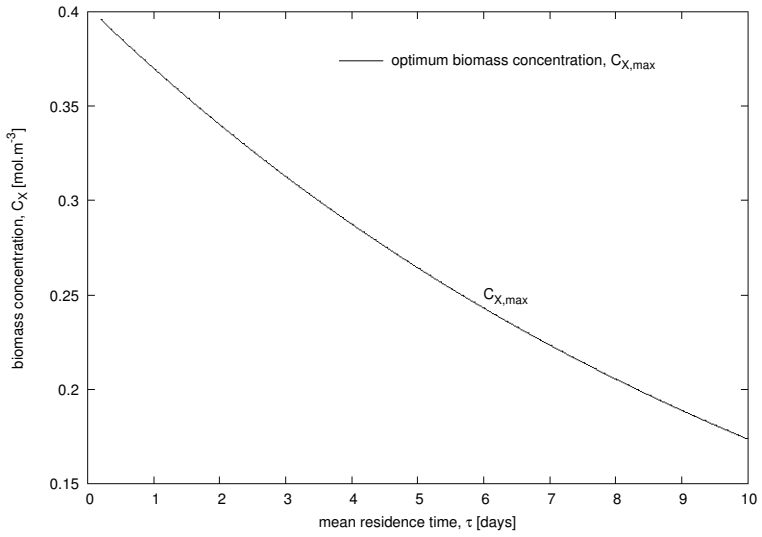

(a)

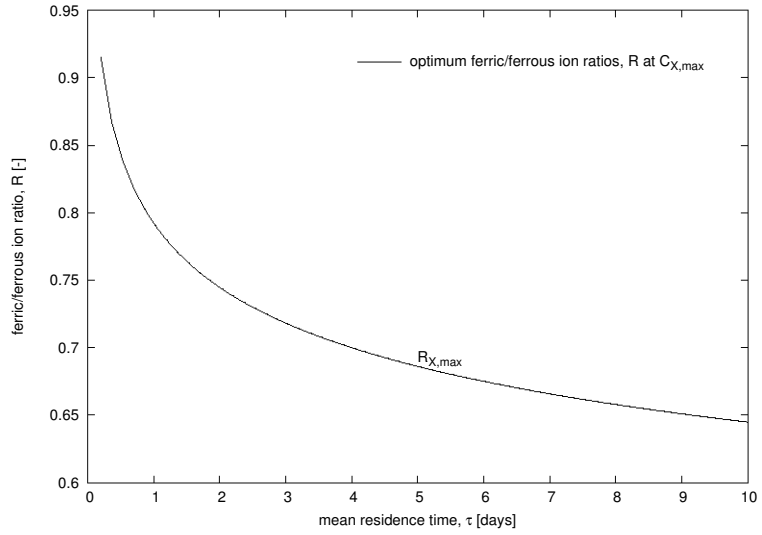

(b)

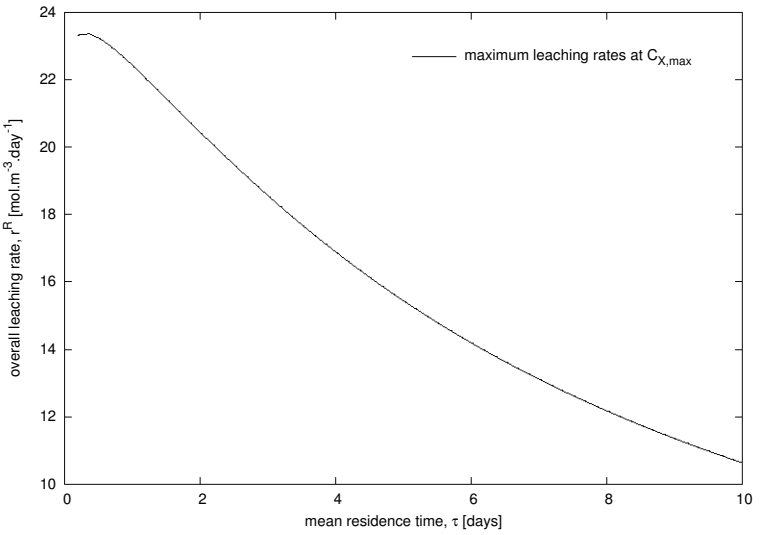

(c)

Figure 6.8: Locus of optimum (a) biomass concentrations $C_{X,max}$ with (b) corresponding ferric/ferrous ion ratios $R_{X,max}$ and (c) maximum bioleaching rates r^R as a function of mean residence time τ.

6.6 Control

In the following section control strategies to achieve maximum rates are introduced. Figure 6.8 revealed that the highest rates are obtained at high flow rates or low mean residence times, while the sensitivity analysis revealed that a critical concentration exists prior to the system shifting from high overall rates at intermediate ferric/ferrous ion ratios to low rates at high ferric/ferrous ion ratios (Figures 6.2). The challenge is therefore to keep the system at an optimum by controlling the relevant process variables. From the dynamics analysis for a continuous flow system, it is clear that maximum rates can be achieved by either controlling the reactor mean residence time or the biomass concentration.

In the following section, control procedures to keep the system at high bioleaching rates are proposed.

6.6.1 Mean Residence Time

From the sensitivity analysis, it was determined that the system operating point is determined by the reactor concentration ferric/ferrous ion ratio R_S and not by the inlet or initial ferric/ferric ion ratio. Since a single R-value exists in both space and time, there is only one stable steady state, therefore maintaining maximum rates at $C_{X,max}$ in a single bioleach reactor can, according to Eq. 6.11, only be achieved by adjusting the reactor mean residence time τ [s]. For example, if $C_{X,max} = 0.34$ mol carbon.m^{-3} with $R = 0.65$ for a given reactor mean residence time $\tau = 2$ days in Figures 6.3b and 6.6, the required mean residence time would be $\tau = 0.48$ days to achieve the desired rate (Figure 6.9), which deviates from the 2 days mean residence time. In Figure 6.9, the overall chemical leaching rate is at a maximum at $\tau = 0.48$ days. Thereafter the rate increases with increasing mean residence time. It should be noted that at mean residence times $\tau \leq \frac{1}{Y_{XS} q^{max}_{Fe^{2+}}}$, R_S is less than zero (Eq. 6.11). At these mean residence times, the growth rate is less than the dilution rate and washout of the biomass occurs (Figure 6.9).

Operating at this mean residence time would ensure high bioleaching rates. However, the conversion per tank would be low due to the diminished reaction space-time (Figure 6.9). As a result, the same overall conversion obtained for a reactor with mean residence time $\tau = 2$ days could be achieved using quarter sized tanks in series operating at maximum extraction rates.

From Eq. 6.11 it was noted that the system will always shift to ferric/ferrous ion ratios R that do not give the optimal leaching rate. Maximum leaching rates could be obtained when the reactor mean residence time was reduced. The reason for the rate enhancement is that any excess biomass that shifts the system to low rates at high redox potentials is washed out. However, since the biomass is generally thought to be uniformly suspended in the solution, lower residence times also result in reduced macro-productivity.

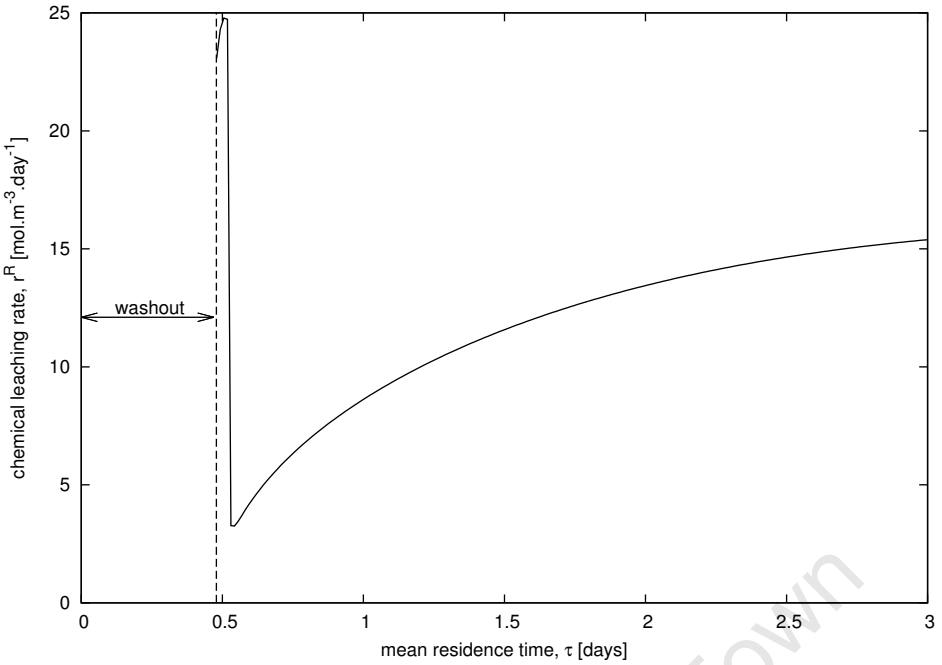

Figure 6.9: The overall chemical leaching rate r^R achieved when the reactor mean residence time is reduced from 2 days to 0.48 days. Washout occurs when $\tau \leq \frac{1}{Y_{XS} q^{max}_{Fe^{2+}}}$

Although reducing the mean residence time results in higher productivity, the system will be operated near the washout point (Figure 6.9). Any fluctuations in the system flow rates may result in complete washout and therefore eliminate any microbial activity driving the system to low overall rates.

It is only through the dynamics analysis that the appropriate mean residence times to achieve high rates could be identified. The analysis revealed that increasing the system flow rate or reducing the reactor mean residence time, would control microbial growth and hence maintain the system at maximum rates.

6.6.2 Biological Stress

The chemical leaching rate of chalcopyrite increases with increasing ferric/ferrous ion ratio until it reaches a maximum at a critical ferric/ferrous ion ratio, after which the rate decreases (see Figure 6.1). From the sensitivity analysis we noted that a critical biomass exists prior to the system switching from increasing to decreasing rates near the critical ferric/ferrous ion ratio (Figures 6.2). It is clear that to operate the bioleach reactor at high rates, the biomass concentration should be kept at levels below the critical biomass concentration. This was further emphasised in the previous section where the mean residence time was used to control the biomass concentration. Although the biomass in the system promotes leaching, it emerged that restricting the biomass concentration levels to below the critical value resulted in higher overall rates. This outcome opens new possibilities in enhancing the achieved reaction rate. Reducing the biomass concentration in the reactor by introducing biological

stress factors, such as high shear stress rates or solids loading (Nemati and Harrison, 2000; Nemati *et al.*, 2000; Raja, 2005; Valencia and Acevedo, 2009) would suppress the biomass concentration to below the critical point $C_{X,b}$ (Figures 6.3 and 6.7) and keep the system at ferric/ferrous ion ratios R within the optimal operating range. In stirred tank reactors biological stresses are induced by high agitation rates and the inclusion of abrasive particles (Raja, 2005). An increase in either of these physical phenomena promotes cell stress and could be used to control the biomass concentration in a reactor. If applied to the system assuming a first order stress rate, the biomass balance in Eq. 6.10 is rewritten as Eq. 6.12.

$$\frac{dC_X}{dt} = \frac{C_{X,inlet} - C_X}{\tau} + Y_{XS} r_{Fe^{2+}} - k_s C_X \qquad [6.12]$$

where k_s $[s^{-1}]$ is the microbial stress rate. The value of k_s can be correlated to the applied stress rate due to agitation and abrasive solids loading.

If the desired biomass concentration $C_{X,max}$ and ferric/ferrous ion ratio $R_{X,max}$ is known, the required steady state stress rate k_s to obtain maximum leaching rates can be calculated (Eq. 6.13). At steady state, the relationship in Eq. 6.13 is observed.

$$k_s = \frac{Y_{XS} q^{max}_{Fe^{2+}}}{(1 + KR)} - \frac{1}{\tau} \qquad [6.13]$$

The stress rates k_s needed to obtain maximum rates at biomass concentrations $C_{X,max}$ and corresponding ferric/ferrous ion ratio $R_{X,max}$ is shown in Figure 6.10. As expected the required stress rate to sustain the system at maximum bioleaching rates is higher at high mean residence times since more biomass accumulates in the reactor as the system approaches batch operation (Figures 6.3b and 6.10, Eq. 6.8).

When applying the optimal stress rate, an effective control procedure can be identified with the objective of maintaining high bioleaching rates. If the reactor operates at a mean residence time $\tau = 2$ days, with maximum rates at $C_{X,max} = 0.34$ mol carbon.m^{-3} and $R_{X,max} = 0.65$ (Figure 6.6) the required stress rate to maintain the optimum operating point can be calculated from Eq. 6.13. The leaching rate decreases as the applied stress rate increases until the optimum ferric/ferrous ion ratio is achieved at $R_{X,max} = 0.65$. At this point the biomass concentration required to maintain maximum rates is at an optimum (see Figure 6.6). This is indicated in Figure 6.11 by the sharp increase in the leaching rate from *ca.* $k_s = 1.65 \times 10^{-5}$ s^{-1} reaching a peak at $k_s = 1.81 \times 10^{-5}$ s^{-1}. With a stress rate $k_s = 1.81 \times 10^{-5}$ s $^{-1}$, it can be seen in Figure 6.11 that the overall bioleaching rate increases by 56% compared to a system that does not incorporate any biological stress ($k_s = 0$ s^{-1}).

From the dynamics analysis of chalcopyrite bioleaching in a flow system, we note that in addition to the biomass concentration C_X and ferric/ferrous ion ratio R, the inlet ferric ion concentration $C_{Fe^{3+},inlet}$ and reactor mean residence time τ directly affects the dynamic structure of the system. The latter parameters affect the magnitude by which the chemical leaching rate function r^S_L is offset by the flow term in Eq. 6.8, thereby shifting the system to lower rates.

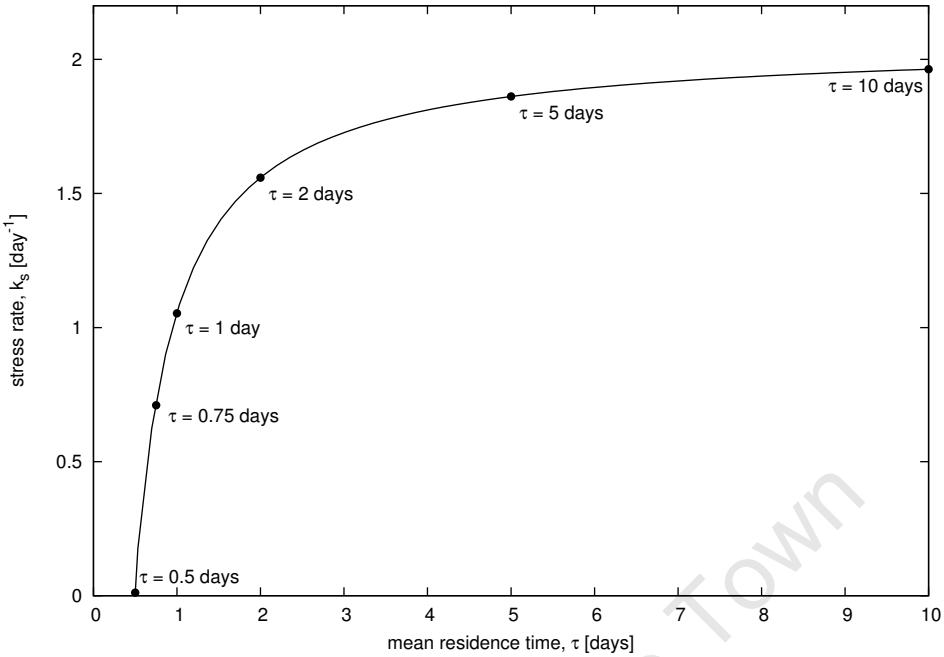

Figure 6.10: Hydrodynamic stress rate k_s required to maintain maximum overall bioleaching rates r^R as a function of mean residence time.

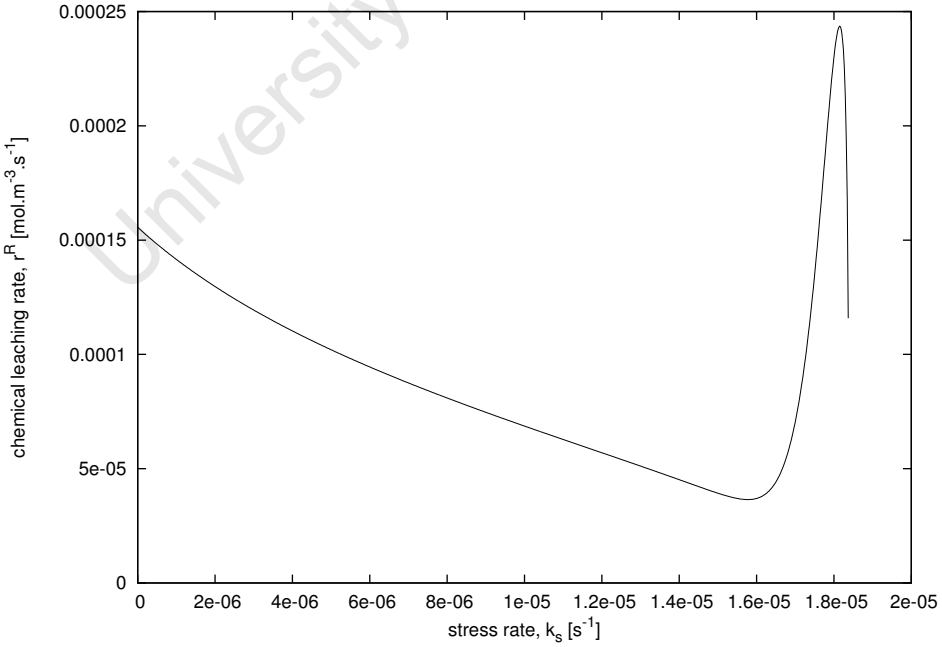

Figure 6.11: Comparison of the overall chemical leaching rate r^R achieved when the hydrodynamic stress to the reactor is progressively increased from $k_s = 0\ s^{-1}$. A maximum rate is observed when a stress rate of $k_s = 1.81 \times 10^{-5}\ \mathrm{s}^{-1}$ is applied.

By performing a dynamics analysis, factors that influence the overall rate and hence the productivity of the system were determined. To maximise the rate, the ferric/ferrous ion ratio and hence the biomass concentration, could be controlled by either reducing the reactor mean residence time or by applying external hydrodynamic stresses to the bioleach system.

In the following section, a dynamics analysis is performed on experimental data obtained from Raja (2005). Data relating to increased biological stress due to increased solids loading, defined as the mass of particles relative to the reactor volume [m/v], are presented. A dynamics analysis is then performed on a continuous flow system, applying the experimental data obtained from Raja (2005), to show that the biomass and redox potential in a bioleach system can be effectively controlled at optimum conditions, using the analysis outlined in this study.

6.7 Experimental Validation

Raja (2005) investigated the biological response of a *Sulfolobus metallicus* culture to hydrodynamic stress in a batch reactor at 341.15 K by increasing the solids loading. Inert quartzite particles, with a size fraction similar to the chalcopyrite concentrate 38×10^{-6} m to 75×10^{-6} m, were utilized in the experiments. Quartzite solids loading of 0, 6, 9 and 12% [m/v] were investigated for experiments containing 3% [m/v] chalcopyrite loading at a constant impeller tip speed. Raja (2005) observed low leaching rates throughout their experiments and attributed these low rates to high initial solution potentials at which passivation was considered to occur. Raja (2005) observed an increase in biological stress with an increase in solids loading, which resulted in a decrease in the redox potential, biomass concentration and hence the overall rate (Figure 6.12).

The results obtained from Raja (2005) provide a framework for establishing an effective control system to maintain high leaching rates in a continuous flow system. Since the leaching rate constants A [mol.m^{-2}.s^{-1}] and B [mol.m^{-2}.s^{-1}], biomass yield Y_{XS} [-] and biological stress rate k_s [s^{-1}] are unknown in these experiments, they were used as fitting parameters when validating the model with the experimental data. Microbial oxidation rate constants $q^{max}_{Fe^{2+}}$ for the *Sulfolobus metallicus* culture was assumed to correspond to the Arrhenius relationship established by Searby (2006) and taken to equal 2.74×10^{-3} mol Fe^{2+}.mol^{-1} carbon.s^{-1} at 341.15 K with the inhibition constant $K = 0.019$ [-] (Searby, 2006).

When fitting the data to the model, it was assumed that no biological stress was present in experiments with 0% [m/v] quartzite and 3% [m/v] chalcopyrite solids loading. Intrinsic leaching rate constants $A = 1.35 \times 10^{-6}$ mol.m^{-2}.s^{-1} and $B = 5.67 \times 10^{-9}$ mol.m^{-2}.s^{-1} and biomass yield $Y_{XS} = 0.0021$ [-] were found to best fit this data and therefore maintained constant in subsequent fits to experimental data containing 6, 9 and 12% [m/v] quartzite solids. The biological stress rate in experiments containing 6, 9 and 12% [m/v] quartzite solids was found to be 1.24×10^{-6}, 1.30×10^{-6} and 2.21×10^{-6} s^{-1}, respectively (Figure 6.12) and increased linearly with an increase in solids loading (Figure 6.13).

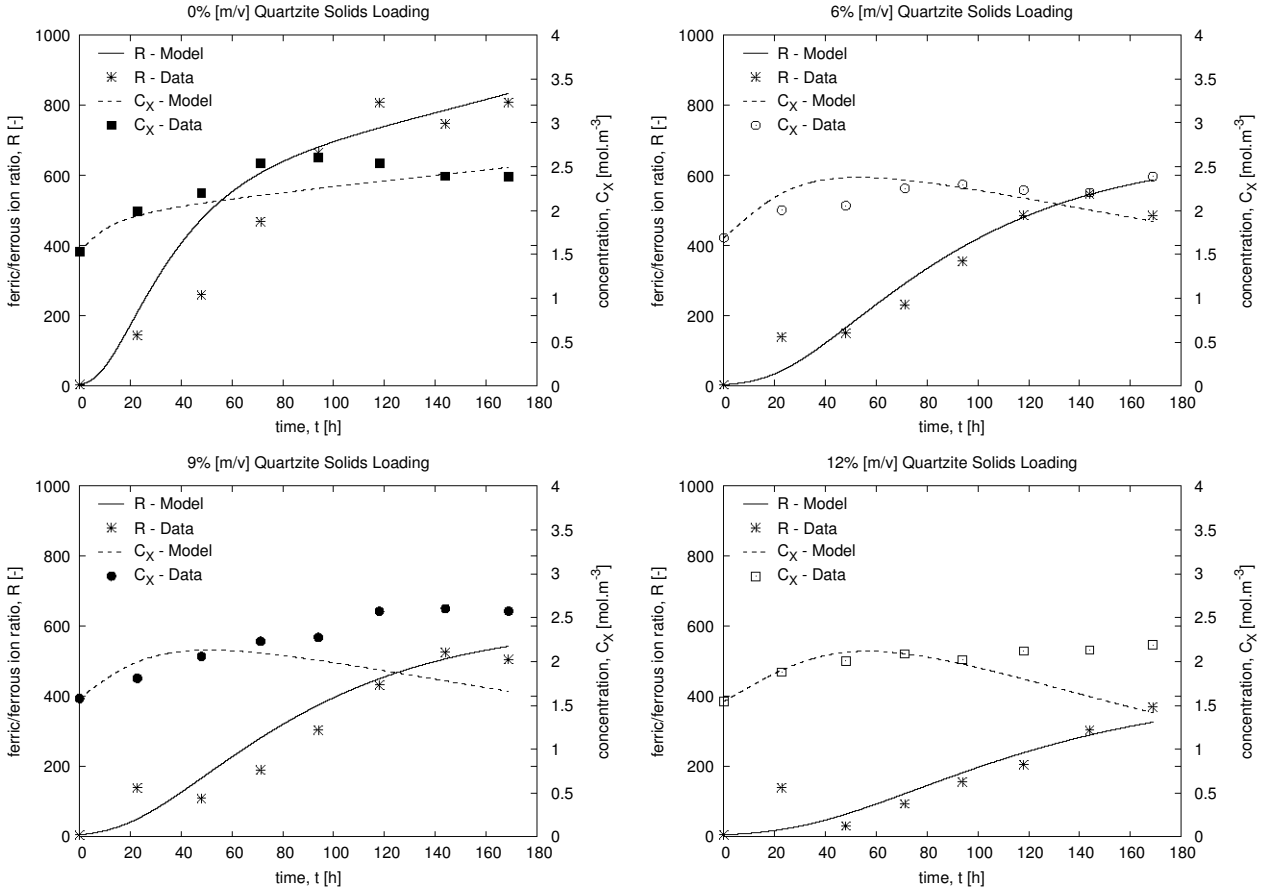

Figure 6.12: Model fit to batch ferric/ferrous ion ratio R and biomass concentration C_X data obtained from Raja (2005) for quartzite solids loadings ranging from 0-12% [m/v].

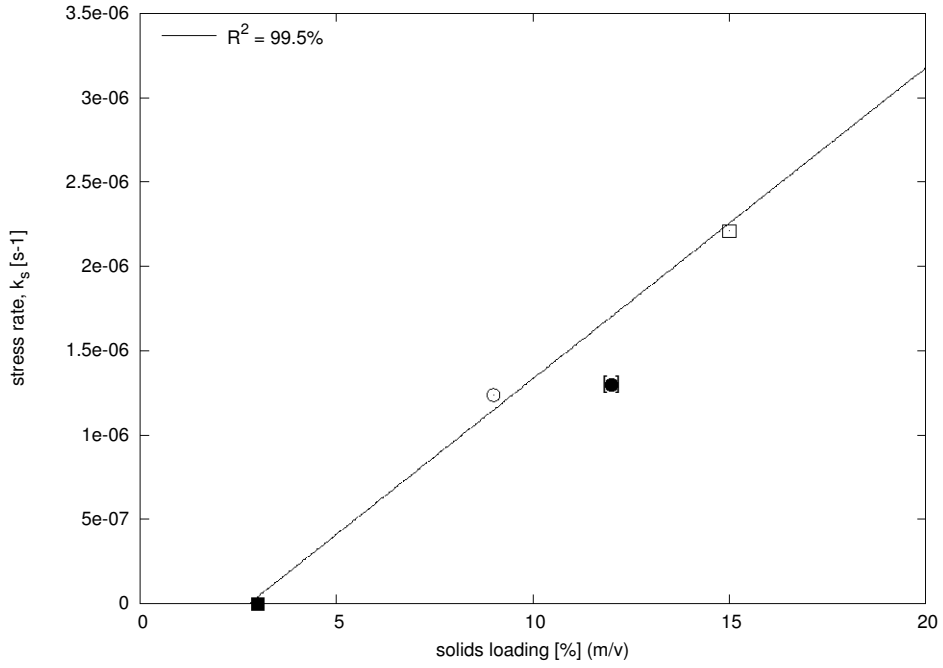

Figure 6.13: Resultant stress rates k_s obtained when 0-12% [m/v] quartzite solids loadings are applied to a batch reactor containing 3% [m/v] chalcopyrite concentrate.

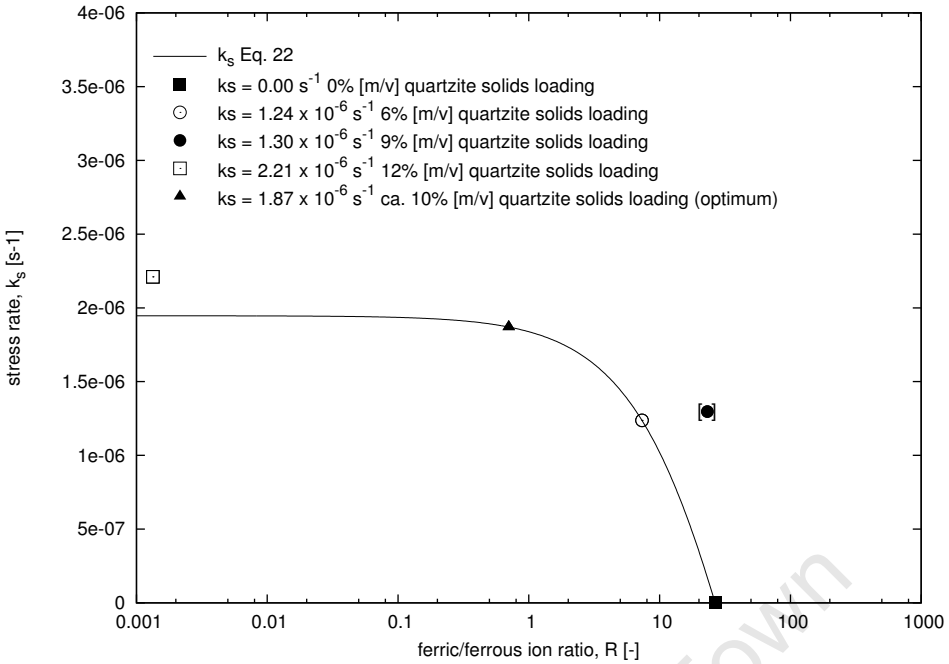

Figure 6.14: The biological stress rate as a function of ferric/ferrous ion ratio R. Stress rates regressed from batch experiments performed by Raja (2005) correspond well to the theoretical correlation outlined in Eq. 6.13.

The kinetic constants obtained by fitting the batch data obtained from Raja (2005) was applied to a dynamics analysis on a continuous flow system. To determine whether the batch data could be used in the continuous flow system, the biological stress rates k_s for the batch system were plotted with theoretical stress rates achieved for a continuous flow system operating at a mean residence time of 3 days using Eq. 6.13 (Figure 6.14). The model was able to predict the biological stress rates with reasonable accuracy and therefore reinforced the validity of a dynamics analysis on a continuous flow system using the data obtained from Raja (2005).

Since the relationship between the solids loading and the resultant stress rate was established, an optimum stress rate to achieve high leaching rates in the continuous system can be determined using the procedure outlined in the previous section. The dynamics analysis revealed that optimum leaching rates are achieved at $R_{X,max} = 0.70$ [-] and $C_{X,max} = 0.39$ mol carbon.m^{-3}. Using Eq. 6.13, it was found that maximum rates could be achieved at the aforementioned conditions using a stress rate $k_s = 1.87 \times 10^{-6}$ s^{-1} (Figure 6.15). According to the experimental results obtained from Raja (2005) and the relationship established in Figures 6.13 and 6.14 and Eq. 6.13 for biological stress rates resulting from increased solids loading in a bioleach reactor, *ca.* 10% [m/v] quartzite solids loading are required to maintain the system at optimum rates (Figure 6.15).

Figure 6.15a was generated by varying the reactor initial conditions. Two scenarios were considered. In the first case, the initial biomass concentration was maintained at the optimum $C_{X,max} = 0.39$ mol carbon.m^{-3} while the ferric/ferrous ion ratio was varied between $0.5 - 500$ [-]. Thereafter the ferric/ferrous ion ratio was kept constant at the

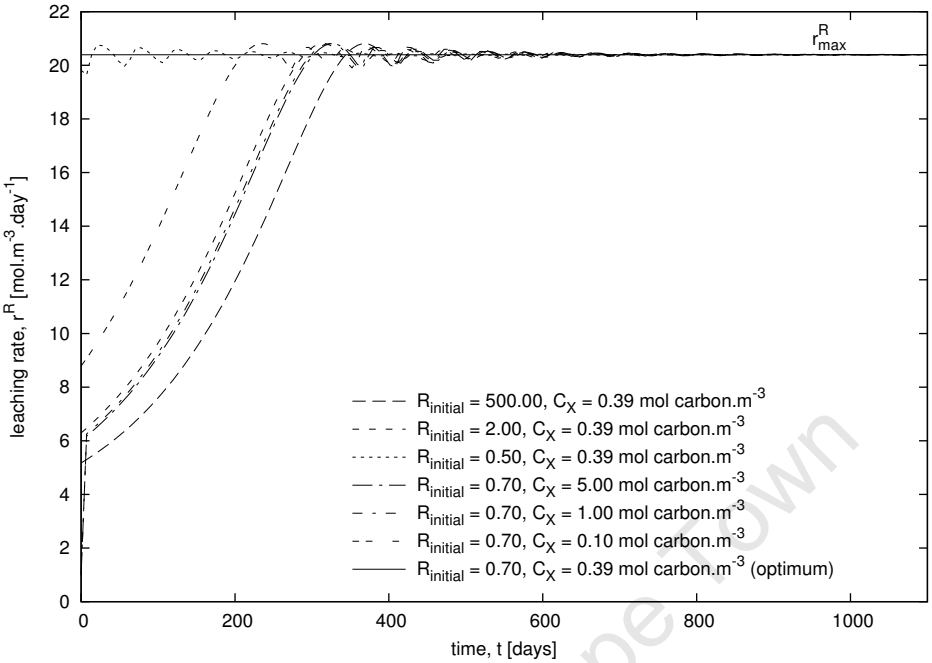

(a) Maximum leaching rate achieved using varying inlet condtions

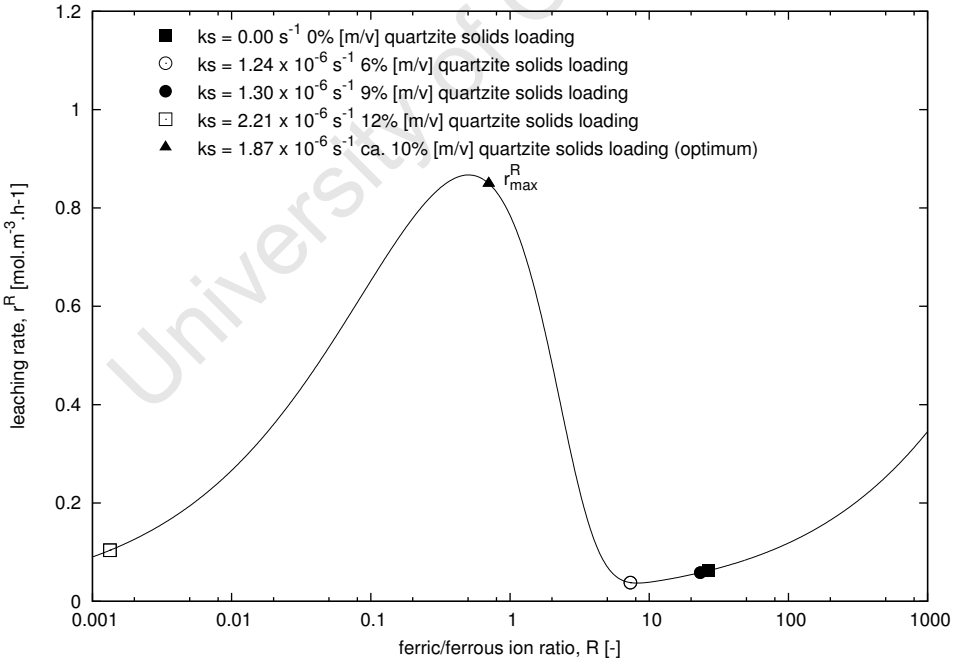

(b) Chemical leaching rates achieved applying varying biological stress rates k_s

Figure 6.15: Overall leaching rate obtained in continuous flow system. Maximum rates r^R_{max} are achieved when a solids loading corresponding to ca. 10% [m/v] with a biological stress rate $k_s = 1.87 \times 10^{-6}$ s^{-1}, is applied.

optimum operating point $R_{X,max} = 0.70$ [-] while the biomass concentration was varied between $0.1 - 5.0$ mol carbon.m^{-3}. High rates r^R_{max} were obtained at ca. 10% [m/v] solids loading irrespective of the reactor inlet conditions when the applied stress rate was kept at $k_s = 1.87 \times 10^{-6} s^{-1}$ (Figure 6.15).

Figure 6.15 verifies that, by applying a dynamics analysis to the bioleaching system, the system can be effectively driven to maintain the maximum rate (Figure 6.15b). This rigorous approach to the dynamics analysis of chalcopyrite bioleaching shows that factors required to maintain high bioleaching rates can be identified using the analysis presented in this study.

6.8 Conclusions

It is evident that as many as three steady states are possible in both batch and continuous flow reactor systems with stable steady states appearing at low ($R < R_{crit}$) and high ($R > R_{crit}$) solution potentials with an unstable steady state at intermediate ferric/ferrous ion ratios R. It was shown, that by controlling either the reactor mean residence time or biomass concentration by application of a biological stress, the bioleach reactor could be operated at an optimum where up to 56 % gains in the overall bioleaching rate could be achieved.

Up to this point, the hydrodynamics of the system are considered constant. However, in practice flow rates to and from the reactor are seldom operated at steady state. This is especially evident when gravity overflow from the preceding tank in a series of reactors is the inlet to subsequent tanks in the series. Given the dynamics analysis performed in this chapter, it is clear that any disturbances in system operating conditions could result in the system being driven to low rates. Consequently, in the following chapter a reactor model is developed, which eliminates the steady state assumption by incorporating recent advancements in RTD theory developed by Rawatlal and Starzak (2003). A dynamics analysis for the bioleaching of chalcopyrite is then performed on the unsteady state system by determining the influence of time-varying mean residence time, perturbations in the particle size distribution and reactor solids loading, for the purpose of maximizing overall bioleach production rate.

7

Development of an Unsteady State Reactor Model

7.1 Introduction

BIOLEACHING reactors are multi-phase systems composed of a solid and an aqueous phase, and may be considered to be well mixed (Breed and Hansford, 1999b; Crundwell, 1994). Since particle size changes with reaction, the RTD must be integrated into the reactor model formulation for accurate prediction of reactor performance (Rawatlal, 2004). Most often, when developing reactor models, RTD are applied to perfectly mixed systems at steady state, restricting model application to design-type rather than controls problems.

In industry, bioleaching is often carried out in tanks in series, where each tank operates under different reaction conditions. The inlet stream to the subsequent tank in the series is the preceding reactor exit stream. These stream flow rates may vary with time and be generally different from each other, resulting in unsteady particle flow rates. Even so, all bioleach reactor models published in the literature are restricted to equally sized tanks at steady state, operating at the same reaction conditions (Pinches *et al.*, 1987; Breed and Hansford, 1999b; Brochot *et al.*, 2004; Crundwell, 1994; 1995; 2001; 2005). These models cannot effectively predict unsteady state operation nor can they successfully predict individual reactor conditions.

The studies into the dynamics of chalcopyrite bioleaching in Chapters 5 and 6 showed that the location of system steady states in the property space were influenced by the temperature, ferric-to-ferrous ion ratio and microbial concentration. These studies showed that bioleaching rates could be maintained at a maximum by controlling the microbial concentration to a critical point, whose location was dependent on the ferric/ferrous ion ratio. As the maximum operating point coincided with a bifurcation point, defined as a critical point at which the dynamic structure of the system changes from multiple steady states to a single steady state, operating at this point could cause the system to fall away from the optimum operating point with any small fluctuation in the reactor inputs or operating conditions. This indicates that a system operating in unsteady state mode easily falls to low overall bioleaching rates. Any fluctuation in reactor flow rates would result in unfavourable rates, thus compounding the

need for effective control systems in bioleach processes. The most common perturbations in reactor systems are due to irregular flow rates. This further highlights the importance of developing a reactor model which incorporates unsteady state RTD theory which describes the hydrodynamics of the system due to changing flow rates with time.

If step changes are applied to either inlet or exit flow rates to a bioleach reactor, the increase or decrease in the flow rate affects the residence time or age of the particles within the reactor. For example, an increase in inlet flow rate increases the population of age zero particles. Therefore, any perturbation introduced to either flow rate causes the RTD to change accordingly at the time of the step change.

Zacca *et al.* (1996) developed an unsteady state RTD for two populations, the original and fresh population. The solution was unfortunately unfeasible for application in multi-vessel systems due to its fragmentary nature (Rawatlal and Starzak, 2003). The multiple population concept was overcome by extending the domain of the boundary conditions for the fresh population domain to include the original population domain resulting in a simpler RTD function requiring a single equation (Eq. 7.1, Rawatlal and Starzak, 2003).

$$I(t,\theta) = \frac{h_{in}(t-\theta)}{H(t)} exp\left[-\int_{t-\theta}^{t} \frac{h_{out}(t')}{H(t')} dt'\right] \quad [7.1]$$

where h_{in} [kg.s^{-1}] is the inlet flow rate to the reactor, h_{out} [kg.s^{-1}] the exit flow rate from the reactor and H the fluid holdup. The reactor mean residence time τ is defined as the relative ratio of the reactor holdup H to the exit flow rate h_{out}. Applying the above RTD function to a reactor model, the total rate of particle dissolution, or the performance of a bioleach reactor, can be determined for cases when the inlet and exit flow rates vary with real time.

The objective of this section is to develop a control strategy to maintain the bioleaching system at the maximum rate given the complication that the flow rate to the reactor is not steady. A reactor model based on the segregation approach is initially developed to determine the suitability of the model to unsteady state operation by validating the data against experimental data. A sensitivity analysis based on the results from the dynamics analysis carried out in Chapter 6 is performed to determine which process conditions have the greatest influence on the dynamic structure of the system and applied to the control strategy.

7.2 Model Formulation

The modified PBM developed in Chapter 4 was formulated assuming steady state operation. For the sake of completeness, fundamentals relating the particles dynamics formulated in Chapter 4, are reproduced in this section and later extended to unsteady state conditions.

A mathematical model predicting the overall reaction rate r^R [mol.m^{-3}.s^{-1}] of a bioleach reactor system was developed to describe reactor performance with the inlet particle size l_0 [m] and residence time or age θ [s] as model inputs. The shrinking particle model in Eq. 7.2 was used to describe the rate of change in particle mass.

$$\frac{dM^p}{d\theta} = r'' A(\theta, l_0) MM_{MS} \qquad [7.2]$$

where M^p [kg] is the particle mass, r'' [mol.m^{-2}.s^{-1}] the surface area based intrinsic chemical reaction rate, $A(\theta, l_0)$ the particle surface area defined as the product of the particle mass M^p [kg] and the particle specific surface area A^p [m^2.kg^{-1}] and MM_{MS} [kg.mol^{-1}] is the molar mass of the mineral sulphide particles.

Applying the relevant substitutions into Eq. 7.2, assuming spherical particles and constant particle density ρ [kg.m^{-3}], the differential in particle size based on the exposure time of a particle to the reaction environment was formulated (Eq. 4.7)

$$\frac{dl}{d\theta} = -\frac{2r''}{\rho} MM_{MS} \qquad [4.7]$$

Particles with a non-trivial distribution in size enter the reactor and are exposed to the aqueous phase for different periods of time. By applying the segregation approach and incorporating the age $I(\theta)$ and size $f_0(l_0)$ distributions, and defining $I(\theta)$ and $f_0(l_0)$ such that $I(\theta)\Delta\theta$ and $f_0(l_0)\Delta l_0$ are the fraction of particles in the age range $[\theta, \theta + \Delta\theta]$ and size range $[l_0, l_0 + \Delta l_0]$, respectively, the overall reaction rate r^R [mol.m^{-3}.s^{-1}] was formulated (Eq. 6.7)

$$r^R = \int_0^\infty \int_0^\infty r'' A^p(\theta, l_0) \frac{M^p(\theta, l_0)}{V^R} \phi_{MS} N^T I(\theta) f_0(l_0) d\theta dl_0 \qquad [6.7]$$

where A^p [m^2.kg^{-1}] is the particle specific surface area, M^p [kg] the particle mass, V^R [m^3] the volume of the reactor and ϕ_{MS} [-] the fraction of the mineral sulphide in the particles.

At steady state, the flow rate across the boundaries of the reactor is constant. For the case in which the particle flow rates change with time, the duration of particle exposure to the reacting environment changes with time, and therefore the change in particle size is dependent on the reactor dynamics and the particle-solution contact time.

To simulate the performance of the bioleach reactor using Eq. 6.7 the use of accurate reaction kinetics is required. As previously noted, most mineral sulphide ores have intrinsic chemical leaching rate expressions in the form of Eq. 5.2.

$$-r'' = k \left(\frac{C_{Fe^{3+}}}{C_{Fe^{2+}}} \right)^n \qquad [5.2]$$

where k is the intrinsic rate constant [mol.m^{-2}.s^{-1}] and n can be approximated to be 0.5 (Crundwell, 2005). However, the concentrations of the ionic species in solution in Eq. 5.2

may be time functions thus making the intrinsic leaching rate r'' a function of real-time $r''(t)$. The change in particle size in Eq. 4.7 is therefore rewritten to incorporate this possible time variance (Eq. 7.3).

$$\frac{d\Delta l}{d\theta} = -\frac{2r''(t)}{\rho} MM_{MS} \quad [7.3]$$

where Δl is the difference between the current particle size $l(t, \theta, l_0)$ at time t and age θ and the inlet particle size $l_0 = l(t, \theta = 0, l = l_0)$, such that $\Delta l = l(t, \theta, l_0) - l_0$.

The age of a particle θ [s] is defined as the difference between the time the particle enters the reactor t_0 [s] and the time the particle leaves the reactor t [s]. The entrance time of particles to the reactor can therefore be expressed as $t_0 = t - \theta$ time units. Integrating Eq. 7.3 over a time range $[t - \theta, t]$ with initial condition $l(t - \theta) = l_0$, a relationship between the particle size l [m], real time t [s] and particle age θ [s] can be determined (Eq. 7.4).

$$l(t, \theta) = l_0 - MM_{MS} \int_{t-\theta}^{t} \frac{2r''(t')}{\rho} dt' \quad [7.4]$$

Since the current particle size l [m] is dependent on both real time t and age θ (Eq. 7.4), the rate of change in particle size Δlcan be expressed by the Partial Differential Equation (PDE) in Eq. 7.5.

$$\frac{d\Delta l}{dt} = \frac{\partial \Delta l}{\partial t} \cdot \frac{\partial t}{\partial t} + \frac{\partial \Delta l}{\partial \theta} \cdot \frac{\partial \theta}{\partial t} = \frac{\partial \Delta l}{\partial t} + \frac{\partial \Delta l}{\partial \theta} \quad [7.5]$$

The change in particle size Δl can be rewritten to include variations in size due to real time t and particle residence time or age θ by substituting Eq. 7.3 into Eq. 7.5. Since a unit change in age θ equals a unit change in time t, $\partial\theta/\partial t = 1$ and hence Eq. 7.5 reduces to Eq. 7.6.

$$\frac{d\Delta l}{dt} = -\frac{\partial \Delta l}{\partial \theta} - \frac{2r''(t)}{\rho} MM_{MS} \quad [7.6]$$

The change in particle size is a function of particle age θ and real time t and inlet particle size l_0, therefore the particle specific surface area $A^p(t, \theta, l_0)$ in Eq. 7.7 and mass $M^p(t, \theta, l_0)$ are also functions of the aforementioned variables.

$$A^p(t, \theta, l_0) = \frac{6}{\rho l(t, \theta, l_0)} \quad [7.7]$$

The performance equation in Eq. 6.7 can therefore be rewritten to obtain an unsteady state reaction rate $r^R(t)$ that is based on the time that the particles enter and age spend within the reactor (Eq. 7.8).

$$r^R(t) = \int_0^\infty \int_0^\infty r''(t) A^p(t, \theta, l_0) \frac{M^p(t, \theta, l_0)}{V^R} \phi_{MS} N^T I(t, \theta) f_0(l_0) d\theta dl_0 \quad [7.8]$$

where $I(t, \theta)$ is defined such that $I(t, \theta)\Delta\theta$ is the fraction of particles in the reactor at time t in age range $[\theta, \theta + \Delta\theta]$.

Now that the unsteady state reactor model has been formulated for the bioleaching of mineral

sulphide particles in flow reactor systems, the influence of unsteady flow on the overall reactor performance can be investigated.

7.3 Hydrodynamics

Since industrial conditions are rarely steady, the sensitivity of the bioleach reactor model to unsteady state flow conditions are investigated. Rawatlal and Starzak (2003) demonstrated the suitability of the residence time distribution function developed in Eq. 7.1 to flow reactor operating at unsteady state by initially applying a steady state flow rate to a continuous flow reactor. The RTD did not vary with real time t under conditions of steady state, therefore the distribution obtained was the familiar exponential decay function for continuous flow reactors, simply repeated for all (real) time t (Rawatlal and Starzak, 2003).

Further, a step increase in the inlet flow rate to the bioleach reactor was investigated with a gravity-driven exit flow rate. The exit flow rate was taken to be directly proportional to the square root of the height of the liquid level in the tank, which is, in turn, proportional to the square root of the reactor holdup $H(t)$ such that $h_{out}(t) = k_{out}\sqrt{H(t)}$, where k_{out} [$\mathrm{kg}^{0.5}.\mathrm{s}^{-1}$] is the exit flow rate constant. By increasing the inlet flow rate, an increase in age zero $\theta = 0$ particles in the reactor was noted due to the linear dependence of Eq. 7.1 on inlet flow rate, thus increasing the holdup of particles in the reactor (Rawatlal and Starzak, 2003). However, the consequent increase in the holdup will only occur if the exit flow rate lags the inlet flow rate. In the case of bioleaching, initiating a step increase in the inlet flow rate to the reactor would cause more particles to come in contact with the reaction phase for a longer period of time, increasing the rate of particle dissolution resulting in smaller particles. Due to the increased presence of smaller particles in the reactor, the particle specific surface area A^p in Eq. 7.7 increases, thus increasing the overall chemical leaching rate r^R.

As shown above, several case studies were presented by Rawatlal and Starzak (2003) for an unsteady state system. For the sake of illustrating the influence of fluctuating flow rates to the bioleach system, the RTD developed by Rawatlal and Starzak (2003) will be presented for the case where a sinusoidal flow profile is applied to the entrance of the bioleach reactor with a gravity driven exit flow rate as described above (Figure 7.1).

A flow rate that can be described by a sine wave goes through increasing and decreasing rates. As noted by Rawatlal and Starzak (2003), an increase in the inlet flow rate would increase the number of age zero fluid elements to the reactor thus increasing the holdup. This increase is attributed to the direct proportionality of the RTD function to the inlet flow rate h_{in} in Eq. 7.1. It can therefore be similarly noted that a decrease in the inlet flow rate would result in a decrease in the holdup and of age zero particles in the bioleach reactor (Figure 7.1).

The overall chemical leaching rate in Figure 7.1d decreases and increases following the same trend as the inlet flow rate in Figure 7.1a. Analogous to a step increase in the entrance

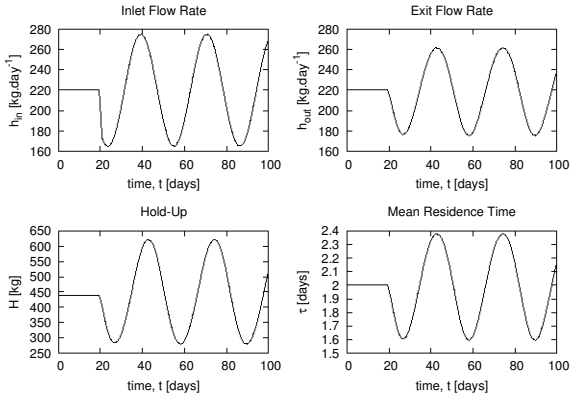

(a) Hydrodynamics

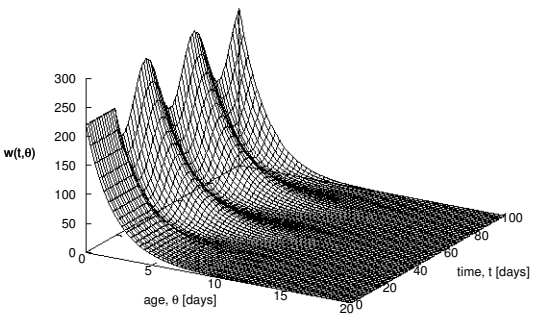

(b) RTD

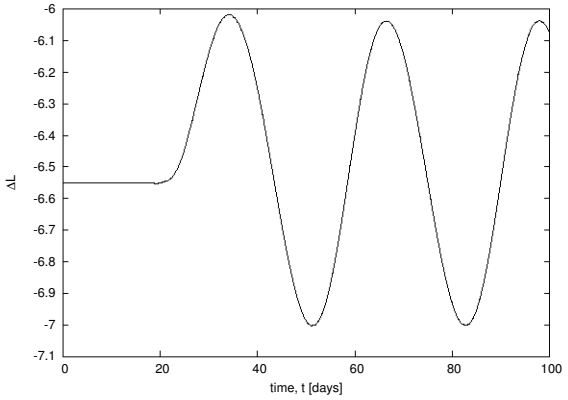

(c) Change in Particle Size

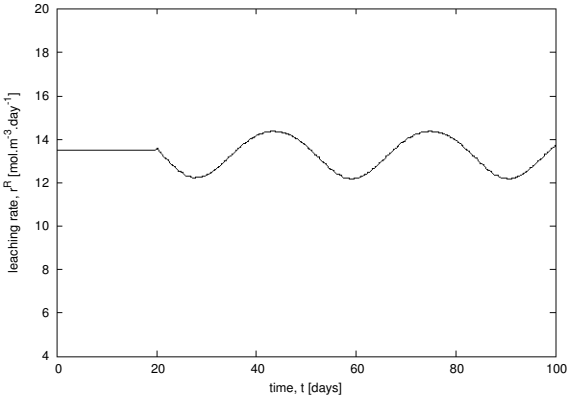

(d) Leaching Rate

Figure 7.1: Hydrodynamic, size and rate profiles for a continuous flow reactor when a sinusoidal inlet flow rate is applied. The resultant RTD and chemical leaching rate is shown in Figures (b) and (d), respectively. Where $w(t,\theta) = H(t)I(t,\theta)$

flow rate, an increase in the inlet flow rate results in an increase in the number of age zero particles (Figure 7.1) to the reaction phase and an increase in the mean residence time and holdup (Figure 7.1a), while a decrease in the inlet flow rate decreases the number of zero aged particles in the reactor and decreases the holdup and mean residence time. Consequently, the concentration of the fluid components and overall chemical leaching rate (Figure 7.1d) go through increasing and decreasing trends relative to the inlet flow rate. Comparable to increasing the entrance flow rate, decreasing rates are observed when the inlet flow rate decreases due to less particles being in contact with the solution phase for a shorter period of time (Figure 7.1a) decreasing the rate of particle dissolution (Figure 7.1c).

It is evident from the above analysis that the rate of particle dissolution, the solution concentrations and hence the overall reaction rate will not remain constant if the flow rates across the reactor are not maintained at steady state. The application of a steady state RTD for perfectly mixed systems will therefore not adequately predict the change in the fluid dynamics due to varying reactor flow rates. Consequently, the inability to sustain steady state operation in industry requires that an unsteady state RTD, such as that proposed by Rawatlal and Starzak (2003), be utilised when developing a model for the bioleaching of sulphide mineral particles in flow reactor systems. To illustrate this, the model developed in the previous sections will be validated against unsteady state experimental data.

7.4 Model Validation

The unsteady state chemical leaching rate $r^R(t)$ developed in Eq. 7.8 was validated against experimental data obtained from Mintek in South Africa for an Aguablanca ore concentrate, which is a polymetallic sulphide comprised of, amongst others, chalcopyrite and pentlandite. The influence of redox potential, temperature, grind size and feed solids concentration on the leach kinetics and metal extraction rates of copper and nickel during the bioleaching of the polymetallic sulphide concentrate were studied (Gericke and Govender, 2011). The concentrate, with a grind size between $d_{90} = 10 \times 10^{-6}$ and 40×10^{-6} m, was bioleached in the presence of a mixed thermophilic culture of *Acidianus brierleyi* (dominant species), *Metallospeara sedula* and *Sulfolobus sp.* at 343.15 K. The stream was fed to a series of reactors operated either in single, three or four stages, by a peristaltic pump with subsequent reactors in the series fed by the same peristaltic pump (Gericke and Govender, 2011). As low flow rates were required, the reactors were only fed every 30 minutes to achieve 3 days mean residence time in the primary reactor. In a peristaltic pump, the fresh feed passes through the pump by means of the compression of a flexible tube by means of a rotor contained in the pump casing. As the tube opens behind the compression action, fresh feed is once again introduced to the pump. This compression-release action together with the pump being turned on and off results in an inherently irregular flow pattern, which corresponds to unsteady state flow dynamics. The data obtained from Mintek is therefore obtained under unsteady flow conditions, and as such is appropriate for the purpose of validating the unsteady state reactor model developed in the preceding sections.

When modelling the Aguablanca concentrate, it was assumed that two competing chemical leaching reactions of chalcopyrite (Eq. 5.1) and pentlandite (Eq. 7.9) occur within the bioleach reactor with different rates of extraction facilitated by microbial oxidation (Eq. 1.2).

$$CuFeS_2 + 4Fe^{3+} \rightarrow 5Fe^{2+} + Cu^{2+} + 2S^0 \quad [5.1]$$

$$CuFeS_{0.89} + 4Fe^{3+} \rightarrow 5Fe^{2+} + Ni^{2+} + 0.89S^0 \quad [7.9]$$

$$4Fe^{2+} + O_2 + 4H^+ \rightarrow 4Fe^{3+} + 2H_20 \quad [1.2]$$

For the purpose of validating the data obtained from Mintek to the unsteady state model for both competing reactions in Eqs. 5.1 and 7.9, it was assumed that the chemical leaching of pentlandite (Eq. 7.9) and chalcopyrite have intrinsic leaching kinetics in the form of Eq. 5.2 and Eq. 2.19, respectively. In Figure 7.2a, it is clear that the solids loading to the principle reactor is not constant. The solids loading, while continuously varying with time, was increased from an average 10% to 11% [m/v] after 23 days. It was assumed that the near sinusoidal irregularity in the solids loading was due to a fluctuating inlet flow rate. These fluctuations are typical of industrial conditions since maintaining a constant flow rate and hence a constant mass of mineral sulphide solids to volume ratio is not always practically possible, especially when the feed to the bioleach reactors is due to gravity overflow from the preceding reactor. It therefore becomes increasingly important that the reactor model incorporate unsteady operation by means of unsteady state residence time distribution theory.

In validating the unsteady state reactor model to the experimental data, some degree of sine-wave smoothing of the solids loading, which is the known input to the reactor, was required to fit the exit Cu^{2+} and Ni^{2+} concentration data. The amplitude and frequency of the fitted sine wave was then used to approximate the variation in the inlet flow rate to the continuous flow bioleach reactor (Figure 7.2a).

The offset c_1, amplitude c_2 and frequency of the irregularity c_3 in the reactor inlet flow rate was simulated by fitting the solids loading (Figure 7.2a) to a sine curve in the form of $c_1 + c_2 sin(c_3 \cdot t)$ to the inlet flow rate to maintain an overall mean residence time of $\tau = 3$ days (Figure 7.2b). The concentration profiles predicted from the model (Eq. 7.8) were fitted to the concentration data obtained from Mintek by adjusting rate constants k (Eq. 5.2), A and B (Eq. 2.19) for the chemical leaching of pentlandite and chalcopyrite, respectively (Figure 7.2c).

Figure 7.2c illustrates that the model, which includes the age θ, initial particle size l_0 and changes in reactor flow rates, by incorporating the unsteady state RTD developed by Rawatlal and Starzak (2003), is able to achieve good agreement with the data.

As it can be seen in Figures 7.2 c and d, the concentration profiles and hence the overall chemical leaching rates of Cu^{2+} and Ni^{2+} fluctuate with varying inlet flow rate according the change in the feed solids loading [m/v] (Figure 7.2b). As expected, the chemical leaching

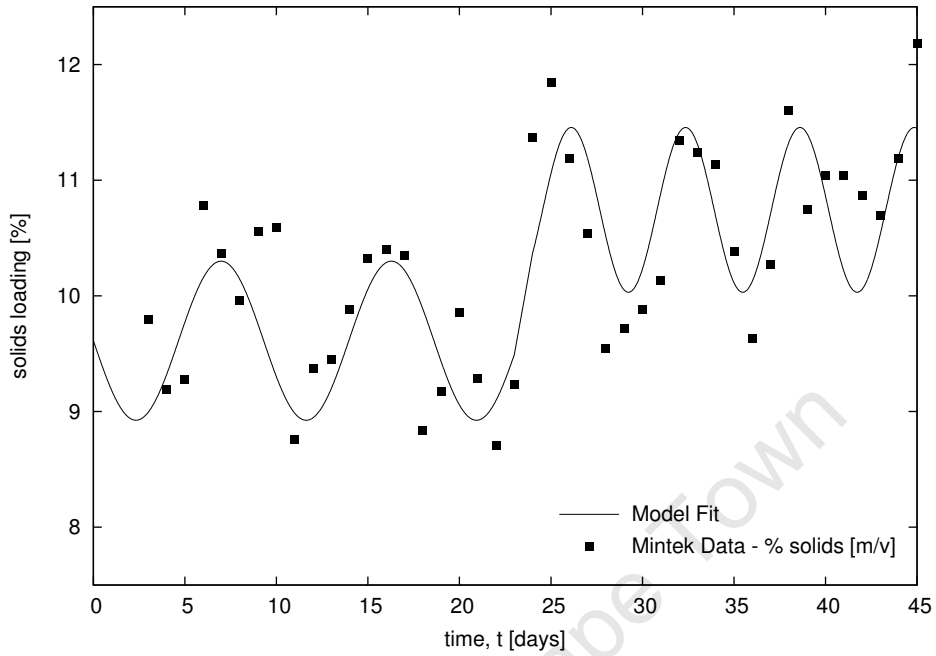

(a) Solids loading

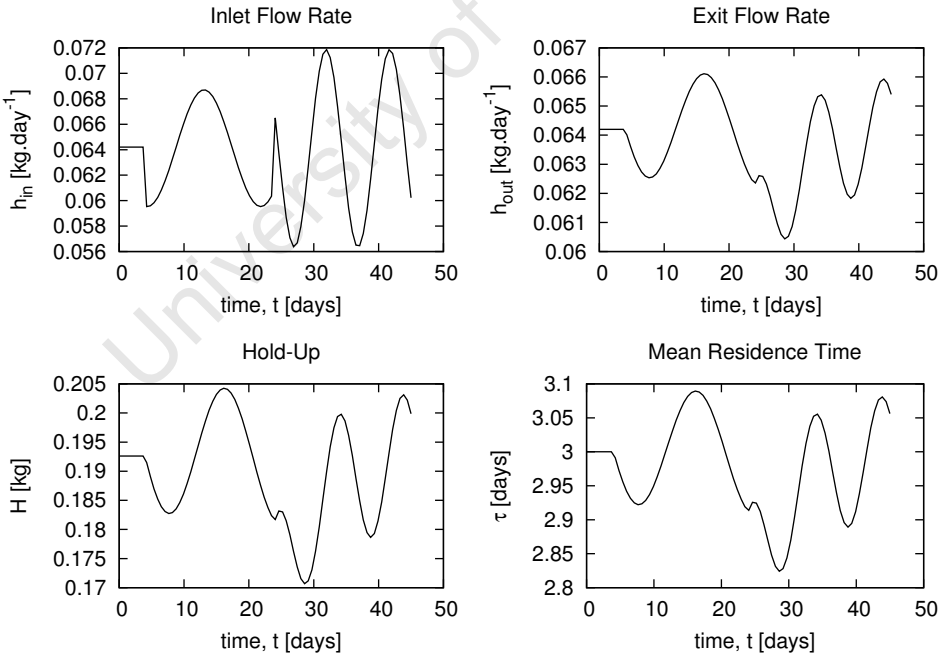

(b) Hydrodynamics

Figure 7.2: Validation of the unsteady state PBM developed using a segregation approach against data obtained from Mintek for Aguablanca ore...continued on next page.

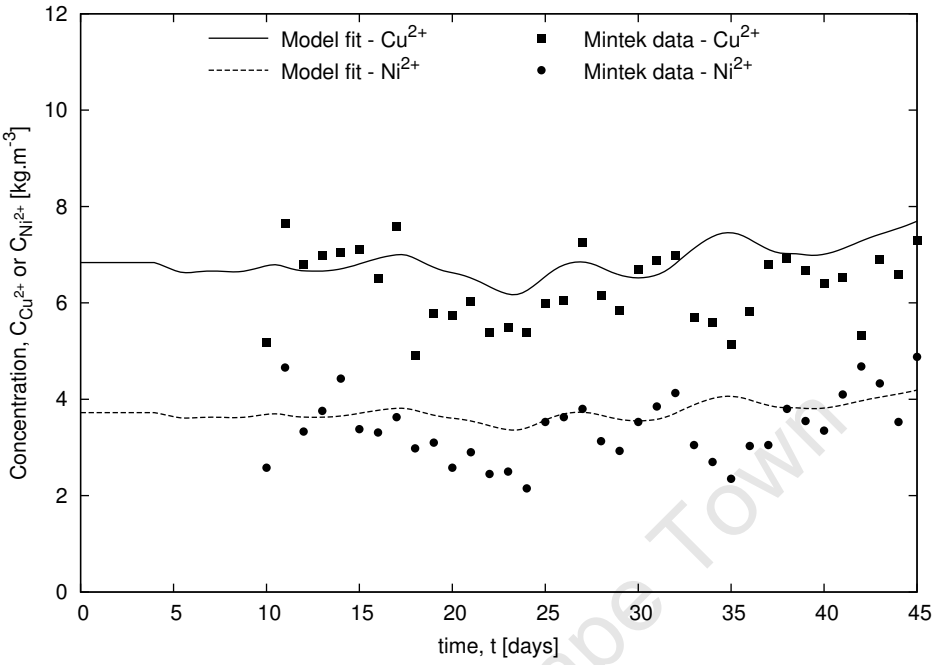

(c) Concentrations

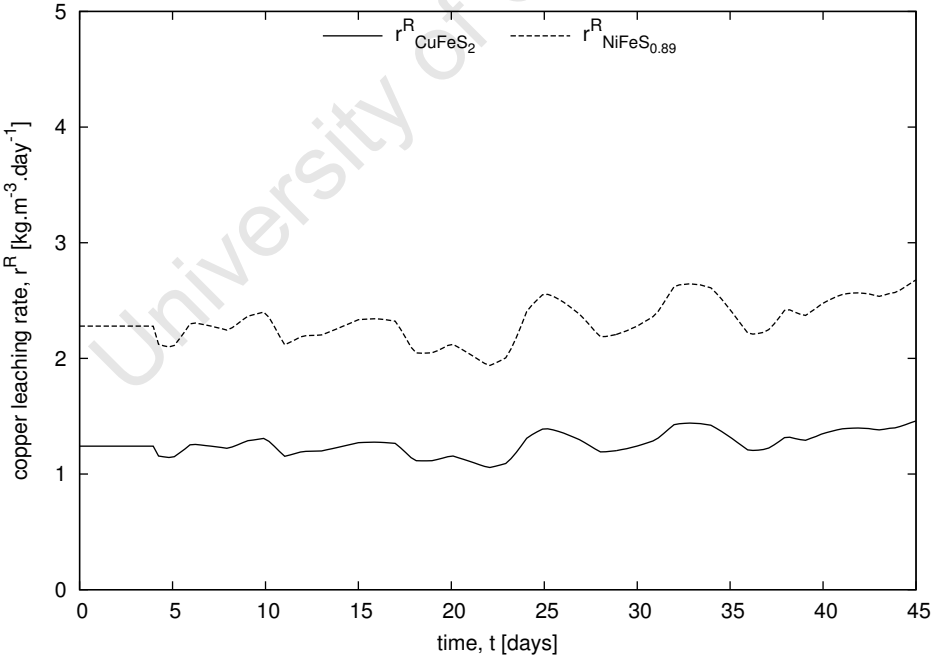

(d) Chemical leaching rate

Figure 7.2: Validation of the unsteady state PBM developed using a segregation approach against data obtained from Mintek for Aguablanca ore.

rates of Cu^{2+} and Ni^{2+} increase with an increase in the solids loading. This is due to the increased number of particles in contact with the reaction phase, which implies that more active sulphide mineral is available for reaction. Similarly, the reaction rate decreases when the number of particles or solids loading to the reactor decreases. Furthermore, fluctuations in the inlet flow rates result in varying reactor mean residence times (Figure 7.2b). An increase in the mean residence time relative to the change in the reactor inlet flow rate increases the chemical leaching rates (Figures 7.2 b and d). With increasing mean residence time the sulphide mineral particles remain in contact with reactants for longer periods of time thus promoting the metal extraction of metals. If a steady state model was applied to the unsteady state data, fluctuations in the concentration and rate profiles would not be accurately predicted and any perturbations in the inlet process variables would not be reflected in the reactor outputs. The implications of irregular inlet process variables on system steady states will therefore require further study.

Earlier analyses into the dynamics of chalcopyrite bioleaching (see Chapters 5 and 6) have shown that there exists within such systems sufficient complexity to warrant further investigation and adaptation to the unsteady state case. Since the model predicts reactor performance with reasonable accuracy, a dynamics analysis on a unsteady state reactor system in which either the inlet flow rate, Particle Size Distribution (PSD) or solids loading are not constant, can be investigated for the purpose of maximising the reaction rate. The results of the analysis will be used to develop strategies at maintaining the system at maximum rates.

7.5 System Dynamics

The dynamics of chalcopyrite bioleaching was extensively studied in batch and continuous flow reactors for a range of ferric/ferrous ion ratios, biomass concentrations, temperature conditions and mean residence times. It was established that the generally-reported steady state by Breed and Hansford (1999b), which assumes that the rate of ferrous ion production during chemical leaching equals the rate of ferrous ion consumption during microbial oxidation, only holds for ferrous ions.

Steady state(s) for the bioleach system were evaluated by making the necessary substitutions into Eq. 5.3 for the ferric and ferrous ion material balances for the corresponding reactor configuration. In the case of continuous flow reactor systems, a general expression that can predict the system steady states was derived (Eq. 6.8).

$$\underbrace{(R+1)\cdot r_{Fe^{2+}}}_{r_M} = \underbrace{(\beta R+\alpha)\cdot r^R - \frac{C_{Fe^{3+}_{inlet}}}{\tau}\left(1-\frac{R}{R_{inlet}}\right)}_{r_L^S} \qquad [6.8]$$

where r_M is the microbial oxidation rate function and r_L^S is the overall chemical leaching rate function that incorporates a time-varying particle surface area due to reaction and flow.

It was clear from the sensitivity analysis that the dynamic structure of the system was sensitive to the biomass concentration C_X, which directly affects the microbial oxidation rate $r_{Fe^{2+}}$, the mean residence time and inlet ferric/ferrous ion ratio R_{inlet}.

Since the influence of biomass concentration, solution redox potential, mean residence time and time-varying particle surface areas on the dynamics is known for a steady state system in which flows across the boundaries of a continuous flow reactor are constant, the dynamics analysis of chalcopyrite bioleaching can be extended to an unsteady state system. Accordingly, the influence of inlet flow rate, PSD and solids loading on the dynamic structure of the system are investigated in the following section.

7.6 Sensitivity Analysis

In the following section, the sensitivity of the bioleach system to reactor inputs will be investigated with the view to identifying suitable control strategies. It is clear from Eq. 7.8 that the overall performance of the bioleach reactor is determined by the rate contribution of all particles of all possible size and age classes and is directly proportional to the mass of particles M^p relative to the reactor volume V^R. Since $f_0(l_0)$ and $I(t,\theta)$ (Eq. 7.1) are functions of particle size and flow rate, respectively, the dependence of the dynamic structure on PSD $f_0(l_0)$, RTD $I(t,\theta)$ and solids loading M^p/V^R to the reactor must be established.

7.6.1 Influence of Inlet Flow Rate

At steady state the inlet and exit flow rates to and from the reactor, respectively, are constant and hence the reactor mean residence time is also constant. If either flow rate varies, the reactor mean residence time would change relative to the change in the flow rate thus shifting the system steady state (Figure 7.1). The R-X plane in Figure 7.3, which is the locus of steady states for a continuous flow reactor system, was plotted to illustrate the shift in steady states due to perturbations in reactor flow rates. The sensitivity of steady states to changes in the inlet flow rate, specifically a step change and sinusoidal inlet flow rate, are investigated. The reactor mean residence time was increased from 1 day to 6 days when a step change was applied at the inlet while the mean residence time fluctuated between *ca.* 1.2 days to 2.7 days when a sinusoidal inlet flow rate was applied.

When a step increase in the entrance flow rate is applied such that the reactor mean residence time is increased from 1 day to 6 days, there is an increase in the concentration of fresh particles in the reactor, as well as an increased holdup in the reactor (Rawatlal and Starzak, 2003). Similarly, with a sinusoidal inlet flow rate, increasing flows result in an increase in the holdup while a decrease in the flow rate decreases the holdup. Since the mean residence time is defined as the relative ratio of the holdup to the flow rate at the exit, the mean residence time increases with increasing inlet flow rate and decreases with decreasing inlet flow rate

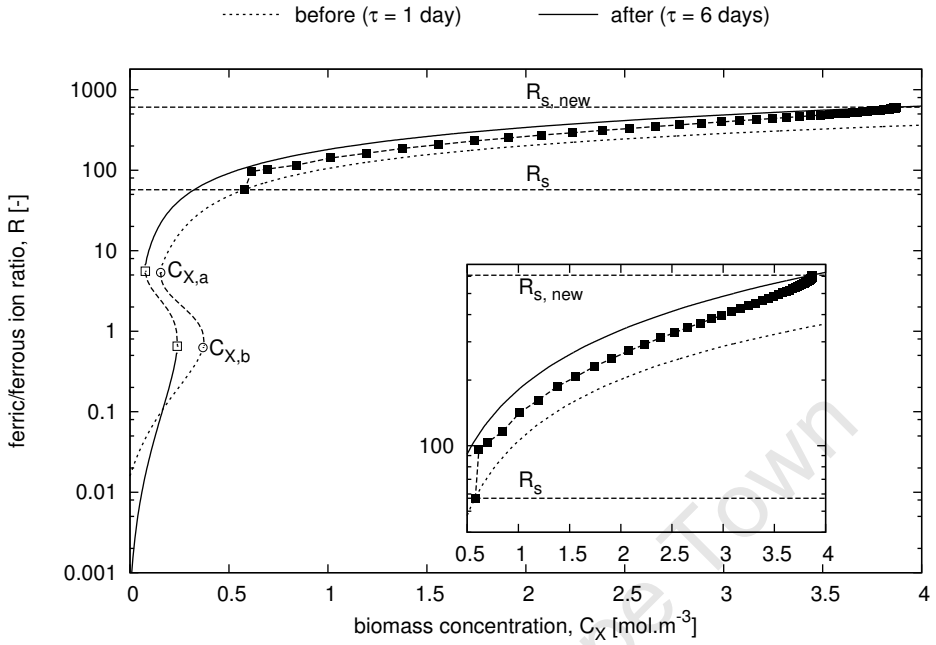

(a) Step change in inlet flow rate

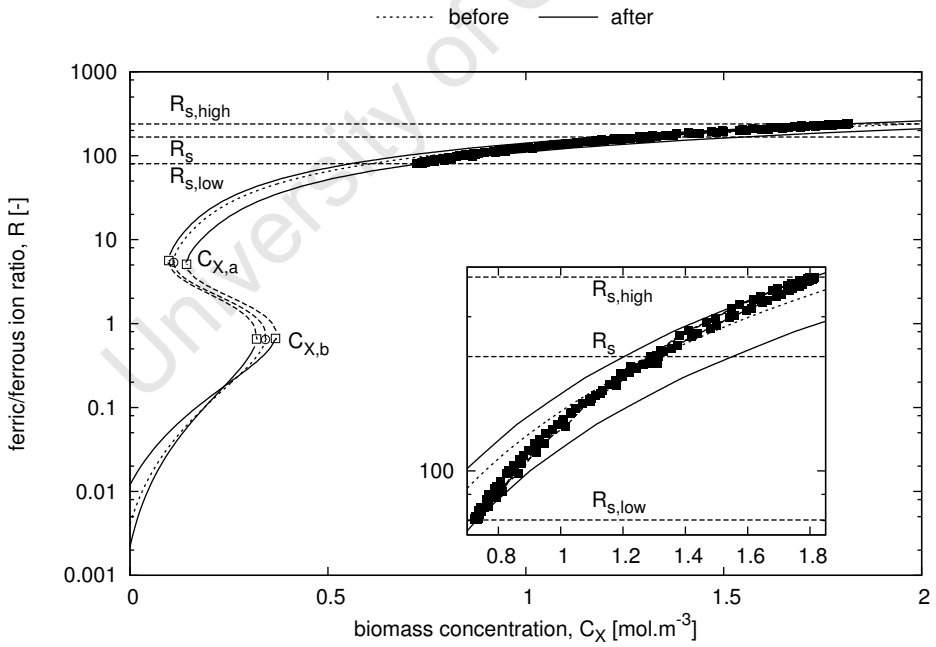

(b) Sinusoidal inlet flow rate

Figure 7.3: The change in system steady states when (a) a step change and (b) sinusoidal inlet flow rate is applied to the bioleach reactor.

when a gravity-driven exit flow rate is applied. The observed increase/decrease in the reactor mean residence time with flow rate is therefore not expected but can be explained by the delayed response of the exit flow rate to the perturbation at the inlet. The resultant increase in the holdup only occurs if the exit flow rate lags the inlet flow rate. The ratio of the reactor holdup to the exit flow rate will therefore result in an increase in the mean residence time. It is often the case in unsteady state mode that space-time θ and mean residence time τ are not always equal.

Points $C_{X,a}$ and $C_{X,b}$ in Figure 7.3 indicate bifurcation points, which are critical points at which the dynamic structure of the system changes from multiple steady states to a single steady state. This is to say that as the microbial concentration C_X increases, the number of intersections between the microbial oxidation rate curve and chemical leaching rate curve changes from one to three intersections and *vice versa*. This effectively means that there is a change in the number of steady states before and after critical points $C_{X,a}$ and $C_{X,b}$, which classifies these points as bifurcation points. With increasing mean residence time, steady states at high ferric/ferrous ion ratios above $C_{X,a}$ shift to higher ferric/ferrous ion ratios (Figures 7.3 a and b) while steady states shift to lower ferric/ferrous ion ratios when the mean residence time decreases (Figure 7.3b). When either a step increase or sinusoidal inlet flow rate is applied, an increase in the biomass concentration is observed due to the increase in reaction space-time resulting in increased reactor reaction rate. When a step increase is applied at the entrance flow rate, such that the reactor mean residence time is increased from 1 day to 6 days, the steady state ferric/ferrous ion ratio R_S increases from $R_S = 57.3$ when the reactor is operated at $\tau = 1$ day, to $R_{S,new} = 606.7$ when the mean residence time is increased to 6 days (Figure 7.3a). However, the steady state R-value fluctuates between $R_{S,low} = 80.2$ ($\tau = 1.2$ days) and $R_{S,high} = 239.0$ ($\tau = 2.7$ days) when a sinusoidal inlet flow rate is applied to a reactor initially operating at $\tau = 2$ days with steady state $R_S = 167.2$ (Figure 7.3b). As observed in Chapter 6, a single steady state R-value at R_S was observed when either a step inlet or sinusoidal inlet flow rate was applied to the reactor, but since the reactor mean residence time changes with flow rate and real time, the steady state R-value R_S changes in direct proportion to the applied change as indicated by Eq. 6.11.

From the analysis, we note that the reactor mean residence time changes according to changes in the entrance flow rate to the reactor. In the case when the reactor mean residence time increases due to an increase in the entrance flow rate, the mineral sulphide particles remain in the reactor for a longer period of time promoting ferrous ion (Eq. 5.1) and hence ferric ion production (Eq. 1.2) thus increasing the microbial concentration and ferric/ferrous ion ratio, respectively. Consequently, increases or decreases in the reactor mean residence time resulting from perturbation in the entrance flow rate influence both the steady state microbial concentration and ferric/ferrous ion ratio and significantly affects the overall dynamics of the bioleach reactor.

Perturbations in the entrance flow rate may also result in perturbations in the uniformity of the particle feed rate. Variances in either the Particle Size Distribution (PSD) or solids loading to the reactor are likely not to be constant if there are fluctuations in the entrance

flow rate. The sensitivity of system steady states due changes in the PSD and solids loading should therefore be studied.

7.6.2 Influence of Inlet Particle Size Distribution (PSD)

It is often the case when developing a reactor model for the bioleaching of sulphide minerals that the inlet PSD $f_0(l_0)$ is approximated by a normal distribution which assumes that a set of random particles accumulate around a mean particle size μ evenly dispersed over a range of sizes. The spread of particle sizes around the mean μ is commonly referred to as the standard deviation σ. In a steady state system, it is assumed that the mean μ and standard deviation σ remain the same at all times, however in reality these may differ due to inhomogeneity in the feed.

To establish the influence of varying inlet PSD on the overall reactor performance and hence the dynamics of the system, a range of mean particle sizes and standard deviations were explored. Initially the influence of standard deviation ($\sigma = 2.50 \times 10^{-6}$ m, 1.25×10^{-6} m, 2.50×10^{-7} m, 1.25×10^{-7} m) of particles around a constant mean $\mu = 12.50 \times 10^{-6}$ m was investigated, thereafter the effect of changing the mean particle size (μ = 6.50 μ m, 12.50 μ m, 21.25 μ m) assuming a narrow standard deviation $\sigma = 1.25 \times 10^{-7}$ m was examined (Figure 7.4). With every applied change in either the mean particle size μ or standard deviation σ (Figure 7.4a), the change in the overall leaching rate r^R (Figure 7.4b), and hence the shift in system steady states (Figures 7.4 c and d), was monitored to determine the sensitivity of the system to changes in the PSD.

Figure 7.4 illustrates the change in the PSD (Figure 7.4a), overall leaching rate (Figure 7.4b) and system steady states (Figures 7.4 c and d) due to changes in the mean and standard deviation for a normally distributed set of particles entering a continuous flow bioleach reactor. In Figure 7.4, it can be seen that as the standard deviation is decreased from $\sigma = 2.50 \times 10^{-6}$ m to $\sigma = 2.50 \times 10^{-7}$ m over a mean particle size $\mu = 12.50 \times 10^{-6}$ m (Figure 7.4a), the overall leaching rate decreases by *ca.* 27.73 % (Figure 7.4 b). By decreasing the standard deviation, the distribution of particles narrows to include mostly particles of similar size to the mean reducing the fraction of small and large sized particles, thus decreasing the particle specific surface area A^p. Since the overall leaching rate in Eqs. 6.7 and 7.8 is directly proportional to the particle specific surface area A^p, the rate decreases, shifting the system steady states to lower overall biomass concentrations C_X at ferric/ferrous ion ratio R_S (Figure 7.4c). The biomass concentration decreases due to the reduction in the ferrous ion substrate production resulting from the decrease in the chemical leaching rate.

When investigating the influence of changing the mean particle size from $\mu = 6.58 \times 10^{-6}$ m to 21.25×10^{-6} m, the chemical leaching rate decreases by ca. 47.78 % with increasing mean particle size (*viz.* $\mu = 12.50 \times 10^{-6}$ m to 21.25×10^{-6} m in Figures 7.4 a and b) while increasing when the mean is reduced to $\mu = 6.58 \times 10^{-6}$ m. Similar to decreasing the standard deviation, increasing the mean particle size decreases the particle specific surface

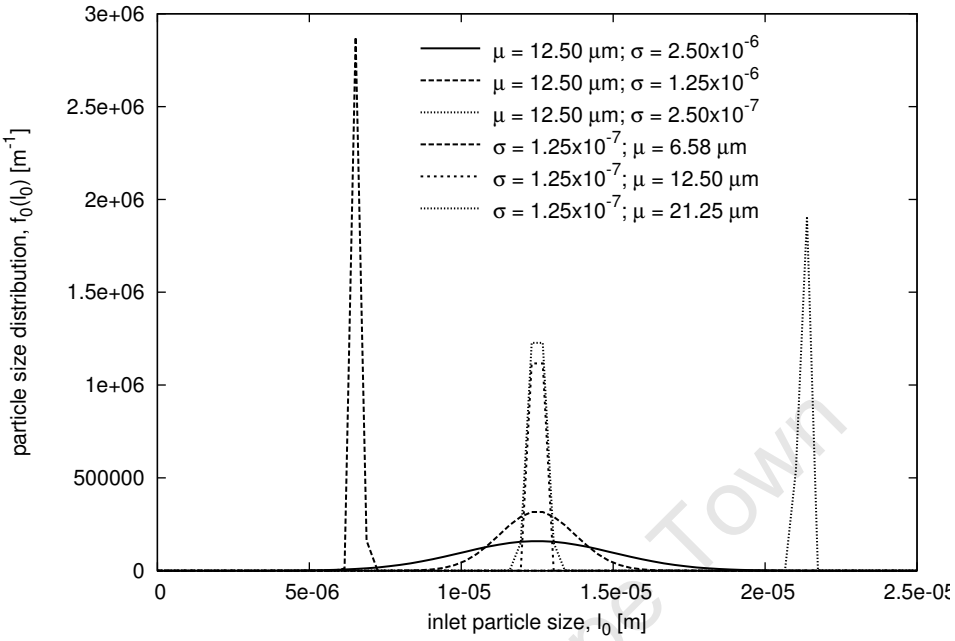

(a) PSD

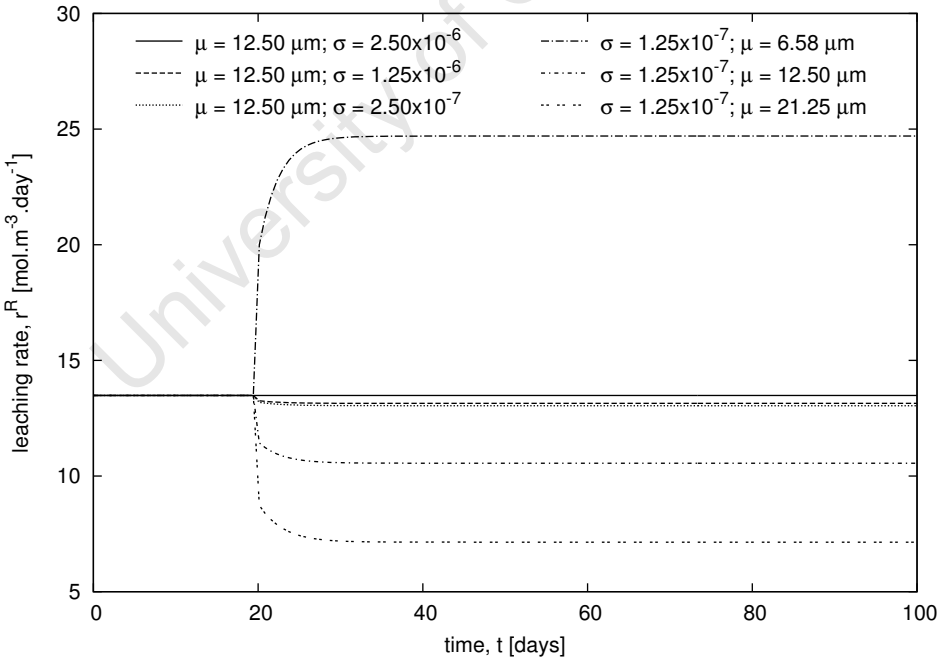

(b) Influence of varying PSD on chemical leaching rate

Figure 7.4: Influence of step changes in the inlet PSD to a continuous flow reactor on the overall leaching rate...continued on next page.

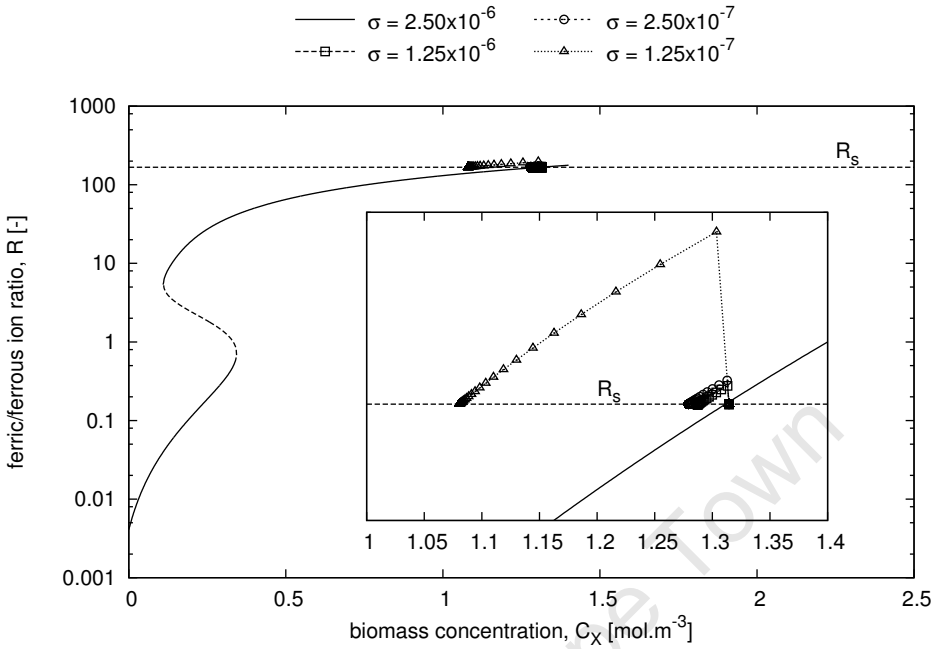

(c) Influence of varying PSD standard deviation on system steady-states

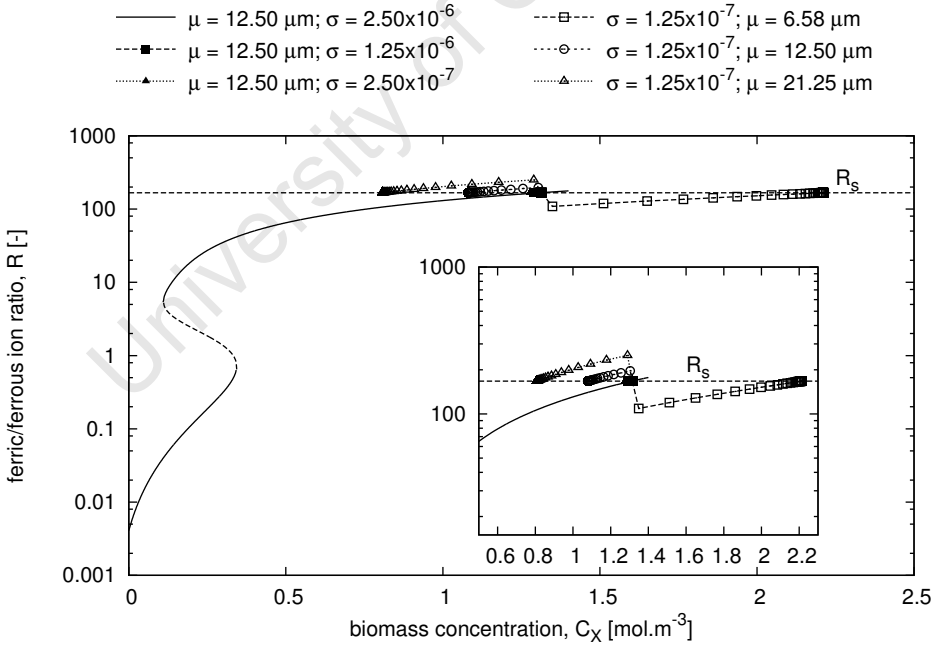

(d) Influence of varying mean PSD μ on system steady-states

Figure 7.4: Influence of step changes in the inlet PSD to a continuous flow reactor on the overall leaching rate.

area and hence decreases the overall rate shifting the system to steady states that correspond to lower biomass concentrations C_X while maintaining the ferric/ferrous ion ratio at the steady state R-value R_S (Figures 7.4 b and d). However, decreasing the mean particle size implies that more small particles are introduced to the reactor and hence increases the particle specific surface area and thus the rate. With an increase in the chemical leaching rate, there is an increase of ferrous ion substrate production (Eq. 5.1) which promotes microbial growth thus shifting steady state operation to higher biomass concentrations C_X (Figures 7.4 b and d). These observations, where the steady state ferric/ferrous ion ratio remains constant, confirmed the findings in Chapter 6 that the system operating point is determined by the steady state ferric/ferrous ion ratio R_S, irrespective of the change in biomass concentration due to changes in the reactor inlet conditions (Eq. 6.11).

From the above analysis, it is apparent that the system steady state ferric/ferrous ion ratio R_S is relatively insensitive to changes in the PSD while significant changes up to *ca.* 68.19 % in the steady state microbial concentration are observed (*viz.* Figures 7.4 c and d). However, prior to achieving steady state after the applied perturbation in the PSD, there is a significant departure from the steady state point prior to the system once again returning to steady operation. It was shown in the dynamics analysis for a continuous flow reactor, operating at steady state, that maximum rates could coincide with a bifurcation point. Therefore any small changes in the operating conditions would drive the system to unfavourable low bioleaching rates. In such cases, it is important that influence of the PSD to any control strategy applied takes into account the influence of varying PSD.

7.6.3 Influence of Solids Loading

The solids loading is defined as the mass of particles relative to the reactor volume M^p/V^R. In Eqs. 6.7 and 7.8, it is clear that the overall chemical leaching rate is directly proportional to M^p/V^R and therefore it is expected that an increase or decrease in the solids loading will increase or decrease the rate, respectively (Figure 7.5). However, effective bioleaching occurs when the solids loading is below 18-20% [m/v] after which hydrodynamic stress due to the increase in the solids loading significantly inhibits microbial growth and hence biooxidation (Sissing and Harrison, 2003; Nemati and Harrison, 2000; Raja, 2005). Since the influence of solids loading on the dynamics of the system is to be investigated, Figure 7.5 was generated assuming that growth inhibition due to hydrodynamic stress resulting from high solids loading, was absent. Solids loadings ranging from 10% to 40% [m/v] were investigated.

In Figure 7.5, it can be seen that the rate increases with solids loading (Figure 7.5a). Increasing the solids loading to 40% shifted the system steady states to higher biomass concentrations while reaching the same overall steady state ferric/ferrous ion ratio R_S (Figure 7.5b). This shift in system steady states is due to the increased concentration of ferrous ion substrate in solution resulting from the chemical leaching of the increased concentration of chalcopyrite (Eq. 5.1) which promotes microbial growth and hence shifts

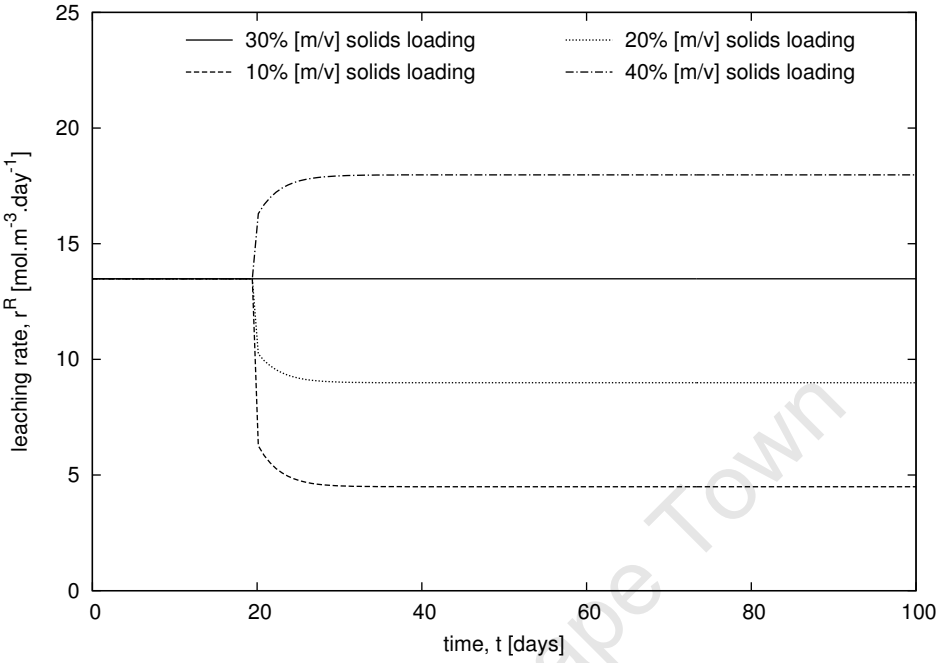

(a) Chemical leaching rate, r^R

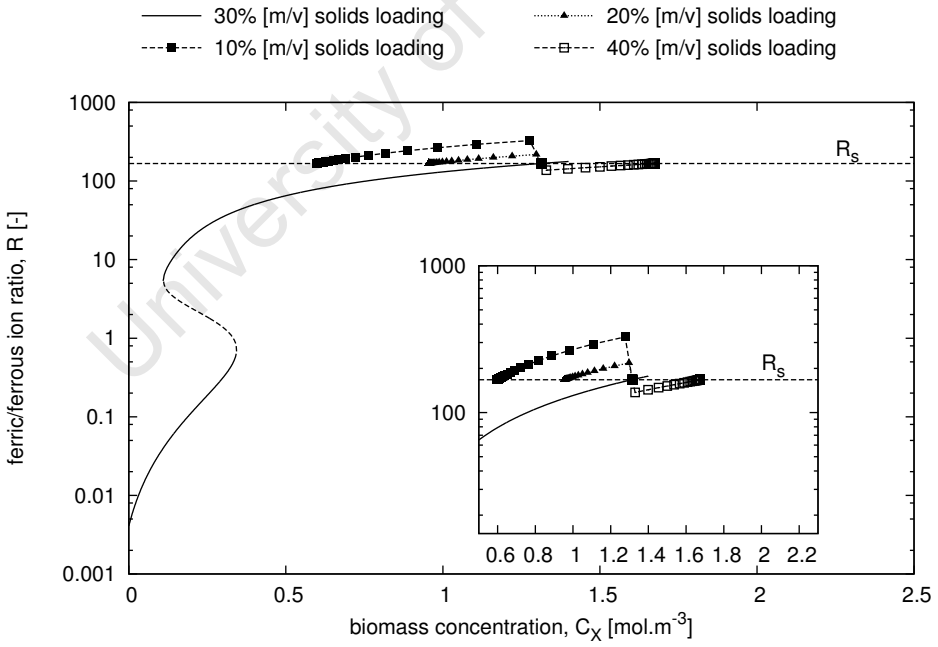

(b) R-X Plane

Figure 7.5: The influence of solids loading on the overall leaching rate rR and bioleaching steady states.

steady states to higher biomass concentrations (Figure 7.5b). Similarly, a decrease in the solids loading decreased the chemical leaching rate resulting in steady states at lower biomass concentrations while reaching the same steady state ferric/ferrous ion ratio R_S. Although the rate increased or decreased due to a change in the solids loading, the steady state operating point of the continuous flow bioleach reactor reached the same overall ferric/ferrous ion ratio R_S indicating once again that the dynamics of the system is determined by the steady state R-value R_S and is not affected by the inlet conditions to the reactor.

Similarly to PSD, the system is only sensitive to changes in the solids loading when the system transitions to the new steady state point after the applied perturbation. During this transition period, there is either an increase (*viz.* 10 % and 20 % [m/v] solids loading in Figure 7.5b) or decrease (*viz.* 40 % [m/v] solids loading in Figure 7.5b) in the ferric/ferrous ion ratio prior to reaching the same overall steady state ferric/ferrous ion ratio R_S indicating that a change in the solids loading would have a significant influence on any control strategy.

In Chapter 6, it was shown that the bioleach system is sensitive to reactor mean residence time τ, biomass concentration C_X and the inlet ferric ferrous ion ratio R_{in}. An increase or decrease in either of these process conditions influenced the dynamic structure of the system and thus steady state operation. Below a critical ferric/ferrous ion ratio, an increase in the mean residence time shifted steady state operation to higher biomass concentrations, while above the critical point steady states were driven to lower overall biomass concentrations. Due to the direct proportionality of the microbial oxidation rate to the biomass concentration, an increase or decrease in the biomass concentration shifted the microbial oxidation rate to respectively higher or lower rates thus shifting the system from multiple steady states to a single steady state. Above a certain critical biomass concentration, the system transitioned from high to low overall bioleaching rates with increasing biomass concentration. In the following section, these observations in combination with the preceding sensitivity analysis are incorporated into the development of an effective control strategy to maintain the operation of the bioleach reactor at optimum rates to maximise overall reactor performance.

7.7 Control

The objective in a control system is to maintain a set of control variables at the desired process conditions to sustain plant operation at the optimum. In bioleaching, one useful optimality criterion is the overall leaching rate.

It has been shown that low rates are achieved at ferric/ferrous ion ratios greater than 1, while high rates are achieved at ratios approximately equal to unity (Petersen and Dixon, 2006). However, it should be noted that due to the non-monotonic shape of the rate curves, the maximum rate also coincides at a point at which a bifurcation occurs. Operating near the bifurcation point is undesirable since any disturbance in process inputs may result in the system being rapidly driven away from the operating point to lower stable steady state

leaching rate points. In unsteady state systems, fluctuations in inlet or exit flow rates, irregularities in the reactor loading or particle size distribution as well as changes in the biomass concentration, redox potential and reactor mean residence time are commonplace. From the sensitivity analysis, it is clear that small changes in reactor inputs can significantly influence the operation point, which means the system can stray from the intended operating point with little provocation.

It is clear from the sensitivity analysis performed in Chapters 5 and 6 that a critical biomass concentration exists prior to the system being driven from high rates to low overall rates. It emerged from this study that controlling the biomass concentration to below that critical biomass concentration, which coincides with the bifurcation biomass concentration $C_{X,b}$, maximum overall rates could be maintained by introducing a first order biological stress factor k_s, assuming steady state operation (Eq. 6.13). The required steady state stress rate to keep the system at maximum rates, k_s, was determined from the optimum biomass concentration $C_{X,max} = C_{X,b}$ and corresponding ferric/ferrous ion ratio $R_{X,max}$ (Eq. 6.13).

$$k_s = \frac{Y_{XS} q^{max}_{Fe^{2+}}}{(1 + KR)} - \frac{1}{\tau} \qquad [6.13]$$

where the value of the biological stress rate k_s [s^{-1}] can be correlated to the applied stress due to agitation and abrasive solids loading. In the Chapter 6, Eq. 6.13 was developed for a system where the flow rates to and from the bioleach reactor were taken as constant. Applying a biological stress rate to the system (determined using Eq. 6.13) proved to be effective at controlling the biomass concentration at levels below the critical point, to control the reaction rate at a maximum. However, the stress rate in Eq. 6.13 was not tested for unsteady state operation in which the flow rates to the bioleaching reactor, were changing with time. In the following section, Eq. 6.13 will be used to control the biomass concentration at the optimum operating point, assuming that high rates are achievable using the steady state assumption for a system operating in unsteady state mode.

Figure 7.6 was generated for an unsteady state system in which a sinusoidal inlet flow rate, with a gravity driven exit flow rate, was applied to the reactor. To maintain the system's operation at maximum rates, the steady state stress rate k_s in Eq. 6.13 was calculated at $C_{X,max} = 0.34$ mol carbon.m^{-3} and corresponding $R_{X,max} = 0.65$ at an average mean residence time $\tau = 2$ days (Figures 7.3 − 7.5) and applied to the bioleach reactor. In this simulation, it was assumed that all other process parameters such as the reactor solids loading and PSD, remained constant.

In Figure 7.6a, it is clear that by applying a steady state stress rate k_s (Eq. 6.13) to an unsteady state system, bioleach operation cannot be maintained at optimal biomass concentrations and ferric/ferrous ion ratios to keep the system at maximum overall rates. Instead, utilising a constant stress rate for a system, in which the mean residence time and reactor volume changes with fluctuations in the entrance flow rate, initiates rapid cell death resulting in low overall rates (Figure 7.6b). Since the reactor volume V^R and mean residence

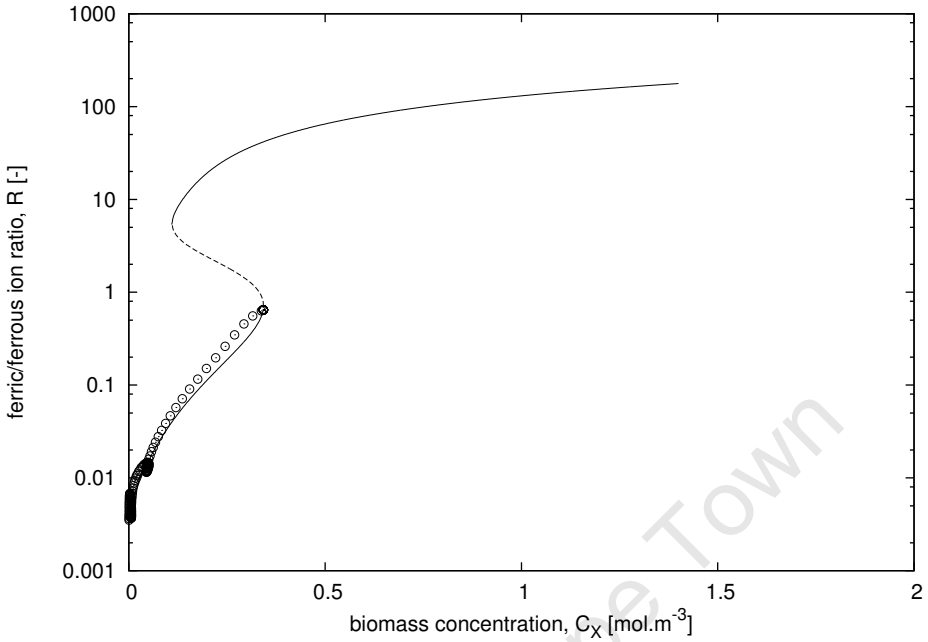

(a) Steady states achieved using constant stress rate k_s

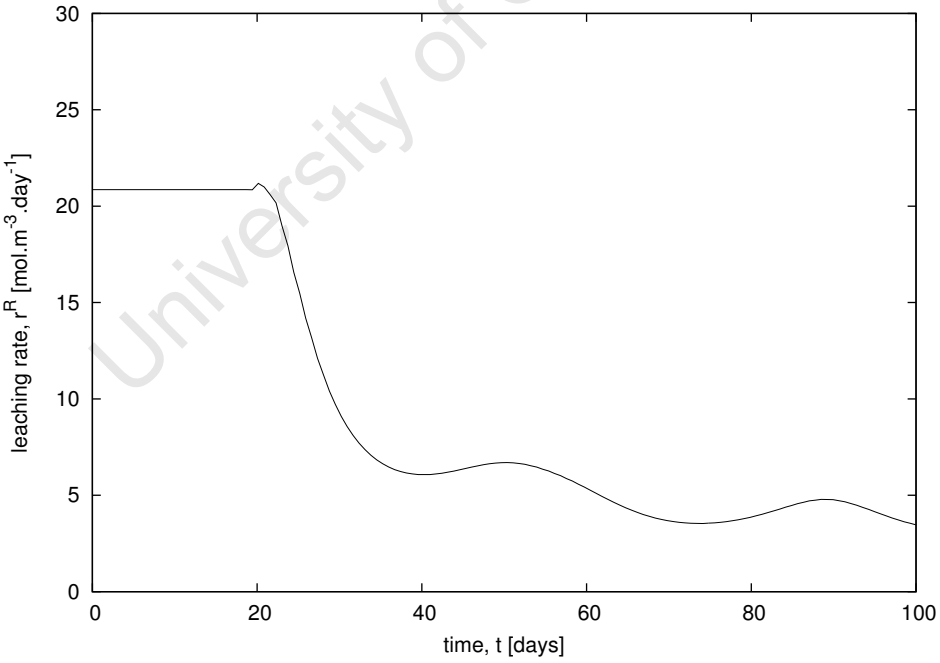

(b) Corresponding leaching rate achieved when applying a constant stress rate k_s

Figure 7.6: Application of a constant stress rate k_s (Eq. 6.13) to a reactor with a sinusoidal inlet flow rate. Points $\odot$ in Figure (a) represent the model prediction assuming a constant stress rate k_s.

time τ change with time a hydrodynamic stress rate that incorporates these changes in an unsteady state system needs to be determined.

To establish the required dynamics dependence of the biomass concentration on the (dynamic) reactor volume, we first develop the unsteady state mass balance over the continuous flow bioleach reactor (Eq. 7.10).

$$C_X \frac{dV^R}{dt} + V^R \frac{dC_X}{dt} = Q_{inlet} C_{X,inlet} - Q_{outlet} C_X + \left(Y_{XS} \cdot r_{Fe^{2+}} - k_s C_X\right) V^R \qquad [7.10]$$

where $C_{X,inlet}$ and C_X [mol carbon.m^{-3}] are the inlet and outlet biomass concentrations, respectively, Q_{inlet} and Q_{outlet} [m^3.s^{-1}] are the inlet and outlet volumetric flow rates to and from the bioleach reactor, respectively and V^R [m^3] the reactor volume.

If the optimum biomass concentration $C_{X,max}$ and ferric/ferrous ion ratio $R_{X,max}$ are known, the derivative $\frac{dC_X}{dt}$ can be approximated by the change in the biomass concentration from the optimum concentration $(C_{X,max} - C_X)$ relative to the desired time period Δt by which the maximum operating conditions should be reached. While $\frac{dV^R}{dt}$ is the change in the reactor holdup determined by Eq. 7.11.

$$\frac{dV^R}{dt} = Q_{inlet} - Q_{outlet} \qquad [7.11]$$

where Q_{outlet} [m^3.s^{-1}] is taken as a gravity-driven exit flow rate.

Making the necessary substitutions into Eq. 7.11 for the microbial oxidation rate expression $r_{Fe^{2+}}$ and the aforementioned assumptions, a time-varying biological stress rate $k_s(t)$ [s^{-1}] for an unsteady state system, required to obtain maximum leaching rates, can be calculated using the relationship derived in Eq. 7.12.

$$k_s(t) = \frac{C_X(t) - C_{X,max}(t)}{C_X(t) \cdot \Delta t} + \frac{Y_{XS} q^{max}_{Fe^{2+}}}{1 + KR} - \frac{Q_{inlet}(t) - Q_{outlet}(t)}{V^R(t)} - \frac{1}{\tau(t)} \qquad [7.12]$$

where $V^R(t)$ [m^3] and $\tau(t)$ [s] are the reactor volume and mean residence time at time t [s] and $C_X(t)$ [mol carbon.m^{-3}], $Q_{inlet}(t)$ [m^3.s^{-1}] and $Q_{outlet}(t)$ [m^3.s^{-1}] are the time variant biomass concentration, inlet and outlet flow rates, respectively. $C_{X,max}(t)$ [mol carbon.m^{-3}] and $R_{X,max}(t)$ [-] are the optimal biomass concentration and ferric/ferrous ion ratio at time t [s].

Since the biological stress rate determined by Eq. 6.13 proved ineffective at maintaining the system at maximum rates, it was assumed that the time-varying stress rate developed in Eq. 7.12 could be applied to determine the trajectory of the bioleaching rate. As biological stress has been shown to increase with increasing impeller tip speed, a transient biological stress rate can be applied by varying the reactor agitation rate as required (Raja, 2005). Optimum biomass concentrations and ferric/ferrous ion ratios were calculated at each time step at which point the chemical leaching r_L^S and microbial oxidation r_M rates were equal and tangent to each other. At the point of tangency the overall leaching rate was at a maximum and the biological stress rate in Eq. 7.12 was recalculated at each time step.

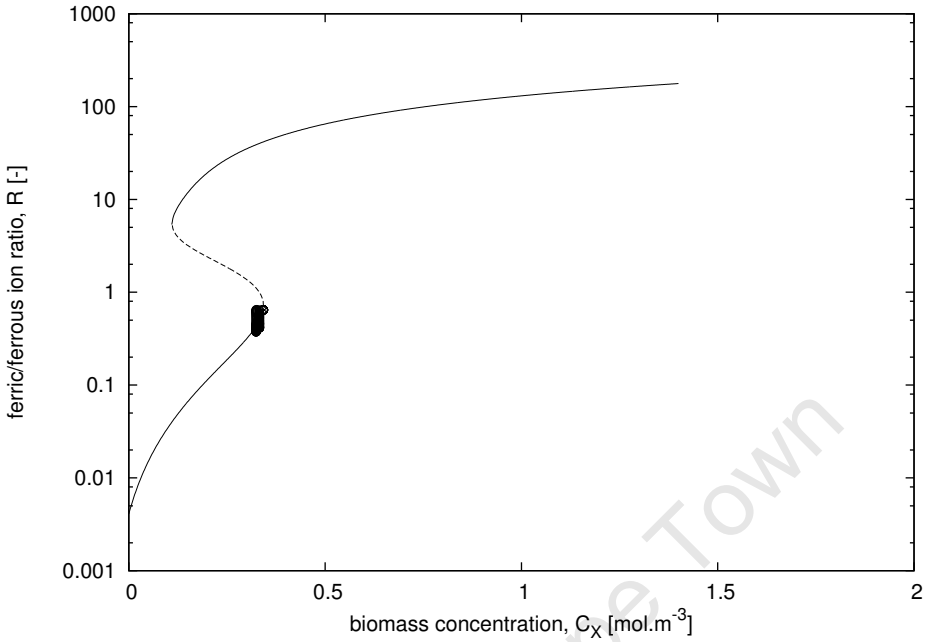

(a) Steady states achieved using time-varying stress rate $k_s(t)$

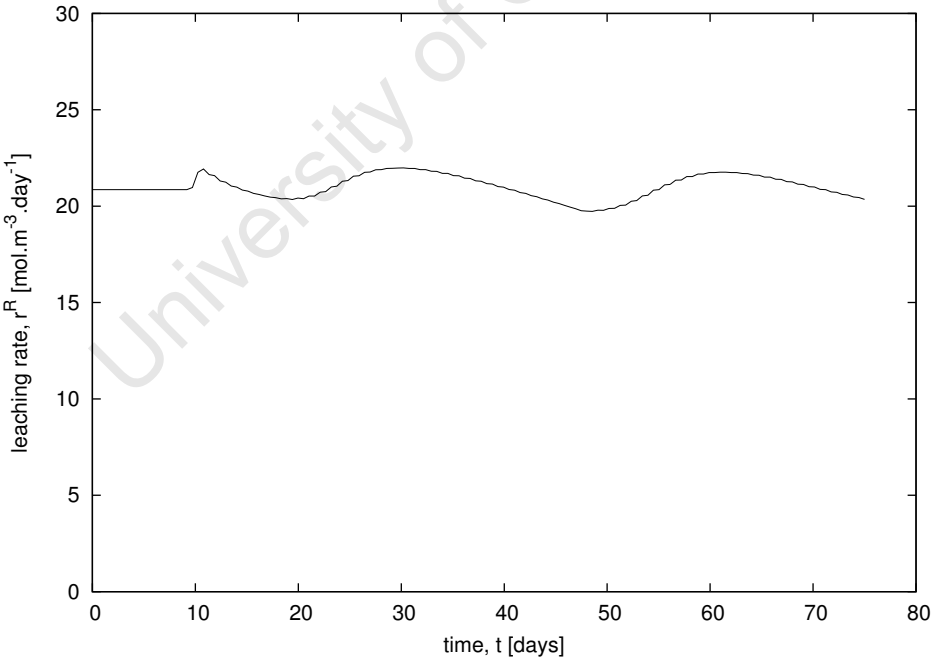

(b) Corresponding leaching rate achieved when applying time-varying stress rate $k_s(t)$

Figure 7.7: Application of a time-varying stress rate $k_s(t)$ (Eq. 7.12) to a reactor with a sinusoidal inlet flow rate. Data points $\odot$ in Figure (a) represent the model prediction assuming a time-varying stress rate $k_s(t)$.

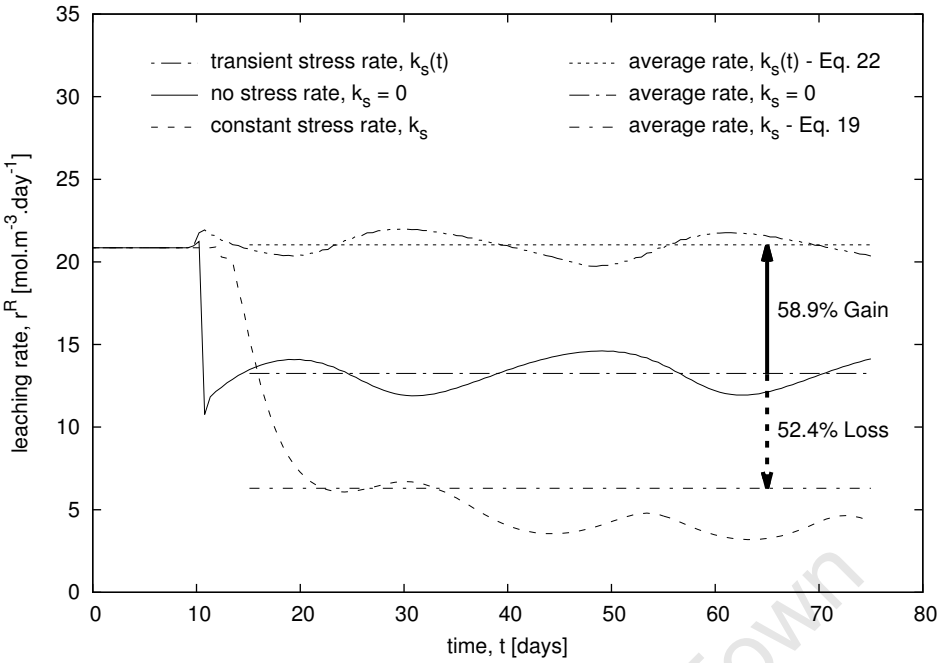

Figure 7.8: A comparison between the overall chemical leaching rates obtained when no biological stress rate is applied ($k_s = 0$ day^{-1}) to when a constant (Eq. 6.13) and transient (Eq. 7.12) biological stress rate is applied to the bioleaching system.

As it can be seen in Figure 7.7a, the overall leaching rate was successfully maintained at the maximum in an unsteady state system by applying the stress rate calculated in Eq. 7.12. This high rate was achieved by recalculating the biological stress rate at each time step t given the optimum microbial concentration $C_{X,max}(t)$ and ferric/ferrous ion ratio $R_{X,max}(t)$, thus correcting for the imposed perturbation at the reactor inlet (Figure 7.7b). Due to the variance in the inlet flow rate, the overall rate fluctuates around the maximum point with changing mean residence time $\tau(t)$ [s] (Figure 7.7c). While an appropriate biological stress could be calculated, even though reactor flow rates are not constant, it is important to note that the effectiveness of such a control system is dependent on the ability to practically achieve the desired stress rate $k_s(t)$ [s^{-1}] within the desired time frame Δt.

To illustrate the influence of applying a constant (Eq. 6.13) and transient (Eq. 7.12) biological stress rate to the bioleach reactor, the reactor was initially operated at steady state at the optimum operating conditions. The system was maintained at these conditions by applying a constant biological stress rate determined by Eq. 6.13 . After 10 days, a sinusoidal disturbance was applied at the inlet. Thereafter, the rates obtained when no biological stress rate was applied to the system was compared to when a constant (Eq. 6.13) and transient (Eq. 7.12) stress rate was applied to the bioleach system, after the applied disturbance (Figure 7.8).

The average rate decreased by 52.4 % when a constant stress rate (Eq. 6.13) was applied to the system, while an average 58.9 % gain in the leaching rate was achieved when the stress rate was adjusted for each time step (Eq. 7.12). Applying a constant stress rate over the entire time domain did not improve the rate of bioleaching. As previously stated, the

maximum operating point in the bioleach reactor is sensitive to any small fluctuations in the operating conditions as the maxima coincides with a bifurcation point (*viz.* $C_{X,b}$ in Figure 7.3), applying a constant stress rate thus proves too restrictive, inhibiting microbial growth and therefore driving the system to low overall rates (Figures 7.6b and 7.8). Clearly, using a stress rate that is corrected for each time step, relative to the fluctuations in the process conditions, improves the overall rate (Figure 7.8).

7.8 Conclusions

By developing a reactor model that can predict reactor performance under unsteady state operating conditions, the sensitivity of the overall leaching rate to the changes in operating conditions could be evaluated. A dynamics analysis on the bioleaching of chalcopyrite showed that, apart from the temperature, ferric/ferrous ion ratio and microbial concentration, the system is sensitive to fluctuations in the reactor flow rates, changes in the PSD and solids loading. By performing a dynamics analysis, the rate could be maximised by controlling the ferric/ferrous ion ratio and hence the biomass concentration in an unsteady system by applying an external biological stress that was adjusted according to the perturbations applied to the bioleach system at each time step.

8

Conclusions

The objective of this study was to develop a reactor model for the bioleaching of sulphide mineral concentrates under unsteady state conditions. Suitable control strategies required to improve the overall bioleach reactor performance were developed for the purpose of maximising the overall rate. Most published reactor models developed for the bioleaching of mineral sulphide particles in continuous flow reactors are formulated under the assumption that the hydrodynamics of the system are at steady state. In reality, the flow rates to and from the reactor are never constant. In this study, an unsteady state reactor model was developed using a segregation approach.

Initially, a mathematical model was developed for a reactor operating under steady state conditions to determine which reactor inputs are necessary to fully describe the dissolution of mineral sulphide particles in the bioleaching process. The model development was complicated by the surface area dependence of the reaction rate. The non-trivial distribution of inlet particle size to the reactor was incorporated in the model by means of a normal distribution while a PFRs and tanks-in-series RTD was used to account for the exit particle age distribution.

Three steady state reactor models were presented. Bioleach reactor models were derived from first principles incorporating material balances with acid-ferric leaching and microbial oxidation kinetics. The reactor performance was initially modeled by applying the most restrictive assumptions in which neither the age nor the size of the particles was included in the model formulation. These simplifying assumptions were later eliminated by first introducing the age distribution of equally sized particles in solution. The model assumptions were further relaxed by incorporating the bioleaching of particles of non-trivial inlet size distribution into the aforementioned reactor model thus accounting for both age and size effects on reactor performance.

As opposed to the models presented by Pinches *et al.* (1987), Breed and Hansford (1999b) and Brochot *et al.* (2004), the proposed model incorporated both chemical leaching and microbial oxidation kinetics while determining the influence of the particle dynamics on the overall reactor conversion. The PBMs proposed by Crundwell (1994; 1995; 2001; 2005) and

Brochot *et al.* (2004) included the effects of particle size on the reactor performance but did not sufficiently explore the influence of particle age and its contribution to the overall bioleaching reaction rate.

Of the three models presented in Chapter 4, the reactor model characterized by the incorporation of variances in both the particle age and size, was the most general. The improved predictive capabilities of this model over preceding models indicated that both age and size contributions of the all particles in the reactor are necessary to fully describe the reactor performance in tank bioleaching. Further, Chapter 4 uncoupled the variation of particle size with time to explicitly consider a distribution in particle age in the reactor. This explicit dependence allowed for the model to be later extended to bioleaching in unsteady state mode of operation.

Due to the non-monotonic relationship between the chalcopyrite leaching rate and solution potential, a dynamic analysis was conducted to determine important operational features that influence system steady states in both batch and continuous flow processes. The dynamics analysis revealed that the system transitions from a single steady state regime at low ferric/ferrous ion ratios to multiple steady states at intermediate ferric/ferrous ion ratios. At high ferric/ferrous ion ratios it was found that once a critical biomass concentration was exceeded the system shifted to, once again, a single steady state with low overall rates, irrespective of the reactor type. A procedure to identify these steady states was proposed. In general, it was found that the overall bioleaching rate in both batch and continuous flow reactor systems is sensitive to the solution redox potential, system temperature and biomass concentration and, in the case of the continuous system, the mean residence time.

For the batch system, a method for determining optimal operation for given biomass concentration and temperatures was proposed. Using this technique, the domains of steady states and their stability with respect to the operating variables, *viz.* temperature and biomass concentration was used to identify regions of optimal operation. The dynamics analysis revealed that increasing both the system temperature and the biomass concentration within a defined feasible region, increased chalcopyrite bioleaching rates could be realized at high redox potentials.

Initial studies into the dynamics of chalcopyrite bioleaching in continuous flow reactor systems were conducted using a fixed particle surface area assumption to determine the influence of the biomass concentration, redox potential and mean residence time. The dynamics for a continuous flow reactor, which incorporated the transient change in particle surface area *via.* the modified PBM developed in Chapter 4, was found to be similar to that of the batch reactor when offset by a flow term. The extent of the offset was determined by the magnitude of the mean residence time and inlet ferric ion concentration. Steady states in the continuous flow reactor were achieved at lower biomass concentrations at similar corresponding ferric/ferrous ion ratios to those achieved in the batch system.

Control systems to maximise the overall reaction rate were introduced. To verify whether the theoretical phenomena outlined in the dynamics analysis do occur in reality, the analyses

were applied to experimental data. For the batch system, experimental data obtained from Third *et al.* (2000), showed that the model was able to accurately predict the observed steady states at low and high ferric/ferrous ion ratios. A dynamics analysis of the data verified the existence of multiple steady states in chalcopyrite bioleaching, and that overall rates are sensitive to the combination of the ferric/ferrous ion ratio with the biomass concentration and system temperature.

Control systems to maximise the overall reaction rate in continuous flow reactor systems were introduced. The reactor mean residence time and the introduction of a biological stress rate proved effective at sustaining the system at maximum rates. Excess biomass in the reactor could be controlled to below a critical concentration, by either reducing the reactor mean residence time or applying an optimum stress rate determined using Eq. 6.13, to increase the overall rate by up to 56 %. Application of the dynamic analysis to experimental data obtained from Raja (2005) showed that the model was able to predict a solids loading that provides a biological stress rate that was able to control the ferric/ferrous ion ratio and biomass concentrations at an optimum conditions to achieve maximum rates.

$$k_s = \frac{Y_{XS} q^{max}_{Fe^{2+}}}{(1 + KR)} - \frac{1}{\tau} \qquad [6.13]$$

The dynamics analyses for the bioleaching of chalcopyrite in both batch and continuous flow reactor systems revealed that maximum rates coincide with a bifurcation point. As such, operating at this point was deemed undesirable since any small fluctuation in system inputs or operating conditions would drive the system to low rates. These observations verified the importance of developing a reactor model that incorporates unsteady state hydrodynamics.

An unsteady state reactor model was developed using a segregation approach. The model incorporated recent advancements in residence time distribution theory (Rawatlal and Starzak, 2003), which accounts for fluctuating reactor flow rates. Changes in the feed inlet flow rate to the reactor were investigated to determine the influence of perturbations on the overall reaction rate and hence the reactor performance. The reactor holdup increased with an increase in the entrance flow rate and as a result, the RTD also increased relative to the applied increase to the system flow rate. Hence, the overall leaching rate increased due to more particles being in contact with the reaction environment for longer periods of time. The model was validated against experimental data obtained from Mintek, South Africa for a polymetal sulphide concentrate and was found to predict reactor performance with reasonable accuracy.

A dynamic analysis was performed to determine the influence of perturbations to the reactor inlet flow rate, variances in the PSD and fluctuations in the solids loading would have on the dynamic structure of the system. It was found that step increases to the entrance flow rates shift system steady states to higher solution potentials at increased biomass concentrations. Further, sinusoidal type inlet flow rates resulted in steady state operation fluctuating between steady states at high ferric/ferrous ion ratios with increasing and decreasing biomass concentrations relative to the inlet flow rate. The overall leaching

rate decreased by *ca.* 47.78 % when particles size distributions with predominantly large particles were introduced to the reactor while an increasing rate was observed when smaller particles were introduced due to the increase in the particle specific surface area. The leaching rate increased by as much as 33.33 % when the reactor solids loading was increased due to the increased availability of reactive mineral sulphide concentrate. In both the PSD and solids loading analyses, system steady states were determined by the solution redox potential. Steady state operation in both cases reached the same overall steady state ferric/ferrous ion ratio irrespective of the disturbance in either the particle size distribution or reactor solids loading.

The results of the sensitivity analysis were used to establish control procedures to maintain the bioleach reactor at optimum performance by maintaining the system at maximum rates. Maximum rates were obtained by keeping the biomass concentration and ferric/ferrous ion ratios at the optimum operating point, identified in the dynamic analysis. Results indicated a system that incorporates external biological stress factors to reduce the ferric/ferrous ion ratio to optimal potentials, was able to maintain the bioleaching of chalcopyrite at maximum overall rates. Gains up to 58.9 % in the reaction were obtained when a transient biological stress rate in the form of Eq. 7.12 was applied to the bioleach reactor.

$$k_s(t) = \frac{C_X(t) - C_{X,max}(t)}{C_X(t) \cdot \Delta t} + \frac{Y_{XS} q^{max}_{Fe^{2+}}}{1 + KR} - \frac{Q_{inlet}(t) - Q_{outlet}(t)}{V^R(t)} - \frac{1}{\tau(t)} \qquad [7.12]$$

These results showed that observed low rates of chalcopyrite bioleaching traditionally explained by the formation of a passivating layer on the mineral particle surface or the susceptibility of the biomass cell structure to mechanical stress at elevated temperatures are in fact simply artifacts of the dynamics of chalcopyrite bioleaching, and the many reports about the influence of these parameters on the bioleaching rate must be subjected to a rigorous dynamic analysis to integrate them into a consistent understanding of the underlying kinetics. It was evident from this study that by performing a dynamics analysis, the performance of the bioleach reactor can be improved. By investigating the influence of unsteady state operation on the dynamic behaviour of the system, suitable control strategies were developed highlighting the potential opportunities in processes optimisation in bioleaching.

9

Future Work

THIS study focussed on developing a modified population balance model *via.* a segregation approach to determine the performance of a bioleach reactor in both steady and unsteady state operation. The latter was achieved by incorporating an unsteady state residence time distribution function into the multi-phase reactor model accounting for particle size and residence time distributions. Further, control strategies based on a dynamics analysis of the bioleach reactor were developed to maintain the system at maximum overall rates.

The objective of future studies in process modelling is to extend the knowledge obtained in this project to further improve the developed model. Aspects that should be explored to improve the reactor model are the incorporation of an improved particle model, an energy balance to further facilitate control procedures in the bioleach process and to develop an efficient control strategy to achieve optimum reactor performance.

In bioleaching, most reactor models utilize the shrinking particle model to determine the change in the particle surface area. However, there is physical evidence that pores or channels are formed on the particle surface. If a particle model is developed that includes both internal (pore generation) and external surface area changes and is incorporated in the reactor model, how will this influence the predictive capabilities of the model for the overall rate or conversion in a bioleaching system?

Reaction-controlled shrinking core models assume that the reaction at the particle surface is unaffected by the presence of an unreactive surface. Most reactor models assume uniform particle surface area changes following the shrinking particle model. The shrinking particle model can be improved by incorporating both external and internal surface area changes with varying pore diameters. External surface area changes can be accounted for by the application of the shrinking particle model, while internal surface area changes can be similarly modeled with mass changes resulting from the formation of pores. Hence a shrinking particle model will be developed that can be used to approximate surface area changes frequently observed in bioleaching thus improving the predictive capabilities of the reactor model.

Microorganisms within the bioleach system, which facilitate the bioleaching of sulphide minerals to valuable metals, are only active within narrow operating temperature range. This becomes an issue due to bioleaching being a highly exothermic reaction. Incorporating an energy balance over the bioleach system will further extend the reactor model but may also influence the dynamic structure of the system. As most reaction kinetics follow an Arrhenius temperature dependent model, the reaction rate will most likely increase with increasing temperature and thus shift system steady states to higher operating regions. To establish how these steady states are influenced by temperature a rigorous dynamics analysis is required which would further facilitate to development of efficient control systems.

The bioleaching reaction is exothermic, which indicates that heat is generated during the leaching process. The following questions therefore need to be answered:

- How would the change in temperature influence the dynamic structure of the system or system steady states? i.e. how sensitive is the bioleach system to fluctuations in the operating temperature? Also,
- What control procedures can be enforced to maintain the temperature within optimal conditions?

Optimum plant operation is typically achieved by maximising the overall reaction rate thus making it an important optimisation parameter. A dynamics analysis can be used to optimise and evaluate optimum input conditions to maximise overall production rate. Using Dijkstra's algorithm, control strategies can be developed to maintain the muti-phase system at maximum rates. Dijkstra's algorithm is used to find the shortest or quickest path between two or more nodes. As such, the algorithm can be used to develop an efficient control strategy to obtain the required optimum conditions to achieve the desired operating point using the least amount of operating steps thus lowering overall operating costs.

By improving the predictive capabilities of the reactor model, industrial applications can be achieved with the minimum expenditure of time and effort. This can be further facilitated by the developing suitable control procedures to maximise production output. Currently, in bioleaching very little research is undertaken in this area. By developing appropriate control strategies the overall performance of the system may be improved thus reducing system resources and hence energy requirements. Further, by improving the efficiency of the system energy requirement will be reduced and any harmful effluent from the process will be decreased thereby reducing the systems impact on the environment.

Ultimately, once the aforementioned areas have been incorporated into the reactor model and validated against experimental data, plant scale testing of the reactor model and proposed control strategies should be put into practice.

Bibliography

Acevedo F. The use of reactors in biomining processes. *Electronic Journal of Biotechnology*, 3:184–194, 2000.

Acevedo F. Present and future of bioleaching in developing countries. *Electronic Journal of Biotechnology*, 5:196–199, 2002.

Almendras E, Arriagada F, Bustos S, Herrera L, Ruiz P, Vargas T, Wiertz J and Badilla-Ohlbaum R. Surface transformation and electrochemical response of chalcopyrite in a bacterial leaching process. In: P Norris and DP Kelly, eds., *Biohydrometallurgy, Proceedings of the 7th International Symposium*, pages 259–271. Warwick, Science and Technology Letters, Surrey, UK, 1987.

Arrendondo R, Garcia A and Jerez CA. Partial removal of lipopolysaccharide for *Thiobacillus ferrooxidans* affects its adhesion to solids. *Applied Environmental Microbiology*, 60:2846–2851, 1994.

Baes CF Jr. *The Hydrolysis of Cations*. Wiley-Interscience, New York, 1976.

Bailey AD and Hansford GS. Oxygen mass transfer limitation of batch bio-oxidation at high solids concentration. *Minerals Engineering*, 7:293–303, 1994.

Bailey JE and Ollis DF. *Biochemical Engineering Fundamentals*. McGraw-Hill, Singapore, 2nd edition, 1986.

Barron JL and Luecking DR. Growth and maintenance of *Thiobacillus ferrooxidans* cells. *Applied Environmental Microbiology*, 56:2801–2806, 1990.

Battaglia-Brunet F, Clarens M, d'Hugues P, Godon JJ, Foucher S and Morin D. Monitoring of a pyrite-oxidising bacterial population using DNA single strand conformation polymorphism and microscopic techniques. *Applied Microbiology and Biotechnology*, 60:206–211, 2002.

Batty JD and Rorke GV. Development and commercial demonstration of the BioCop^{TM} thermophile process. In: STL Harrison, DE Rawlings and J Peterson, eds., *Proceedings of the 16th International Biohydrometallurgy Symposium*, pages 153–161. Cape Town, South Africa, 2005.

Bennett JC and Tributsch H. Bacterial leaching patterns on pyrite crystal surfaces. *Journal of Bacteriology*, 134:310–319, 1978.

Blight K, Ralph DE and Thurgate S. Pyrite surfaces after bio-leaching: a mechanism for bio-oxidation. *Hydrometallurgy*, 58:227–237, 2000.

Boogerd FC, van Beemd C, Stoelwinder T, Bos P and Kuenen JG. Relative contributions of biological and chemical reactions to the overall rate of pyrite oxidation at temperatures between 30 and 70^oC. *Biotechnology and Bioengineering*, 38:109–115, 1991.

Boon M. *Theoretical and experimental methods in the modelling of the bio-oxidation kinetics of sulphide minerals*. Ph.D. thesis, Delft University of Technology, Delft, The Netherlands, 1996.

Boon M, Brasser HJ, Hansford GS and Heijnen JJ. Comparison of the oxidation kinetics of different pyrites in the presence of *Thiobacillus ferrooxidans* or *Leptospirillum ferrooxidans*. *Hydrometallurgy*, 53:57–72, 1999a.

Boon M, Hansford GS and Heijnen JJ. Recent developments in modelling bio-oxidation kinetics part ii: Kinetic modelling of the bio-oxidation of sulphide minerals in terms of the critical sub-processes involved. In: D Holmes and R Smith, eds., *Minerals Bioprocessing II, Proceedings of Engineering Foundation Conference*. The Minerals Metals and Materials Society, Salt Lake City, 1994.

Boon M, Hansford GS and Heijnen JJ. The role of bacterial ferrous iron oxidation in the bio-oxidation of pyrite. In: T Vargas, CA Jerez, JV Wiertz and H Toledo, eds., *Biohydrometallurgical Processing I*, pages 153–163. University of Chile, Santiago, 1995.

Boon M and Heijnen JJ. Chemical oxidation kinetics of pyrite in bioleaching processes. *Hydrometallurgy*, 48:27–41, 1998a.

Boon M and Heijnen JJ. Gas-liquid mass transfer phenomena in bio-oxidation experiments of sulphide minerals: A critical review of literature data. *Hydrometallurgy*, 48:187–204, 1998b.

Boon M, Heijnen JJ and Hansford GS. The mechanism and kinetics of bioleaching sulphide minerals. *Mineral Processing and Extractive Metallurgy Review*, 19:107–115, 1998.

Boon M, Meeder TA, Thone C, Ras C and Heijnen JJ. The ferrous iron oxidation kinetics of *Thiobacillus ferrooxidans* in continuous cultures. *Applied Microbiology and Biotechnology*, 51:820–826, 1999b.

Boon M, Ras C and Heijnen JJ. The ferrous iron oxidation kinetics of *Thiobacillus ferrooxidans* in batch cultures. *Applied Microbiology and Biotechnology*, 51:813–819, 1999c.

Braddock JF, Luong HV and Brown EJ. Growth kinetics of *Thiobacillus ferrooxidans* isolated from arsenic mine drainage. *Applied and Environmental Microbiology*, 48:48–55, 1984.

Brandl H. Microbial leaching of metals. In: HJ Rehm and G Reed, eds., *Biotechnology Set*, pages 191–224. Wiley-VCH Verlag GmbH, 2nd edition, 2008.

Breed AW. *Studies on the mechanism and kinetics of bioleaching with special reference to the bioleaching of refractory gold-bearing arsenopyrite/pyrite concentrates*. Ph.D. thesis, University of Cape Town, Cape Town, South Africa, 2000.

Breed AW, Dempers CJN, Searby GE, Gardner MN, Rawlings DE and Hansford GS. The effect of temperature on the continuous ferrous-iron oxidation kinetics of a predominantly *Leptospirillum ferrooxidans* culture. *Biotechnology and Bioengineering*, 65:44–53, 1999.

Breed AW and Hansford GS. Effect of pH on ferrous-iron oxidation kinetics of *Leptospirillum ferrooxidans* in continuous culture. *Biochemical Engineering Journal*, 3:193–201, 1999a.

Breed AW and Hansford GS. Modelling continuous bioleach reactors. *Biotechnology and Bioengineering*, 64:671–677, 1999b.

Brierley CL. Mining Biotechnology: Research to commercial development and beyond. In: DE Rawlings, ed., *Biomining: Theory, Microbes and Industrial Processes*, pages 3–17. Springer-Verlag, Berlin, Germany, 1997.

Brierley JA and Brierley CL. Present and future commercial applications ob biohydrometallurgy. *Hydrometallurgy*, 59:233–239, 2001.

Brochot S, Durance MV, Villeneuve J, d'Hugues P and Mugabi M. Modelling of the bioleaching of sulphide ores: application for the simulation of the bioleaching/gravity section of the Kassese Cobalt Company Ltd process plant. *Minerals Engineering*, 17:253–260, 2004.

Brock TD and Madigan MT. *Biology of Microorganisms*. Prentice-Hall, New Jersey, USA, 6^{th} edition, 1991.

Bronnenmeier R and Märkl H. Hydrodynamic stress capacity of microorganisms. *Biotechnology and Bioengineering*, 24:553–578, 1982.

Cherry RS and Papoutsakis ET. Hydrodynamic effects on cells in agitated tissue culture reactors. *Bioprocess Engineering*, 1:21–41, 1986.

Clark DA and Norris PR. Oxidation of mineral sulphides by thermophilic microorganisms. *Minerals Engineering*, 9:1119–1125, 1996.

Coker AK. *Modeling of chemical kinetics and reactor design*. Gulf Professional Publishing Company, Houston, Texas, 2001.

Colmer AR and Hinkle HE. The role of microorganisms in acid mine drainage: Preliminary report. Technical report, Agricultural and Engineering Experiment Stations, West Virginia University, 1947.

Coram NJ and Rawlings DE. Molecular relationship between two groups of genus *Leptospirillum* and the find that *Leptospirillum ferriphilum* sp. nov. dominates South African commercial biooxidation tanks that operate at 40^oC. *Applied Environmental Microbiology*, 68:838–845, 2002.

Crundwell F. The leaching number: Its definition and use in determining the performance of leaching reactors and autoclaves. *Minerals Engineering*, 18:1315–1324, 2005.

Crundwell FK. Kinetics and mechanism of the oxidative dissolution of a zinc sulphide concentrate in ferric sulphate solutions. *Hydrometallurgy*, 19:227–242, 1987.

Crundwell FK. Mathematical modelling of batch and continuous bacterial leaching. *The Chemical Engineering Journal and the Biochemical Engineering Journal*, 54:207–220, 1994.

Crundwell FK. Progress in the mathematical modelling of leaching reactors. *Hydrometallurgy*, 39:321–335, 1995.

Crundwell FK. The kinetics of the chemiosmotic proton circuit of the iron-oxidizing bacterium *Thiobacillus ferrooxidans*. *Bioelectrochemistry and Bioenergetics*, 43:115–122, 1997.

Crundwell FK. Modelling, simulation and optimization of bacterial leaching reactors. *Biotechnology and Bioengineering*, 71:255–265, 2001.

Crundwell FK. How do bacteria interact with minerals? *Hydrometallurgy*, 71:75–81, 2003.

Danckwerts PV. Continuous flow systems: Distribution of residence times. *Chemical Engineering Science*, 2:1–13, 1953.

Dempers CJN, Breed AW and Hansford GS. The kinetics of ferrous-iron oxidation by *Acidithiobacillus ferrooxidans* and *Leptospirillum ferrooxidans*: Effect of cell maintenance. *Biochemical Engineering Journal*, 16:337–346, 2003.

Devasia P, Natarajan KA and Rao GR. Role of bacterial growth conditions and adhesion in the bioleaching of chalcopyrite by *Thiobacillus ferrooxidans*. *Minerals and Metallurgical Processing*, 13:82–86, 1996.

Deveci H. Effect of solids on viability of acidophilic bacteria. *Minerals Engineering*, 15:1181–1189, 2002.

Deveci H. Effect of particle size and shape of solids on the viability of acidophilic bacteria during mixing in stirred tank reactors. *Hydrometallurgy*, 71:385–395, 2004.

Dew DW. Comparison of performance for continuous bio-oxidation of refractory gold ore flotation concentrates. In: T Vargas, CA Jerez, JV Wiertz and H Toledo, eds., *Biohydrometallurgical Processing*, volume 1, pages 239–251. Santiago: Univ. Chile Press, 1995.

Dew DW, Lawson EN and Broadhurst JL. The BIOX® process for biooxidation of gold-bearing ores or concentrates. In: *Biomining: Theory, Microbes and Industrial Processes*, chapter 3, pages 45–61. 1997.

Dopson M and Lindström EB. Analysis of community composition during moderately thermophilic bioleaching of pyrite, arsenical pyrite and chalcopyrite. *Microbiology and Ecology*, 48:19–28, 2004.

Drossou M. *The kinetics of the bioleaching of a refractory gold-bearing pyrite concentrate.* Master's thesis, University of Cape Town, Cape Town, South Africa, 1986.

Dunlop EH and Namdev PK. Effect of fluid shear forces on plant cell suspensions. *Chemical Engineering Science*, 49:2263–2276, 1994.

Dutrizac JE. The dissolution of chalcopyrite in ferric sulphate and ferric chloride media. *Metallurgical Transactions B*, 12:371–378, 1981.

Dutrizac JE, MacDonald RC and Ingraham TR. The kinetics of dissolution of synthetic chalcopyrite in aqueous acidic ferric sulfate solutions. *Trans. Metall. Soc. AIME*, 245:955–959, 1969.

Dutrizac JE and MacDonald RJC. Ferric ion as a leaching medium. *Minerals Science and Engineering*, 2:59–100, 1974.

Dutta R. *Fundamentals of Biochemical Engineering*. Springer, 2008.

Ehrlich HL. Past, present and future of biohydrometallurgy. *Hydrometallurgy*, 59:127–134, 2001.

Faires JD and Burden RL. *Numerical Methods*. PWS Publishing Company, Boston, USA, 1993.

Garrels RM and Thompson ME. Oxidation of pyrite by iron sulfate solutions. *American Journal of Science, Bradley Volume*, 258A:57–67, 1960.

Gehrke T, Telegdi J, Thierry D and Sand W. Importance of extracellular polymeric substances from *Thiobacillus ferrooxidans* for bioleaching. *Applied Environmental Microbiology*, 64:2743–2747, 1998.

Gericke M and Govender Y. Bioleaching strategies for the treatment of nickel-copper sulphide concentrates. *Minerals Engineering*, 24:1106–1112, 2011.

Gericke M, Govender Y and Pinches A. Tank bioleaching of low-grade chalcopyrite concentrates using redox control. *Hydrometallurgy*, 104:414–419, 2010.

Gericke M, Neale JW and van Staden PJ. A Mintek perspective of the past 25 years in minerals bioleaching. *The Journal of the South African Institute of Mining and Metallurgy*, 109:567–585, 2009.

Gilbertson BP. Creating value through innovation: biotechnology in mining. *Mineral Processing and Extractive Metallurgy*, 109:61–67, 2000.

Goebel BM and Stackebrandt E. Cultural and phylogenetic analysis of mixed microbial populations found in natural and commercial bioleaching environments. *Applied Environmental Microbiology*, 60:1614–1621, 1994.

Gomez JM and Cantero D. Kinetic study of biological ferrous sulphate oxidation by iron-oxidising bacteria in continuous stirred tank and packed bed bioreactors. *Proc Biochem*, 38:867–875, 2003.

Gomez JM, Caro I and Cantero D. Kinetic equation for growth of *Thiobacillus ferrooxidans* in submerged culture over aqueous ferrous sulfate solutions. *Journal of Biotechnology*, 48:147–152, 1996.

Grishin S and Tuovinen O. Fast kinetics of Fe^{2+} oxidation in packed-bed reactors. *Applied Environmental Microbiology*, 54:3092–3100, 1988.

Guay R, Silver M and Torma AE. Ferrous iron oxidation and uranium extraction by *Thiobacillus ferrooxidans*. *Biotechnology and Bioengineering*, 19:727–740, 1977.

Hansford GS. Recent developments in modelling the kinetics of bioleaching. In: DE Rawlings, ed., *Biomining: Theory, Microbes and Industrial Processes*, pages 153–176. Springer-Verlag, Berlin, Germany, 1997.

Hansford GS and Chapman JT. Batch and continuous bio-oxidation kinetics of a refractory gold-bearing pyrite/arsenopyrite concentrate. *Minerals Engineering*, 5:597–612, 1992.

Hansford GS and Drossou M. In: PR Norris and DP Kelly, eds., *Biohydrometallurgy, Science and Technology Letters*. Surrey, UK, 1988.

Hansford GS and Miller DM. Biooxidation of a gold-bearing pyrite-arsenopyrite concentrate. *FEMS Microbiology Reviews*, 11:175–182, 1993.

Hansford GS and Vargas T. Chemical and electrochemical basis of bioleaching processes. *Hydrometallurgy*, 59:135–145, 2001.

Harvey PI and Crundwell FK. Growth of *Thiobacillus ferrooxidans*: a novel experiment design for batch growth and bacterial leaching studies. *Applied and Environmental Microbiology*, 63:2586–2592, 1997.

Hirato T, Majima H and Awakura Y. The leaching of chalcopyrite with ferric sulfate. *Metallurgical Transactions B*, 18:489–496, 1987.

Hiroyoshi N, Hirota M, Hirajima T and Tsunekawa M. A case of ferrous sulfate addition enhancing chalcopyrite leaching. *Hydrometallurgy*, 47:37–45, 1997.

Hiroyoshi N, Hirota M, Hirajima T and Tsunekawa M. Inhibitory effect of iron-oxidizing bacteria on ferrous-promoted chalcopyrite leaching. *Biotechnology and Bioengineering*, 64:478–483, 1999.

Hiroyoshi N, Kuroiwa S, Miki H, Tsunekawa M and Hirajima T. Synergistic effect of cupric and ferrous ions on active-passive behavior in anodic dissolution of chalcopyrite in sulfuric acid solutions. *Hydrometallurgy*, 74:103–116, 2004.

Hiroyoshi N, Miki H, Hirajima T and Tsunekawa M. A model for ferrous-promoted chalcopyrite leaching. *Hydrometallurgy*, 57:31–38, 2000.

Hiroyoshi N, Miki H, Hirajima T and Tsunekawa M. Enhancement of chalcopyrite leaching by ferrous ions in acidic ferric sulfate solutions. *Hydrometallurgy*, 60:185–197, 2001.

Holdren GR Jr. Fine particle dissolution behavior and its effect on the apparent dissolution kinetics of primary silicate minerals (abstr.). *Geol. Soc. Amer. Abstr. Prog.*, 13:475, 1981.

Holmes PR and Crundwell FK. The kinetics of the oxidation of pyrite by ferric ions and dissolved oxygen: An electrochemical study. *Geochimica et Cosmochimica Acta*, 64:263–274, 2000.

Huberts R. *Modelling of ferrous sulphate oxidation by iron oxidising bacteria - chemiosomotic and electrochemical approach.* Ph.D. thesis, Department of Chemical Engineering, University of the Witwatersrand, Johannesburg, South Africa, 1994.

Hulbert HM and Katz S. Some problems in particle technology: A statistical mechanical formulation. *Chemical Engineering Science*, 19:555–574, 1964.

Jaffer A. *An investigation into the mechanism of bioleaching of a predominantly chalcopyrite concentrate with mesophiles.* Master's thesis, University of Cape Town, Cape Town, South Africa, 2002.

Johnson KA and Goody RS. The original Michaelis constant: Translation of the 1913 Michaelis-Menten paper. *Biochemistry*, 50:8264–8269, 2011.

Jones CA and Kelly DP. Growth of *Thiobacillus ferrooxidans* on ferrous iron in chemostat culture: Influence of product and substrate inhibition. *Journal of Chemical Technology and Biotechnology*, 33B:241–261, 1983.

Jones E, Oliphant T, Peterson P *et al.* SciPy: Open source scientific tools for Python. http://www.scipy.org/, 2001.

Kametani H and Aoki A. Effect of suspension potential on the oxidation rate of copper concentrate in a sulphuric acid solution. *Metallurgical Transactions B*, 16B:695–705, 1985.

Kawabe Y, Inoue C, Suto K and Chida T. Inhibitory effect of high concentrations of ferric ion on the activity of *Acidithiobacillus ferrooxidans. Bioscience and Bioengineering*, 96:375–379, 2003.

Kawakami K, Sato J, Kusunoke K, Kusakabe K and Morooka S. Kinetic study of oxidation of a pyrite slurry by ferric chloride. *Industrial & Engineering Chemistry Research*, 27:571–576, 1988.

Kelly DP and Jones CA. Factors affecting metabolism and ferrous iron oxidation in suspensions and batch cultures of *Thiobacillus ferrooxidans*:relevance to ferric iron leach generation. In: LE Murr, AE Torma and JA Brierley, eds., *Metallurgical Applications of Bacterial Leaching and Related Microbiological Phenomena*, pages 19–44. Academic Press, New York, 1978.

Kelly DP and Wood AP. Reclassification of some species of *Thiobacillus* to the newly designated gerera *Acidithiobacillus* gen. nov., *Halothiobacillus* gen. nov. and *Thermithiobacillus* gen. nov. *International Journal of Systematic and Evolutionary Microbiology*, 50:511–516, 2000.

King WE Jr and Perlmutter DD. Pyrite oxidation in aqueous ferric chloride. *AIChE Journal*, 23:679–685, 1977.

Konishi Y, Kubo H and Asai S. Bioleaching of zince sulphide concentrate by *Thiobacillus ferrooxidans. Biotechnology and Bioengineering*, 39:66–74, 1992.

La Motta EJ. Kinetics of continuous growth cultures using the logistic growth curve. *Biotechnology and Bioengineering*, 18:1029–1032, 1976.

Lacey DT and Lawson F. Kinetics of the liquid-phase oxidation of acid ferrous sulfate by the bacterium *Thiobacillus ferrooxidans*. *Biotechnology and Bioengineering*, 12:29–50, 1970.

Leduc LG, Trevors JT and Ferroni GD. Thermal characterization of different isolates of *Thiobacillus ferrooxidans*. *FEMS Microbiology Letters*, 108:189–194, 1993.

Levenspiel O. *Chemical Reaction Engineering*. John Wiley & Sons, Inc., New York, 2nd edition, 1972.

Liu MS, Branion RMR and Duncan DW. The effects of ferrous iron, dissolved oxygen, and inert solids concentrations on the growth of *Thiobacillus ferrooxidans*. *The Canadian Journal of Chemical Engineering*, 66:445–451, 1988.

Lizama HM and Suzuki I. Rate equations and kinetic parameters of the reactions involved in pyrite oxidation by *Thiobacillus ferrooxidans*. *Applied and Environmental Microbiology*, 55:2918–2923, 1989a.

Lizama HM and Suzuki I. Synergistic competitive inhibition of ferrous iron oxidation by *Thiobacillus ferrooxidans* by increasing concentrations of ferric iron and cells. *Applied and Environmental Microbiology*, 55:2588–2591, 1989b.

Loayza C and Ly ME. Biooxidation of arsenopyrite concentrate for industrial plant Tamboraque using acid mine drainage. In: *Biomine '99: Conference Proceedings*, pages 162–167. Perth, Australia, 1999.

Loia G, Mura A, Trois R and Rossi G. Bioreactor performance versus solids concentration in coal biodepyritization. *Fuel Processing Technology*, 40:251–260, 1994.

MacDonald DG and Clark RH. The oxidation of aqueous ferrous sulphate by *Thiobacillus ferrooxidans*. *The Canadian Journal of Chemical Engineering*, 48:669–676, 1970.

MacMullin RB and Weber M. The theory of short-circuiting in continuous-flow mixing vessels in series and kinetics of chemical reactions in such systems. *Trans. AIChE Journal*, 31:409–458, 1935.

Mathews CT and Robins RG. The oxidation of iron disulphide by ferric sulphate. *Australian Chemical Engineering*, pages 21–25, 1972.

May N, Ralph DE and Hansford GS. Dynamic redox potential measurement for determining the ferric leach kinetics of pyrite. *Minerals Engineering*, 10:1279–1290, 1997.

McKibben MA. *Kinetics of aqueous oxidation of pyrite by ferric iron, oxygen, and hydrogen peroxider from pH 1−4 and 20−40°C*. Ph.D. thesis, Pennsylvannia State University, 1984.

McKibben MA and Barnes HL. Oxidation of pyrite in low temperature acidic solutions: Rate laws and surface textures. *Geochimica et Cosmochimica Acta*, 50:1509–1520, 1986.

Meruane G, Sahle C, Wiertz J and Vargas T. Novel electrochemical-enzymatic model which quantifies the effect of the solution Eh on the kinetics of ferrous iron oxidation with *Acidithiobacillus ferrooxidans*. *Biotechnology and Bioengineering*, 80:280–288, 2002.

Meruane G and Vargas T. Bacterial oxidation of ferrous iron by *Acidithiobacillus ferrooxidans* in the pH range 2.5-7.0. *Hydrometallurgy*, 71:149–158, 2003.

Michaelis L and Menten ML. Die kinetik der invertinwirkung. *Biochemische Zeitschrift*, 49:333–369, 1913.

Michaels JD, Mallik AK and Papoutsakis ET. Sparging and agitation-induced injury of cultures animal cells: Do cell-to-bubble interactions in the bulk liquid injure cells? *Biotechnology and Bioengineering*, 51:399–409, 1996.

Mikkelsen D, Kappler U, McEwan AG and Sly LI. Archaeal diversity in two thermophilic chalcopyrite bioleaching reactors. *Environmental Microbiology*, 8:2050–2055, 2006.

Miller DM and Hansford GS. Batch biooxidation of gold-bearing pyrite-arsenopyrite concentrate. *Minerals Engineering*, 5:613–629, 1992.

Mishra D, Kim DJ, Ahn JG and Rhee YH. Bioleaching: A microbial process of metal recovery; A review. *Metals and Materials International*, 11:249–256, 2005.

Monod J. The growth of bacterial cultures. *Annual Review of Microbiology*, 3:371–394, 1949.

Moses CO and Herman JS. Pyrite oxidation at circumneutral pH. *Geochimica Cosmochimica Acta*, 50:471–482, 1991.

Moses CO, Nordstrom DK, Herman JS and Mills AL. Aqueous pyrite oxidation by dissolved oxygen and by ferric iron. *Geochimica et Cosmochimica Acta*, 51:1561–1571, 1987.

Nagpal S, Dahlstrom D and Oolman T. A mathematical model for the bacterial oxidation of a sulfide ore concentrate. *Biotechnology and Bioengineering*, 43:357–364, 1994.

Nemati M and Harrison STL. Effect of solid loading on thermophilic bioleaching of sulfide minerals. *Journal of Chemical Technology and Biotechnology*, 75:526–532, 2000.

Nemati M, Harrison STL, Hansford GS and Webb C. Biological oxidation of ferrous sulphate by *Thiobacillus ferrooxidans*: a review on the kinetic aspects. *Biochemical Engineering Journal*, 1:171–190, 1998.

Nemati M, Lowenadler J and Harrison STL. Particle size effects in bioleaching of pyrite by acidophilic thermophile *Sulfolobus metallicus* (bc). *Applied Microbiology and Biotechnology*, 53:173–179, 2000.

Nemati M and Webb C. A kinetic model for biological oxidation of ferrous iron by *Thiobacillus ferrooxidans*. *Biotechnology and Bioengineering*, 53:478–486, 1997.

Nemati M and Webb C. Inhibition effect of ferric iron on the kinetics of ferrous iron. *Biotechnology Letters*, 20:873–877, 1998.

Nicholson RV, Gillham RW and Reardon EJ. Pyrite oxidation in carbonate-buffered solution: I. experimental kinetics. *Geochimica Cosmochimica Acta*, 52:1077–1085, 1988.

Nikolov LN and Karamanev DG. Kinetics of the ferrous iron oxidation by resuspended cells of *Thiobacillus ferrooxidans*. *Biotechnology Progress*, 8:252–255, 1992.

Norris PR. Iron and mineral oxidation studies with *Leptospirillum*-like bacteria. In: G Rossi and AE Torma, eds., *Recent progress in Biohydrometallurgy*, pages 83–96. Associazione Mineraria Sarda, Rome, Italy, 1983.

Norris PR. Acidophile diversity in mineral sulfide oxidation. In: DE Rawlings and DB Johnson, eds., *Biomining*, pages 199–216. Springer-Verlag, Berlin, 2007.

Norris PR, Barr DW and Hinson D. Iron and mineral oxidation by acidophilic bacteria: affinities for iron and attachment to pyrite. In: *Proceedings of the International Biohydrometallurgy Symposium*, pages 43–59. 1988.

Norris PR and Johnson DB. Acidophilic microorganisms. In: K Horikoshi and WD Grant, eds., *Extremophiles: Microbial life in extreme environments*, pages 133–153. Wiley, 1998.

Norris PR and Kelly DP. The use of mixed microbial cultures in metal recovery. In: AT Bull and JH Slater, eds., *Microbial Interactions and Communities*, page 443. Academic Press, London, 1982.

Nurmi P, Özkaya B, Kaksonen AH, Tuovinen OH and Puhakka JA. Inhibition kinetics of iron oxidation by *Leptospirillum ferriphilum* in the presence of ferric, nickel and zinc ions. *Hydrometallurgy*, 2009:137–145, 2009.

Nyavor K, Egiebor NO and Fedorak PM. The effect of ferric iron on the rate of ferrous oxidation by *Thiobacillus ferrooxidans*. *Applied Microbiology and Biotechnology*, 45:688–691, 1996.

Ojumu TV. *The Effects of Solution Conditions on the Kinetics of Microbial Ferrous-Iron Oxidation by Leptospirillum ferriphilum in Continuous Culture*. Ph.D. thesis, University of Cape Town, Cape Town, South Africa, 2008.

Ojumu TV, Peterson J, Searby GE and Hansford GS. A review of rate equations proposed for microbial ferrous-iron oxidation with a view to application to heap bioleaching. *Hydrometallurgy*, 83:21–28, 2006.

Ojumu TV, Peterson J, Searby GE and SHansford G. The kinetics of ferrous-iron oxidation by *Leptospirillum ferriphilum* in continuous culture: The effect of temperature. *Biochemical Engineering Journal*, 46:161–168, 2009.

Okibe N, Gericke M, Hallberg KB and Johnson DB. Enumeration and characterization of acidophilic microorganisms isoltated from a pilot plant stirred tank bioleaching operation. *Applied and Environmental Microbiology*, 69:1936–1943, 2003.

Olson GJ. Rate of pyrite bioleaching by thiobacillus ferrooxidans: Results of interlaboratory comparison. *Applied and Environmental Microbiology*, 57:642–644, 1991.

Olson GJ, Brierley JA and Brierley CL. Bioleaching Review Part B: Progress in bioleaching: applications of microbial process by the minerals industries. *Appl Microbiol Biotechnol*, 63:249–257, 2003.

Özkaya B, Sahinkaya E, Nurmi P, Kaksonen AH and Puhakka JA. Kinetics of iron oxidation by *Leptospirillum ferriphilum* dominated culture at pH below one. *Biotechnology and Bioengineering*, 97:1121–1127, 2006.

Pesic B and Olivier DJ. An electrochemical method of measuring the oxidation rate of ferrous to ferric iron with oxygen in the presence of *Thiobacillus ferrooxidans*. *Biotechnology and Bioengineering*, 33:428–439, 1989.

Peters E. Direct leaching of sulfides: chemistry and applications. *Metallurgical Transactions B*, 7:505–517, 1976.

Petersen J and Dixon DG. Competitive bioleaching of pyrite and chalcopyrite. *Hydrometallurgy*, 83:40–49, 2006.

Petrovich R. Kinetics of dissolution of mechanically comminuted rock-forming oxdes and silicates. I. Deformation and dissolution of quartz under laboratory conditions. *Geochimica et Cosmochimica Acta*, 45:1665–1674, 1981.

Pinches A, Chapman JT, te Riele WAM and van Staden M. The performance of bacterial leach reactors for the preoxidation of refactory gold bearing sulphide concentrates. In: PR Norris and DP Kelly, eds., *Biohydrometallurgy, Proceedings of the 7th International Symposium*, pages 329–344. Warwick, Science and Technology Letters, Surrey, UK, 1987.

Pletcher D. *Industrial electrochemistry*. Chapman and Hall, New York, 1984.

Poulin R and Lawrence RW. Economic and environmental niches of biohydrometallurgy. *Minerals Engineering*, 9:799–810, 1996.

Raja SB. *The effect of particulate-induced hydrodynamic stress on the bioleaching of chalcopyrite by a Sulfolobus sp.* Ph.D. thesis, Department of Chemical Engineering, University of Cape Town, Cape Town, South Africa, 2005.

Ratkowsky DA, Lowry RK, McMeekin TA, Stokes AN and Chandler RE. Model for bacterial culture growth rate throughout the entrire biokinetic temperature range. *Journal of Bacteriology*, 154:1222–1226, 1983.

Ratkowsky DA, McMeekin TA and Ball A. Relationship between temperature and growth rate of bacterial cultures. *Journal of Bacteriology*, 149:1–5, 1982.

Rawatlal R. *Unsteady-state modelling of Ziegler-Natta catalyzed olefin polymerization reactor systems*. Ph.D. thesis, University of Kwa-Zulu Natal, Kwa-Zulu Natal, South Africa, 2004.

Rawatlal R and Starzak M. Unsteady-state residence-time distribution in perfectly mixed vessels. *AIChE Journal*, 49:471–484, 2003.

Rawlings DE. Industrial practice and the biology of leaching of metals from ores - The 1997 pan labs lecture. *Journal of Industrial Microbiology & Biotechnology*, 20:268–274, 1998.

Rawlings DE. Heavy metal mining using microbes. *Annual Review of Microbiology*, 56:65–91, 2002.

Rawlings DE, Dew D and du Plessis C. Biomineralization of metal-containing ores and concentrates. *TRENDS in Biotechnology*, 21:38–44, 2003.

Rawlings DE and Johnson DB. The microbiology of biomining: development and optimization of mineral-oxidizing microbial consortia. *Microbiology*, 153:315–324, 2007.

Reedy BJ, Beattie JK and Lowson RT. A vibrational spectroscopic ^{18}O tracer study of pyrite oxidation. *Geochimica et Cosmochimica Acta*, 55:1609–1614, 1991.

Riekkola-Vanhanen M and Heimala S. Electrochemical control in the biological leaching of sulfidic ores. In: AE Torma, JE Wey and VL Lakshmanan, eds., *Biohydrometallurgical Technologies. The Minerals, Metals and Materials Society*, pages 561–570. 1993.

Rimstidt JD and Newcom WD. Measurement and analysis of rate data: The rate of reaction of ferric iron with pyrite. *Geochimica et Cosmochimica Acta*, 57:1919–1934, 1993.

Rodriguez-Leiva M and Tributsch H. Morphology of bacterial leaching patterns by *Thiobacillus ferrooxidans* on synthetic pyrite. *Arch Microbiol*, 149:401–405, 1988.

Rohwerder T, Gehrke T, Kinzler K and Sand W. Bioleaching Review Part A: Progress in bioleaching: fundamentals and mechanisms of bacterial metal sulfide oxidation. *Applied Microbiology and Biotechnology*, 63:239–248, 2003.

Salmon SU and Malmström ME. Quantification of mineral dissolution rates and applicability of rate laws: Laboratory studies of mill tailings. *Applied Geochemistry*, 21:269–288, 2006.

Sand W and Gehrke T. Extracellular polymeric substances mediate bioleaching/biocorrosion via interfacial processes involving iron (iii) ions and acidophilic bacteria. *Research in Microbiology*, 157:49–56, 2006.

Sand W, Gerke T, Hallmann R and Schippers A. Sulphur chemistry, biofilm, and the (in)direct attack mechanism - a critical evaluation of bacterial leaching. *Applied Microbiology and Biotechnology*, 43:961–966, 1995.

Sand W, Gerke T, Jozsa PG and Schippers A. (bio)chemistry of bacterial leaching - direct vs. indirect bioleaching. *Hydrometallurgy*, 59:159–175, 2001.

Schippers A, Jozsa PG and Sand W. Sulfur chemistry in bacterial leaching of pyrite. *Applied Environmental Microbiology*, 62:3424–3431, 1996.

Searby GE. *An investigation of the kinetics of thermophilic microbial ferrous iron oxidation in continuous culture*. Ph.D. thesis, University of Cape Town, Cape Town, South Africa, 2006.

Shrihari RK and Gandhi KS. Modelling of Fe^{2+} oxidation by *Thiobacillus ferrooxidans*. *Applied Microbiology and Biotechnology*, 33:524–528, 1990.

Shuler ML and Kargi F. *Bioprocess Engineering: Basic Concepts*. Prentice Hall PT, New Jersey, 2nd edition, 2002.

Silverman MP and Ehrlich HL. Formation and degradation of minerals. *Advances in Applied Microbiology*, 6:174–187, 1964.

Silverman MP and Lundgren DG. Studies on the chmoautotrophic iron bacterium *Ferroobacillus ferrooxidans*: II. Manometric studies. *Journal of Bacteriology*, 78:326–331, 1959.

Singer PC and Stumm W. The rate determining step in the production of acidic mine wastes. *American Chemical Society, Division of Fuel Chemistry, Preprints*, 13:80–87, 1967.

Sissing A and Harrison STL. Thermophilic mineral bioleaching performance: A compromise between maximizing mineral loading and miximizing microbial growth and activity. *The Journal of the South African Institute of Mining and Metallurgy*, 103:139–142, 2003.

Smith JR, Luthy RG and Middleton AC. Microbial ferrous iron oxdiation in acidic solution. *Journal (Water Pollution Control Federation)*, 60:518–530, 1988.

Southwood MJ and Southwood AJ. Mineralogical observations on the bacterial leaching of auriferous pyrite: A new mathematical model and implications for the release of gold. In: RW Lawrence, RMR Branion and HG Ebner, eds., *Fundamentals and Apploied Biohydrometallurgy*, page 98. Elsevier, 1986.

Suzuki I, Lizama HM and Tackaberry PD. Competitive inhibition of ferrous iron oxidation by *Thiobacillus ferrooxidans* by increasing concentration of cells. *Applied and Environmental Microbiology*, 55:1117–1121, 1989.

Tal P. The effect of the iron(III) to iron(II) ratio on the rate of dissolution of pyrite. *Council of Mineral Technology, Hydrometallurgy Division Technical Memorandum No. 18255*, 1986.

Third KA, Cord-Ruwisch R and Watling HR. The role of iron-oxidizing bacteria in stimulation inhibition of chalcopyrite bioleaching. *Hydrometallurgy*, 57:225–233, 2000.

Tributsch H. Direct versus indirect bioleaching. *Hydrometallurgy*, 59:177–185, 2001.

Valencia P and Acevedo F. Are bioleaching rates determined by the available particle surface area concentration? *World Journal of Microbiology and Biotechnology*, 25:1010–1016, 2009.

Valencia P, Gentina JC and Acevedo F. Effect of pulp density and particle size on the biooxidation rate of a pyritic gold concentrate by *Sulfolobus metallicus*. In: *Proceedings of the International Biohydrometallurgy Symposium*. Athens, Greece, 2003.

van Aswegen PC, van Niekerk J and Olivier W. The BIOX® process for the treatment of refractory gold concentrates. In: DE Rawlings and DB Johnson, eds., *Biomining*, pages 1–34. Springer-Verlag, Berlin, 2007.

van Scherpenzeel DA, Boon M, Ras C, Hansford GS and Heijnen JJ. Kinetics of ferrous iron oxidation by *Leptospirillum* bacteria in continuous cultures. *Biotechnology Progress*, 14:425–433, 1998.

Wadsworth CL. *Leaching – Metals applications*. John Wiley and Sons, New York, New York, 1987.

Watling HR. The bioleaching of sulphide minerals with emphasis on copper sulphides – a review. *Hydrometallurgy*, 84:81–108, 2006.

Wiersma CL and Rimstidt JD. Rates of reaction of pyrite and marcasite with ferric iron at pH 2. *Geochimica et Cosmochimica Acta*, 48:85–92, 1984.

Williamson MA and Rimstidt JD. The kinetics and electrochemical rate-dtermining step of aqueous pyrite oxidation. *Geochimica et Cosmochimica Acta*, 58:5443–5454, 1994.

Witne JY and Phillips CV. Bioleaching of 0k tedi copper concentrate in oxygen-and carbon dioxide-enriched air. *Minerals Engineering*, 14:25–48, 2001.

Yagi S and Kunii D. Fluidized-solids reactors with continuous solids feed. I. Residence time of particles in fluidezed beds. *Chemical Engineering Science*, 16:364–371, 1961.

Zacca JJ, Debling JA and Ray WH. Reactor residence time distribution effects on the multistage polymerization of olefins - I. basic principles and illustrative examples, polypropylene. *Chemical Engineering Science*, 51:4859–4886, 1996.

Zheng CQ, Allen CC and Bautista RG. Kinetic study of the oxidation of pyrite in aqueous ferric sulphate. *Industrial & Engineering Chemistry Process Design and Development*, 23:308–317, 1986.

Zimmerley SR, Wilson DG and Prater JD. Cyclic leaching process employing iron oxidising bacteria. US Patent 2,829,964, 1958.

A

Mintek Data

A.1 Bioleaching of Aguablanca Ore – Data provided by Mintek

Table A.1: Experimental Data for the Bioleaching of Polymetallic Sulphide Mineral, Aguablanca – Data provided by Mintek, South Africa

Time [days]	Solids Loading [%]	ORP ($Ag/AgCl$) [mV]	Soluble Cu^{2+} [g/L]	Soluble Ni^{2+} [g/L]
0	7.70	636	0.00	0.00
1	7.70	623	0.98	0.90
2	8.00	610	1.95	1.80
3	9.80	597	2.93	2.70
4	9.19	603	3.85	2.38
5	9.28	607	3.93	2.25
6	10.78	590	4.00	2.45
7	10.37	600	4.45	2.90
8	9.96	611	4.73	3.08
9	10.56	604	4.50	2.40
10	10.59	590	5.18	2.58
11	8.76	604	7.65	4.65
12	9.37	623	6.80	3.33
13	9.45	591	6.98	3.75
14	9.88	601	7.09	4.43
15	10.32	588	7.10	3.38
16	10.40	615	6.50	3.30
17	10.35	592	7.58	3.63
18	8.84	595	4.90	2.98
19	9.17	608	5.78	3.10
20	9.86	592	5.73	2.58
21	9.29	582	6.03	2.90
22	8.71	582	5.38	2.45
23	9.23	597	5.48	2.50
24	11.37	592	5.38	2.15
25	11.85	590	5.98	3.53
26	11.20	593	6.05	3.63
27	10.54	619	7.25	3.80
28	9.55	590	6.15	3.13
29	9.72	594	5.85	2.93
30	9.88	580	6.70	3.53
31	10.13	604	6.88	3.85
32	11.34	572	6.98	4.13
33	11.24	581	5.70	3.05
34	11.14	599	5.60	2.70
35	10.39	588	5.13	2.35
36	9.63	586	5.83	3.03
37	10.27	588	6.80	3.05
38	11.60	591	6.93	3.80
39	10.75	588	6.68	3.55
40	11.04	609	6.40	3.35
41	11.04	601	6.53	4.10
42	10.87	585	5.33	4.68
43	10.70	580	6.90	4.33
44	11.19	586	6.60	3.53
45	12.18	557	7.30	4.88